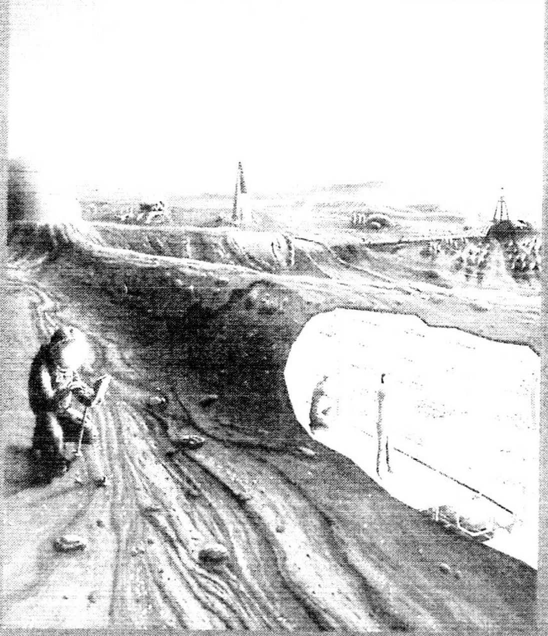

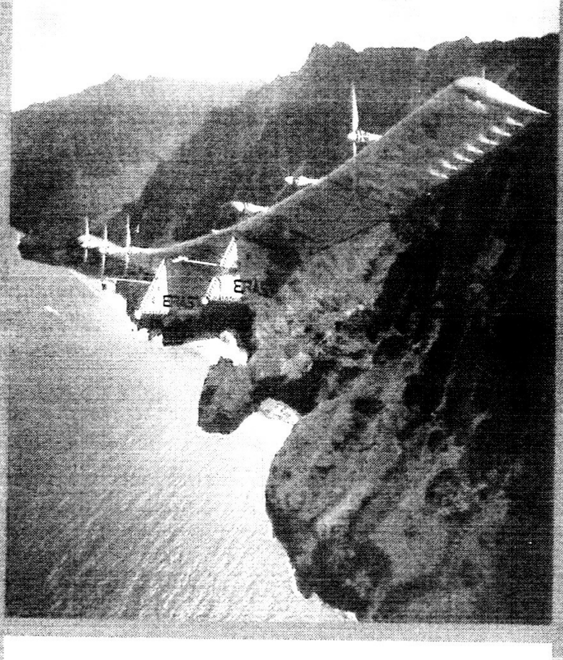

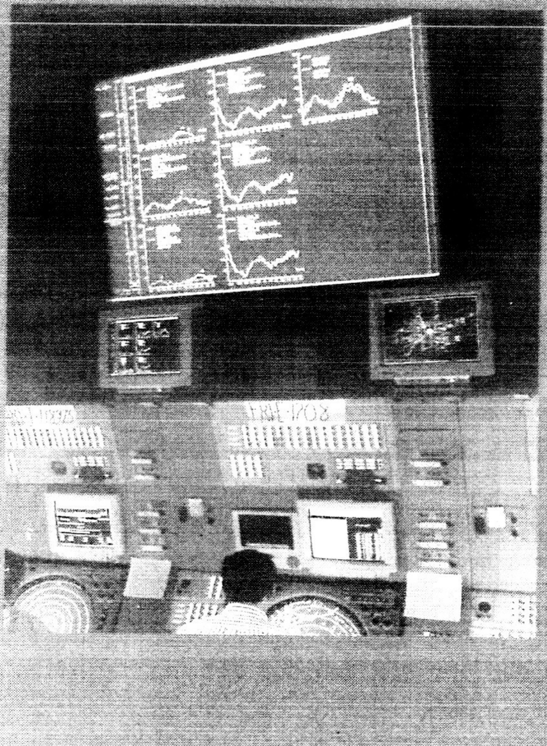

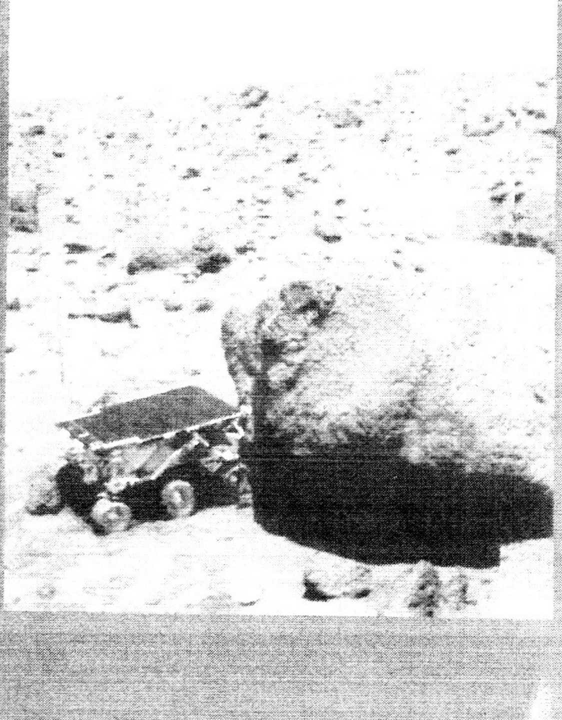

1997

RESEARCH & TECHNOLOGY

NASA AMES RESEARCH CENTER

RESEARCH & TECHNOLOGY

NASA AMES RESEARCH CENTER

1997

National Aeronautics and Space Administration • **Ames Research Center** • Moffett Field, California

NASA/TM–98-112240

Acknowledgment

The NASA Ames Research Center acknowledges Dr. Unmeel Mehta for his major contributions in publishing the annual *Ames Research and Technology Report*. During the past three years, Dr. Mehta has worked as the report's Managing Editor, taking time from his own research to provide valuable technical assistance and advice. His innovations have led to the report's inclusion of the Overviews and reorganization of the report's content to align it with NASA's four Strategic Enterprises.

Available from:

NASA Center for AeroSpace Information
7121 Standard Drive
Hanover, MD 21076-1320
(301) 621-0390

National Technical Information Service
5285 Port Royal Road
Springfield, VA 22161
(703) 487-4650

Foreword

This report highlights the challenging work accomplished during fiscal year 1997 by Ames research scientists and engineers. The work is divided into accomplishments that support the goals of NASA's four Strategic Enterprises: Aeronautics and Space Transportation Technology, Space Science, Human Exploration and Development of Space (HEDS), and Earth Science. A key purpose of this report is to communicate information to our stakeholders, customers, and the people of the United States about the scope and diversity of Ames' mission, and the nature of Ames' research and technology activities.

Ames Research Center is making significant contributions to the Aeronautics and Space Transportation Enterprise. The Center has core competencies in the areas of human factors, air-traffic management, information systems, rotorcraft, vertical/short takeoff and landing technology, and thermal protection systems technology. The Center is leading the Agency's mission in such areas as Aviation Operations Systems, Aviation System Capacity, and Rotorcraft. Ames is making significant contributions to the Access to Space pillar by characterizing the aerothermal environment around next generation reusable launch vehicles such as the X-33 and X-34 vehicles.

NASA Ames Research Center's research effort in the Space, Earth, and HEDS Enterprises is focused in large part to support Ames' lead role for Astrobiology, which broadly defined is the scientific study of the origin, distribution, and future of life in the universe. This NASA initiative in Astrobiology is a broad science effort embracing basic research, technology development, and flight missions. Ames' contributions to the Space Science Enterprise are focused in the areas of exobiology, planetary systems, astrophysics, and space technology. Ames supports the Earth Science Enterprise by conducting research and by developing technology with the objective of expanding our knowledge of the Earth's atmosphere and ecosystems. Finally, Ames supports the HEDS Enterprise by conducting research, managing spaceflight projects, and developing technologies. A key objective is to understand the phenomena surrounding the effects of gravity on living things.

Ames has also been designated the Agency's Center of Excellence for Information Technology. The three cornerstones of Information Technology research at Ames are automated reasoning, human-centered computing, and high performance computing and networking. The mission critical capabilities enabled by NASA's three cornerstones of Information Technology span all four of NASA's strategic enterprises. They include the Design and Fabrication in the Virtual Environment, Human Exploration of Space, Robotic Exploration of Space, Aircraft Operations, and Science Understanding. State-of-the-art capability in Information Technology is essential in realizing the challenge of the NASA Administrator, Dan Goldin, to do it "faster, better, and cheaper."

For further information on Ames research and technology projects, please contact the person designated as the point of contact at the end of each article. For further information about the report itself, contact Stephanie Langhoff, Chief Scientist, Mail Stop 230-3, NASA Ames Research Center, Moffett Field, CA 94035. An electronic version of this report is available on the Ames home page.

Henry McDonald,
Director

Aeronautics and Space Transportation Technology Enterprise

Overview 1

Global Civil Aviation/Safety

The Concept of Airspace Complexity and Its Use in Air-Traffic Management 3
Banavar Sridhar, Gano Chatterji, Kapil Sheth

Conflict Prediction and Resolution Technology Field Test 4
Dave McNally, Ralph Bach, William Chan

Conflict Probe Performance Evaluation 5
Karl D. Bilimoria

Collaborative Arrival Planning 6
Rick Zelenka

T-NASA Taxi Test at Atlanta Airport 8
David C. Foyle, Anthony Andre, Becky Hooey, Robert McCann

Analysis of Civil Helicopter Accidents 10
Sandra G. Hart

Simulation Motion Requirements in Coordinated Maneuvers 11
Jeffrey A. Schroeder, William W. Y. Chung, Soren Laforce

Human Motion Perception: Error Metrics and Neural Models 12
Lee Stone

Eye Movement Metrics of Human Motion Perception and Search 13
Lee Stone, Brent Beutter, Jeffrey B. Mulligan

Image Processing for High-Precision Eye-Movement Tracking 15
Jeffrey B. Mulligan

Measuring Human Detection Templates 16
Albert J. Ahumada, Jr., Andrew B. Watson, Bettina L. Beard

High-Fidelity Virtual Environments 18
Stephen R. Ellis

Effect of System Latency in Dynamic Virtual Acoustic Environments 20
Elizabeth M. Wenzel

Hybrid Systems Research 22
George Meyer

Aeronautics and Space Transportation Technology Enterprise (continued)

Global Civil Aviation/Affordability

CTAS Joint Software Development 23
Michelle M. Eshow

Object-Oriented Design of a Dynamic Planner for Air-Traffic Control Real-time Sequencer, Scheduler, and Runway Allocator 24
Gregory L. Wong, Harry N. Swenson

Daily Use of the Traffic Management Advisor 26
Harry N. Swenson, Shawn Engelland, Ty Hoang

Surface Movement Advisor 27
Stan Harke

Surface Flow Visualization on a Hovering Tiltrotor Blade 28
Gloria K. Yamauchi, Alan J. Wadcock, James T. Heineck

Wake Visualization of a Full-Scale Tiltrotor in Hover 29
Benton H. Lau, Alan J. Wadcock, James T. Heineck

Skin-Friction Measurements on a Rotor in Hover 31
Alan J. Wadcock, Gloria K. Yamauchi

Characterization of Dynamic Stall on the UH-60A 32
William G. Bousman

Modeling UH-60A Control System Stiffness 33
Robert Kufeld

On-Blade Control of Rotor Blade Vibration 34
Mark V. Fulton, Robert A. Ormiston

Aeroelastic Stability Testing 36
Thomas Maier, David Sharpe, Robert A. Ormiston

Flight Mechanics of Helicopter Sling-Load Systems 36
Luigi Cicolani, Mark Tischler, Allen McCoy, George Tucker

Canard Rotor Wing Conversion Test 39
C. W. Acree, Jr., John F. Madden

Advanced Methods for Testing Rotor Performance 40
Francis X. Caradonna

Computational Fluid Dynamics in Rotor Design 42
Francis X. Caradonna

Control/Display Integration Issues for STOVL Aircraft 43
James A. Franklin

Aeronautics and Space Transportation Technology Enterprise (continued)

Global Civil Aviation/Affordability (continued)

Improved Experimental/Computational Aerodynamics Comparisons 44
Michael Olsen

Turbulence Modeling Validation Study 46
J. E. Bardina, P. G. Huang, T. J. Coakley

Boundary-Layer Receptivity 47
Anthony J. Dietz

Evolution of Strained Plane Wakes 49
Michael M. Rogers

A Model for the Limiting Piston Stroke in Vortex Ring Formation 50
K. Shariff

B-Spline Method for Turbulent Flow Simulation 51
A. Kravchenko, P. Moin, K. Shariff

Low-Speed Pressure-Sensitive Paint Research 52
Rabindra D. Mehta, Owen C. Brown

Area Measurement of Skin Friction in Complex Three-Dimensional Flows 54
James L. Brown

Global Interferometric Skin-Friction Measurements on a Wingtip Model 56
Gregory Zilliac

Global Civil Aviation/Environmental Compatibility

Flight Test of Civil Tiltrotor Noise-Abatement Approach 57
William A. Decker, Rickey C. Simmons

Methods for Predicting Blade-Vortex Interaction Noise 58
F. X. Caradonna, C. Kitaplioglu, M. McCluer

Closed-Loop Neural Control of Rotor Noise and Vibration 60
Sesi Kottapalli

Are Surface Shear-Stress Fluctuations a Valid Source of Sound? 61
K. Shariff, M. Wang

Aeronautics Design/Test Environment Phased Microphone Array Technology 62
Michael Watts

Sonification of Multivariate Data 64
Jim Stevenson

Aeronautics and Space Transportation Technology Enterprise (continued)

Revolutionary Technology Leaps/Innovative Technology and Tools

X-36 Tailless Fighter Agility Research Aircraft 65
Mark Sumich, Rodney O. Bailey

Aeronautics Design/Test Environment Condition-Based Maintenance for the 12-Foot Pressure Wind Tunnel 66
Ann Patterson-Hine

DARWIN 68
David Korsmeyer

New Technique for Visualizing Unsteady Flow 69
David Kao, Han-Wei Shen

New Release of Field Encapsulation Library 70
Patrick Moran, Chris Henze, Steve Bryson, David Kenwright

Portable Batch System Expands Its Customer Base 71
Robert Henderson

Adaptive Refinement and Structured Grids for Unsteady Aerodynamics 72
Robert Meakin

Multi-Level Parallelism: A New Computing Technique 73
James R. Taft

Carbon-Nanotube-Based Nanotechnology 74
Subhash Saini

Nanoelectronic Devices for the 21st Century 75
M. P. Anantram, Bryan A. Biegel, T. R. Govindan, Subhash Saini, Toshishige Yamada

Modeling Carbon Nanotube Electronic Devices 77
Richard L. Jaffe, Jie Han

Interaction Energy of Nitrogen Molecules 78
Harry Partridge, James R. Stallcop

Revolutionary Technology Leaps/Supersonic Technology

Clutter-Rejection for Obstacle Detection in Radar Data 79
Yair Barniv

Detection of Aircraft in Video Images 80
Jeffrey W. McCandless, Albert J. Ahumada, Mary K. Kaiser

Surface Operations Research and Evaluation Vehicle 81
Mary K. Kaiser

Direct Simulation of a Supersonic Turbulent Boundary Layer 83
S. Guarini, R. D. Moser, K. Shariff

Aeronautics and Space Transportation Technology Enterprise (continued)

Access to Space

Aerothermal Analysis of the X-33 Vehicle 84
Mike Green, Dinesh Prabhu, Grant Palmer, Mark P. Loomis, Ethiraj Venkatapathy, Dean Kontinos, William Henline, Susan Polsky, Periklis Papadopoulos, Carol B. Davies

Aerothermal Analysis of the X-34 Vehicle 86
Grant Palmer, Susan Polsky

Sharp Leading Edges for Hypervelocity Vehicles 87
Joan S. Salute, Paul Kolodziej, Jeffrey D. Bull

Arc-Jet Flow Characterization 88
Douglas G. Fletcher

Space Science Enterprise

Overview 91

Exobiology

Implementing a Strategy for Mars Exopaleontology 94
Jack D. Farmer, David J. Des Marais

Molecular Biomarkers in Living Stromatolites 95
Linda L. Jahnke, Jack D. Farmer, Harold P. Klein

Amino Acids in Meteorites 97
Narcinda R. Lerner

Genetic Network Modeling 98
Shoudan Liang, Zoltan Szallasi, Stefanie Fuhrman, Roland Somogyi

Dynamical Behavior of Networks and Cellular Automata 99
Jeffrey Scargle, Silvano Colombano, Shoudan Liang

Prebiotic Synthesis of Activated Amino Acids 100
Arthur L. Weber

Space Science Enterprise (continued)

Planetology

Mars Pathfinder Virtual Reality Model (MarsMap) 101
Ted Blackmon

Primary Accretion in the Protoplanetary Nebula 103
J. N. Cuzzi, R. C. Hogan, J. M. Paque, A. R. Dobrovolskis

Telltale Electric Currents During Impacts on Rocks 104
Friedemann Freund, Jerome G. Borucki, Marshall Lisé

Nitrogen Dissociation in Earth's Lower Thermosphere 106
Winifred M. Huo, Christopher E. Dateo

Transient Meteor Activity 107
Peter Jenniskens

Solar System Dynamics 108
Jack J. Lissauer

Virtual Reality on Mars Pathfinder 109
C. Stoker, T. Blackmon, M. Sims, E. Zbinden

Cratering Rates on the Galilean Satellites 111
Kevin Zahnle, Luke Dones

Astrophysics

The Structure of the Solar Nebula 113
K. Robbins Bell, P. Cassen

Molecules in Stellar Photospheres 114
Duane Carbon, David Goorvitch, Martin Cohen

NICMOS Images of Orion 115
Edwin F. Erickson, Michael Kaufman, Sean Colgan

Star Formation Studies 116
D. Hollenbach, K. Robbins Bell, P. Cassen

Galactic Bulge Observations 117
Thomas L. Roellig, Kin-Wing Chan

Photochemistry of Interstellar and Cometary Ice Analogs 117
Scott Sandford, Max Bernstein, Louis Allamandola, Robert Walker

Hot Water Decoded 119
David W. Schwenke

Discovery of Polycyclic Aromatic Hydrocarbon Ions in NGC 1333 120
Gregory Sloan, Louis Allamandola, Jesse Bregman, Doug Hudgins, Tom Hayward, Becky Devito

Space Science Enterprise (continued)

Space Technologies

Submicron Optical Aerosol Spectrometer 121
Mark L. Fonda, David M. Stratton

Gravity Probe B Project 122
J. Goebel

Modeling of Steady Secondary Flows in Pulse Tube Cryocoolers 123
Jeffrey M. Lee, Peter Kittel

Validating Requirements for Fault-Tolerant Systems Using Model Checking 125
Francis Schneider, Jack Callahan, Steve Easterbrook

Bonded Capillary Columns 126
Thomas Shen, Jr-Lung Chen

2-D Super Resolution Used on Mars Pathfinder 128
Bob Kanefsky, Peter Cheeseman, C. Stoker

Human Exploration and Development of Space Enterprise

Overview 131

Inducing Presyncope in Men: A Comparison of Two Stimuli 134
Patricia S. Cowings, William B. Toscano, Bruce Taylor

Ultrasonic Measurement of Intracranial Pressure Waveforms 135
Toshiaki Ueno, Richard E. Ballard, Lawrence M. Shuer, William T. Yost, John H. Cantrell, Alan R. Hargens

Evolutionary Adaptations of Intracranial Pressure to Gravity 137
Masayuki Matsuyama, Toshiaki Ueno, Christopher Yang, Shi-Tong T. Hsieh, Harvey B. Lillywhite, Alan R. Hargens

Calcium Metabolism in Bion 11 Monkeys 138
Sara B. Arnaud, Richard E. Grindeland, Meena Navidi

Human Immunology and Osmolality: An Hypothesis 140
John E. Greenleaf, Meghan A. McKenzie, Robin Looft-Wilson, Paul R. Barnes

Neurolab Technologies Enable Space Life Sciences Neuroscience Research 141
James P. Connolly, Paul D. Savage

Human Exploration and Development of Space Enterprise (continued)

Advanced Life Support Research and Technology Development Activities 142
Mark Kliss

U.S. Army Application for NASA Technology 144
Patricia S. Cowings, William B. Toscano, Charles DeRoshia

Virtual Environment Surgery and the Virtual Hospital 146
Muriel D. Ross, Jeffrey D. Smith

Earth Science Enterprise

Overview 149

Ecosystem Science and Technology

Remote-Sensing Data in Estimating Inputs to Ecosystem Models 151
Joseph Coughlan, Jennifer Dungan

Paleoenvironmental Studies 151
Hector L. D'Antoni

Global Land Surface Monitoring with Low-Resolution Satellite Imagery 154
Christine A. Hlavka, Jennifer Dungan

CRUSH Project 155
Lee F. Johnson, Brad Lobitz

Modeling Leaf and Canopy Reflectance 155
Lee F. Johnson, Christine A. Hlavka

Amazon Ecology from Space 156
Christopher Potter

Ultraviolet Radiation Effects on Carbon Isotope Fractionation 157
Lynn Rothschild, David DesMarais, Anne Tharpe

Perceptual Image-Compression Prototype 158
Andrew B. Watson

Earth Science Enterprise (continued)

Atmospheric Chemistry

Aircraft-Borne Meteorological Measurement Systems 160
T. Paul Bui, K. Roland Chan, Leonhard Pfister, Antonio A. Trias, Stuart W. Bowen, Jonathan Dean-Day, Cecilia Chang, Elizabeth Moore, David Bui

Studies of Stratospheric Bromine Compounds 161
Timothy J. Lee, Srinivasan Parthiban

Analysis of Stratosphere-Troposphere Exchange 162
Leonhard Pfister

Convectively Generated Gravity Waves 163
Leonhard Pfister

Measuring Tropospheric Nitrogen 164
James R. Podolske

Atmospheric Effects Of Aircraft Emissions: SONEX 164
Hanwant B. Singh, James Eilers

Airborne Tracking Sunphotometry 165
Philip B. Russell, John M. Livingston, Beat Schmid, Damon Ried

Environmental Research Aircraft and Sensor Technology 166
Steve Wegener

Atmospheric Physics

Multidimensional Simulations of Marine Stratocumulus Clouds 167
Andrew Ackerman

Quantitative Infrared Spectroscopy of Minor Constituents of Earth's Atmosphere 169
Charles Chackerian, Jr., Lawrence P. Giver

Spreading and Growth of Contrails in a Sheared Environment 169
Eric Jensen

The Roles of Aerosols in Stratospheric Ozone Chemistry 171
Anthony W. Strawa, Rudolf F. Pueschel, Guy V. Ferry

Developing and Validating an Aerosol Model for the Upper Troposphere 172
Azadeh Tabazadeh

Aeronautics and Space Transportation Technology Enterprise

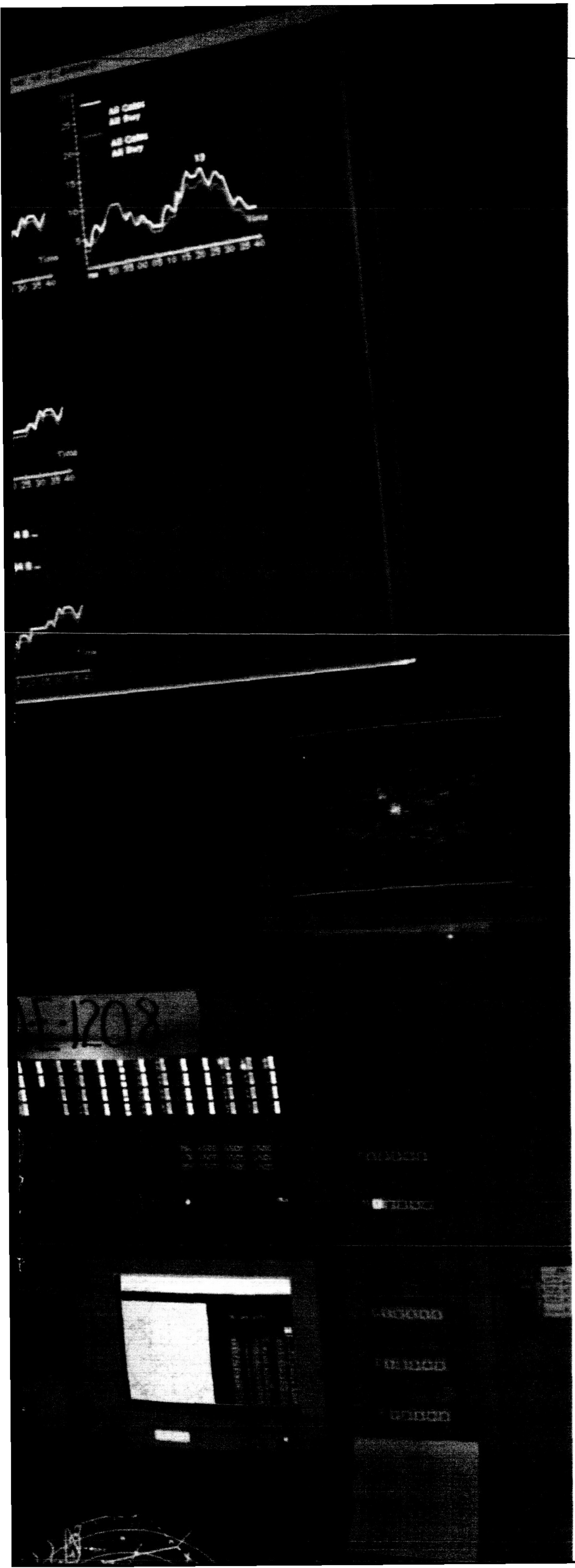

Overview

NASA's mission for the Aeronautics and Space Transportation Technology (ASTT) Enterprise is to pioneer the identification, verification, transfer, application, and commercialization of high-payoff aeronautics and space transportation technologies. Research and technology programs conducted for dramatic improvements in aviation and space transportation by the Enterprise contribute to national security, economic growth, and the competitiveness of U.S. aerospace companies.

The Agency manages principally through Enterprises. The ASTT Enterprise manages a clearly defined portfolio of technology investments through designated Center Missions and Lead Centers having the responsibility to manage the implementation and execution phases of the technology programs. To support the ASTT Enterprise, Ames Research Center is responsible for the Agency's mission in Aviation Operations Systems. Ames leads the Agency's programs for the Aviation System Capacity Program, the High-Performance Computing and Communications Program, and research and technology base programs in aviation operations systems, information technology, and rotorcraft. Ames leads the Enterprise in the core competency areas of human factors research, air-traffic management, information system technologies, rotorcraft, vertical/short takeoff and landing technology, and thermal protection systems technology. In addition, Ames is the Center of Excellence for Information Technology.

The ASTT Enterprise directly supports national policy in both aeronautics and space, documented in "Goals for a National Partnership in Aeronautics Research and Technology," "National Space Policy," and "National Space Transportation Policy." The national goals drive the Enterprise goals. These goals are grouped into three areas, or as they are called, three pillars: "Global Civil Aviation" for enabling U.S. leadership in global aviation through safer, more affordable, cleaner, and quieter air travel; "Revolutionary Technology Leaps" for revolutionizing air travel and the way in which aircraft are designed, built, and operated; and "Access to Space" for enabling the full commercial potential of space and expansion of research and exploration. The following sections present Ames' FY97 accomplishments toward achieving most of the goals listed under these pillars.

Global Civil Aviation

Increasing the safety and throughput of the nation's air transportation system while reducing the costs of aircraft operations and avoiding environmental impacts are major challenges. Ames has unsurpassed expertise in the key disciplines to address these challenges. They include innovative integrated design techniques, human centered designs of automated air traffic management tools, research and development of computational tools to optimize aircraft performance, rotorcraft systems like the Short Haul Civil Tiltrotor, and information technologies to manage and communicate knowledge. Ames maintains key national facilities. These efforts are all part of Ames' contributions to the safety, capacity, and affordability goals.

Airlines and businesses lose billions of dollars annually as a result of delays and lost productivity owing to weather and congestion in the airspace system. Under capacity and affordability goals, Ames' major effort in the research and development of automation for air traffic management has provided new decision support tools to the Federal Aviation Administration (FAA) that are currently being incorporated in many of the major air traffic facilities in the United States. Ames leads the Agency in working with the FAA to develop aviation system capacity technologies.

Research supporting the environmental compatibility goals includes significant aeroacoustic research and testing capabilities, the most recent advance in those capabilities being the upgrade of the Ames' National Full-Scale Aerodynamics Complex. An aeroacoustic modification, which is being completed this fiscal year, will permit the highest speed acoustic wind tunnel testing in the world of large models.

Revolutionary Technology Leaps

NASA's charter is to explore high-risk technology areas that can revolutionize air travel and create new markets for U.S. industry. The technology challenges for NASA include accelerating the application of technology advances, eliminating the barriers to affordable supersonic travel, and expanding general aviation. These technology advances may at times require the use of experimental aircraft.

The next-generation design tools will dramatically affect the way in which business is conducted. Its effect will be felt across the three pillars, contributing to every technology goal. Research is done at Ames in information technology to elevate the power of computing tools through fuzzy logic, neural networks, and artificial intelligence. These tools will integrate multidisciplinary product development activities to dramatically cut design cycle times. Examples of accomplishments include neural control of rotorcraft vibration, coupling of flow-field optimization tools, and advances in computational tools. Experimental aircraft are also invaluable tools for exploring the possibility of new technology. One example is the use of advanced aerodynamics and flight controls on the X-36 aircraft, which includes the completion of 31 successful flights.

Under the high-speed transport goal, Ames has diverse activities in wind tunnel testing and simulation, external visibility, sonic boom minimization, and wing aerodynamic optimization. Ames continues to support the program with the simulation and wind tunnel facilities, as well as the computational and code development capabilities.

Access to Space

In coming decades, NASA envisions the space frontier as a busy crossroads of U.S.-led international science, research, commerce, and exploration. Experience with this vast resource has already yielded new treasures of scientific knowledge, life-enhancing applications for use on Earth, and fantastic celestial discoveries.

Ames is charged with developing new thermal protection systems that will enable vehicles of the future to be built more economically and will enable existing ones to be upgraded at reduced cost. Ames maintains one of the world's premier arc-jet complexes for providing realistic simulations of entry environments. These simulations are essential for technology development, system validation, and system qualifications. Ames supports the U.S. aerospace community in developing Thermal Protection Systems that will be necessary for the nation's future space vehicles.

Aviation and space transportation have always been exciting and innovative areas. With continued strong partnership among industry, government, and academia, Ames' role in aerospace will continue to be strong and far reaching. As we continue to leverage information technology to the successful execution of our programs, Ames Research Center's contribution will become even more significant as we enter the 21st century.

The Concept of Airspace Complexity and Its Use in Air Traffic Management

Banavar Sridhar, Gano Chatterji, Kapil Sheth

The growth in air traffic and the new concepts in air traffic management (e.g., free flight) have increased the need to develop models and measures to describe traffic in the national airspace in order to predict air traffic controller workload and to make flow management decisions like resectorization. The complexity of the airspace depends on both *structural* measures and *flow* measures. The structural measures are fixed for a Sector/Center and depend on the spatial and physical features of the Sector. They are a function of attributes like terrain, number of airways, airway crossings, and navigation aids. The flow measures vary as a function of time and depend on such factors as the number of aircraft, mix of aircraft, weather, separation between aircraft, closing rates, aircraft speeds, and flow restrictions.

The Radio Technical Commission for Aeronautics task force report has emphasized the need to understand how airspace complexity affects controller workload. Controller workload has been measured in two ways: one based on the physiological state of the controller and another based on the physical interaction of the controller with the displays and other communication devices.

An effort was undertaken to develop and validate a measure of airspace complexity called dynamic density, which can be computed, in real time, from air traffic data inputs. The dynamic density function was developed based on interviews and survey techniques using qualified air traffic controllers. An activity catalog tool was developed to measure the controller activity. The dynamic density function has been linked with the Center/TRACON (Terminal Radar Approach Control) Automation System (CTAS) software. Preliminary results from tests of the density function at the Denver Air Route Traffic Control Center (ARTCC) airspace show a good correlation between dynamic density and controller activity.

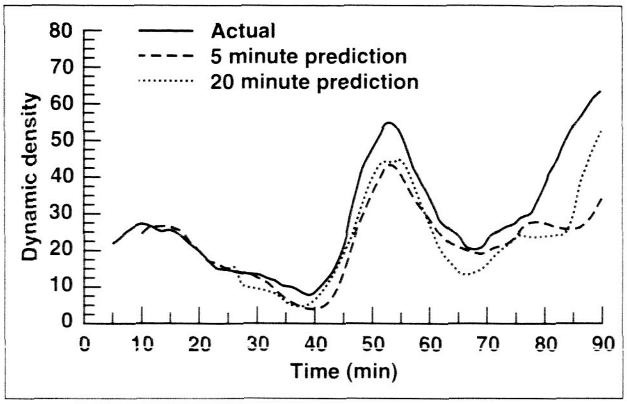

Fig. 1. Predictions of dynamic density at Denver Air Route Traffic Control Center.

Currently, Ames is evaluating application of the dynamic density measure, developed using data from the Denver Center, to traffic situations in other Centers; in addition, alternative measures for dynamic density are being developed.

In order for dynamic density to be useful as a planning tool, it is necessary to be able to predict its behavior. The figure shows the prediction of dynamic density 5 and 20 minutes in the future for Sector 16 at Denver Center. The prediction faithfully depicts the "ups" and "downs" of the actual dynamic density. The predictions deviate from actual values when the number of aircraft and their "intent" information are not known to CTAS software. This limitation can be overcome in the future when intercenter data become available to the system.

Point of Contact: B. Sridhar
(650) 604-5450
bsridhar@mail.arc.nasa.gov

Conflict Prediction and Resolution Technology Field Test

Dave McNally, Ralph Bach, William Chan

The Center/TRACON (Terminal Radar Approach Control) Automation System (CTAS) conflict-prediction capability, developed for the Descent Advisor function, was recently expanded and improved. The new CTAS conflict-prediction function processes all flight phases (climb, cruise, descent). A trial planning function was added to help the user confirm that a conflict-resolution trajectory is conflict-free before issuing a clearance to an aircraft. It was desirable to field test the conflict-prediction function stand-alone before re-integration with the Descent Advisor and other planned technologies for user-preferred trajectories. For field test purposes, the conflict-prediction and conflict-resolution functions were incorporated into a stand-alone tool that displays conflict information and helps the controller quickly build and check a trial plan route using turn vector, direct route, altitude, or speed changes.

The tool was field tested at the Denver Air Route Traffic Control Center September 8–25, 1997. During Phase I (first week) the objective was to obtain a quantitative comparison of conflict prediction and resolution with and without the aid of the tool. One hundred tool-aided conflict resolutions were developed by test controllers and stored for analysis, but they were not communicated to sector controllers on duty. Actual conflict resolutions for the corresponding conflict pairs were also observed and recorded. Part (a) of the first figure shows the distribution of tool-aided resolution types used by test controllers. The second part of the figure shows the actual resolutions issued by the sector controllers for the corresponding set of conflicts. As shown, test controllers were able to resolve 44% of the conflicts by sending one aircraft directly to a future point along its planned route, whereas sector controllers used a direct route in only 12% of the conflicts. A direct route shortens the aircraft path and requires one less clearance (radio communication) by the controller. The 12% no-resolution cases (part (a)) are cases in which trial plans were accepted that predicted less than legal separation between the aircraft. This anomaly is believed to be a result of improper use of the tool caused by limited training. The no-action cases (part (b)) are cases in which the aircraft were not vectored by the sector controller because there was adequate separation.

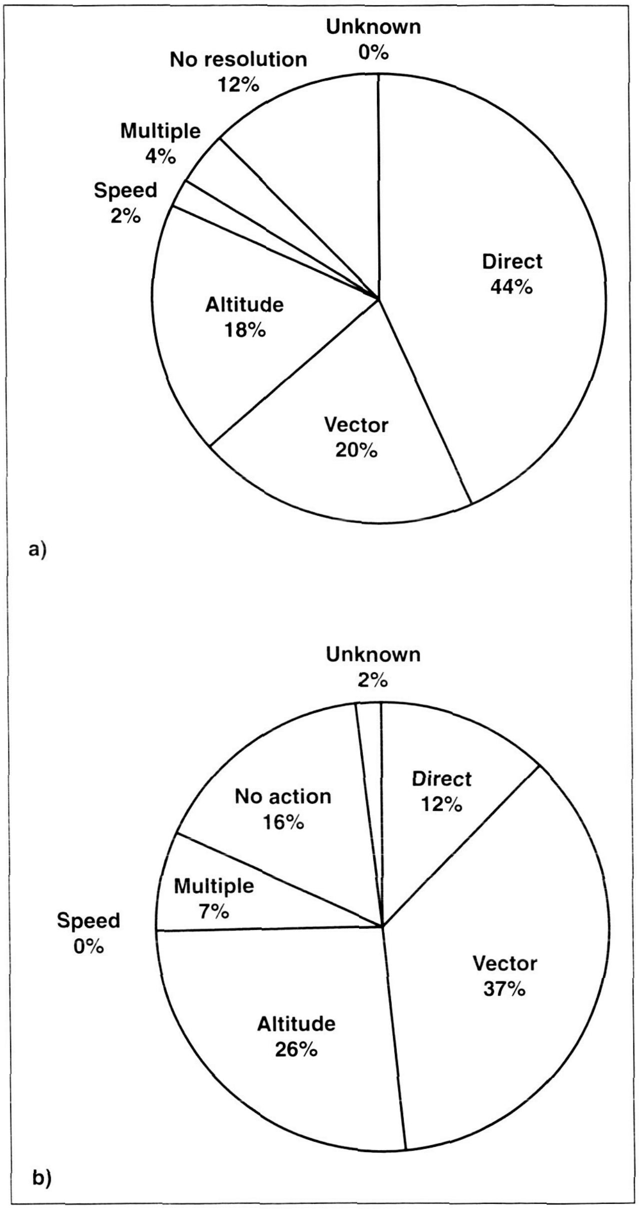

Fig. 1. Resolution types used (a) by test controllers and (b) by sector controllers.

During Phase II (second and third weeks) the tool was set up next to the sector controller positions at

Sectors 16, 17, and 28. The second figure shows the tool at Sectors 16 and 17. Conflict-resolution trajectories were developed by test controllers using the tool, and the trajectories were then suggested to the sector controllers for clearance to the aircraft. During 88 sector-hours of testing, 175 tool-aided resolutions were suggested to sector controllers and about 72% of these resulted in clearances to aircraft. Compared with the Phase I results, there was a 26% increase in the number of direct route resolution clearances actually issued to aircraft. The tool's ability to confirm that a trial plan resolves a conflict and does not create other conflicts was consistently rated as "highly beneficial" by the controllers.

Point of Contact: D. McNally
(650) 604-5440
dmcnally@mail.arc.nasa.gov

Fig. 2. Conflict prediction and resolution tool setup at Sectors 16 and 17, Denver Center, September 1997.

Conflict Probe Performance Evaluation

Karl D. Bilimoria

A conflict probe is a software tool that assists air traffic controllers in maintaining safe separation between aircraft by predicting conflicts up to 20 minutes in advance, using information on aircraft state (track data), intent (flight plans), and atmospheric conditions (wind and temperature). Such a tool would be especially useful in a "free-flight" environment, which is expected to have a less structured traffic flow than is afforded by the current operating environment. The objective of this research is to develop a comprehensive method for quantitatively evaluating the performance of any conflict probe, and then to apply the method to the Center/TRACON (Terminal Radar Approach Control) Automation System (CTAS) Conflict Probe Tool developed at Ames Research Center.

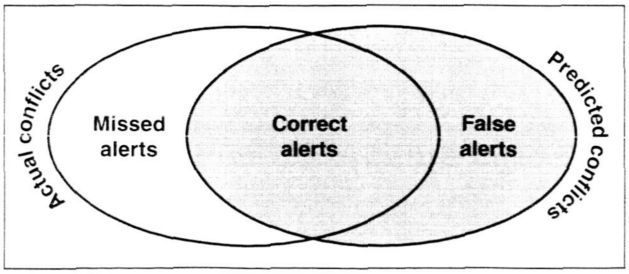

Fig. 1. Schematic of conflict probe primary metrics.

Several metrics of conflict probe performance have been developed and evaluated. The missed-alert rate and false-alert rate are primary metrics that quantify the reliability of a conflict probe. As shown in the first figure, missed alerts are actual conflicts that were not predicted, false alerts are conflicts that were predicted but did not actually occur, and correct alerts are conflicts that were predicted and actually occurred. The mean conflict warning time and root-mean-square errors in key conflict prediction parameters such as minimum horizontal and vertical separations are important secondary metrics that quantify the accuracy of a conflict probe. The CTAS Conflict Probe Tool was exercised with almost 4000 tracks of actual traffic data from the Denver Air Route Traffic Control Center, using expanded conflict windows (see the second figure). Techniques have been developed to identify those conflicts associated with imprecise intent information (e.g., controller clearances not entered as flight plan

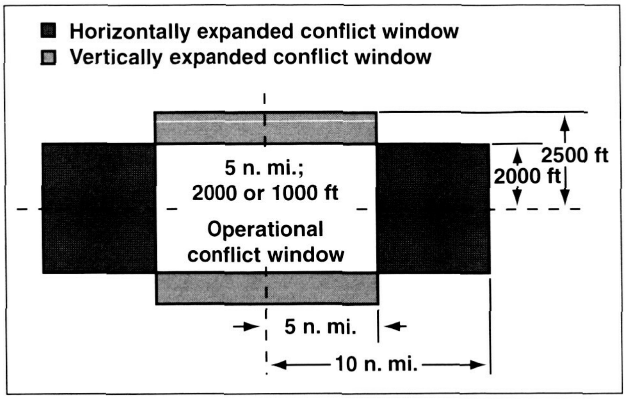

Fig. 2. Examples of expanded conflict windows.

amendments), and to appropriately adjust missed- and false-alert rates for those cases.

Preliminary results indicate that overall conflict probe performance is dependent on conflict geometry distributions and on the parameters of the expanded conflict windows. It is expected that the final results will provide guidelines for the performance that can be expected from a conflict probe based on current technology for aircraft tracking and weather prediction.

Point of Contact: K. Bilimoria
(650) 604-1638
kbilimoria@mail.arc.nasa.gov

Collaborative Arrival Planning

Rick Zelenka

The continued expansion of air-traffic and air-carrier economic pressures is necessitating changes in the relationship between the air traffic control service provider and the system user. Such pressures have resulted in efforts to increase the flexibility of air traffic management operations and allow collaboration between the service provider and system user. The government/industry "free-flight" initiative, whose ultimate vision is to allow users to select their own flightpath and speed in real time with air traffic control (ATC) imposing restrictions only when necessary, is the most visible of such efforts. Shared decision making and collaboration between system users and service providers have been identified as providing benefits necessary to support subsequent phases of free flight.

In the terminal arrival phase of flight, many restrictions and a high degree of control are placed on system users without regard for individual user operational preferences. Air traffic procedures do not allow the system users to prioritize their arrival sequence. For example, in hub operations, airlines may have preferences based on ensuring connections to overseas flights or gate availability that significantly affect their economics of operation.

The Collaborative Arrival Planning (CAP) service-provider/system-user decision-support tools should increase air traffic management flexibility and increase the economic efficiencies for system users. CAP is an extension of the Center/TRACON (Terminal Radar Approach Control) Automation System (CTAS), a suite of decision-support tools that provide computer-generated advisories for both en route and terminal-area controllers to manage and control arrival traffic more efficiently. CTAS has been selected by the Federal Aviation Administration (FAA) for national deployment. CTAS CAP will allow the user to request and influence intra-airline arrival characteristics without negatively affecting ATC operations. A tactical CAP tool will assist and improve the handling of individual aircraft arrival preferences. The strategic CAP tool will alter the CTAS arrival sequence within an individual airline's planned arrivals based on relative priority without affecting the priorities of other carriers.

Specific CAP accomplishments during FY97 include the following:

1. The design and development of a specialized airline CTAS "repeater" system. This system shares the CTAS arrival scheduling and airspace management information with the airspace user. Such real-time sharing of scheduling information is a significant first step in airspace user and service-provider collaboration and more efficient airline operations.

2. The design and development of a simulated airline "hub management" workstation to support the

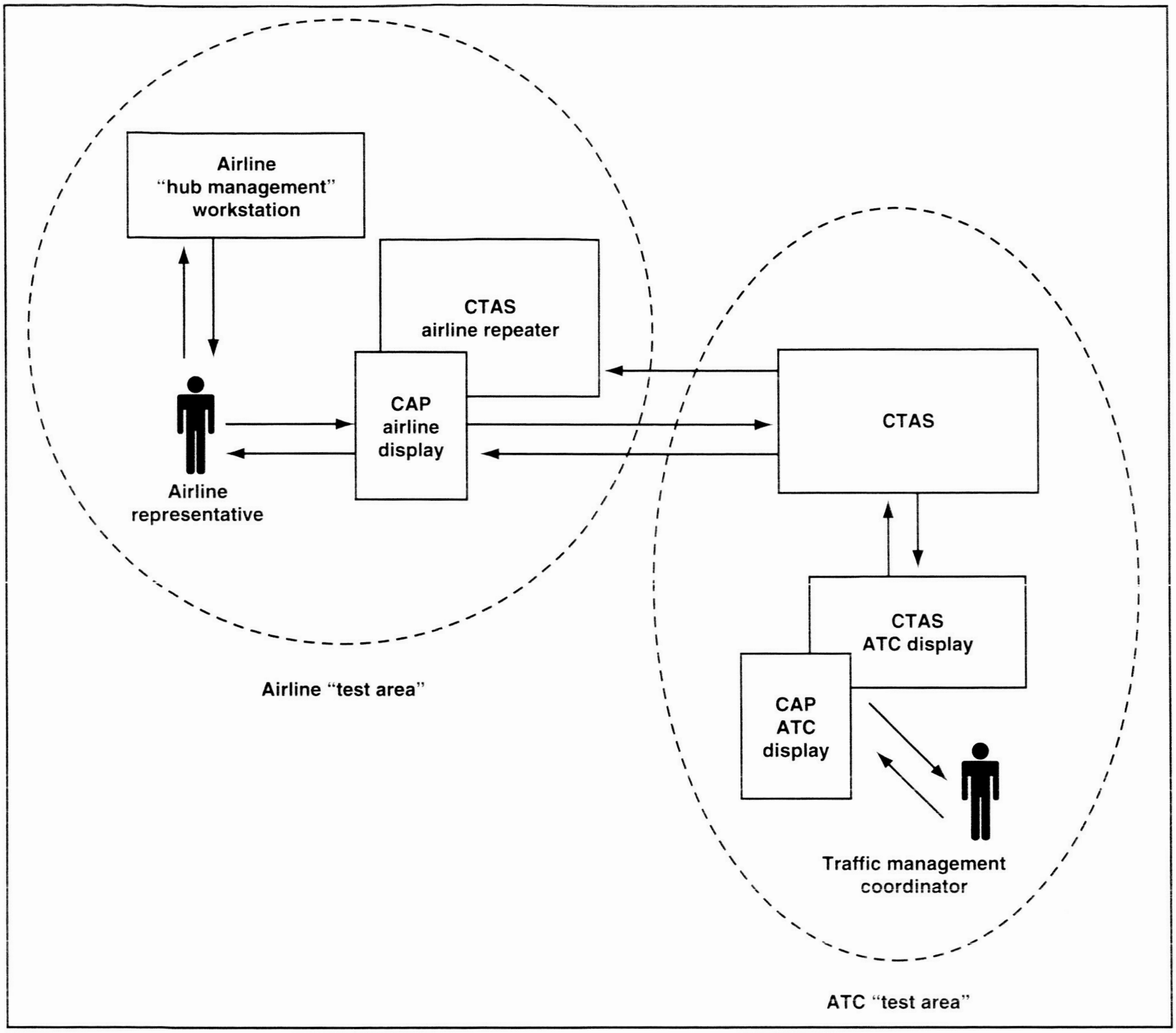
Airline
"hub management"
workstation
CTAS
airline repeater
CAP
airline
display
Airline
representative
CTAS
CTAS
ATC display
CAP
ATC
display
Traffic management
coordinator
Airline "test area"
ATC "test area"

Fig. 1. Collaborative Arrival Planning (CAP) decision-support tool laboratory development environment.

laboratory development of CAP decision-support tools (see figure). The workstation presents a "gant chart" display of arriving and departing aircraft sorted by airport gate, as typically used by "hub-and-spoke" air carriers in their hub airport ramp towers.

3. A unique three-party memorandum of agreement (MOA) between NASA, the FAA, and airline participants. The MOA will allow the installation of the CTAS repeater system at airlines operating in the Dallas/Fort Worth area, the location of NASA CTAS field testing.

Point of Contact: R. Zelenka
(650) 604-5433
rzelenka@mail.arc.nasa.gov

T-NASA Taxi Test at Atlanta Airport

David C. Foyle, Anthony Andre, Becky Hooey, Robert McCann

The Terminal Area Productivity Program/Low-Visibility Landing and Surface Operations element is developing cockpit technologies to enable safe and efficient surface operations in Category IIIB (300–700-feet runway visual range) visibility conditions. Ames Research Center is developing an integrated display system, the T-NASA (Taxiway Navigation and Situation Awareness) system, consisting of conformal symbology on a head-up display (HUD; see first figure), an electronic moving map (EMM; second figure), and three-dimensional (3-D) audio alerts for impending traffic incursions. The T-NASA Taxi HUD uses scene-linked symbology projected on glass overlaying the forward scene to present taxi route information, situational awareness information, and ground speed. The EMM depicts the cleared taxi route on the airport surface, as well as real-time information about own-ship position, other airport traffic, and hold-short locations. The 3-D Audio Ground Collision Avoidance System (GCAS) presents spatially localized auditory traffic and navigation warnings.

A joint flight test was conducted at Atlanta's Hartsfield International Airport to evaluate Ames Research Center's HUD and EMM components of the T-NASA system. Langley Research Center conducted the integration of T-NASA into NASA's 757 aircraft, and the Federal Aviation Administration developed the airport surveillance and data-link technologies.

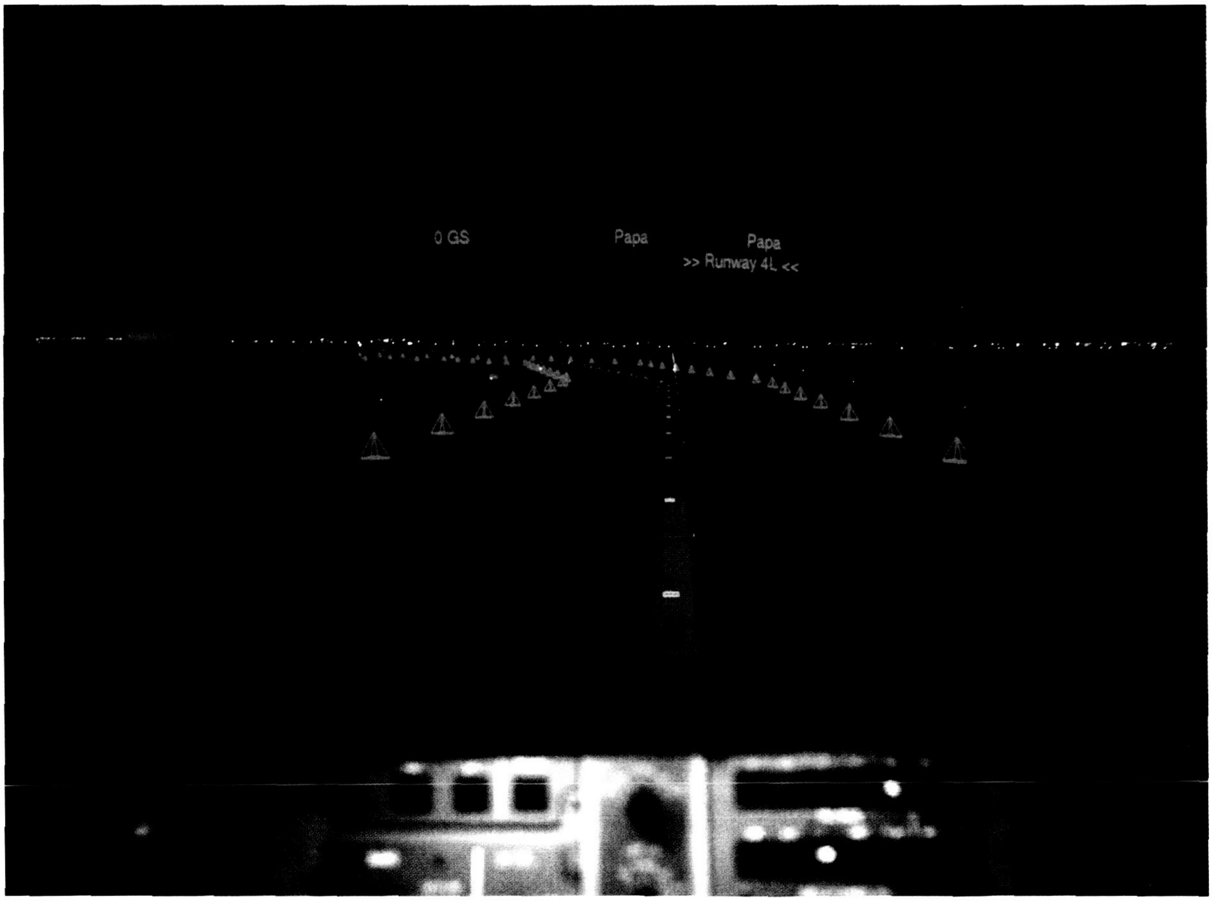

Fig. 1. Scene-linked T-NASA Taxi HUD symbology (green) showing high-speed exit off of runway and cleared taxi route overlaid on night airport scene. Text symbology shows ground speed and current position.

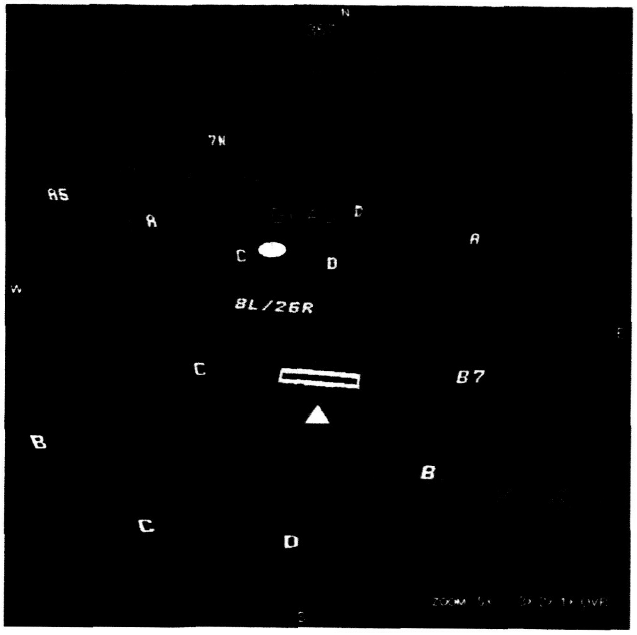

Fig. 2. Electronic moving map display of Atlanta's Hartsfield International Airport from field test. Features shown are the current location of the test aircraft (white triangle); the cleared taxi route (magenta line); the position of another taxiing airplane with flight tag information (white circle); and hold bar indicating air traffic control hold short of the active runway (yellow and red bar).

Fifty-three flights were conducted by two NASA test pilots and four commercial pilots from different airlines. Taxi operations were conducted under night visual flight rules (VFR) conditions to emulate low-visibility conditions. Pilots completed taxi trials with three different T-NASA configurations: (1) Baseline—Jeppesen paper chart only; (2) EMM only; and (3) EMM plus HUD. Aircraft state data, such as velocity and heading, were electronically recorded. Formal questionnaire assessments were made by the pilots after each trial, and a questionnaire and debriefing interview was administered after each day of testing.

Pilot reports indicated that T-NASA reduced overall taxi times by allowing for increased taxi speeds; by requiring less route planning time, less time at confusing intersections, and fewer stops while taxiing; by improving situation awareness; and by providing greater confidence in the aircraft's position on the airport surface. These subjective reports were supported by objective velocity data collected during the flight test. Further, during one of seven baseline taxi trials in which the T-NASA system was turned off, the pilot turned onto the wrong taxiway—this never happened when the T-NASA system was activated. This was a good example of lowered situational awareness and time wasted at confusing intersections without the T-NASA system.

All four commercial pilots agreed that T-NASA technology would improve taxi safety, primarily by reducing the likelihood of incursions. As another indication of safety, pilots stated that the Jeppesen chart "distracted" them from taxiing and that neither the EMM nor the EMM-plus-HUD configurations were distracting. T-NASA system allowed the pilots to spend more time looking out the window and less time head-down consulting the Jeppesen chart. Also, all pilots unanimously agreed that both the EMM and the EMM-plus-HUD configurations increased situational awareness and reduced mental navigational workload during taxi operations. Furthermore, pilots noted that T-NASA system improved communications with ground control and between crew members, because there was less need for communication and communications were clearer. One pilot's company trip report succinctly summarizes the flight tests: "This research by NASA represents a quantum step in air operations safety and technology, on the same level as the development of the Ground Proximity Warning System and the Traffic Collision Avoidance System," and "this system is very usable and demonstrated its design goal of improving the speed and accuracy of ground operations, reducing task loading, and enhancing overall situation awareness and safety in a complex, high-density traffic environment."

Point of Contact: D. Foyle
(650) 604-3053
dfoyle@mail.arc.nasa.gov

Analysis of Civil Helicopter Accidents

Sandra G. Hart

NASA formed the Aviation Safety Program in mid-1997 to respond to the ambitious safety challenge posed by President Clinton. To guide the development of a safety investment strategy for the helicopter element of this program, a team of experts, drawn from helicopter manufacturers, operators, and governmental agencies, was formed and tasked with analyzing representative fatal helicopter accidents to identify prevention opportunities. The 34 accidents analyzed included a range of vehicle makes and models, missions, flight phases, types of operation, and accident characteristics. Using information contained in the official National Transportation Safety Board accident dockets, the team developed a sense of what happened (the chain of Events), identified issues or problems that might have existed with the aircraft, maintainers, environment, pilot actions, and air traffic control, and the quality of the information in the report itself (the Problems), and hypothesized what might have prevented an accident entirely or at least mitigated its severity (Solutions).

On average, 16 Events were identified per accident, ranging from 5 to 33 Events across accidents. To illustrate repeating patterns observed in the accidents reviewed, 14 representative (but hypothetical) scenarios were described. These will be made available to operators for training and safety meetings. Eventually, the written narratives will be accompanied by graphic recreations to illustrate the important points even more clearly.

The number of Problems identified in the 34 accidents ranged from 3 to 21, averaging 16 per accident. Because similar Problems occurred in several accidents, a coding system was developed to group entries into 14 categories and 58 subcategories. Examples of categories include preflight planning, safety culture, maintenance, training, pilots' judgments and actions, communications, situation awareness, and the failure of helicopter parts or systems. Postcrash survivability problems included vehicle crashworthiness, restraint systems, postcrash fires, sinking, or capsizing, and delayed rescue.

There were an average of 13 Solutions suggested per accident, ranging from 4 to 25 across accidents. Some of the solutions were available or emerging technologies, whereas others addressed nontechnological solutions, such as changes in procedures, training, or attitudes, or broader issues, such as the need for more complete accident investigation information. Since similar interventions were suggested for different problems and accidents, a coding scheme was developed to group Solutions into 8 categories and 54 subcategories. Improving the information available in the cockpit to enhance pilot situational awareness was suggested as a solution in many accidents. Examples included enhanced/synthetic vision systems, moving maps with weather and terrain overlays, possibly coupled with sensor data, decision aids, and hazard detection and warning. To be effective in reducing the overall fatality rate, however, such technology solutions must be cost-effective, certifiable, and capable of being retrofitted to the existing fleet. Improved preflight planning might have prevented other accidents. In several accidents, the responses of pilots to emergencies were delayed because they were not aware that a problem was developing, did not recognize the nature of the problem, or did not know the correct way to resolve it.

Real-time performance monitors, health and usage monitoring systems (HUMS) and associated technologies offered potential solutions. In more than half of the 34 accidents, those related to equipment failures and malfunctions might have been avoided had HUMS been available for either on-condition maintenance or improved cockpit warnings. The potential benefits of real-time performance monitors and pilot aids, such as envelope-limiting, were discussed as well. Maintenance was another area that received considerable attention; in one-third of the accidents the team felt that improved maintenance procedures or better supervision of maintainers might have prevented subsequent part or system failures that contributed to a fatal accident. The indirect benefits of an improved "safety culture" were proposed as a means of breaking a fundamental link in the chain of events that led to several of the accidents analyzed. Improved initial, recurrent, and transition training was identified as a potential solution in many of the accidents reviewed. Finally, ways of improving postcrash survivability and accident and incident databases were proposed.

Using databases that captured the output of the accident analysis sessions, team members developed summary definitions of the types of Problems and Solutions found and nominated safety investments that should produce the greatest safety benefits. These represent the most promising Solutions grouped into research areas. The results of this helicopter accident analysis effort have been presented to industry and are available in a report.

Point of Contact: S. Hart
(650) 604-6072
shart@mail.arc.nasa.gov

Simulation Motion Requirements in Coordinated Maneuvers

Jeffrey A. Schroeder, William W. Y. Chung, Soren Laforce

If a pilot does not feel a lateral acceleration during a roll maneuver, the maneuver is said to be coordinated. During these maneuvers, the ball on the cockpit turn-and-slip indicator is centered. To accurately represent these coordinated maneuvers in a flight simulator, the motion platform must translate laterally when it rolls. However, most simulators do not have enough lateral displacement available to maintain coordination. As a result, the pilot feels an inappropriate, or false, lateral acceleration in the simulator. This study examined the effect of this false simulator cue. In addition, the effort suggested a criterion for simulator manufacturers and users that can be used to select the required size of future simulators. In the study, pilots flew a helicopter model in the world's largest displacement flight simulator, which is located at Ames Research Center. The large displacement of this unique simulator allowed coordinated maneuvers to be flown as a baseline. Subsequent reductions in the commanded roll and lateral simulator displacements allowed the examination of the false cueing effects. Measures of pilot-vehicle performance and pilot workload quantified the effect of these reductions in displacement.

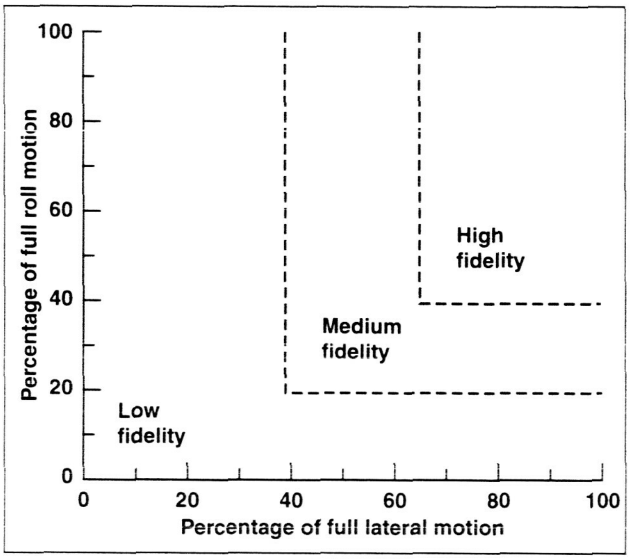

Fig. 1. Three fidelity regions superimposed on the percentage of full-roll motion versus the percentage of full-lateral motion.

The figure shows three fidelity regions superimposed on the percentage of full-roll motion versus the percentage of full-lateral motion. High fidelity means that the simulator motions felt like those of real flight. Medium fidelity means that the simulator motions were noticeably different from flight, but not objectionably so. Low fidelity means that the simulator motions were both noticeably different from those of flight and objectionable. Since medium fidelity is desired as a minimum, the criterion indicates that simulators should provide at least 20% of the full-roll motion and 40% of the full-lateral motion.

Point of Contact: J. Schroeder
(650) 604-4037
jschroeder@mail.arc.nasa.gov

Human Motion Perception: Error Metrics and Neural Models

Lee Stone

Pilots and astronauts have to make accurate judgments of their self-motion (or of that of the craft they are controlling) to navigate safely and effectively. In many critical aerospace tasks, such as flying a helicopter at low altitude under low-contrast conditions or landing the shuttle after several weeks of adaptation to microgravity, human performance in self-motion estimation is pushed to its limits, yet any perceptual error could have disastrous consequences. The goal of this research project is to identify visual conditions under which humans are likely to make perceptual errors in visual motion judgments and to understand at the neural level why these errors occur, as part of a strategy to develop methods of preventing or mitigating them. The specific aims are (1) to develop predictive biologically based models of human performance in heading estimation and related motion perception tasks, and (2) to identify empirically those conditions that lead to human error, as part of an effort to test, refine, and validate some models, while ruling out others. The availability of validated quantitative models of human self-motion perception will aid in the design of training regimes for pilots, in the development of displays and automation systems that interact more effectively with human pilots while they fly aircraft or spacecraft, and in the evolution of artificial vision systems based on the massively parallel architecture of the human brain.

In collaboration with Dr. Thompson at the University of York in the United Kingdom, human errors associated with low-contrast motion stimuli (such as motion seen through fog) have been identified. In FY97, by showing that flicker and speed

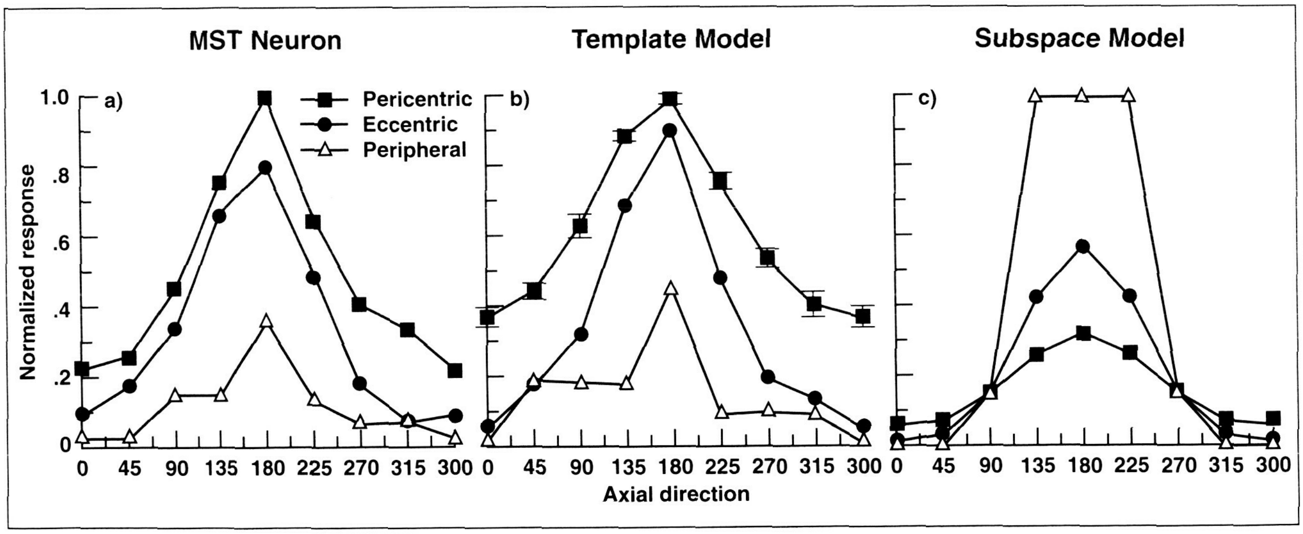

Fig. 1. (a) The responses of a real neuron in MST area as a function of heading direction along a series of axial directions at three eccentricities (from Duffy and Wurtz, 1995); (b) the responses of a template model "neuron" to the same set of visual stimuli (from Perrone and Stone, 1994); and (c) the response of a subspace model "neuron" to the same set of visual stimuli (from Lappe and Rauscheker, 1993).

perception errors have the opposite contrast dependence, the class of models of human speed perception that rely on flicker to derive motion can be ruled out almost entirely. In collaboration with Dr. Perrone at the University of Waikato in New Zealand, a neural "template" model of human visual self-motion estimation was developed in 1994. In FY97, it was demonstrated that the neural elements within the Ames-developed template model can quantitatively mimic the response properties of neurons in the Medial Superior Temporal area, a visual processing area within the primate brain thought to underlie self-motion perception, whereas the neural units of subspace models cannot (see figure). The template model also correctly predicts that during self-motion along a curved path, human perception will show a small bias in the direction of the turn, but will not show errors associated with discontinuities in the environmental layout (as is predicted by decomposition models).

Point of Contact: L. Stone
(650) 604-3240
lstone@mail.arc.nasa.gov

Eye Movement Metrics of Human Motion Perception and Search

Lee Stone, Brent Beutter, Jeffrey B. Mulligan

Visual display systems provide critical information to pilots, astronauts, and air traffic controllers. The goal of this research project is to develop precise and reliable quantitative metrics of human performance based on nonintrusive eye-movement monitoring that can be used in applied settings. The specific aims are (1) to refine the hardware, optics, and software of eye-trackers to allow the nonintrusive acquisition of high-temporal and high-spatial precision eye-position data; (2) to measure quantitatively the links between eye-movement data and perceptual-performance data during tracking and search tasks; and (3) to develop biologically based computational models of human perceptual and eye-movement performance. Validated quantitative models of human visual perception and eye-movement performance will assist in designing computer and other display systems optimized for specific human tasks, in the development of eye-movement-controlled machine interfaces, and in the evolution of artificial vision systems.

In FY97, considerable progress was made in the technical effort to improve the spatial and temporal resolution of infrared video-based systems. In collaboration with ISCAN Inc., a high-speed infrared video-based prototype eye-tracker was benchmarked to have a precision of 0.12 degree at a 240-hertz sampling rate, although with a limited range of approximately ±5 degrees. In collaboration with Dr. Krauzlis at the National Eye Institute, benchmark data from the state-of-the-art invasive eye-tracker (an eye-coil system) were gathered for comparison.

By measuring direction judgments and eye movements simultaneously, the use of signal-detection theory to predict the errors in direction judgments from eye movements was validated. Preliminary evidence suggests that the spatiotemporal integration rule used to drive pursuit eye movements is not simple vector averaging and, at least for luminance-defined (black-and-white) targets, appears to be similar to that used for perception. However, perception and eye movements may not share the same motion processing for color and contrast-defined targets. In collaboration with Dr. Eckstein of the Cedars-Sinai Medical Center, signal-detection theory was also applied to a search (target-location) task. The perceptual judgments and eye movements follow similar trends. As the figure shows, in an easy condition both the first eye movement and the final perceptual decision were correct, whereas in the hard condition both were incorrect. A computational model based on signal-detection theory was used to quantify these trends and to compare the amount of information about target location available for controlling eye movements and for the final perceptual decision. The situations under which the eye-movement data provide reliable information about the human observer's perceptual state are being identified by systematically measuring and comparing perceptual and eye-movement responses under a number of display and task conditions.

Point of Contact: L. Stone
(650) 604-3240
lstone@mail.arc.nasa.gov

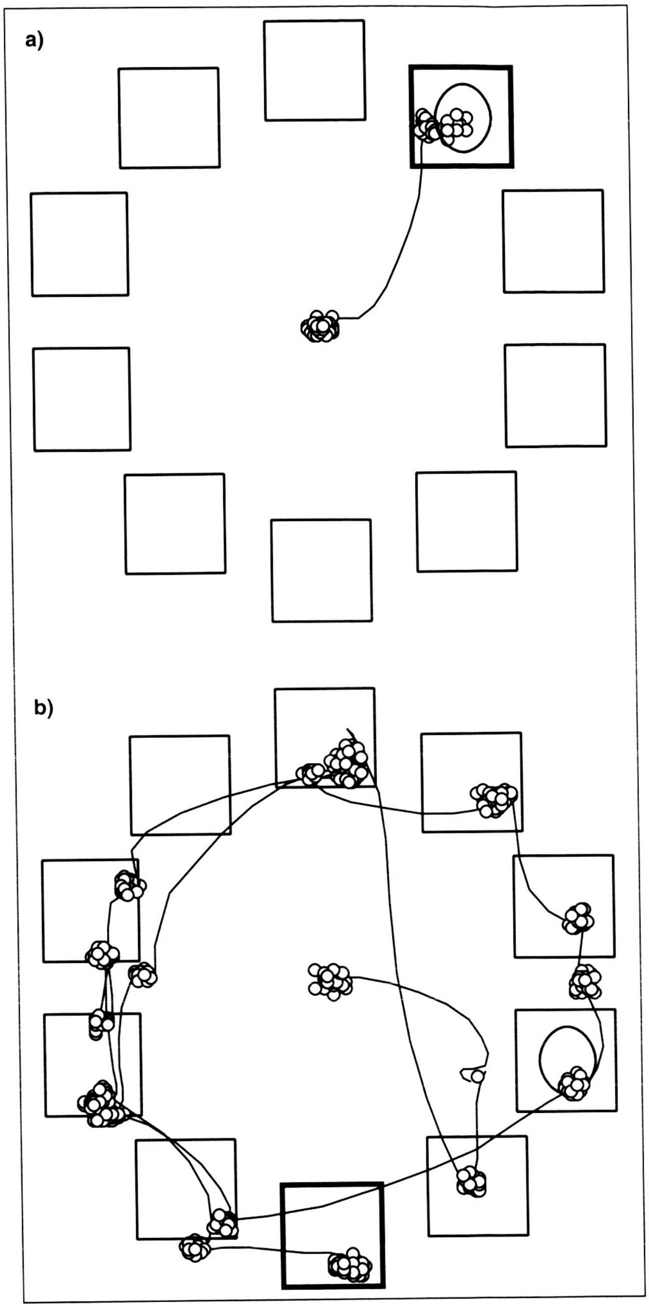

Fig. 1. Search Task. The observer was given 4 seconds to find a disk target embedded in noise in one of 10 locations (squares). The bold square indicates the location of the target; the big open circle, the final decision; and the small solid circles, eye position during fixations. (a) In this high signal-to-noise trial, both the first eye movement and the decision quickly indicated the correct location; (b) in this low signal-to-noise trial, the eye examined many locations and the final decision was wrong.

Image Processing for High-Precision Eye-Movement Tracking

Jeffrey B. Mulligan

Eye movements can provide a wealth of information about how human operators perceive and process visual information. Video-based measurement systems offer considerable advantages over competing approaches for use in applied contexts outside the laboratory: first, they do not require physical contact with the eye, and second, they do not restrict the subject's movement. This research investigates image processing methods in an effort to obtain greater accuracy from video images of the eye.

Currently available commercial systems use special hardware to compute eye position in real time from images of the eye's anterior structures (first figure). To attain real-time performance, these systems must use relatively simple processing algorithms. This project is concerned with maximizing the final accuracy by the application of more sophisticated image processing, even when the calculations cannot be performed in real time on present-day microcomputers.

The first challenge was to develop efficient and convenient methods for continuous digital recording of video data. Two approaches to this problem have shown promise. In one, the application of hardware image compression reduces the data rate to one easily handled by a single computer disk. Results obtained using simulated data indicate that moderate levels of compression have negligible effects on the final accuracy. In the other, an array of parallel disk drives achieves a data rate capable of storing video with no compression.

Digital storage of the video images and off-line processing allow sophisticated processing algorithms to be applied. A particularly difficult problem has been reliable tracking of the fourth Purkinje image, formed by reflection of the illuminator from the posterior surface of the crystalline lens of the eye (the small bright spot in the first figure). The position of the fourth Purkinje image is especially useful, because the distance between this feature and the bright corneal reflex, or first Purkinje image (the large bright spot in the figure), is directly related to the direction of gaze, unlike the positions of the individual features that confound translations of the head with shifts of gaze directions. Difficulties in tracking the fourth Purkinje image arise from its small size and low contrast. This project has now succeeded in tracking the fourth Purkinje image by using a Gaussian curvature computation on an image from which the corneal reflex and pupil margin have been masked off.

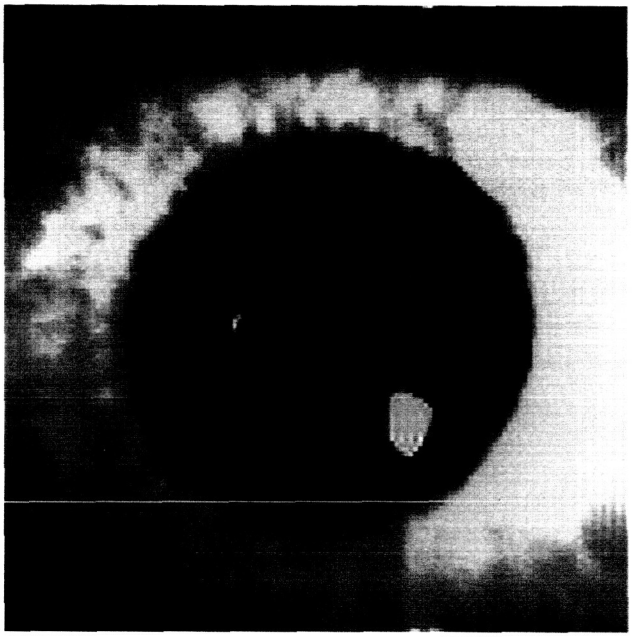

Fig. 1. Subsampled video image of the anterior structures of the eye. The central dark disk is the pupil, formed by the edge of the iris. The two bright spots within the pupil are the first (large) and fourth (small) Purkinje images, whose relative positions give a precise indication of gaze direction.

Although images of the pupil are easy to obtain simply by pointing a camera at the eye, greater accuracy still can be achieved by ophthalmoscopic imaging of the retina (second figure). This requires a special optical setup, and currently requires that the subject's head be stationary; however, it permits much greater optical magnification, with consequent increases in resolution and accuracy for small eye movements. This project has developed a computer program that constructs a large retinal mosaic for each subject. Using techniques similar to those used

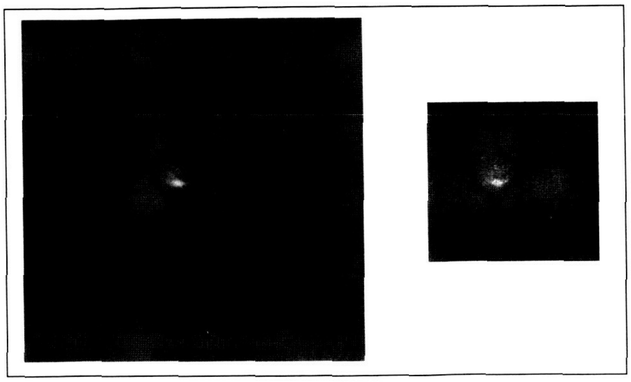

Fig. 2. Retinal images obtained with a table-top video ophthalmoscope. The left-hand panel shows a subsampled version of a single video field, in which a faint image of the optic disk and retinal blood vessels may be seen on a large background of camera noise. The right-hand panel shows a composite image constructed by registering and averaging approximately 1000 images like the one shown in the left panel.

in the analysis of satellite imagery, the program registers and averages a large number of images, each of which covers just a small part of the subject's retina. Once this mosaic or template has been constructed, subsequent records are analyzed by registering the individual frames to the template. In addition to images obtained in the laboratory, the software has been applied to images obtained with a scanning laser ophthalmoscope, a clinical instrument used in the diagnosis of various ocular disorders.

For both classes of imagery described, the software developed in this project provide a level of accuracy commensurate with the inherent physiological noise (about 1 arc minute), significantly better than commercially available video-based systems and comparable to the best invasive methods.

Point of Contact: J. Mulligan
(650) 604-3745
jmulligan@mail.arc.nasa.gov

Measuring Human Detection Templates

Albert J. Ahumada, Jr., Andrew B. Watson, Bettina L. Beard

As part of NASA's goal to improve aircraft safety and performance, Ames is developing models that can be used to predict a human observer's ability to detect visual targets. Often these models perform well because they mimic visual system processing. When task performance depends on the observer's memory of a target, these models should include a characterization of these internal representations, or memory templates.

A technique was developed to measure these templates when an observer is discriminating two different targets. The technique involves adding a small amount of random noise to each target stimulus. The two targets are then presented to the observer. The observer's discrimination response is then correlated with the lightness or darkness of the noise at each location, or pixel, in the image. If a particular pixel significantly contributes to the observer's decision, then the resulting response correlation image will show lighter or darker areas in those regions. The response correlation image illustrates the contribution of each noise image pixel to the observer's decision and can represent which features of the stimulus are being used to make the discrimination.

At Ames, this technique was demonstrated using a well-studied visual discrimination task, vernier acuity. Vernier acuity refers to the smallest misalignment of two lines that an observer can detect. The first figure illustrates the two stimuli presented in a vernier acuity discrimination task. One stimulus is a pair of lines in alignment. The other is the same except the right line is elevated by a single pixel (0.005 degree of visual angle). Human observers are quite precise in detecting misalignment and it is of interest to know what features of the stimulus are used that can account for such precise discriminations. This knowledge can greatly improve model predictions of target detection and discrimination.

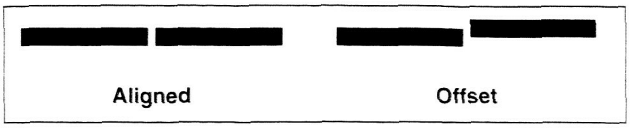

Fig. 1. Vernier acuity stimulus. In this example, the vernier stimulus is composed of two line features that are 0.02 degree of visual angle in length. On each trial, the right line will either be aligned with the left, or displaced upward relative to the left line. The task is to categorize the trial as "aligned" or "offset."

The second figure shows the response correlation image obtained after correlating the added noise pixel values with the observer responses. Current visual discrimination models that mimic visual system processing, but ignore observer templates, typically predict that the right side of the image should show a blurred version of the difference stimulus, as does appear. However, these models predict that nothing should appear around the left vernier feature since the images are the same in this region. The response correlation image shows that contrary to this prediction, the observers pay approximately equal attention to the fixed line on the left.

The response correlation technique can make an important contribution to current visual discrimination models by improving predictions of target detectability. This technique is useful for a variety of tasks in clarifying the underlying features used to form and upgrade memory templates.

Point of Contact: A. Ahumada, Jr.
(650) 604-6257
aahumada@mail.arc.nasa.gov

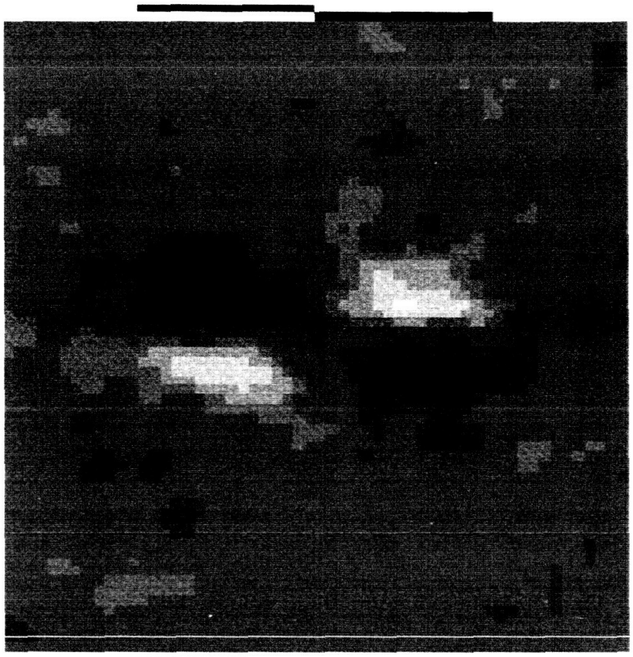

Fig. 2. Response correlation images for a vernier acuity task. A response correlation image is shown for the combined data sets of three observers. Dark areas mean that darker noise pixels in these locations led to more "offset" responses. Light areas in the image mean that lighter pixels led to the "offset" response.

High-Fidelity Virtual Environments

Stephen R. Ellis

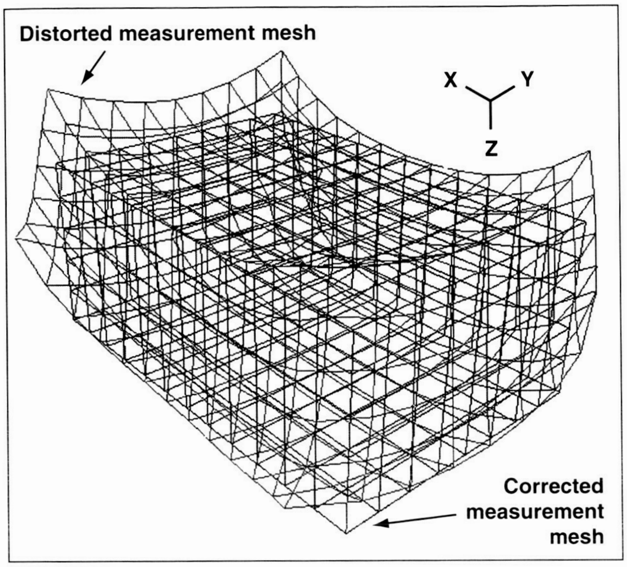

Fig. 1. Mesh of position-sensor distortion.

Virtual environments are personal simulators. They are interactive, head-referenced computer displays that create an illusion that causes their users to feel displaced to another location. This illusion is created through the operation of three types of equipment: (1) sensors, such as head position sensors, to detect the operator's body movements, (2) effectors, such as stereoscopic displays, to stimulate the operator's senses, and (3) special-purpose hardware to interlink the sensors and effectors to produce sensory experiences resembling those encountered by inhabitants immersed in a physical environment. In a virtual environment this linkage is accomplished by a simulation computer. In a head-mounted teleoperator display the linkage is accomplished by the robot manipulators, vehicles, control systems, sensors, and cameras at a remote work site. Both virtual environments and head-mounted teleoperator displays have applications in mechanical design, data visualization, robotics, and as aids for mechanical assembly.

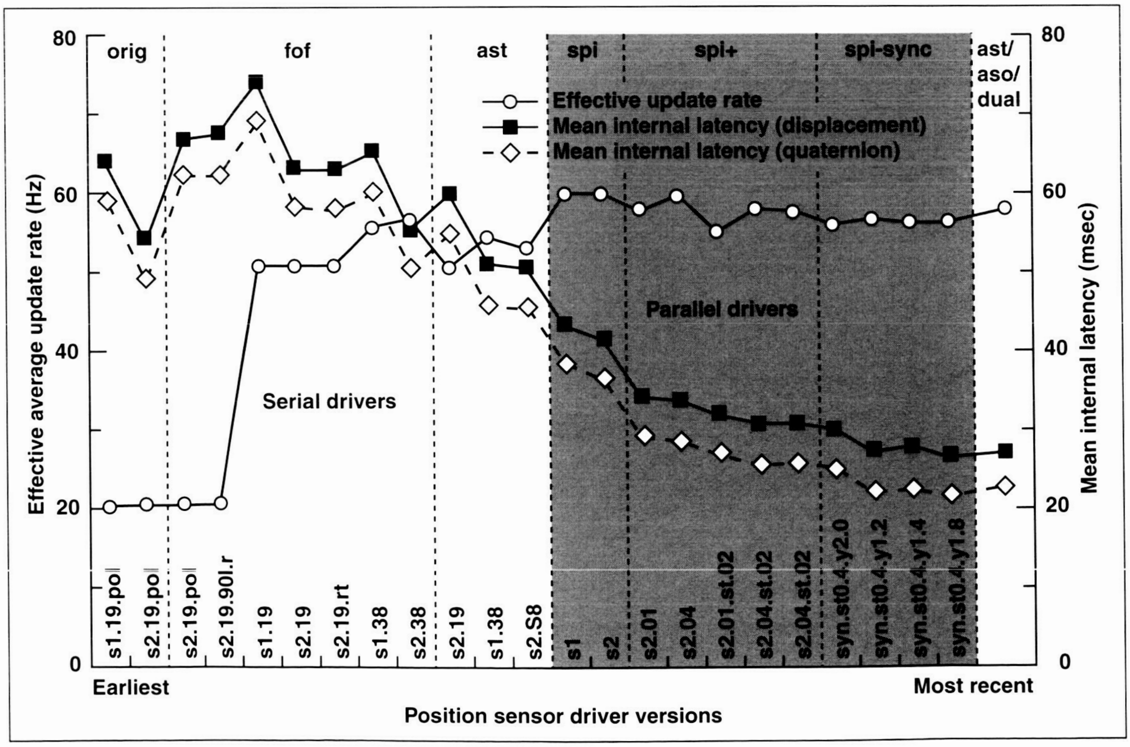

Fig. 2. Performance of improved position-sensor drivers.

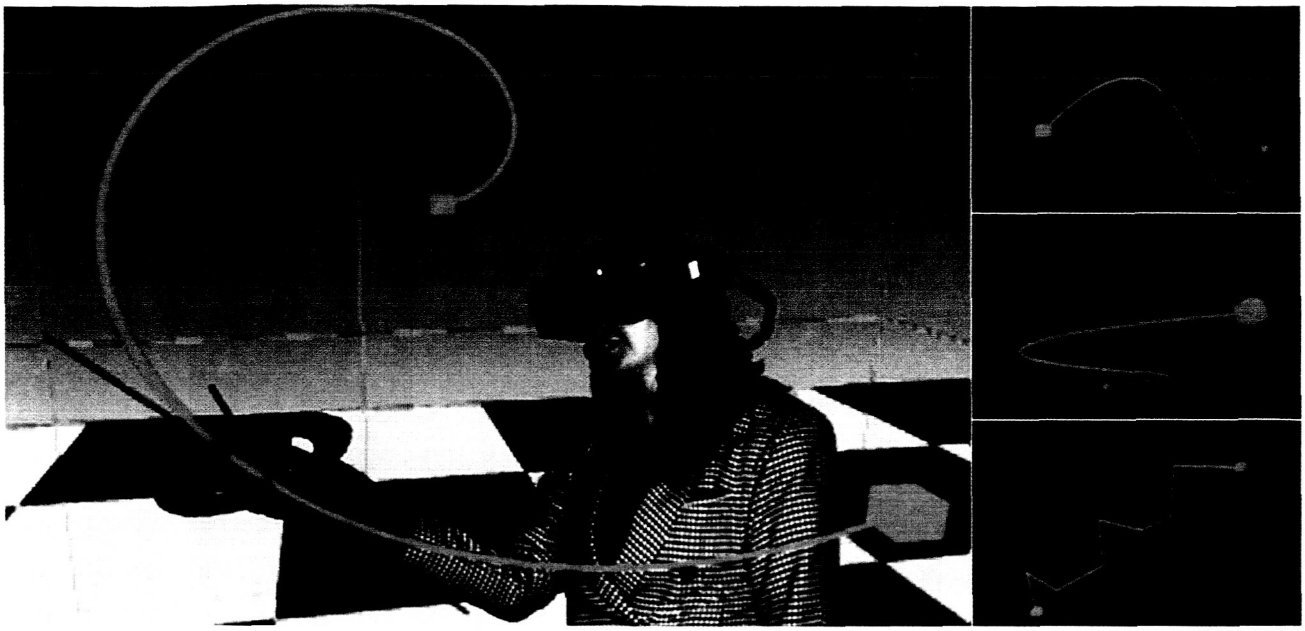

Fig. 3. Subject tracing a virtual path with a virtual ring attached to her hand.

Current virtual environment systems commonly use electromagnetic position trackers to sense operator head and hand positions in order to generate virtual environment simulations. The most common of these sensors suffer from uncorrected distortion in measurements of operator position; when interfaced to simulation computers, they produce objectionable time lags. Though these defects are acknowledged problems, their effect on the objective and subjective aspects of operator behavior within immersing virtual environments has not been studied and they have not been minimized.

The objective of the current work has been to measure and correct the position distortion of common position sensors (first figure) and to minimize simulation system visual lag during virtual environment rendering (second figure). These improvements are then tested with a manual tracing task in which operators attempt to move a virtual ring over a virtual path (third figure, left and center right) without making contact with it. Path complexity and ring diameter are changed (third figure, right) to study the precision with which operators can accomplish the task as a function of display conditions.

The precision and accuracy with which users can interact with virtual objects in virtual environments have been improved by correcting spatial distortion in common position sensors used to produce virtual environment simulations and by improvements in the latency and update rates with which these environments may be created. Position and orientation of a FasTrak position sensor were measured and corrected comparing linear and nonlinear interpolation schemes adapted from the computational geometry used in computational fluid dynamics. These algorithms have been ported to run on popular computer graphics workstations.

Point of Contact: S. Ellis
(650) 604-6147
sellis@mail.arc.nasa.gov

Effect of System Latency in Dynamic Virtual Acoustic Environments

Elizabeth M. Wenzel

The aviation environment contains multiple channels of auditory and visual information that must be accessed under high-stress, high-workload conditions. Auditory displays that controllers and pilots currently use can be significantly enhanced by utilizing three-dimensional (3-D) audio technology. Separate channels of auditory information can be placed at different virtual locations (1) to enhance situation awareness (e.g., airborne or ground traffic collision avoidance alerts, taxiway navigation aids and announcements); (2) to increase intelligibility (through the use of binaural delivery systems); and (3) to reduce auditory fatigue. Enabling these displays requires the development of specialized hardware systems for rendering virtual audio, the assessment of their engineering performance characteristics, and the perceptual validation of the spatial cues rendered by such systems.

Previous research suggests that auditory localization errors are minimized when a virtual acoustic environment (VAE) is dynamic, that is, when listeners are allowed to move their heads and the spatial cues change appropriately in real time. In such a display, knowledge of system parameters such as latency is critical for assessing real-time performance, and it is important that these parameters be carefully defined and measured. Psychoacoustic parameters such as the minimum audible movement angle (MAMA) can then be used as target guidelines to assess whether a given system meets perceptual requirements. In addition, such measurements enable systematic perceptual studies of the effect of degrading system latency on localization accuracy.

In a VAE, the total system latency (TSL) refers to the time elapsed from the initiation of an event or action, such as a movement of the head, until the consequences of that action cause the equivalent change in the virtual sound source location. Latencies are contributed by individual components of a VAE system, including tracking devices, signal processors, software to control these devices, and communications lines. There is no reason to expect that a system's latency remains constant over time. Thus, measurements of the mean, standard deviation, and range of the TSL provide a better characterization of this parameter.

This article reports on measurements of TSL for the virtual audio system used in previous studies of localization with and without head motion. The system consisted of a Convolvotron spatialization device that simulates direct-path spatial cues using 256-point, minimum-phase head-related transfer functions (HRTFs). It received head-position data from a Polhemus Fastrak (40-hertz update rate). In order to measure latency, a special HRTF map was constructed, which contained a single impulse at one map location and zeroes at all other locations. Latency measurements were conducted using the testbed shown in the first figure. The Fastrak receiver was mounted on the end of a mechanical swing arm with an optical switch that detected when the arm passed through a preset threshold position. This event threshold was considered analogous to the initiation of head (or source) motion in a VAE and began the universal counter's TSL timing cycle. At the same time, the tracker sent data to the Convolvotron in polled mode via a serial line, and a signal generator fed a 6000-hertz square wave to one of the input channels. Before the threshold was crossed, the Convolvotron was set to a zeroed map location so that no signal passed through the output channel. The experimenter then pushed the swing arm through the threshold position. The next tracker data sample that was received after threshold crossing caused the Convolvotron to switch to the nonzero map location. The square wave then passed through the system and terminated the timing cycle of the universal counter whose reading was considered to be the TSL. A total of 117 such measurements were taken: mean = 54.3, standard deviation = 8.8, range = 35.4 to 74.6 milliseconds.

Examination of the head motions that listeners use to aid localization suggests that the angular velocity of some head motions (in particular, left-right yaw) may be as fast as about 175 degrees per second for short time periods (e.g., about 1 second). A maximum TSL of 75 milliseconds could potentially result in short-term undersampling of relative listener-source motion as well as positional instability of the simulated source. For example, in the second figure, head motion yaw for an individual listener is plotted

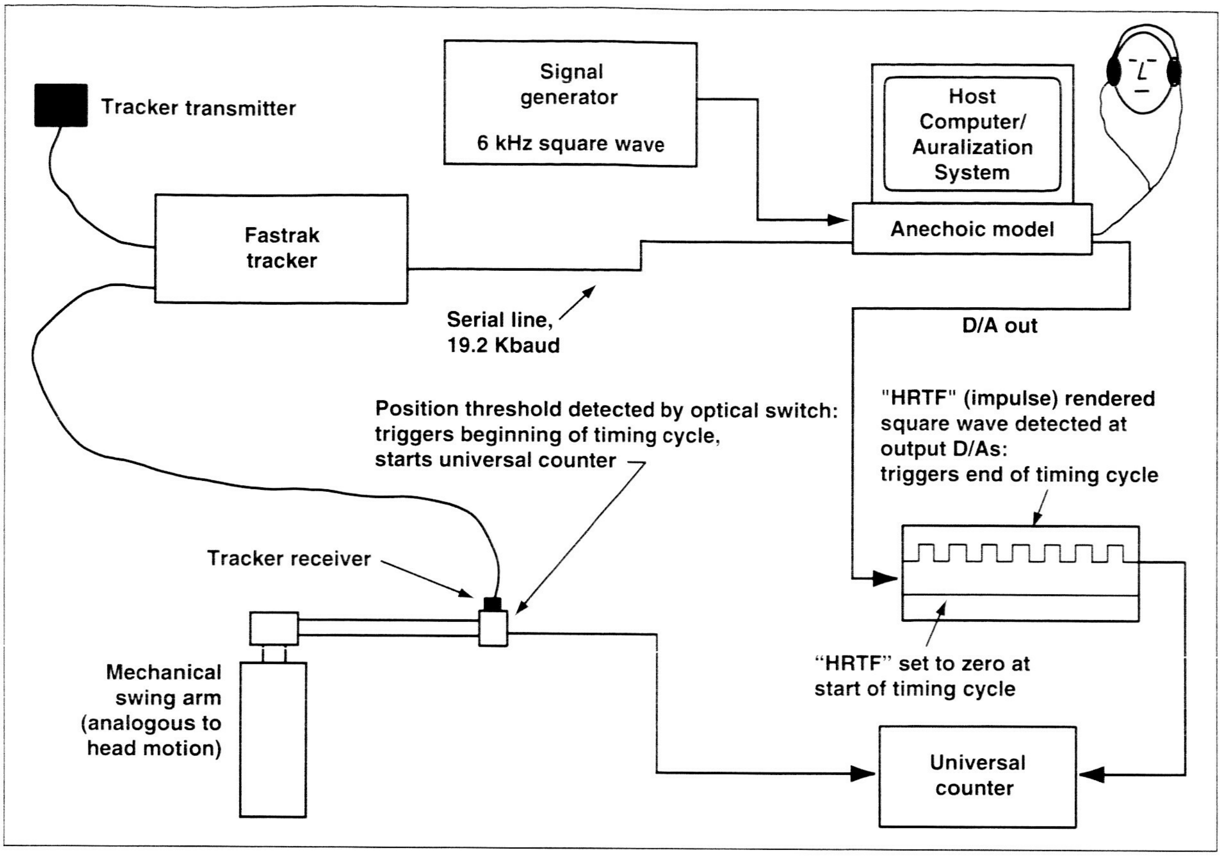
Tracker transmitter
Signal generator
6 kHz square wave
Host Computer/ Auralization System
Anechoic model
Fastrak tracker
Serial line, 19.2 Kbaud
D/A out
Position threshold detected by optical switch: triggers beginning of timing cycle, starts universal counter
"HRTF" (impulse) rendered square wave detected at output D/As: triggers end of timing cycle
Tracker receiver
Mechanical swing arm (analogous to head motion)
"HRTF" set to zero at start of timing cycle
Universal counter

Fig. 1. Testbed for measuring total system latency.

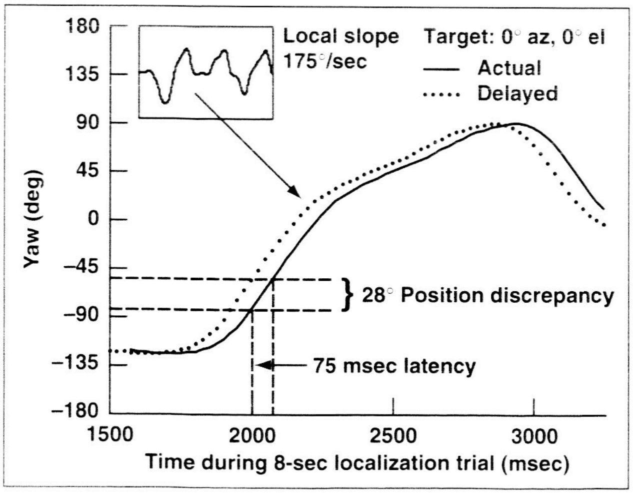

Fig. 2. Illustration of position displacement caused by latency.

as a function of time (undelayed and delayed by 75 milliseconds) during localization of a virtual source. The inset shows the entire 8-second trial. In regions of the head-motion trace where angular head motion is large (local slope = 175 degrees per second), a TSL of 75 milliseconds could result in a relative position discrepancy of about 28 degrees between actual head orientation and the rendered direction of the source. From psychophysical studies of the MAMA for real, moving sound sources, one can infer that the minimum perceptible TSL for a virtual audio system should be no more than about 69 milliseconds for an angular source velocity of 180 degrees per second. Thus, the positional displacement of the simulated source caused by TSL may have occasionally exceeded the perceptible threshold. In fact, listeners did not report any obvious instability in source position.

Point of Contact: E. Wenzel
(650) 604-6290
bwenzel@mail.arc.nasa.gov

Hybrid Systems Research

George Meyer

Hybrid systems are dynamic systems in which discrete and continuous behaviors coexist and interact. Broadly speaking, they are systems in which change occurs in response to events that take place discretely, asynchronously, and sometimes nondeterministically and also in response to dynamics that represent causal evolution as described by differential and difference equations of time. Often, as shown in the figure, a given system may be represented as a parallel composition of simpler hybrid systems. Each such subsystem is represented by an automaton with discrete states and events. Each discrete state supports a continuous multidimensional state space, shown as a fiber in the figure, on which the system evolves according to a given state equation defined on states, controls, and disturbances. Conditions on a fiber, such as departure from normal operation represented as a subset of the state space, may cause discrete state transitions. Certain of the discrete states are designated as unsafe states. The two primary concerns are system safety and system liveness. A hybrid system is safe if it visits only safe states. It is lively if it performs its intended function.

The objective of the research is to develop, in collaboration with the universities, a rigorous theory for the design and analysis of hybrid systems. The focus of the research has been on the combined system comprising an aircraft, cockpit, and pilot. The continuous part in this case describes aircraft motion including translation, rotation, aerodynamics, and power, requiring all together at least a 14-dimensional state space. The autopilot, with its control modes and the control panel, determines the discrete part of the system.

The concept of minimally restrictive legal controllers has been developed. Such controllers enforce safety with the fewest restrictions on liveness. Algorithms for the design of minimally restrictive legal controllers have been developed for a class of hybrid systems.

Point of Contact: G. Meyer
(650) 604-5750
gmeyer@mail.arc.nasa.gov

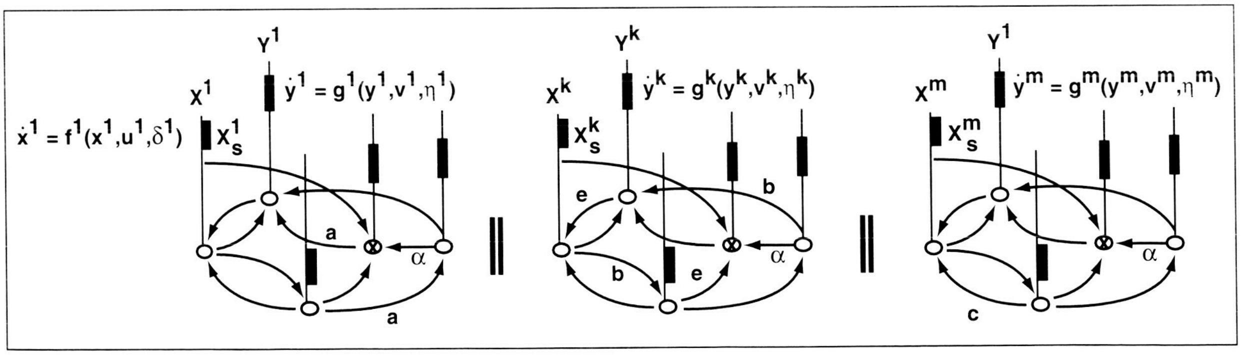
Y^1
X^1
$\dot{y}^1 = g^1(y^1, v^1, \eta^1)$
$\dot{x}^1 = f^1(x^1, u^1, \delta^1)$
X_s^1
a
α
a
$\|$
Y^k
X^k
$\dot{y}^k = g^k(y^k, v^k, \eta^k)$
X_s^k
e
b
b
e
α
$\|$
Y^1
X^m
$\dot{y}^m = g^m(y^m, v^m, \eta^m)$
X_s^m
α
c

Fig. 1. Model of hybrid systems.

Global Civil Aviation / Affordability

CTAS Joint Software Development

Michelle M. Eshow

The Federal Aviation Administration (FAA) has decided to field major elements of the Center/TRACON (Terminal Radar Approach Control) Automation System (CTAS) to many air traffic control facilities across the United States. To facilitate the deployment, NASA, the FAA, and their contractors have conceived and implemented an innovative software development approach known as Joint Development. Under Joint Development, NASA and the FAA are working in a common baseline of software that combines the products of CTAS enhancements produced by NASA with the FAA-generated elements necessary for a fielded operational system. This approach contrasts with previous efforts in which there was a single discrete handoff of software or technology from a research organization to the FAA.

The primary benefit of this Joint Development approach is that new CTAS functionalities and even entirely new tools developed as part of NASA's research programs can be fielded very quickly, because they are included in the common software baseline as soon as they are proven beneficial in field evaluations. The alternative would be to transfer the new functionalities in the form of written specifications to the FAA, which would then have to redevelop them for the operational system. In the past this approach has proved technically difficult and prohibitively expensive.

However, the Joint Development approach presents its own unique challenges. The software developed by NASA and its contractors must be written to conform to the same standards as that for the operational system. And, the configuration management of the software is a complex task that must be managed jointly by NASA, the FAA, and their contractors. These challenges are being met with a combination of process improvement and strategic use of advanced, commercially available products for configuration management and change tracking. In particular, the ClearCase/Multi-Site configuration management tool is being used for parallel development of CTAS at four locations across the country. Every few weeks, the software developed at the four sites is merged, thus incorporating the work of all the organizations.

The Joint Development process has been in full operation since July 1997, and many benefits have already been realized. In fact, the FAA is leveraging this approach to move up the initial deployment of CTAS by 2 years, to 2000.

Point of Contact: M. Eshow
(650) 604-5272
meshow@mail.arc.nasa.gov

Object-Oriented Design of a Dynamic Planner for Air Traffic Control Real-Time Sequencer, Scheduler, and Runway Allocator

Gregory L. Wong, Harry N. Swenson

The Dynamic Planner (DP) was designed, implemented, and integrated into the Center/TRACON (Terminal Radar Approach Control) Automation System (CTAS) to assist Traffic Management Coordinators (TMCs) in their task of planning and scheduling arrival traffic when that traffic is approximately 35 to 200 nautical miles from the destination airport. The TMC may input to the DP a series of current and future scheduling constraints that reflect the operational and environmental conditions of the airspace. Under these constraints, the DP uses flight plans, track updates, and estimated-time-of-arrival (ETA) predictions to calculate favorable runway assignments and arrival schedules that ensure a smooth flow of traffic into the terminal area. These runway assignments and schedules can be shown directly to controllers or they can be used by other CTAS tools to generate advisories to the controllers. Additionally, the TMC may override some of the decisions made by the DP and manually enter schedules, runway assignments, and sequences as the TMC sees fit. The DP will adapt its computations to accommodate these manual inputs. Should the TMC opt for a new plan, the constraints to the DP may be changed, and the DP will compute new runway assignments and schedules in real time.

In designing the DP, an object-oriented approach was used. Object-oriented design techniques were selected because of the ease with which the implementation task could be divided among the programming resources, as well as the ease with which the design could be maintained. Since the DP's operational deployment in 1996, a number of changes and new functionalities have been requested by air traffic controllers and researchers. The object-oriented approach to the DP's design and implementation made it possible for software engineers to readily modify the DP in response to these requests. This has resulted in short turnaround times and in rapid deployment of the new functionalities for evaluation in the field. As a result, the DP continues to evolve to meet the needs of air traffic controllers, TMCs, and researchers.

The Object Modeling Technique (OMT) object-oriented design method, developed by Rumbaugh (General Electric Research and Development Center, Schenectady, New York) and others, was used. The figure shows the high-level object model of the DP. Note that the Traffic Management Advisor (TMA) components external to the DP are shown as objects in the diagram. These external components are the Communications Manager (CM), Route Analyzer (RA), Timeline Graphical User Interface (TGUI), and a set of site-adapted data files known collectively as Site Dependencies.

The DP sequences and schedules arrival aircraft to the outer meter fix, meter fix, and runway in such a way as to maximize airport and TRACON capacity without compromising safety. Note that a blocked slot is a fake aircraft synthesized by a TMC to hold a place for a real aircraft which has not been entered into the system. Aircraft and blocked slots are collectively referred to as Schedulable Objects (SOs).

The DP's Sequence object puts the SOs into a first-come-first-served (FCFS) order at the meter fix. This is the order that TMCs are most comfortable with. However, a TMC may alter this order by manually entering one or more Sequence Constraints using the TGUI. The Sequence object will take these Sequence Constraints into account when setting the SO order.

The DP's Schedule object takes the order generated by the Sequence object and computes the scheduled time of arrival (STA) for each SO such that all Scheduling Constraints are satisfied. Scheduling Constraints are entered by the TMC using the TGUI. Scheduling Constraints reflect the landing rate at the airport, as well as the desired spacing between the aircraft near the meter fix and while landing. Furthermore, Scheduling Constraints may indicate that no aircraft may be scheduled to land during an interval of time set by the TMC. In addition to the Scheduling Constraints, the Schedule object takes into account the ETA of each SO as provided by the RA. The ETA represents the earliest possible time that an SO could arrive at a point if there were no other traffic in the

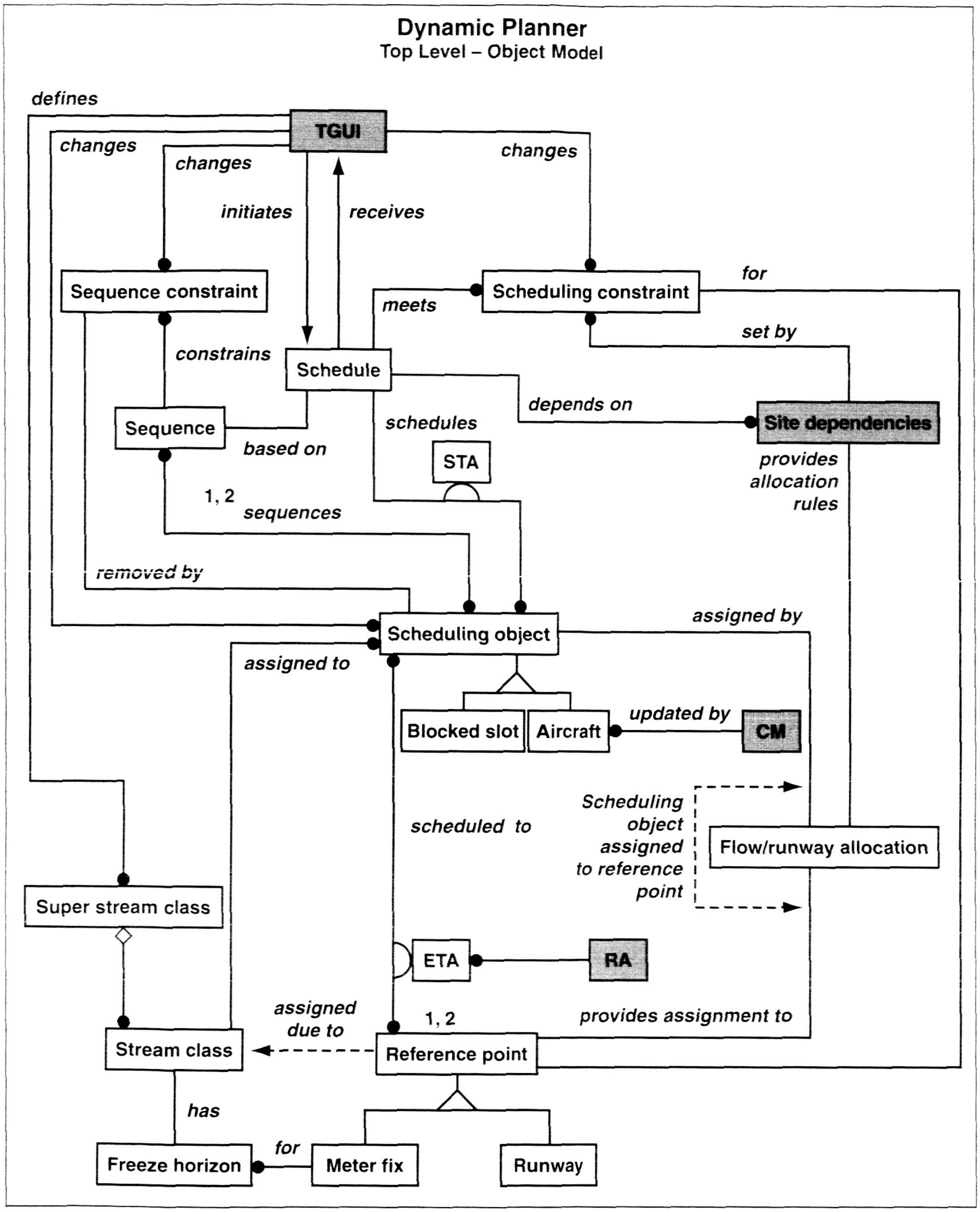
Dynamic Planner
Top Level – Object Model
defines
TGUI
changes
changes
changes
initiates
receives
Sequence constraint
Scheduling constraint
for
meets
set by
constrains
Schedule
depends on
Site dependencies
Sequence
schedules
based on
STA
provides allocation rules
1, 2
sequences
removed by
assigned by
Scheduling object
assigned to
Blocked slot
Aircraft
updated by
CM
Scheduling object assigned to reference point
scheduled to
Flow/runway allocation
Super stream class
ETA
RA
assigned due to
1, 2
provides assignment to
Stream class
Reference point
has
Freeze horizon
for
Meter fix
Runway

Fig. 1. Object model of the Dynamic Planner.

system. Thus, the STA of an SO computed by the Schedule object will not be earlier than the ETA of the SO.

In order to optimize the schedule that it computes, the DP will allocate SOs to the allowable runways using its Flow/Runway Allocation object. For each SO, the Flow/Runway Allocation object will assign the SO to each allowable runway and compute a set of STAs for all SOs as a result of that runway assignment. The runway assignment that minimizes the overall delay of all SOs is selected.

The scheduling and runway allocation processes are repeated periodically by the DP to ensure that the

STAs take into account the most recent traffic situation. This periodic update approximately corresponds to the rate at which aircraft-track updates are received. In addition, manual inputs by the TMCs, such as scheduling constraints, sequence constraints, and changes in the airport configuration, will trigger the DP to compute a new set of STAs and runway assignments to accommodate these changes.

The DP, as part of the TMA, has been in daily operational use throughout 1997 at the Traffic Management Unit at the Fort Worth Air Route Traffic Control Center. Feedback from TMCs, air traffic controllers, and researchers has defined new requirements that were unknown during the initial analysis and design phase. Because of the object-oriented design approach, however, these changes were quickly incorporated into the DP without disrupting its daily use.

Point of Contact: G. Wong/H. Swenson
(650) 604-1439/5469
glwong@mail.arc.nasa.gov
hswenson@mail.arc.nasa.gov

Daily Use of the Traffic Management Advisor

Harry N. Swenson, Shawn Engelland, Ty Hoang

The growth of commercial air travel and the "hub-and-spoke" operations used by many air carriers have put a severe strain on the Nation's air traffic capacity. This strain is safely, but many times inefficiently, absorbed by routine airborne and ground delays of aircraft. These delays cost the traveling public several billion dollars per year. The Center/TRACON (Terminal Radar Approach Control) Automation System (CTAS) is a joint NASA/Federal Aviation Administration (FAA) program that has as its goal the development of decision-support automation tools to efficiently reduce delays while maintaining a safe and reasonable level of controller workload.

The Traffic Management Advisor (TMA), developed under the CTAS program, is a time-based strategic planning and tactical advisory tool for traffic management coordinators and en route air traffic controllers. The TMA assists these air traffic control (ATC) specialists in efficiently and safely optimizing the capacity of a demand-impacted airport. The TMA software consists of highly accurate trajectory prediction, safety and ATC constraint-based scheduling with fuel-efficient delay distribution, traffic flow visualization, and controller advisories.

The TMA was installed and evaluated during a limited operational assessment in the summer of 1996 at the Fort Worth Air Route Traffic Control Center (ARTCC) and the Dallas/Fort Worth (DFW) Terminal Radar Control Facility, two of the busiest ATC facilities in the world. The benefits demonstrated during the assessment indicated that routinely the TMA saves 2 minutes of delay for every aircraft and, because of its efficient delay distribution scheduling, the routine landing capacity of the DFW TRACON was increased by 5%.

Following the success shown by the initial assessments, the FAA requested that NASA maintain the TMA on a daily use status throughout 1997. The figure shows the TMA as installed in the Traffic Management Unit at the Fort Worth ARTCC. The objective of this research was to expose the TMA to the broad spectrum of ATC personnel, as well as to

Fig. 1. Traffic Management Advisor installation at Fort Worth ARTCC.

the broad range of ATC conditions that could not be captured during the initial assessment. The TMA, used as the primary traffic management tool throughout the year, yielded an estimated annual savings of $5.6 million as a result of reduced delays. The evaluation during this extended period led to significant redesign of the configuration, scheduling, and mode-control interfaces, which reduced the workload associated with the use of the TMA. Another feature developed during FY97 to reduce controller workload was an automated delay-reporting system that for the first time provided the ATC facilities with a tool that accurately measures their performance. The TMA was also exposed to numerous anomalous events and provided the means to quickly provide solutions so that at the end of the year, the FAA had changed its acquisition strategy from one of a long-term development to a spiral deployment of the NASA prototype.

Point of Contact: H. Swenson/T. Hoang
(650) 604-5469/1980
hswenson@mail.arc.nasa.gov
thoang@mail.arc.nasa.gov

Surface Movement Advisor

Stan Harke

The Surface Movement Advisor (SMA) is a joint Federal Aviation Administration (FAA) and NASA project whose purpose is to help current airport facilities operate more efficiently. Currently installed and operational at Atlanta-Hartsfield International Airport, SMA is demonstrating how advanced information systems technologies can be implemented to improve coordination and planning of ground airport traffic operations.

The SMA system is based on a client-server architecture. A fiber backbone between the airlines, the airport management, the ramp towers, and the FAA control tower links the SMA system together. Various traffic data are collected in real time by the SMA server. The SMA system integrates the airline schedules, gate information, flight plans, radar feeds, and runway configuration (departure split and landing direction). This integrated information is then retransmitted over the network system and shared between ramp operators, airport managers, airline operators, and FAA controllers and supervisors.

SMA provides air traffic and ramp controllers with automated aircraft identification and tracking. It combines tracking and identification data with arrival and departure flight-sequencing data (such as the surface operations and aircraft taxi routing information provided to air traffic controllers, airline operators, and airport operators).

The first SMA proof-of-concept/prototype (Build-1) has been successfully demonstrating SMA functional capabilities at the FAA-selected test site, Atlanta-Hartsfield International Airport, since early 1996.

An official report released by the FAA in October 1997 measured the cost benefit of the SMA in Atlanta conservatively at $20 million a year. The total investment was $4.1 million with a development time of only 18 months. This cost benefit was measured based on taxi times and for departures only. The report also cites benefits not quantified, including increased airline productivity, assistance to ground and ramp controllers in reduced visibility, and reduced communication time between tower and ramp, and between tower and pilots.

Point of Contact: S. Harke
(650) 604-5012
sharke@mail.arc.nasa.gov

Surface Flow Visualization on a Hovering Tiltrotor Blade

Gloria K. Yamauchi, Alan J. Wadcock, James T. Heineck

Fluorescent mini-tufts were used to visualize the flow behavior on the upper surface of the blade of a full-scale, hovering XV-15 tiltrotor installed in the Ames 80- by 120-Foot Wind Tunnel. The objectives of the test were to determine whether the flow direction could be deduced from the tuft motion and whether this visualization technique could be practically implemented for forward flight. A dual camera/strobe system was used to acquire inboard and outboard images of approximately 2500 tufts on the upper surface of one blade. The tufts were approximately 0.625 inch in length; tuft diameters of 0.002 and 0.006 inch were used. Tuft images were acquired for a range of thrust conditions up to and including stall.

The first part of the figure shows three overlaid images for the inboard blade region of a stalled condition. There are several 0.002-inch-diameter tufts near the trailing edge that are pointing upstream. Since the centrifugal force causes the tufts to point toward the tip, aerodynamic forces must be responsible for the upstream-pointing tufts. Therefore, areas of the local flow are reversed. The second part of the figure shows overlaid images of the outboard blade region for the same condition. An area of highly localized flow disturbance is shown centered at approximately r/R = 0.895 (where R is the rotor tip radius and r is the radial station). One explanation for this disturbance is that the flow is separated. Another possibility is that the disturbance is caused by interaction with the tip vortex from the preceding blade. The formation of the tip vortex is evident in the two rows nearest the blade tip (note tufts near trailing edge pointing toward tip). Although tuft sizes were selected to minimize the effect of centrifugal force on the tufts, distinguishing between the effects of aerodynamic and centrifugal forces on the tufts was not always possible. Nevertheless, the tuft motion can provide useful information about the behavior of the flow on the upper surface of the blade.

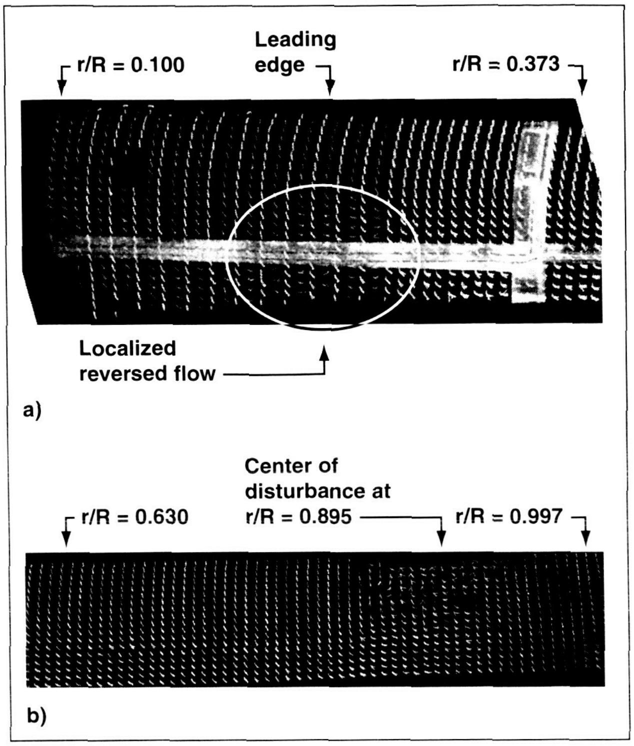

Fig. 1. Overlaid images of XV-15 upper blade surface tuft pattern: thrust coefficient = 0.0145; figure of merit = 0.702; tip Mach number = 0.56. (a) Inboard, (b) outboard.

This experimental setup was tailored for acquiring images in hover; however, images of similar quality are possible in forward flight, given some modification to the light source.

Point of Contact: G. Yamauchi
(650) 604-6719
gyamauchi@mail.arc.nasa.gov

Wake Visualization of a Full-Scale Tiltrotor in Hover

Benton H. Lau, Alan J. Wadcock, James T. Heineck

The objectives of this program were to measure the tip-vortex trajectory of a full-scale, hovering tiltrotor and to compare the vortex trajectory of the baseline rotor with that of the subwing rotor (first figure). The subwing, which is mounted at the blade tip, can split the strong concentrated tip vortex into two weaker vortices, and weakening the vortex can reduce the blade–vortex interaction noise. Two sets of subwings with different incidence angles were tested in this program.

The wake-visualization program was conducted on a right-hand XV-15 tiltrotor in the Ames 80- by 120-Foot Wind Tunnel. A smoke dispenser was installed near the rotor tip and an optics pod was placed below the rotor plane on the wind tunnel floor. When fed with a laser beam via a fiber-optic cable, the pod generated a thin laser sheet and illuminated the entrained smoke in the rotor wake. Images of the rotor-wake geometry were recorded on videotapes and later digitized on a Macintosh for analysis.

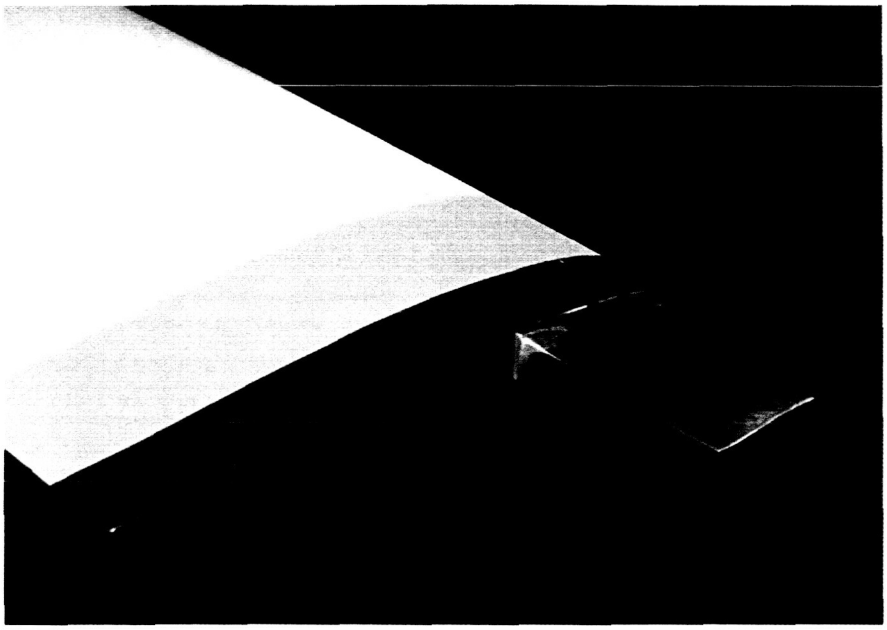

Fig. 1. Subwing blade.

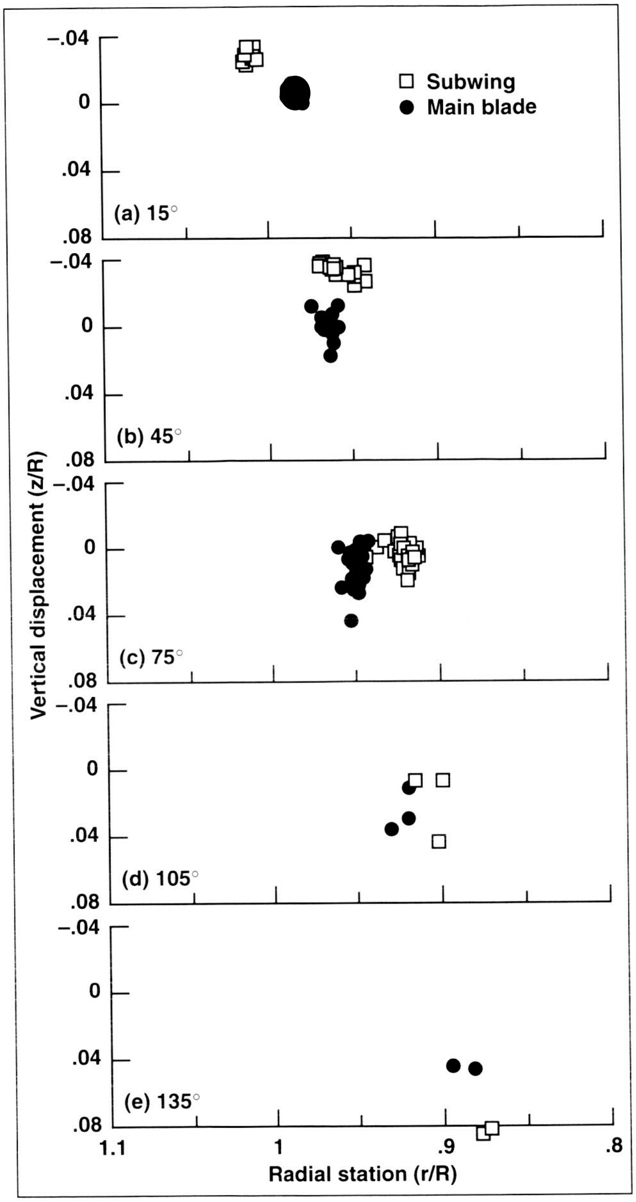

Fig. 2. Interaction of the subwing vortex with the main-blade vortex at different wake ages.

For both subwing rotors, the laser sheet illuminated a vortex pair rotating in the same direction. The trailing vortex generated by the subwing appears to be weaker than that of the main blade. Initially the subwing wake contracts faster than the main-blade wake. As the vortex pair is convected downstream, the two vortices rotate, relative to each other, approximately half a revolution in a 75-degree blade rotation (second figure). Subsequently, the vortex pair combine into a single vortex at a wake age between 150 degrees and 165 degrees. The trajectory of the combined vortex has the same trajectory as the baseline rotor. A small improvement in hover performance over that of the baseline rotor is observed for both subwing rotors.

Point of Contact: B. Lau
(650) 604-6714
blau@mail.arc.nasa.gov

Skin-Friction Measurements on a Rotor in Hover

Alan J. Wadcock, Gloria K. Yamauchi

A means of acquiring skin-friction measurements on a fixed wing using an oil-flow interferometric technique was developed at Ames in the early 1990s. As long as flow conditions are steady, as they are in hover, this technique can be applied to rotary wings also. During the March 1997 hover test of a full-scale XV-15 tiltrotor in the Ames 80- by 120-Foot Wind Tunnel, this technique was used for the first time to provide detailed skin-friction measurements on a rotor over a wide range of thrust conditions.

The method consists of applying a highly reflective adhesive-backed Mylar film to the rotor blade at each radial station of interest. Six radial stations were chosen for this study: 17%, 28%, 50%, 72%, 83%, and 94% of the rotor radius. To determine the *chordwise* shear stress at a desired location, oil is applied to the Mylar film in a thin line oriented parallel to the blade leading edge. Centrifugal force will act parallel to this radial oil line and therefore play no role in the chordwise development of the oil film.

The first part of the figure represents the initial pattern of oil lines applied to the rotor blade at the 72%-radius location. The lines are staggered in an attempt to prevent adjacent oil films from merging with each other. Also visible is a series of chordwise oil lines applied with the objective of measuring the radial shear stress. The rotor is rapidly spun up and held "on condition" for several minutes before quickly being brought to rest. If the oil films are subsequently photographed using monochromatic light, a series of fringe patterns is made visible, as shown in the second part of the figure. Each fringe pattern provides information about the local oil-film thickness distribution, and this in turn yields a measurement of shear stress. The third part of the figure presents corresponding measurements of the chordwise component of skin friction at the radial station r/R = 72% (where R is the rotor tip radius and r is the radial station) under nominal 1-g hover conditions (coefficient of thrust $C_T = 0.0093$) at design tip Mach number 0.69. Shear stress is directly proportional to fringe spacing, and this latter part of the figure clearly indicates the increase in shear stress associated with the transition from laminar flow to turbulent flow.

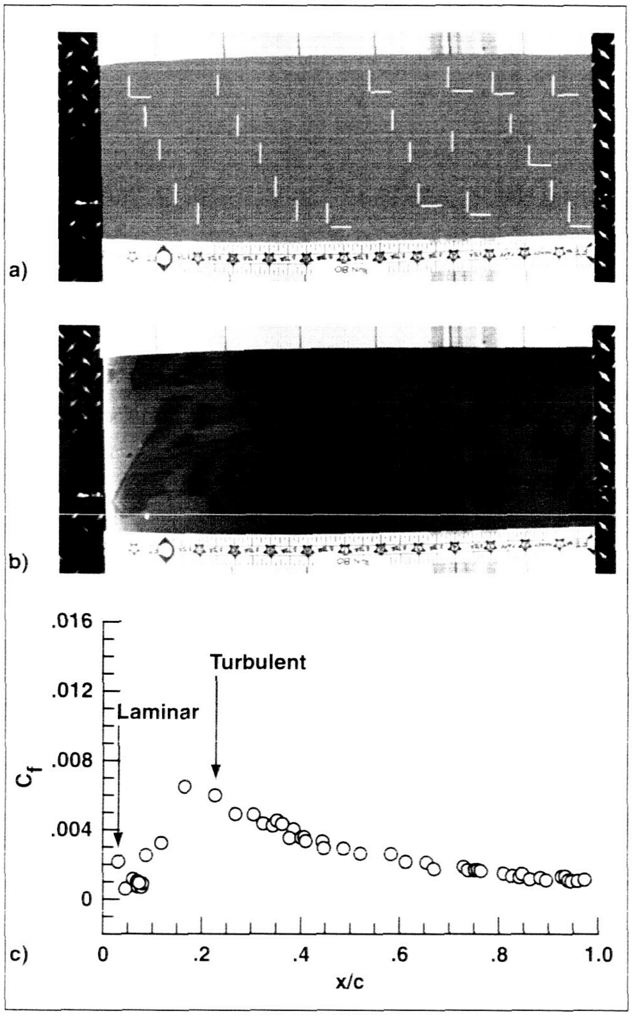

Fig. 1. (a) Initial oil-line pattern; (b) final oil-film pattern; and (c) chordwise skin-friction coefficient for nominal 1-g hover conditions at r/R = 72%.

Point of Contact: A. Wadcock
(650) 604-4573
awadcock@mail.arc.nasa.gov

Characterization of Dynamic Stall on the UH-60A

William G. Bousman

Under severe loading conditions dynamic stall will occur intermittently on a helicopter rotor blade as it makes one revolution of 360 degrees. When dynamic stall does occur, a vortex is shed from the leading edge of the blade; this vortex is translated back along the upper surface of the blade, and then leaves the trailing edge. The shedding of the dynamic-stall vortex in these conditions twists the rotor blade and causes extremely high loads in the helicopter's control system. Indeed, the size and strength of the components in the control system are generally determined by these dynamic-stall loads. Unfortunately, analytical models are unable to compute the dynamic-stall loads because of the nonlinear nature of the aerodynamic loading. A first step in the development of improved analytical models for helicopter design is an accurate characterization of dynamic stall as it occurs in flight as determined by experimental measurements.

A highly instrumented rotor was installed on a UH-60A helicopter, and flight measurements were obtained for a great variety of conditions at Ames in 1993–94. The instrumentation included 242 pressure transducers mounted at nine radial stations on one rotor blade. The variation in measured pressure as the blade makes one revolution can be examined in detail and, with the assistance of two-dimensional wind tunnel tests, regions of dynamic stall can be identified. For the research discussed here, three flight cases were examined. In the first, the helicopter was pulled up very rapidly in an evasive maneuver. This is the so-called UTTAS pull-up, named after the original military requirement for this aircraft: the Utility Tactical Transport Aerial System. This maneuver is quite unsteady and there is a rapid variation in load factor and airspeed. In the second, a high-speed diving turn was examined; this is a steadier maneuver in that the airspeed and load factor are held constant, but the aircraft rates are unsteady. In the third, the helicopter was in level flight, but in an overloaded condition.

From the pressure data measurements it was possible to identify dynamic-stall cycles that involved the repeated shedding of a dynamic-stall vortex as the rotor blade moved through a full revolution. The figure shows a rotor map of the locations of these dynamic-stall events; it can be seen that they occur in three groups or "patches." The rotor blade is rotating counterclockwise in this figure, and the first stall patch is seen at about 180 degrees on the inboard portion of the blade. Then as the blade continues around, the stall moves outward on the blade and leaves the tip at an azimuth of about 280 or 290 degrees. The second and third stall patches occur at approximately 350 and 50 degrees, regardless of the type of maneuver. It is concluded that the first stall cycle is triggered by high angles of attack

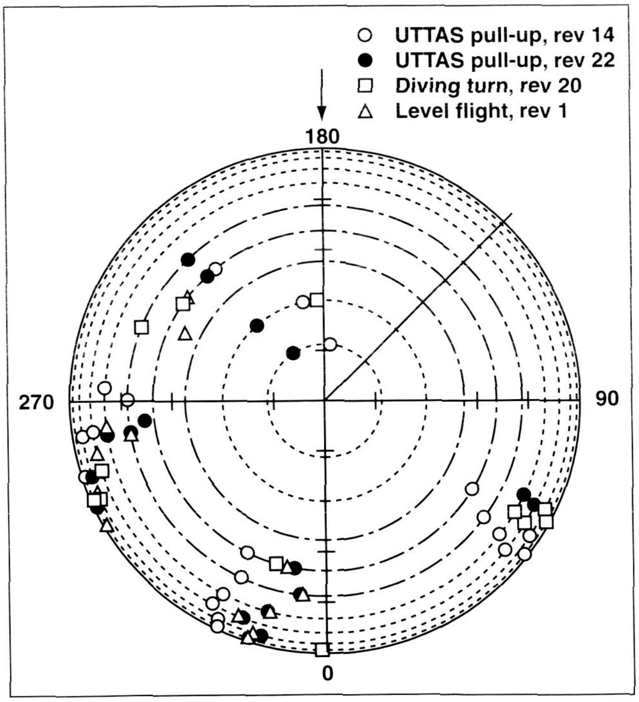

Fig. 1. Rotor map of dynamic-stall locations for four loading conditions.

that are associated with the loading on the blade, whereas the pattern of the second and third cycles is determined by the flexibility of the control system as the twisting forces on the blade cause the blade to oscillate in and out of stall. These results suggest that analytical methods need to be tested for steady flight conditions initially and, if successful there, then applied to maneuvering flight.

Point of Contact: W. Bousman
(650) 604-3748
wbousman@mail.arc.nasa.gov

Modeling UH-60A Control System Stiffness

Robert Kufeld

Accurately predicting the dynamic stall characteristics of a helicopter rotor has become one of the major goals of the rotorcraft industry. The loads during this flight condition are important, for they are used to size the helicopter control system. In addition, improved predictions should reduce the design and development cost of new helicopters. To accurately predict these dynamic stall characteristics, accurate models of the rotor structure, control system stiffness, linear and nonlinear aerodynamics, and rotor inflow are required.

The objective of this work was to focus on improving the control system model of the UH-60A helicopter and thus improve the prediction of its dynamic stall characteristics. The recent flight testing of the UH-60A at Ames Research Center provided a wealth of data on observations of the dynamic stall phenomenon; the data are ideally suited for comparison with calculations from comprehensive rotorcraft analyses. In addition, current models of the UH-60A control system stiffness were based on an analytical estimate and never verified.

A direct measurement of the UH-60A control system stiffness was made, and a summary of the collective loading results is shown in the figure. These data show that the measured collective control-system stiffness is a function of the rotor azimuth, as opposed to the constant value typically used. The data also show that the maximum value of the measured stiffness near 165 degrees rotor azimuth is more than 4 times that used in the current model.

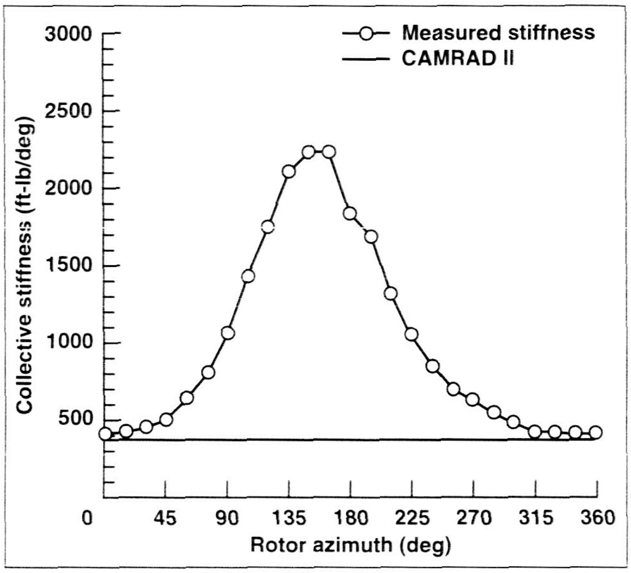

Fig. 1. Measured and calculated UH-60A control-system stiffness versus rotor azimuth.

Point of Contact: R. Kufeld
(650) 604-5664
rkufeld@mail.arc.nasa.gov

On-Blade Control of Rotor Blade Vibration

Mark V. Fulton, Robert A. Ormiston

High levels of vibration in rotorcraft fuselages cause various problems, including structural fatigue, pilot fatigue, reduced rotorcraft readiness, and increased costs of development and maintenance. Current helicopters typically employ *passive* vibration isolation and absorption to reduce fuselage vibration. However, these passive devices are heavy and have various other limitations. Past attempts to further reduce vibration have used *active* techniques such as higher harmonic control of the swashplate and individual blade control by means of active pitch links at the root of each blade. Modern "smart" materials provide an opportunity for on-blade active control, possibly for reduced weight and power. A small-scale, two-bladed rotor with on-blade control surfaces (elevons) was previously designed, fabricated, and tested in hover. The objective of the current project was to test this active rotor in a wind tunnel to determine the effectiveness of the elevon in changing vibratory blade moments in forward flight.

The active rotor is shown in the Ames 7- by 10-Foot Wind Tunnel in the first figure. The model is a two-bladed, 7.5-foot-diameter hingeless rotor that was operated at tip speeds of up to 298 feet/second. Each blade has one 10%-chord, 12%-span elevon that is actuated by two lead zirconate titanate (PZT) bimorphs; a close-up of the active section is shown in the second figure. A command voltage can be applied to the PZT in order to oscillate the elevon at the desired frequency.

The PZT actuator produced average elevon motions exceeding ±5 degrees for frequencies up to four times the maximum rotor speed of 760 revolutions per minute (rpm). The effectiveness of the elevons was measured by varying the elevon phase for five harmonics of the rotor speed (1/rev–5/rev) and recording the vibratory bending and torsion moments at the root of each blade. These phase sweeps were performed at various flight conditions, including low to moderate thrust levels, flight speeds

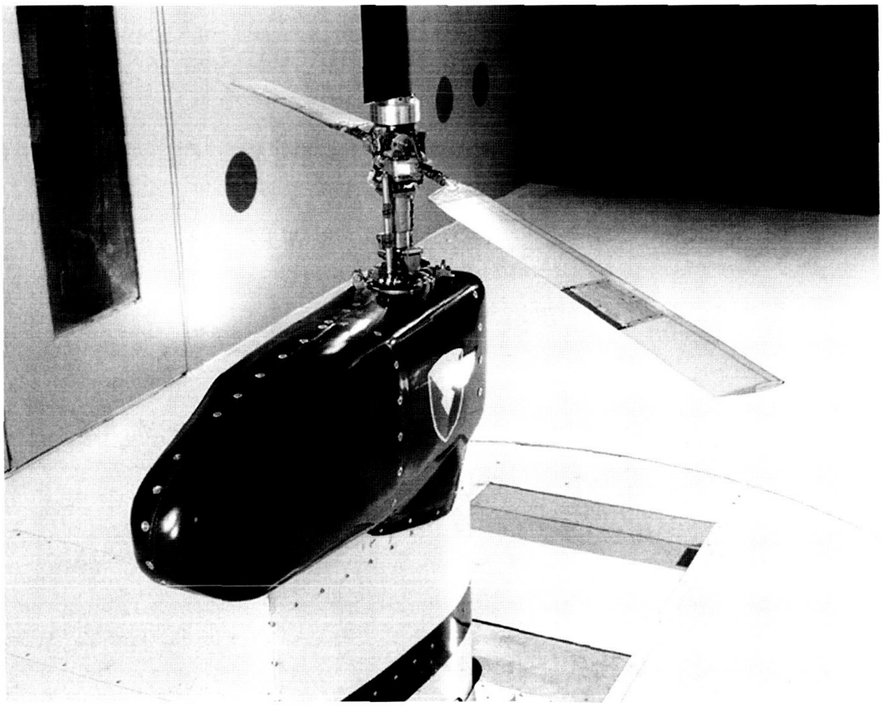

Fig. 1. Rotor with on-blade elevons in the Ames 7- by 10-Foot Wind Tunnel.

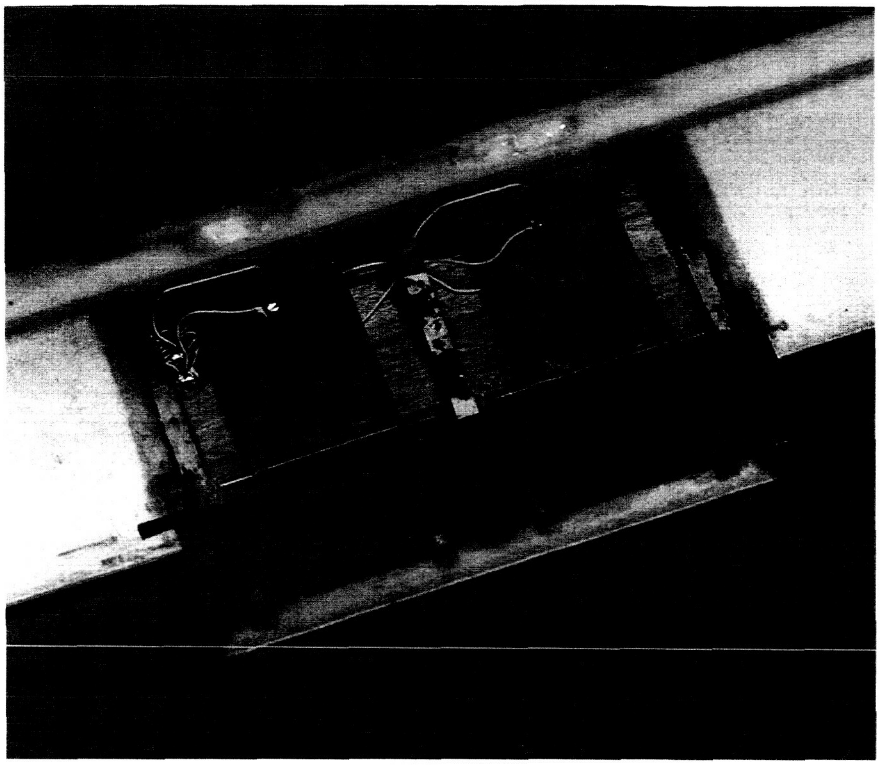

Fig. 2. Close-up of the active section with the access panel removed and the elevon disassembled.

up to 89 feet/second (or 30% of the maximum tip speed), and rotor speeds between 450 and 760 rpm. Changing the rotor speed allowed higher blade loadings, as well as an investigation of the effect of blade aeroelastic properties on elevon effectiveness. The resultant blade-frequency and aeroelastic coupling changes were expected to alter the elevon effectiveness at various harmonics of the rotor speed.

It was shown that the elevon could significantly change blade-root vibratory moments. High-speed effects on actuator performance and elevon effectiveness were measured up to a flight speed of 106 feet/second (or 60% of the tip speed) at essentially zero thrust and 450 rpm. The optimum phase angle for vibratory moment reduction was determined for 1/rev–5/rev excitation. Finally, the optimum amplitude of elevon motion was determined for selected cases. In summary, this project has provided an improved understanding of this on-blade control idea and has shown that on-blade active control holds promise for reducing helicopter fuselage vibration.

Point of Contact: M. Fulton
(650) 604-0102
mfulton@mail.arc.nasa.gov

Aeroelastic Stability Testing

Thomas Maier, David Sharpe, Robert A. Ormiston

An important consideration in the design of helicopter rotor blades is the stability of the isolated rotor and the coupled rotor-body system. Once disturbed, unstable linear systems grow in response without bound until a failure occurs. Therefore, the helicopter design engineer would like an analytical tool that would accurately calculate the stability of these systems. The present work provides an experimental database that is needed to validate these analytical tools. The database, when complete, will include two rotor-blade configurations tested in hover and forward flight. This year's accomplishments include the fabrication and structural testing of the second rotor-blade configuration.

The two configurations include a rectangular blade with center of gravity, elastic axis, tensile axis, and aerodynamic center located on the quarter chord, and a swept-tip blade with small offsets in elastic and inertial properties. The rectangular blade is the simplest of the two structures to analyze. The more complicated swept tip amplifies the coupling of bending and torsion modes. Both blade sets have a hingeless hub design (root pitch motion through a feathering bearing; flap and in-plane motion through a composite root flexure). The rotors are mounted on a relatively rigid test stand to confine the experiment to the physics of interest. Once the operating condition is obtained, hydraulic actuators are used to oscillate the pitch of the blade at the regressive in-plane mode natural frequency, thus exciting this lowly damped mode. The excitation is shut off and the decay of the in-plane bending moment is measured by strain gages bonded to the blade structure. The rectangular-bladed rotor has been tested in hover by varying rotor speed and collective pitch and in forward flight by varying wind speed, collective pitch, and shaft angle at 1700 revolutions per minute.

Point of Contact: T. Maier
(650) 604-3643
tmaier@mail.arc.nasa.gov

Flight Mechanics of Helicopter Sling-Load Systems

Luigi Cicolani, Mark Tischler, Allen McCoy, George Tucker

The specific objectives of this research are (1) to develop and demonstrate the ability to compute the dynamic flight envelope of helicopter and sling-load combinations simultaneously with flight testing, and (2) to develop corresponding simulation models validated with flight-test data.

Helicopter sling-load operations are common in both military and civil operations. The addition of the load can degrade system stability and reduce the safe operating envelope of the combined system below that of the helicopter alone. During its operational life, a utility helicopter will carry a wide variety of loads using a variety of slings, each with different dynamic characteristics. Incidents and accidents can occur when the dynamic limits of the helicopter and load are unknowingly exceeded. To avoid these occurrences, military helicopters and loads are usually qualified for these operations in flight tests, which can be expensive, time consuming, and sometimes risky.

The cost, time, and risks of flight qualification tests can be reduced by developing a system providing real-time analysis of flight-test data. Quantitative assessment of helicopter flying qualities and load-pendulum stability can be accomplished after a test at a given test airspeed and before proceeding to the next test point. Further, the ability to make reliable predictions of load-helicopter stability from simulation models will reduce the requirement for flight-test qualifications to just a few loads, provide knowledge of critical points in advance of flight testing, and allow assessment of loads for which flight-test evaluations are not available.

Flight tests were conducted with an instrumented UH-60A Black Hawk helicopter and an 8- by 6- by 6-foot standard military cargo container. The first figure shows the helicopter carrying its instrumented load. Data were telemetered to a ground station where they were analyzed by using three work stations interfaced with the real-time telemetry system. The computations and the subsequent engineering and safety assessments took 4–8 minutes to complete before the pilot was cleared to proceed to the next test point.

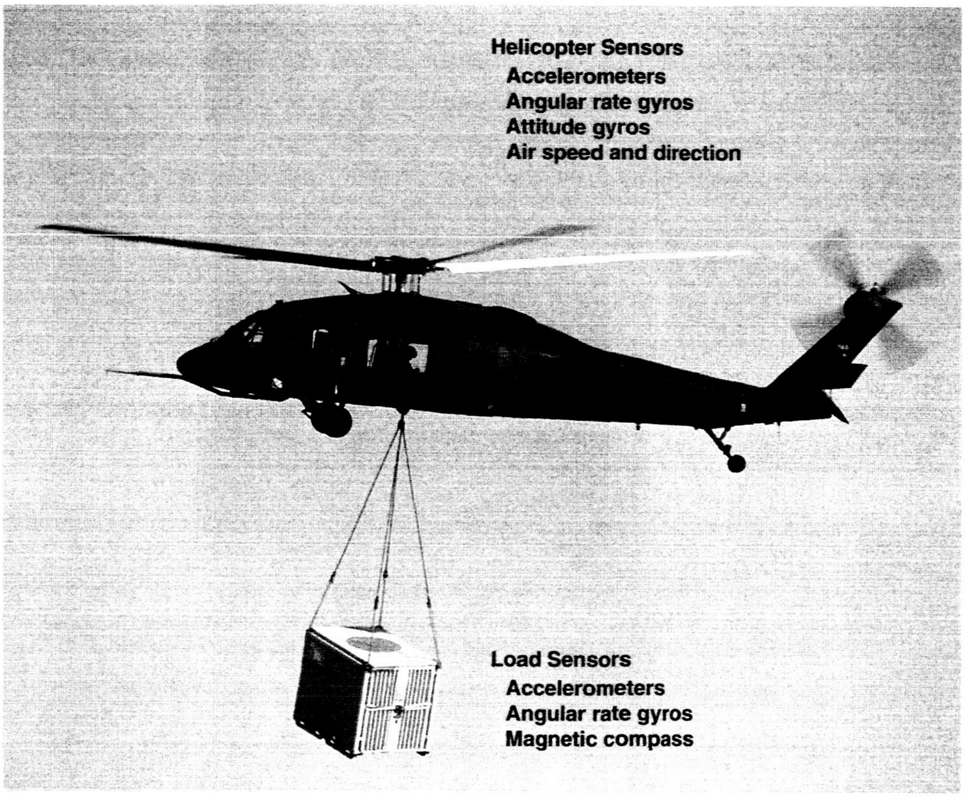
Helicopter Sensors
Accelerometers
Angular rate gyros
Attitude gyros
Air speed and direction
Load Sensors
Accelerometers
Angular rate gyros
Magnetic compass

Fig. 1. Black Hawk helicopter with Conex box load.

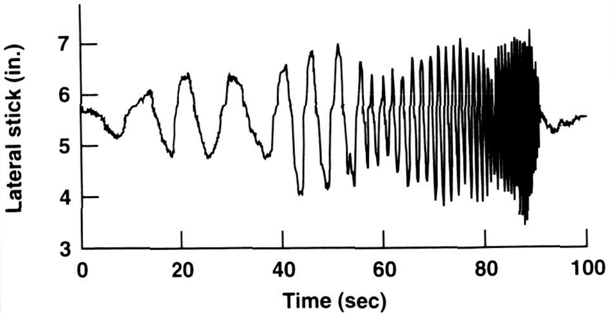

a) Test control input

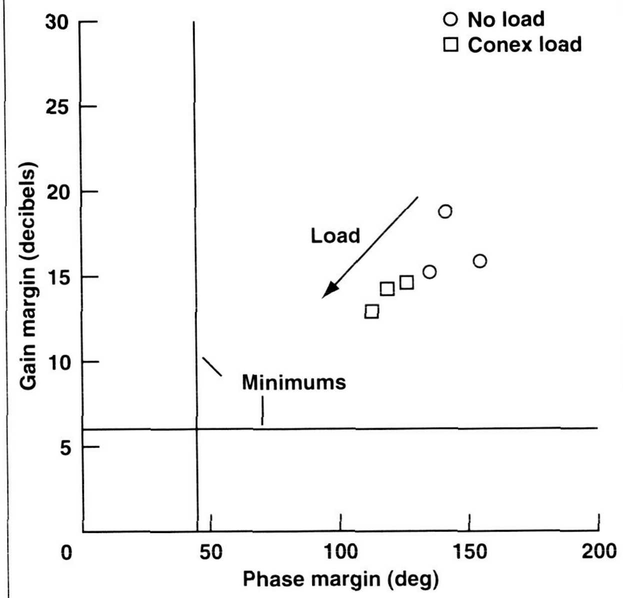

b) Helicopter stability

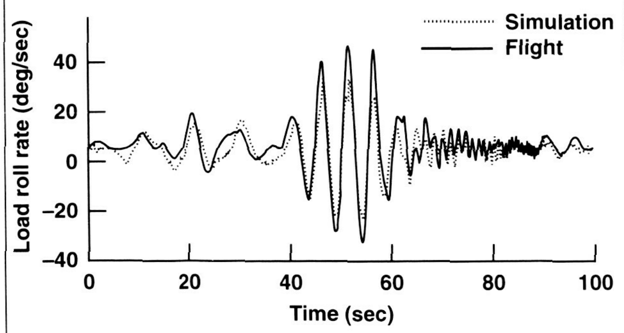

c) Comparison with simulation

Fig. 2. (a) Pilot's test control input; (b) helicopter stability with and without Conex load; (c) comparison with simulation—load roll rate.

The analysis used the CIFER™ software for frequency-domain analysis of flight data. This flight-test software tool was developed previously at Ames. The top portion of the second figure (test control input) shows the sinusoidal control inputs of increasing frequency from 0.05 to 2 cycles per second, which the software uses, along with the corresponding roll response of the helicopter, to calculate phase and gain stability margins of the helicopter-load combination. Results are shown in the middle part of the figure (helicopter stability). A moderate reduction in stability margins at three test airspeeds—hover, 30 knots, and 50 knots—is indicated when the helicopter is carrying the load. Although the Black Hawk has ample available margin above the safe minimums, other load-carrying helicopters do not, and for such aircraft the loss in stability margin seen here could pose a risk.

The load instrumentation package was provided by the Technion (Israel Institute of Technology) under a U.S. Army/Israel memorandum of agreement. It was designed for portability, and provides comprehensive data on the details of load motions—possibly the first such data available for systematic validation of mathematical models of the load-sling motions. The bottom of this second figure (comparison with simulation) shows a sample comparison of flight and simulation responses for load roll rate during a lateral-axis control frequency sweep. There is good agreement in this comparison. However, other data and observations indicate that significant improvements in simulation models are still required to fully predict the helicopter and load motion.

A total of 15 data flights were recorded and archived as a database for simulation validation.

Point of Contact: L. Cicolani
(650) 604-5446
lcicolani@mail.arc.nasa.gov

Canard Rotor Wing Conversion Test

C. W. Acree, Jr., John F. Madden

The canard rotor wing (CRW) design was initiated by McDonnell Douglas Helicopter Systems (now Boeing) for high-speed, vertical takeoff and landing unmanned air vehicles. The teetering, reaction-drive rotor has a symmetric airfoil, allowing it to be stopped and started in flight with good dynamic performance. Conversion from rotary-wing to fixed-wing flight and vice versa at high speeds is the greatest technical challenge of the CRW. A test of a half-scale model in the Ames 7- by 10-Foot Wind Tunnel (first figure) demonstrated full conversions of the bare rotor at airspeeds up to 150 knots. Rotor loads were benign throughout conversion.

The rotor, which is the critical dynamic component of the CRW vehicle system, is illustrated in the second figure. The rotor provides lift for takeoff and landing as it would in a conventional helicopter. The aft-mounted wing and large canard (forward wing) provide lift in cruising flight, which allows the rotor to be stopped and started while unloaded. With the rotor stopped, the CRW can attain much higher speeds than conventional rotorcraft.

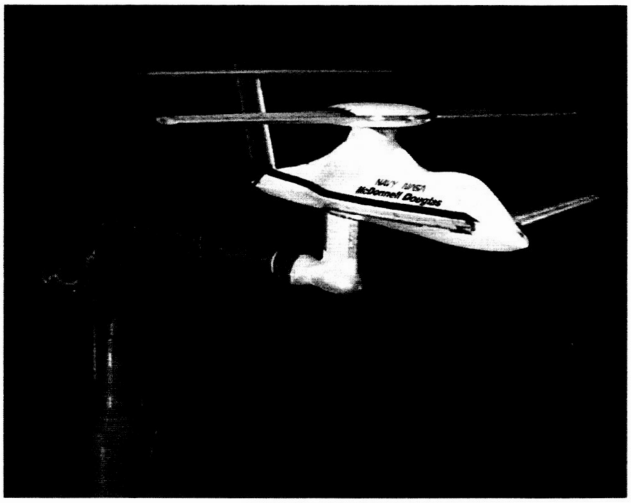

Fig. 1. The CRW rotor (half-scale) in the Ames 7- by 10-Foot Wind Tunnel.

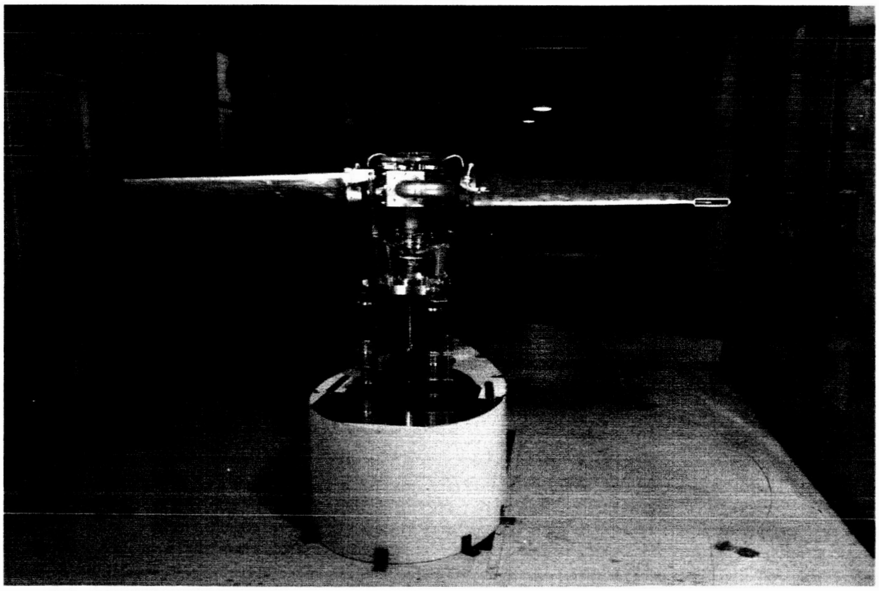

Fig. 2. The CRW fixed-wing model in the Ames 40- by 80-Foot Wind Tunnel.

The rotor is driven by high-pressure air ejected through tip nozzles, which eliminates the need for the usual transmission. The flight vehicle will use turbofan engines to supply high-pressure air to the rotor. In the wind tunnel test, the Ames high-pressure air supply system was used to simulate the engine exhaust.

Previous tests at Ames evaluated performance at high speeds (rotor stopped) and in hover. In the latest test, full conversion was achieved at 150 knots, both with and without hub springs. The test included measurements of rotor loads, stability, control power, and forward flight performance.

Test preparations included addition of a 0.5-megawatt heater to the high-pressure air supply, upgraded air-supply valves, and improved safety protection for the control room. Boeing provided the data-acquisition system.

Point of Contact: C. Acree, Jr.
(650) 604-5423
wacree@mail.arc.nasa.gov

Advanced Methods for Testing Rotor Performance

Francis X. Caradonna

A principal advantage of rotorcraft is their ability to hover, and the efficiency with which they can hover is fundamental to helicopter productivity. It is surprising, therefore, that the ability to predict hover efficiency (and thus design optimum rotors) is limited. This is because the rotor flow field is so sensitive to the rotor wake that there are large analytical errors. This same wake sensitivity also causes large experimental errors. (If a perfect prediction capability existed, there would be no way to know it, because of experimental error.) Therefore, the attainment of greater rotor analysis capability is a twofold problem of improving both computational and experimental accuracy. This effort is directed at the experimental part of the problem.

Measuring hover performance experimentally is complicated, principally because hover flows are plagued by a range of errors that are related to the

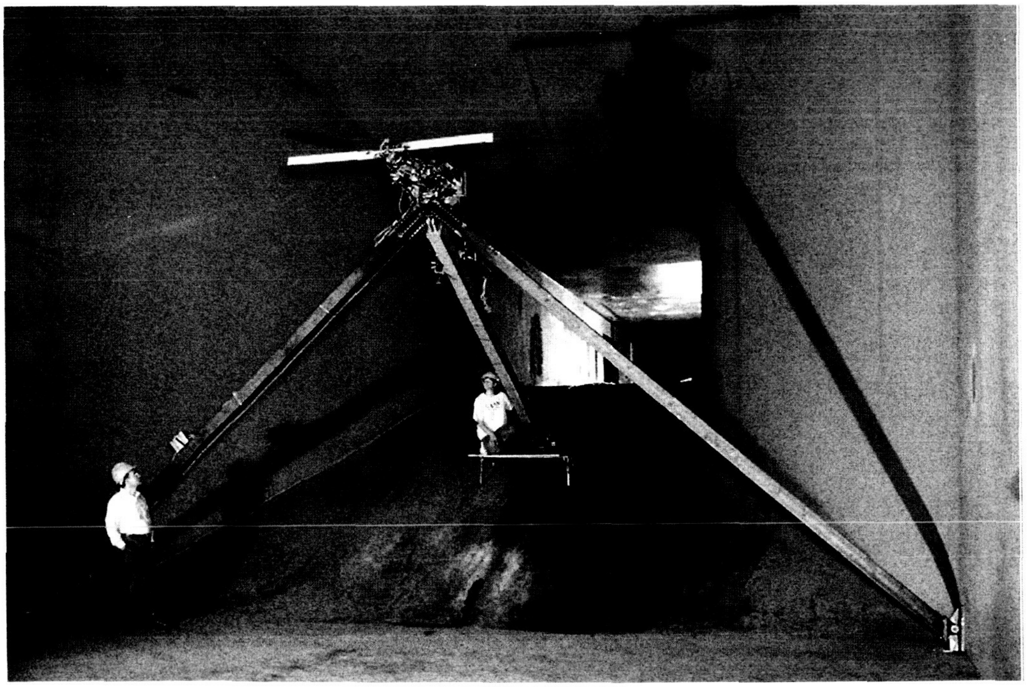

Fig. 1. Setup used to test model rotors in climb.

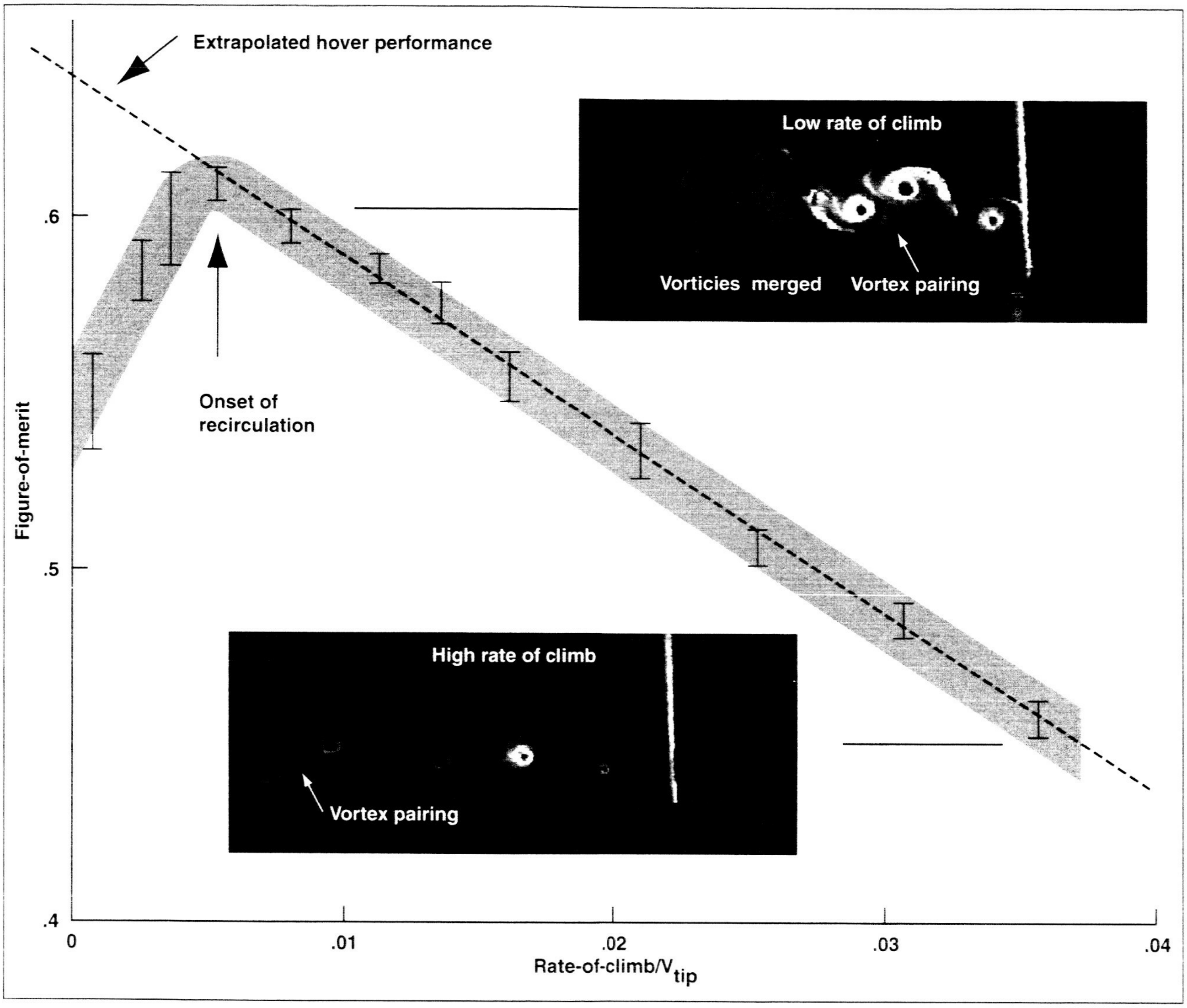

Fig. 2. Plot of the effect of climb on rotor efficiency. The data are very steady and are a linear function of climb rate until the onset of flow recirculation at very low climb. The linear trend can be extrapolated to find the hover performance.

wake sensitivity and to the effects of the ambient environment (including wind effects in outdoor testing and recirculation effects in test chambers). Recently, a new approach to model-rotor performance measurement has been tested. In this approach, the model is mounted horizontally in a wind tunnel settling chamber, thereby simulating climb. The resulting flows are found to suppress chamber recirculation to low-rate-of-climb levels that approach hover very closely. It appears that reliable hover performance can be obtained by a straightforward extrapolation of these climb results. The first figure is a photograph of the test setup in the settling chamber of the Ames 7- by 10-Foot Wind Tunnel. The reliable data trends obtained with this test arrangement are demonstrated in the second figure. The insets in this second figure show the high quality flow visualizations of the rotor wake obtained with this setup—this is a result of the very steady flow that this test approach produces.

Point of Contact: F. Caradonna
(650) 604-5902
fcaradonna@mail.arc.nasa.gov

Computational Fluid Dynamics in Rotor Design

Francis X. Caradonna

Rotorcraft are important because they can hover, and the efficiency of this hover is fundamental to helicopter productivity. It is surprising, therefore, that our ability to predict hover efficiency (and thereby to design optimum rotors) is limited. This is because the rotor flow field is so sensitive to the rotor wake that there are large analytical errors. This same wake sensitivity also causes large experimental errors. (If a perfect prediction capability existed, there would be no way to know it, because of experimental error.) Therefore, the attainment of greater rotor analysis capability is a twofold problem of improving both computational and experimental accuracy. This effort is directed at the computational part of the problem.

The classic problem with the methods of computational fluid dynamics (CFD) is that numerical dissipation severely degrades the wake prediction. The method of vorticity-embedding is unique in that it is the only CFD method that totally obviates this dissipation. This unique ability enables the use of small grids and permits practical computation of the compressible, free-wake rotor flow. This method is now being applied to the analysis of specific rotor configurations in an effort to maximize the hover efficiency that can be attained with currently used fabrication technology.

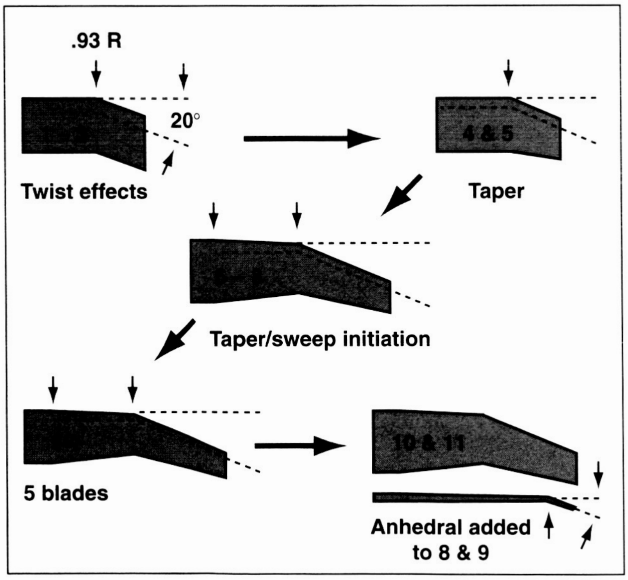

Fig. 1. The tip sections of some rotors under study showing a path of rotor configuration variations leading to an enhanced hover efficiency.

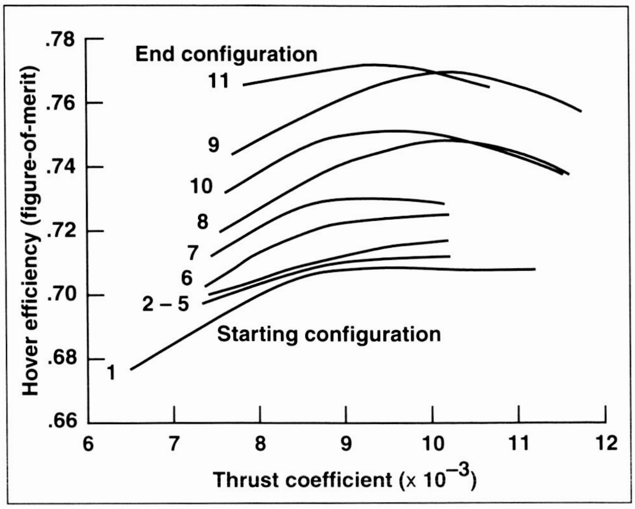

Fig. 2. Graphs of computed rotor efficiency computations performed using vorticity-embedded CFD. These efficiency plots correspond to the configurations shown in the first figure.

The first figure shows one of several configurational development paths that are now being studied. This configurational evolution path includes the combined effects of sweep, taper, twist, and anhedral. The second figure shows the range of performance improvements obtained through this range of configurations. In this particular case the starting rotor is an AH-64A rotor and the resulting efficiency increases are sufficient to increase payload by about 1000 pounds.

Point of Contact: F. Caradonna
(650) 604-5902
fcaradonna@mail.arc.nasa.gov

Control/Display Integration Issues for STOVL Aircraft

James A. Franklin

As a member of the Joint Strike Fighter program team, Ames Research Center is participating in technology development for short takeoff and vertical landing (STOVL) fighter aircraft. NASA's role in the program is to develop design guidelines for integrated flight/propulsion controls, to support technology development for a demonstrator aircraft, and to provide consultation on integrated control design to industry participants. The choices of control response types and of pilot/vehicle interface strongly influence the operational capability for STOVL aircraft. Design criteria are being developed for response characteristics for integrated control systems that have the potential to significantly reduce pilot workload in STOVL operations.

As part of NASA's effort, a simulation model was developed of a lift-fan configuration that represents a prospective STOVL design (see figure). This simulation has recently been used to conduct STOVL operations on the Vertical Motion Simulator at Ames to (1) evaluate the integration of the throttle inceptor with flight-control laws for direct thrust command for conventional flight and for vertical and short takeoff, and for vertical-velocity command for transition and vertical landing; (2) evaluate control-mode blending for transition from wing-borne to jet-borne flight; and (3) evaluate the effect of conformal versus nonconformal presentation of flightpath and guidance display symbols for STOVL operations.

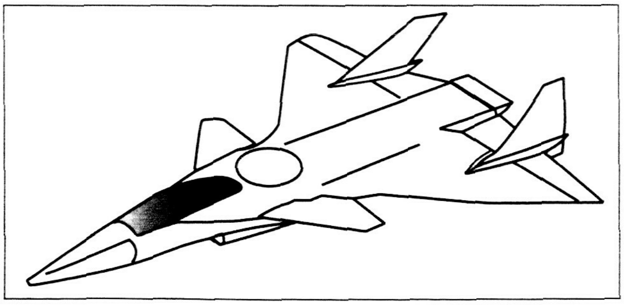

Fig. 1. STOVL lift-fan aircraft.

In the simulations, throttle inceptor integration for thrust and flightpath control functions performed free of transients at mode switch and provided satisfactory control sensitivity to the pilot. Level 1 pilot ratings were obtained for the flightpath and vertical velocity command modes for STOVL land-based and shipboard operations. Blending of pitch control from wing-borne to jet-borne flight was accomplished successfully over a range of speeds in which control of flightpath with attitude becomes ineffective. Blending of roll control was performed over a speed range in which turn-coordination in wing-borne flight gives way to lateral-velocity translation in hover. Blending of yaw control was performed over a broad speed range to reduce abrupt yaw transients as the aircraft accelerates in takeoff or through transition to wing-borne flight. Pilots appreciated conformality of the flightpath and guidance symbols during the approach to hover. However, sensitivity of the symbols for lateral path tracking increased pilot control activity, particularly in the presence of turbulence. Satisfactory tracking accuracy could be achieved with reduced control activity with the symbols scaled less than 1:1. This preference was reinforced by the need to convert the flightpath symbol to scaled lateral velocity at low speed approaching the hover, where angular relationships are inappropriate for lateral flightpath control.

Point of Contact: J. Franklin
(650) 604-6004
jfranklin@mail.arc.nasa.gov

Improved Experimental/Computational Aerodynamics Comparisons

Michael Olsen

Improved turbulence modeling requires accurate computational simulation of carefully controlled experiments. Discrepancies between computational predictions and experimental results are the measure of turbulence model performance. The simulation of experimental conditions is one possible source of discrepancy between computation and experiment. This problem is most acute for the separated flow cases, in which small changes in experimental conditions can sometimes change the flow substantially. An improvement in the simulation of the wind tunnel walls dramatically improves the simulation of wind tunnel experiments at transonic speeds, the speed range in which civil transport aircraft fly.

The improved simulations include the effect of the tunnel-wall boundary layers. The boundary layer is a region, very close to a wall, where the airspeed changes dramatically in a very small distance. In this work, the fidelity of experimental simulations is increased by computing, instead of approximating, the effects of the tunnel-wall boundary layers.

The first figure shows pressures measured on the wind tunnel walls compared with those predicted using the old method (inviscid walls) and the improved method (viscous walls). The viscous-wall simulations improve the prediction of the experimentally measured pressures over the entire tunnel length. The most important differences, however, occur near $x_0 = 0$, where the wing is located. The inviscid-wall solution matches the upper "suction" pressures reasonably well, but misses the lower "pressure" surface by a substantial margin.

Experimental wing pressures are compared with the results of computations in the second figure. Both "viscous-wall" and "inviscid-wall" simulations match the experiment on the wing upper surface. Only the viscous-wall simulations match the lower surface pressures, however. This discrepancy is tied directly

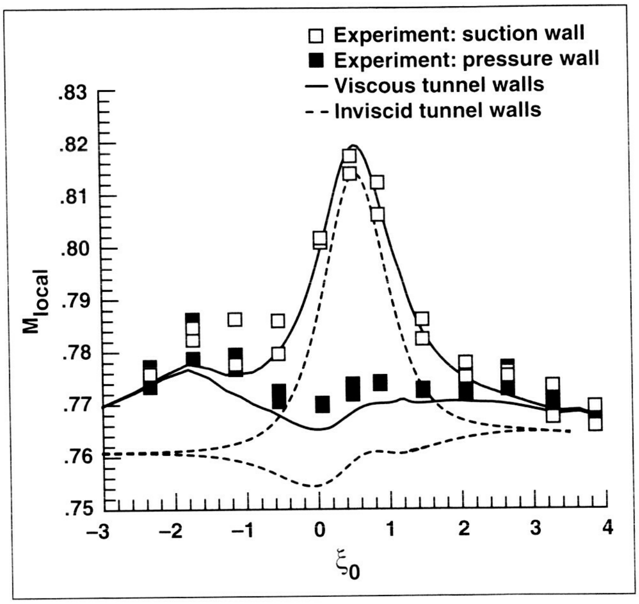

Fig. 1. Wall pressures.

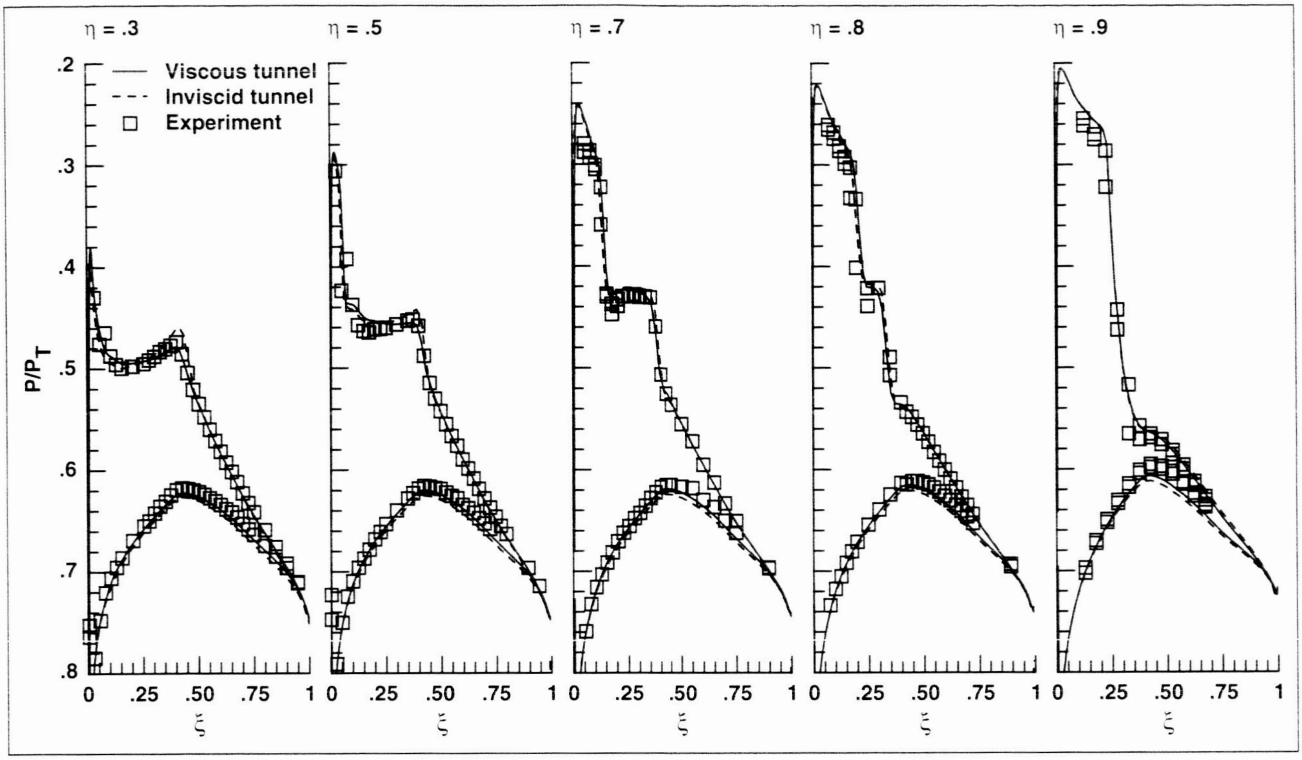

Fig. 2. Wing pressures.

to the effects of the wing pressure field on the tunnel-wall boundary layers. The tunnel-wall boundary layers create an effect similar to that of the divergence of the tunnel walls around the wing, lowering the effective Mach number (airspeed). By including the viscous-wall effects in computational simulations, the local environment of the wing is more accurately simulated.

Point of Contact: M. Olsen
(650) 604-6200
molsen@kyzyl.arc.nasa.gov

Turbulence Modeling Validation Study

J. E. Bardina, P. G. Huang, T. J. Coakley

The present study is part of an ongoing effort to evaluate and develop turbulence models for aerodynamic applications. The objective of the study was to investigate the performance of several turbulence models on a variety of aerodynamic flows and to make recommendations regarding their applicability in aeronautical applications. The models studied were the Jones-Launder k-ε model, the k-ω model of Wilcox, the one-equation model of Spalart and Allmaras, and the two-equation k-ω shear-stress transport (SST) model of Menter. Ten flows were investigated including five free-shear flows and five boundary-layer flows, of which three were complex flows involving separation or shock waves or both. The results of numerical predictions were compared with experimental results, which included surface pressures, skin friction, and profiles of velocity and turbulent kinetic energy and shear stress.

The turbulence models were evaluated on the basis of numerical accuracy with respect to experimental results, numerical sensitivity to grid spacing and refinement, sensitivity to free-stream turbulence conditions, and the choice of the numerical code. Typical results of the study are shown in the figures.

Model Performance

Model	k-ω	k-ε	S-A	SST
Mixing layer	□	■	■	■
Far wake	□	○	■	○
Plane jet	□	■	○	■
Round jet	□	●	□	●
ZPG BL	■	■	■	■
APG BL	○	□	●	■
Trans. bump	○	□	▲	●
RAE 2822	○	□	▲	●

Scale: (Bad) □ ○ ▲ ● ■ (Good)

Fig. 1. Numerical grid and surface pressure distributions for the RAE 2822 transonic airfoil (case 10).

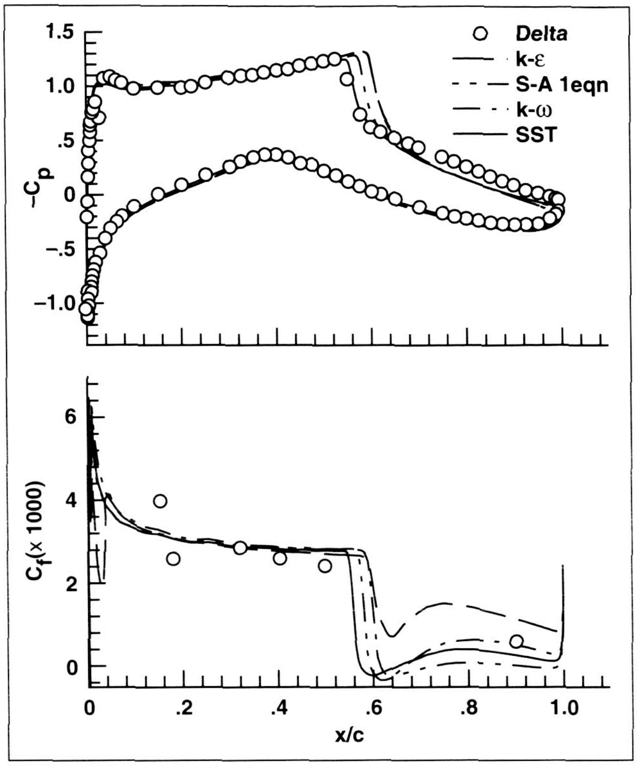

Fig. 2. Numerical performance and sensitivity ratings of turbulence models.

The first figure shows the results for a transonic airfoil flow and indicates the numerical grid used and the measured and computed pressures and skin friction on the surface of the airfoil. Results comparing the performance of the four models for eight of the flows studied and the model sensitivity to various conditions are shown in the second figure. From these results it was found that the Menter SST model gave the best overall results followed by the Spalart-Allmaras model and then the k-ω and k-ε models. With respect to sensitivity, the Spalart-Allmaras model gave the best results, closely followed by the SST model and then the k-ω and k-ε models.

Point of Contact: J. Bardina
(650) 604-2150
jbardina@mail.arc.nasa.gov

Boundary-Layer Receptivity

Anthony J. Dietz

Accurate prediction of boundary-layer transition is crucial to the solution of a wide range of fluid dynamics problems, from the design of low-drag airfoils to the estimation of reentry heat loads. In many flows, transition begins with a receptivity process, in which boundary-layer instabilities are excited by disturbances in the free stream. Understanding of this process has come a long way in recent years. A particular Ames contribution has been in the area of receptivity to vortical disturbances.

An experiment was conducted in a low-turbulence research wind tunnel to investigate the vortical receptivity mechanism in a controlled flow. Small vortical disturbances were introduced into the free stream by a vibrating ribbon, and the effect of these disturbances on the boundary layer of a flat plate was measured with hot-wire anemometry. According to current receptivity theory, a receptivity site with a short-scale variation in the boundary-layer mean flow is required to convert the typically long-wavelength free-stream disturbances into short-wavelength boundary-layer instabilities. Strips of very thin polyester tape were fixed to the surface of the plate to provide such a site.

The first series of tests involved continuous single-frequency disturbances. No instability waves could be detected without roughness on the plate. However, with roughness present, instability waves were measured at downstream locations. The mode shape, growth rate, and phase speed of the waves matched that of the Tollmien-Schlicting (TS) waves predicted by linear-stability theory. Linear-stability calculations were then used to determine the immeasurably small initial amplitudes of the waves at the roughness location from amplitudes measured downstream, thus separating the receptivity (generation) characteristics of the waves from their stability (growth) characteristics.

The experimentally obtained receptivity coefficients agreed well with those predicted by receptivity theory, and both followed similar trends with frequency and Reynolds number. However, these results pertained to continuous single-frequency waves, whereas real-world flows contain broadband transient disturbances. Broadband pulse and random disturbances could also be generated by the ribbon. The response to a pulse disturbance is shown in the first figure, where a TS wave packet, generated by an interaction between the convected pulse and the surface roughness, can be seen lagging the pulse disturbance. The lower propagation speed of the wave packet has separated the two phenomena, allowing each to be analyzed independently.

The receptivity coefficients calculated for pulse and random disturbances are compared with single-frequency coefficients in the second figure. Similar results were obtained for all three disturbance types, demonstrating that the single-frequency theories are applicable to transient and broadband disturbances. The results also confirmed theoretical predictions that receptivity to distributed roughness is nearly an order of magnitude greater than that for single roughness, and that the results for distributed roughness are highly tuned to a resonant frequency at which waves generated at successive roughness elements are in phase and add constructively.

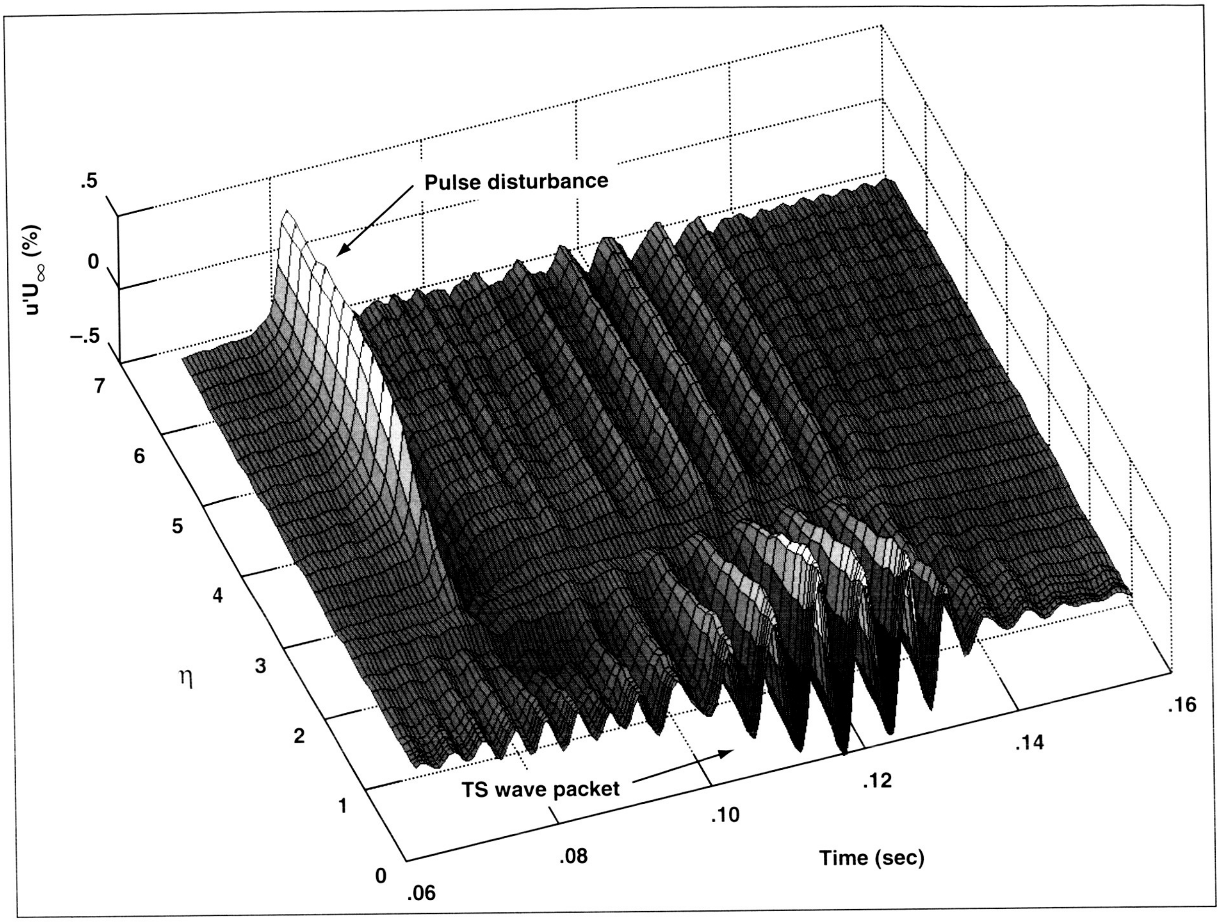

Fig. 1. Boundary-layer response to a pulse disturbance measured downstream of an array of roughness elements. Phase-locked averaged time records of the streamwise velocity fluctuations u', normalized by the free-stream velocity U_∞, are plotted against the nondimensional height above the plate surface $\eta = y/(2\nu x/U_\infty)^{1/2}$.

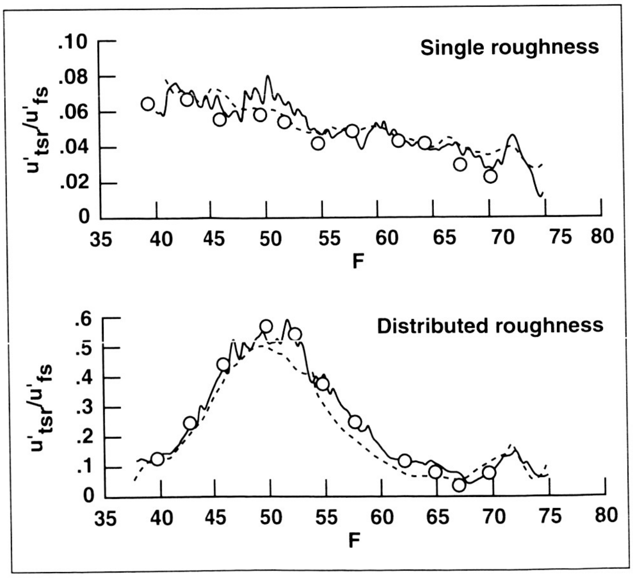

Fig. 2. Variation of receptivity coefficient with frequency for three disturbance types at single and distributed roughnesses. TS wave amplitude at the roughness location (u'tsr) normalized by the free-stream disturbance amplitude at the edge of the boundary layer (u'fs) plotted against the frequency parameter $F = 2\pi f\nu/U_\infty^2 \times 10^6$; single frequency (o), pulse (- - -), random (——).

This experimental verification of the mechanism behind receptivity to convected disturbances is a step toward the still-unrealized goal of transition criteria, which include free-stream disturbance characteristics. Current prediction techniques do not take the free-stream disturbance environment into account and so miss an important aspect of the problem.

Point of Contact: A. Dietz
(650) 604-4137
adietz@mail.arc.nasa.gov

Evolution of Strained Plane Wakes

Michael M. Rogers

Turbulence models currently have difficulty predicting the response of turbulence to additional strains, such as those arising in the flow over a multicomponent airfoil designed to produce high lift. In particular, as the turbulent wake of an upstream airfoil component encounters the pressure gradient produced by a downstream component, it is strained. The response to this strain is poorly predicted by existing turbulence models.

In order to provide insight into the behavior of such flows and to provide a database to aid turbulence modelers, several direct numerical simulations of strained plane wakes have been generated. These simulations are made in a reference frame moving with the free-stream velocity outside the wake and thus they evolve in time. Such temporally evolving flows are computationally simpler to generate and therefore it is possible to achieve higher Reynolds numbers and more realistic turbulence. In the limit of small wake deficits the equations governing the temporally evolving problem are identical to those describing a spatially evolving flow, such as that of a wake in an adverse pressure gradient.

Previous direct numerical simulations of unstrained wakes have been used to generate the initial conditions for the strained wake computations. Once the unstrained wake reaches an apparently self-similar state, the strain is applied to generate the strained wake cases. Six different plane strain geometries have been applied to the wake, with the directions of compression and expansion associated with the strain being aligned with the coordinate axes. The case with compression in the streamwise direction and expansion in the cross-stream (inhomogeneous) direction corresponds to that of a wake developing in the presence of an adverse pressure gradient.

Analysis shows that there is a possible self-similar state for wakes subjected to strain applied at a constant rate. Both the peak velocity deficit of the wake and the wake width are predicted to evolve exponentially in time, with the exponent in both cases being equal to half of the difference between the cross-stream and streamwise total strains. All the Reynolds stresses are predicted to scale with the square of the peak velocity deficit in this self-similar state.

The simulated flows typically do not evolve according to this self-similar solution, although the wake velocity deficits and widths do change exponentially. The wake width in flows that are compressed in the cross-stream direction approaches a constant, whereas it increases exponentially at the same rate as the global strain in flows that are expanded in the cross-stream direction (see figure). For flows in which the cross-stream direction is unstrained the wake spreads at a rate that is similar to the unstrained case. For the case that is analogous to a wake developing in an adverse pressure gradient this is consistent with the rate predicted by the self-similar analysis, and indeed this case does appear to be evolving in accord with the predicted self-similar solution.

The wake mean velocity profile is largely unaffected by the geometry of the strain, remaining approximately Gaussian throughout the flow evolution in all cases. The behavior of the Reynolds stresses, however, varies dramatically, depending on the strain geometry and on whether the global mean strain produces or destroys a particular Reynolds stress component. In most cases (although not in the adverse pressure gradient case), the mean shear

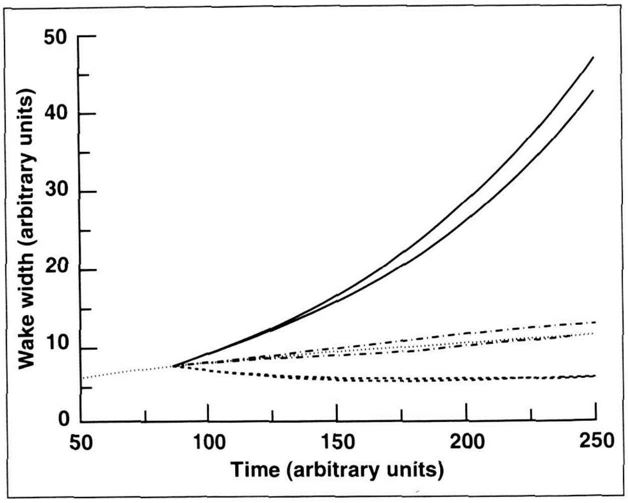

Fig. 1. The evolution of wake widths for a turbulent wake subjected to various plane strains. Solid lines denote flows stretched in the cross-stream direction; dashed lines, flows compressed in the cross-stream direction; and chain-dotted lines, flows with no strain in the cross-stream direction. The dotted line is the result from the unstrained wake simulation.

associated with the wake is found to decay and the flow evolves toward a pure straining flow.

The combination of turbulence production through both strain and time-varying wake shear provides a difficult test case for turbulence models. All terms in the Reynolds stress balance have been computed at several times for each of the simulations and are being compared with predictions of various turbulence models. The detailed information available in the simulations will provide guidance on how to improve the existing models so that they will better predict the turbulent flow over a high-lift airfoil.

Point of Contact: M. Rogers
(650) 604-4732
mrogers@nas.nasa.gov

A Model for the Limiting Piston Stroke in Vortex Ring Formation

K. Shariff

Many devices eject a mass of fluid either in one shot or periodically. Examples include heart valves and flapping wings. Often the goal is to maximize the volume of fluid moving as a coherent vortex ring away from the exit. M. Gharib (California Institute of Technology) used a piston to experimentally study fluid ejected from a pipe and found that the largest coherent mass of fluid was attained at a piston stroke (normalized by diameter) of 4 under a variety of circumstances, including different histories of the piston motion. For longer strokes, the mass broke up into smaller vortices and a trailing jet. He also found that this maximum stroke, when expressed as a time, corresponds to the ejection period of many biological systems, including normal hearts.

The present contribution was a simple model that predicts the limiting stroke and the associated properties of the vortex such as circulation. Reasons for insensitivity to piston motion emerge from the model, and piston motions that maximize the ejected mass were obtained.

The model is based on Lord Kelvin's (1880) result that among all vortex motions with given impulse and circulation, the steady one has maximum energy. In the present situation, one finds that after a certain critical piston stroke, one cannot keep feeding enough energy (in comparison with impulse and circulation) to maintain this maximum and so the vortex becomes unsteady. This critical value agrees with the experiments, is quite insensitive to different piston histories, and correctly predicts the slight dependencies observed experimentally. Subsequently, numerical simulations by M. Rosenfeld

(Tel-Aviv University) found a strong sensitivity of the limiting stroke to the exit velocity profile and a lack of sensitivity of ring circulation to both the exit profile and piston motion. The model reproduces these facts as well. Finally, using an inverse design procedure, piston histories were found that may overcome the limit at a stroke-to-diameter ratio of 4 and thereby lead to larger coherent masses.

Point of Contact: K. Shariff
(650) 604-5361
shariff@nas.nasa.gov

B-Spline Method for Turbulent Flow Simulation

A. Kravchenko, P. Moin, K. Shariff

B-splines are an attractive basis for a numerical method. Because of the continuity of a high number of derivatives, B-splines have resolving power approaching that of spectral functions, but provide greater flexibility in geometry and grid distribution. They are not as flexible as finite elements, but they are much more accurate for the same number of degrees of freedom. Furthermore, if they are used in a Galerkin formulation, the resulting scheme conserves not only the discretized quantities (such as mass and momentum) but quadratic invariants as well (such as kinetic energy for inviscid incompressible flow). This protects the scheme against aliasing and ensures that there is no numerical smoothing of the unresolved scales of motion.

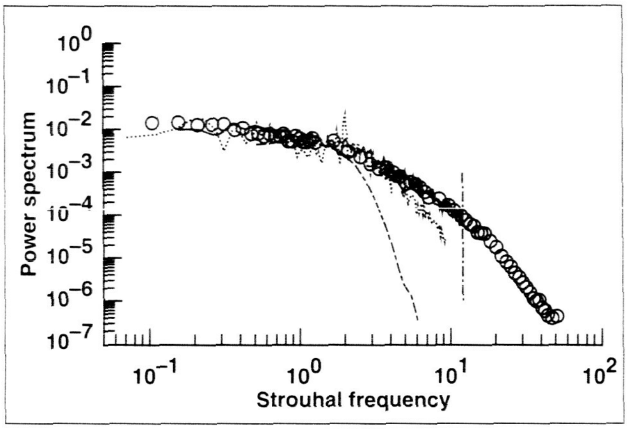

Fig. 1. Frequency spectrum of velocity fluctuations in the wake of a circular cylinder showing the resolving power of various schemes.

The B-spline method was implemented for incompressible flow in two generalized coordinates using a Galerkin formulation. Fourier expansions are used for the third direction. The B-spline zonal mesh capability developed by Shariff and Moser (1995), which gives the same high degree of derivative continuity at zonal boundaries as everywhere else, is used. It increases gridding flexibility and leads to a significant reduction in the number of grid points required. Basis vectors are used that already satisfy the incompressibility constraint. This leads to a reduction in the number of degrees of freedom from four to two per grid point. However, there is a high cost associated with calculating the Galerkin nonlinear term and in inverting the mass matrix. More work is required to improve the efficiency of the method.

In the figure, the experimental (symbols) and computed (lines) frequency spectra in the wake of a turbulent flow past a circular cylinder at a Reynolds number of 3900 are compared. The computations are all large-eddy simulations with the dynamic model. The curves show the result of three different numerical methods. The B-spline method (solid line) with quadratic basis functions gives excellent accuracy up to the smallest scale it resolves (shown by the chain-dotted vertical line). The energy-conserving second-order finite-difference scheme (dashed) is accurate for a smaller range of frequencies, whereas the fifth-order upwind biased scheme (chain-dashed) is much too dissipative for a large range of scales.

Point of Contact: K. Shariff
(650) 604-5361
shariff@nas.nasa.gov

Low-Speed Pressure-Sensitive Paint Research

Rabindra D. Mehta, Owen C. Brown

Pressure-sensitive paint (PSP) is a relatively new measurement technique used in aerodynamic wind tunnel testing. PSP contains a unique sensor molecule that can be excited with light that has an appropriate wavelength. The excited sensor molecule returns to its original state by re-emitting light, or by reactions with nearby oxygen molecules in a process known as "oxygen quenching." The emitted intensity of excited PSP is therefore directly proportional to the local partial pressure of oxygen and hence to the local pressure at the painted surface. Scientific grade charge-coupled device (CCD) cameras are used to record digital images of wind tunnel models painted with PSP. Images are taken with the wind tunnel running and with the wind tunnel turned off (this latter image serving as a reference). Software is used to calibrate the ratio of the wind-on and wind-off image intensities to pressures at various points on the model sensed by conventional pressure taps. Since the intensity-versus-pressure relation is (ideally) linear, only a few pressure taps are needed for proper calibration.

The use of PSP offers a dramatic process improvement in design and testing. PSP provides the capability to record the complete pressure field over a model surface with high spatial resolution. Wind tunnel models can be constructed with only a few pressure taps instead of the thousands of taps typically needed for structural load modeling. This saves precious design-cycle time that would otherwise be spent in constructing a complicated model.

PSP measurements are typically performed at Mach 0.2 or higher. Below these speeds, the intensity changes of the paint (as caused by pressure differences) become relatively small. External factors then interfere with the ability to accurately detect such minute signals. These factors include temperature effects (PSP intensity is also unfortunately influenced by temperature changes), registration errors between the ratioed wind-on and wind-off images, and electronic noise within the CCD camera.

However, PSP measurements at speeds below Mach 0.2 are of potential value. It is in this speed realm that measurements using PSP would be valuable to designers of vertical/short takeoff and landing aircraft, small-scale unmanned air vehicles, and automobiles. Experiments are being conducted at Ames Research Center using PSP on aerodynamic models at low speeds in an effort to further quantify measurement constraints and improve low-speed measurement techniques.

PSP experiments have been conducted in a 12- by 12-inch research wind tunnel on a NACA 0012 airfoil. Data have been obtained in a speed range of 10 to 50 meters per second (equivalent to 22 to 112 miles per hour).

The sources of errors inherent in PSP testing were minimized in an effort to obtain good response in this low-speed test regime. Data acquisition procedures were implemented to allow temperatures to properly stabilize on the model, thus minimizing temperature changes on the model and thereby reducing the effects of temperature-induced errors. A new camera-lighting stabilization mechanism was built that substantially reduced the model movement relative to the imaging equipment. Data averaging methods were applied to reduce electronic CCD noise.

Using the above technique, PSP measurements have been made, with good results in the 10-to-50-meter-per-second speed range. The calibration errors between the PSP pressures and tap pressures are very close to the current theoretical limits of PSP accuracy, and they are among the best currently published.

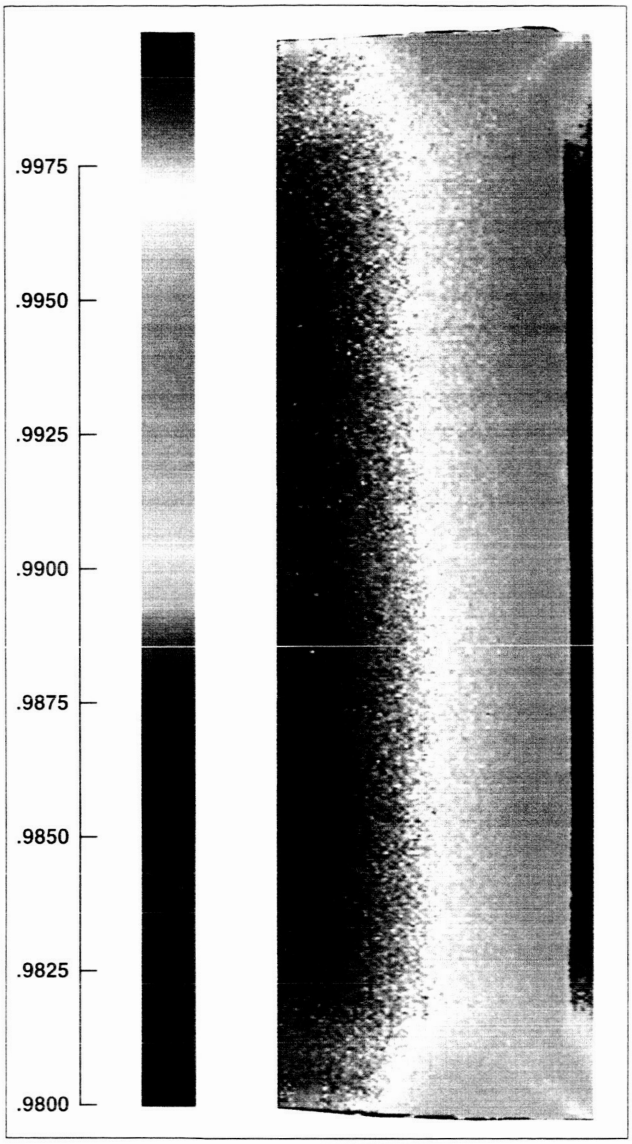

Fig. 1. PSP-measured pressure field on NACA 0012 wing: angle of attack 5 degrees, velocity 30 meters per second.

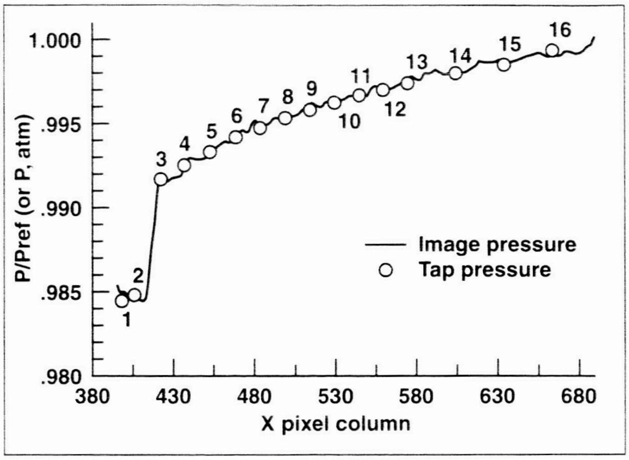

Fig. 2. PSP-measured pressure field versus pressure-tap data.

The first figure shows the pressure field on the NACA 0012 wing at 30 meters per second and at an angle of attack of 5 degrees. The pressure scale is in atmospheres, with the airflow from right to left in the image. The second figure displays the pressures measured by the PSP on the airfoil from leading edge to trailing edge, compared with pressures measured using conventional pressure taps. The root-mean-square error between tap and calibrated PSP pressures is 21.8 pascals (0.04 coefficient-of-pressure units).

Point of Contact: R. Mehta
(650) 604-4141
rmehta@mail.arc.nasa.gov

Area Measurement of Skin Friction in Complex Three-Dimensional Flows

James. L. Brown

A surface-imaging skin-friction instrument provides measurement of the wall shear-stress vector over a large surface region during a single wind tunnel test using an oil-film interference method. During a test, a camera captures images of the fringe pattern produced by illuminating an oil film with quasi-monochromatic light. By using a visual tracer in the oil, the surface streamlines can also be determined. Analysis of the fringe images using a Hilbert-transform-based technique determines the oil thickness distribution in the region where fringes are visible. A combination of the oil thickness and surface direction is then used to calculate the surface shear-stress distribution by numerically solving the thin-oil film equation:

where τ_x and τ_z are the *x*- and *z*-components of the surface shear stress, and μ is the dynamic viscosity of the oil. All quantities in this equation are known from the height measurement except τ_x and τ_z. However, an additional piece of information is needed to solve this equation. If the surface streamline direction γ is obtained from visual tracers or from a streamline image, then $\tau_x = \tau \cos(\gamma)$ and $\tau_z = \tau \sin(\gamma)$, and the equation may be solved for τ.

To test the technique in a demanding situation, it was applied to a three-dimensional (3-D) flow in which a cylinder is mounted normal to a flat plate. An incoming turbulent boundary layer encounters the vertically mounted cylinder and a highly complex 3-D flow results. The first figure shows oil interferograms taken in this flow indicating regions of reverse flow. These images are analyzed, along with surface

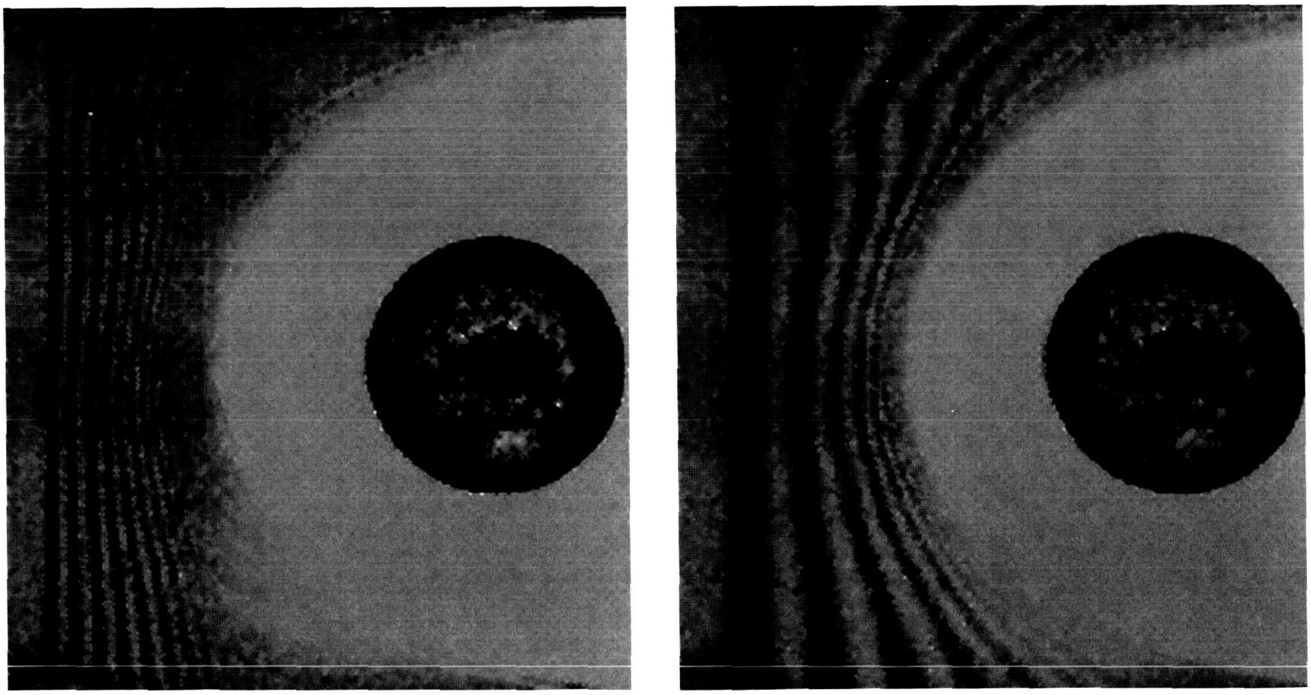

Fig. 1. Oil-film interferogram fringes in front of a cylinder mounted normal to a flat plate.

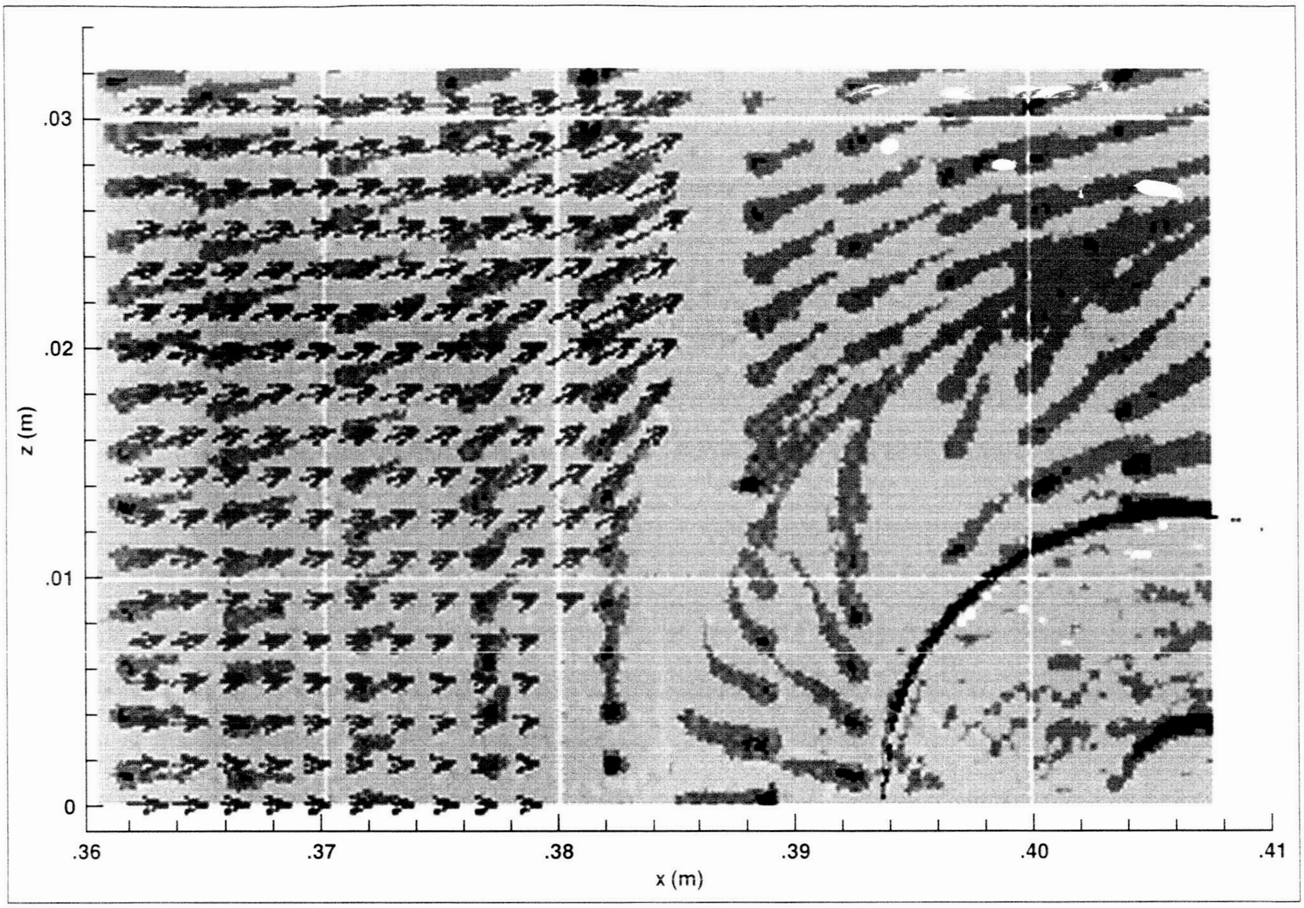

Fig. 2. Shear-stress vectors for a cylinder mounted normal to a flat plate.

streamline images, to determine the surface shear-stress vector field that is shown in the second figure.

The application of the method to the normal cylinder experiment indicates the ability of the instruments to perform in actual flow fields—even in those that are highly complex. An extensive development of the theory has been accomplished to verify the accuracy and theoretical rigor of the analysis techniques used for 3-D flows. A patent assigned to NASA has been applied for and the technology is available for license.

Point of Contact: J. Brown
(650) 604-6229
jlbrown@sunrfe.arc.nasa.gov

Global Interferometric Skin-Friction Measurements on a Wingtip Model

Gregory Zilliac

Skin-friction distribution on surfaces of flight vehicles is desirable for several reasons. Aerodynamicists would like to know where transition occurs and if separation is present. Turbulence modelers are interested in validating skin-friction (drag) predictions. Finally, if it were possible to sum the skin-friction distribution on a lifting wind tunnel model, it would be possible to determine the viscous contribution to the total drag, a quantity not readily measured independently of the induced drag. For these reasons research scientists have expended a great deal of energy in an ongoing effort to develop accurate, high-resolution skin-friction measurement techniques.

A high-resolution fringe-imaging skin-friction system (FISF) has been developed. Skin-friction measurements are made at points on an aerodynamic surface by imaging the flow of oil drops and applying lubrication theory to determine the skin-friction level. At the heart of this system is a wide-field digital camera capable of imaging 4096 × 4096 pixels. The system was recently tested on a wingtip model in the Flight Mechanics Laboratory's 3- by 4-Foot Indraft Wind Tunnel. Image data processing based on digital photogrammetry is a key component of the system and is the enabling technology that permitted the gathering of 2500 independent measurements of skin friction on a wing.

The figure shows the skin-friction magnitude on the suction side of a wingtip model from a Reynolds-averaged Navier–Stokes solver using a Baldwin–Barth turbulence model (left) compared with experimental measurements (right). This comparison shows reasonable agreement on the inboard portion of the wing where the flow is nearly two-dimensional. In the vicinity of the wingtip vortex (top-right corner), where the flow is highly three dimensional, substantial differences in the skin-friction magnitude are seen. These differences are attributed to the turbulence modeling deficiencies in the computed Navier–Stokes solution.

The FISF system described has recently been used in production tests of a Boeing 777 and also of a high-speed research model in the Ames 12-Foot Wind Tunnel.

Point of Contact: G. Zilliac
(650) 604-3904
gzilliac@mail.arc.nasa.gov

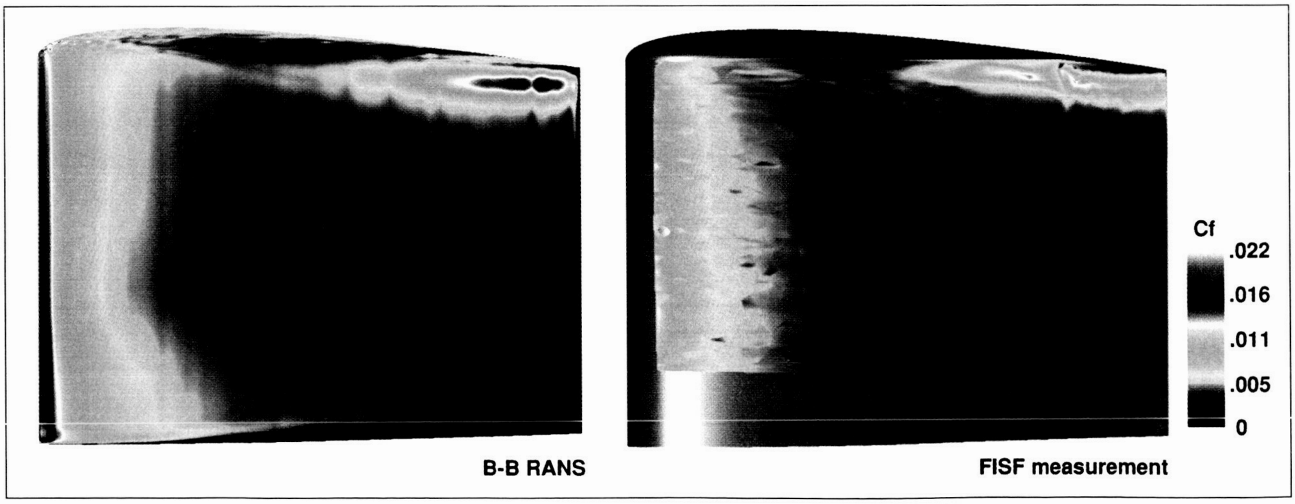

Fig. 1. Comparison of computed and measured skin friction on a wingtip (flow left to right).

Global Civil Aviation / Environmental Compatibility

Flight Test of Civil Tiltrotor Noise-Abatement Approach

William A. Decker, Rickey C. Simmons

Civil tiltrotor transports have the potential to relieve the growing congestion around the Nation's conventional airport runways. Operating as regional transports, civil tiltrotors can operate from airport vertipads, from short, unused runway segments, or directly from urban vertiports located near population and business centers. Safe, all-weather, low-noise terminal-area operations are needed to realize the tiltrotor's potential for improving the capacity of the air transportation system. Rotorcraft noise, particularly that associated with approach operations, must be minimized to facilitate location of vertiports close to population centers.

As first demonstrated for helicopters with a NASA UH-60 flight test, complex, decelerating, noise-abatement approach profiles can be developed from previous fixed operating-point noise measurements. Precision approach guidance can then be developed, using satellite-based position data, and displayed to the pilot on a flight director. Application of this method to the tiltrotor includes proprotor nacelle angle as an additional approach control. Building upon tiltrotor instrument operations experience and flight director design developed in the Ames Vertical Motion Simulator, tiltrotor noise-abatement approach profiles and guidance were developed for flight test using the XV-15 aircraft.

A test team composed of NASA (Ames and Langley Centers), Army, and Bell Helicopter Textron personnel developed 20 approach profiles, guided by a programmable flight director using differential global positioning satellite tracking data, and measured the resulting noise ground footprint. An approach profile, described by the altitude track, airspeed, and nacelle angle, and the resulting ground footprint of the noise for a segmented noise-abatement approach, is shown in the figure. The

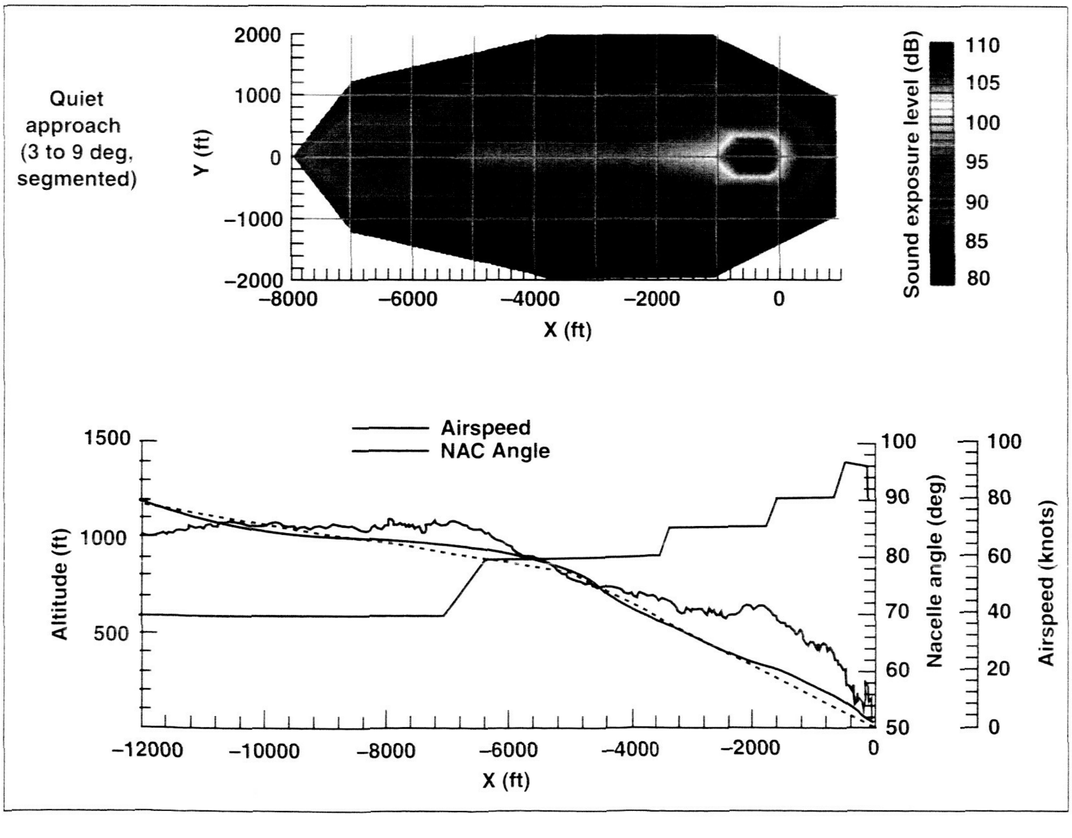

Fig. 1. Noise footprint (above) and approach profile track (below) for tiltrotor noise-abatement approach. The most intense noise is concentrated immediately around the hover pad.

approach profile and tracking are shown from 12,000 feet out from the hover pad. The ground microphone array for the noise footprint extended 8000 feet uprange from the hover pad and 1000 feet beyond. In the figure, the approach track shows the desired height-distance profile as a dashed line, with the actual position track shown as a solid line around it. Airspeed began at 70 knots. Decelerations are initiated by moving the nacelles farther aft, ultimately to the hover position of 90 degrees. Nacelle position is moved in discrete steps, beginning at 70 degrees. A small amount of full aft nacelle position (95 degrees) was used for braking just before coming to a hover over the landing pad. Careful control of the aircraft flight condition as conveyed to the pilot by the flight director results in the concentration of approach noise in the immediate environs of the landing pad while minimizing noise along the approach track.

Point of Contact: W. Decker
(650) 604-5362
wdecker@mail.arc.nasa.gov

Methods for Predicting Blade-Vortex Interaction Noise

F. X. Caradonna, C. Kitaplioglu, M. McCluer

Rotor-vortex interactions have been the subject of many experimental, analytical, and computational studies. Most of this activity is motivated by the importance of blade–vortex interactions (BVIs) as a major source of rotorcraft noise and vibration problems. The conceptual simplicity of the problem has encouraged the development of numerous computational methods, ranging from simple, incompressible two-dimensional analyses to full three-dimensional Euler/Navier–Stokes computational fluid dynamics (CFD) codes. However, experimental data of comparable simplicity were unavailable because of the difficulty of generating sufficiently clean vortices in a wind tunnel environment, and also because of the difficulty of acquiring corresponding loading and acoustic data. These experimental problems have been largely solved by the rotor/vortex-generator approach originally employed by B. McCormick (Pennsylvania State University) and later developed into a full aeroacoustic test at Ames Research Center. The first figure shows the rotor and vortex generator in the Ames wind tunnel setup.

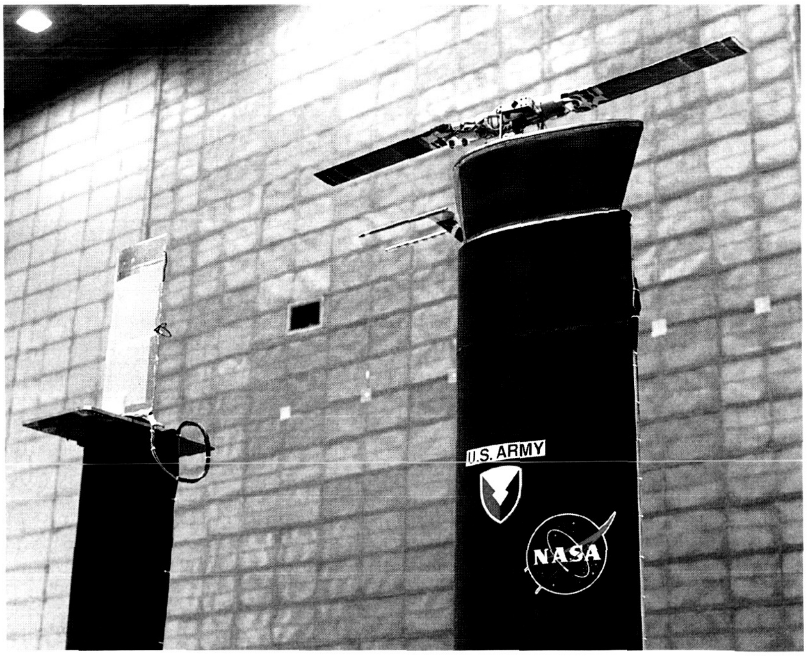

Fig. 1. Parallel BVI experiment in the Ames 80- by 120-Foot Wind Tunnel.

The data obtained from this test were suitable for evaluating computational models and became the focal point for an extensive correlation study. A wide range of participants from industry, academia, and government, both in the United States and abroad, contributed to the study. The results were collated by an ad hoc working group.

The study considered two simple parallel BVI interactions, a near-miss case and (to a more limited extent) a direct-hit case, and determined that the pressure and acoustic data (together with the inferred vortex model) are a suitable basis for the initial validation of computational models. A user of these data should expect to first obtain reasonable comparisons with these blade-surface and acoustic data before proceeding on to compute more complex interactions.

Overall, excellent results were obtained, indicating that a significant capability exists to predict the BVI interaction and its acoustic implications. Representative acoustic results are illustrated in the second figure. This does not imply, however, that the acoustic problem is solved. In this test the vortex location was well known and the vortex structure was fairly well defined. In a full rotor computation, however, these inputs are not known to a great degree of accuracy, and the ability to predict them is probably the greatest challenge for the future.

One of the most interesting results demonstrated that the simplest methods worked quite well compared with far more complex models. Of course, the BVI configuration under study is intrinsically simple and only acoustic applications are being considered. Full rotor-wake computations, wherein loads and performance must be predicted (in addition to acoustics), cannot be expected to yield so easily to the simplest approaches. Nevertheless, for particular, well-understood solution requirements, it is clear that great simplifications can be made.

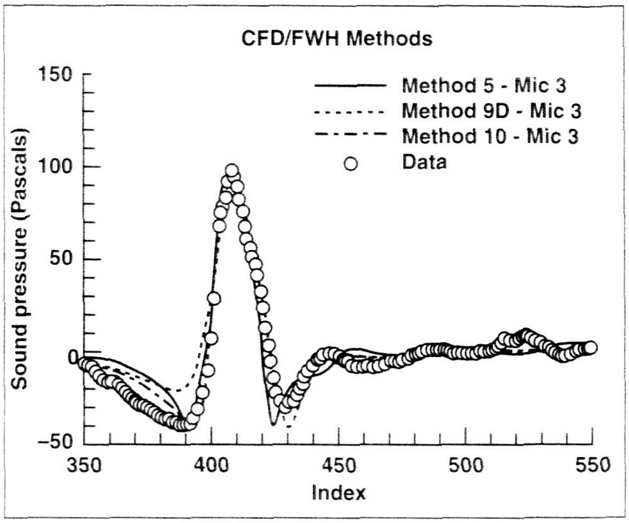

Fig. 2. Comparison of CFD/Ffowcs-Williams Hawkings methods for far-field noise with data for a near-miss parallel BVI.

Point of Contact: F. Caradonna
(650) 604-5902
fcaradonna@mail.arc.nasa.gov

Closed-Loop Neural Control of Rotor Noise and Vibration

Sesi Kottapalli

A study to identify and control helicopter rotor blade–vortex interaction (BVI) noise and vibratory hub loads using neural networks has been initiated at Ames Research Center. BVI noise can make a major contribution to the total rotorcraft noise, and can be annoying. The vibratory hub loads substantially determine the total rotorcraft vibration level. This vibration affects pilot and passenger comfort and the vehicle's structural fatigue life.

Current neural control simulation covers simultaneous control of BVI noise and vibratory hub loads by using an objective function approach. In the present study, the advancing side BVI noise and the vibratory hub load components were represented by two metrics, namely, the noise metric and the hub loads metric. The objective function was composed of the sum of the weighted squares of the noise and hub loads metrics. The closed-loop controller must be fast-executing and must converge quickly (in six iterations or less); gradient-based methods must not be used.

The identification (plant modeling) procedure was completed; it involved the use of a two-hidden-layer radial-basis function neural network with one input and two outputs. A simple, easy-to-implement neural control technique, the "direct inverse" method, was successfully applied and found to be robust. The present approach had the following essential ingredients: accurate plant modeling, halving of the metric in order to accelerate controller convergence, "inverted-axes" control modeling, and a feedback iterative loop. A simple, two-hidden-layer back-propagation neural network used in the control step was successful.

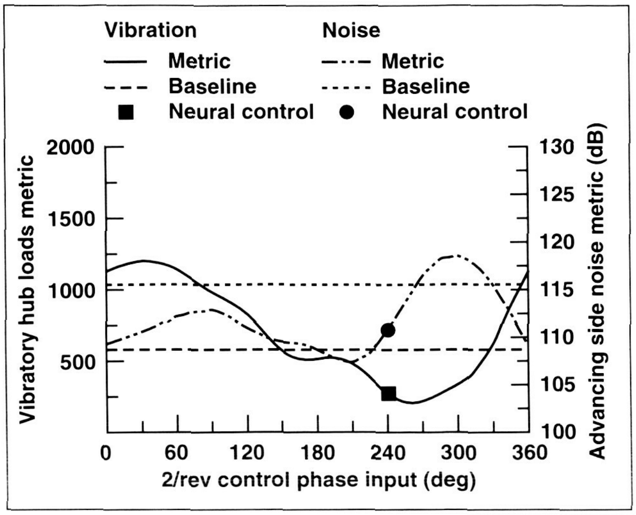

Fig. 1. Simultaneous noise and hub load reductions using present closed-loop neural network controller.

Results from the present, closed-loop neural network controller showed that simultaneous reductions of 5 decibels in the baseline noise and 54% in the baseline vibratory hub loads were achievable in only two controller iterations (these results are shown in the figure).

Point of Contact: S. Kottapalli
(650) 604-3092
skottapalli@mail.arc.nasa.gov

Are Surface Shear-Stress Fluctuations a Valid Source of Sound?

K. Shariff, M. Wang

In aeroacoustics, a complete solution is possible only in rare instances. More often, one cautiously uses the acoustic analogy of Lighthill. In doing this, it is not always clear what to consider as a genuine source of sound and what to consider as a propagation effect. One way such a problem can arise is when the sources of sound cannot be separated from the effects of sound. For instance, it is well known that surface pressure fluctuations, which at first sight looked like a source of sound, actually represent only the reflection of sources located within the flow above the surface. Surface shear-stress fluctuations, the object of the present study, have posed a similar problem because sound propagating above the wall produces its own wall shear fluctuations in addition to those caused by the flow. Those who argue against shear-stress fluctuations being a valid source begin with the fact that only shear-stress fluctuations at the acoustic wavelength can radiate sound. These fluctuations, it is argued, must be a result of the sound itself. Therefore, shear-stress fluctuations are not a true source and provide merely a modification to the sound created by the flow. On the other hand, some investigators have boldly assumed that surface shear-stress fluctuations caused by the flow are a genuine source of dipole sound. Who is right?

Numerical simulation is useful in resolving such issues in the absence of analytical insight. A simple two-dimensional computational experiment was undertaken after modifying a code developed earlier by Mitchell and Lele (Stanford University, Stanford, California), which meets the stringent requirements of accurate aeroacoustic computations. A portion of a wall was oscillated tangentially. This does not prejudice the issue since (unlike normal motion) it is not by itself a source of sound. The first figure shows the sound field computed on a large enough domain to accommodate a few acoustic wavelengths. In comparison, the vortical flow created is in a tiny

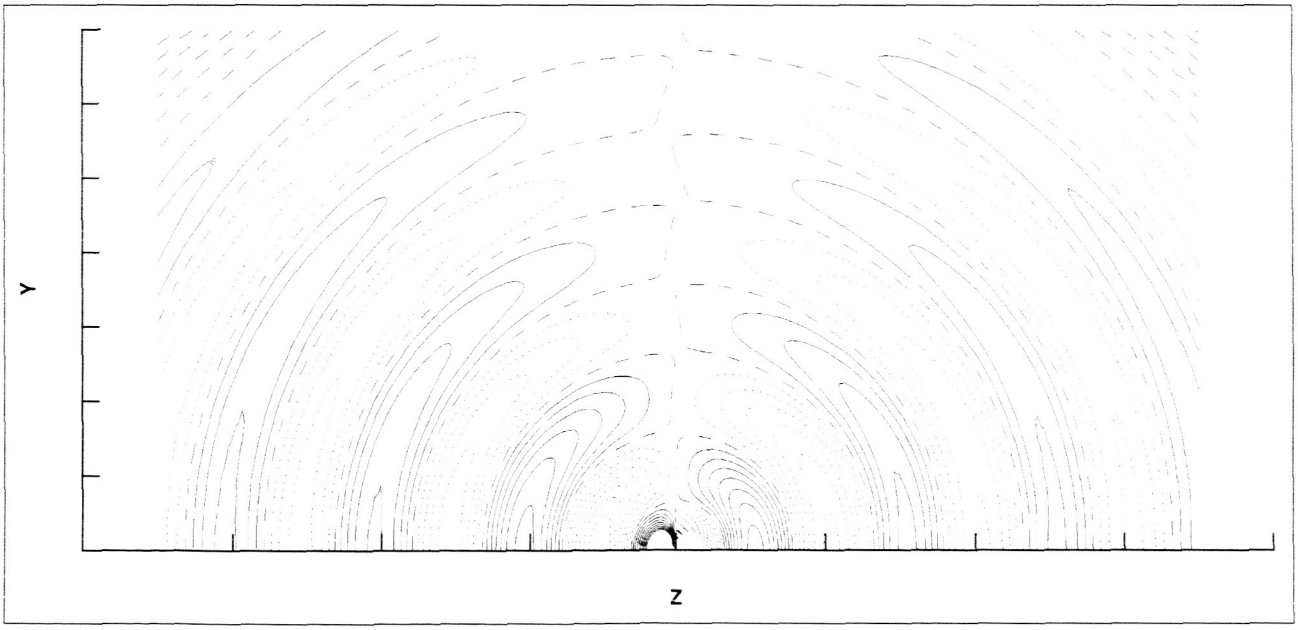

Fig. 1. Contours of acoustic pressure produced by a localized tangential wall oscillation.

region near the origin. The sound field is of dipole character. The second figure shows that the computed amplitude of the sound field (solid line) agrees with a formulation (dashed line) that regards shear-stress fluctuations as acoustically compact and as a genuine source of sound. The argument presented above, against shear-stress fluctuations being a valid source, fails because even at the acoustic wavelength, the flow itself evidently makes a larger contribution to the shear-stress spectrum.

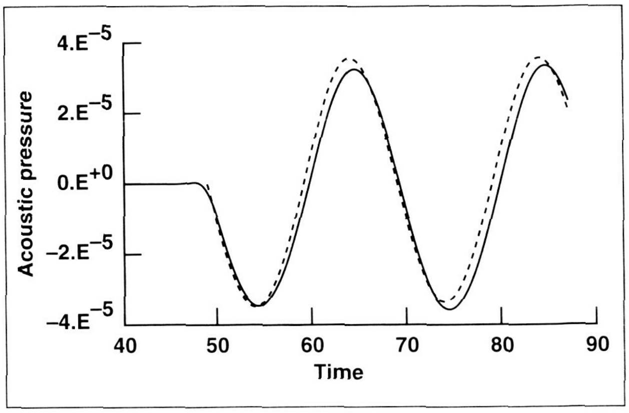

Fig. 2. Comparison of acoustic pressure in the simulation (solid) and a formulation (dashed) which regards surface shear-stress fluctuations as a valid source of sound.

Point of Contact: K. Shariff
(650) 604-5361
shariff@nas.nasa.gov

Aeronautics Design/Test Environment Phased Microphone Array Technology

Michael Watts

Noise has become a major driver in the design of aircraft. The development of low-noise aircraft within a rapid design-cycle process requires that the noise design be done concurrently with other disciplines such as high-lift aerodynamics and landing gear development. Phased Microphone Array Technology (PMAT), currently being developed as part of the Aeronautics Design/Test Environment effort to expand the role of the wind tunnel in the overall aircraft development process, shows great promise for attacking the noise design problem, as well as for being an instrumentation system that can be run concurrently with aerodynamic, performance, controls, and structural loads testing. Because it is nonintrusive, PMAT is compatible with optical measurement technologies that are being developed. Implementation of the array measurement capability will allow designers to evaluate the acoustic effect of design details in parallel with the aerodynamic development. This will result in a significant improvement in the present design-cycle process.

In classic acoustic testing, the result is generally a spectral plot from a single microphone. Although this is informative, it can be ambiguous, for the spectrum contains noise from the environment as well as the noise generated by the test object. PMAT allows researchers to reduce the effect of the background noise and to locate noise sources coming only from the item being tested. This level of detail from the array results shows true effects of parameter changes, while it also reduces the corruption of the signal from the background noise. The figure shows the reduced noise as seen in the spectral plots, but also allows the researcher to see the localized effects of installing the flap fences. This detailed information could not have been acquired without PMAT.

PMAT integrates several instrumentation, computer, and high-speed network systems to produce noise maps at specified frequencies. Sources of noise on aircraft and engine models are identified and isolated through computational analysis of the signals received from the microphone array. The signals are measured with a 100-element microphone array mounted in the wind tunnel and processed on a supercomputer. The current system has the capability of returning results for 200 frequencies within about

- **Demonstrates the ability to localize noise sources (flap and slat edges).**
- **Shows relative amplitude of localized noise sources.**
- **Results obtained during runs provide immediate feedback to researcher.**
- **PMAT complements single microphone measurements.**
- **Flap edge treatments show promise in meeting AST airframe noise reduction goals.**

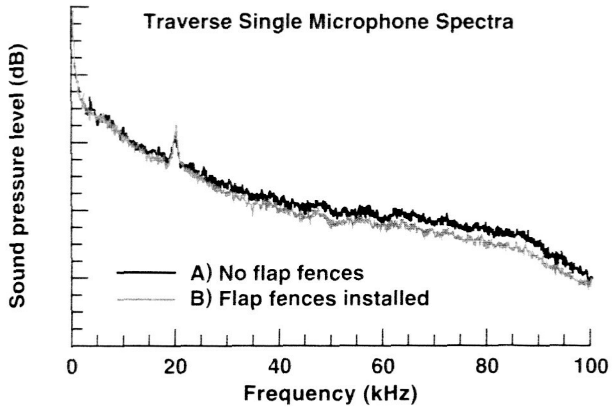

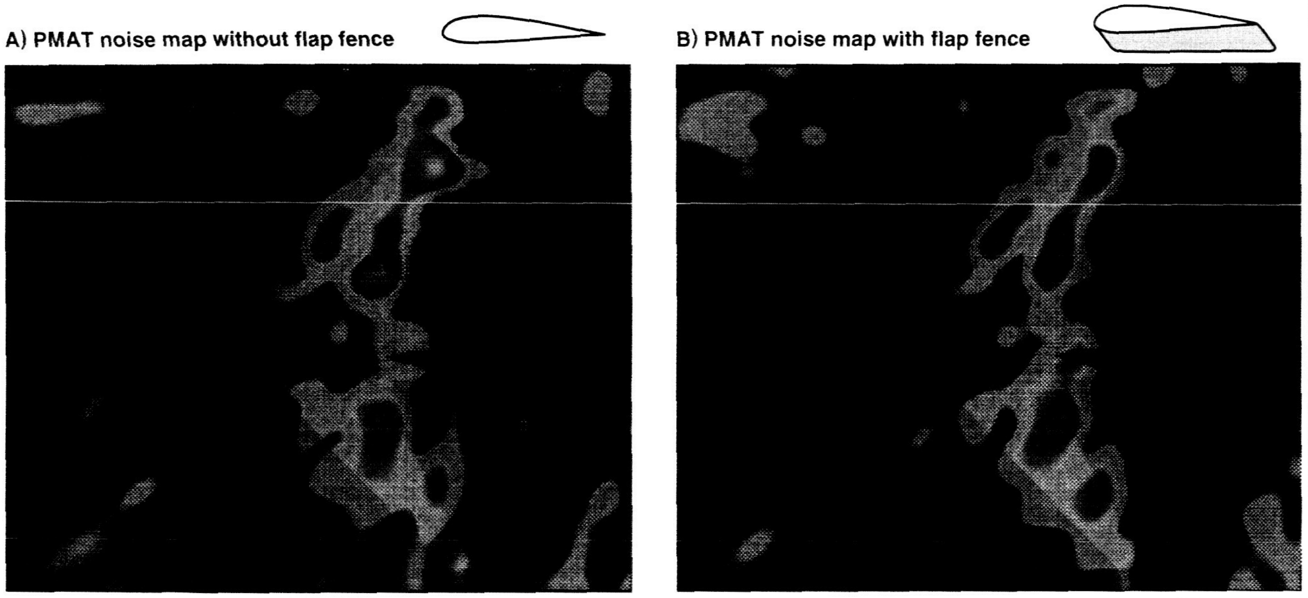
A) PMAT noise map without flap fence

B) PMAT noise map with flap fence

Fig. 1. PMAT array processing results.

8 minutes during a wind tunnel run. Results of the processing are displayed using a simplified, user-friendly interface to the Flow Analysis Software Toolkit software previously developed at Ames Research Center, as well as an interface developed by the PMAT team. The processing of each test point is performed before the next test condition is established. This quick turnaround of data allows researchers to guide the testing to make the best use of the test time available.

In 1997, system software for the current system, running on an HPVX1, was developed and checked out, hardware was acquired and assembled, and the system was successfully tested in an anechoic environment in preparation for the first test in the Ames 7- by 10-Foot Wind Tunnel in early 1998. The software was also tested on data acquired from an array during a Boeing wind tunnel test.

Point of Contact: M. Watts
(650) 604-6574
mwatts@mail.arc.nasa.gov

Sonification of Multivariate Data

Jim Stevenson

Previously, a program called MULTIVAR was developed for sonification of multivariate data. Magnitude was represented by frequency. Rows or columns of the data matrix were sequentially displayed. MULTIVAR contained many switches for sorting or scaling data. Timing of presentation within and between rows of the data matrix was controllable by tables and switches.

Next, programs were developed to drive all the sound-generating registers of the OPL frequency modulator (FM) chip. Its driving tables contain control variables such as frequency, voice number, speaker channel, [volume, attack, decay, sustain, and release] for carrier and modulator, and many others including a percussion mode and a four-parameter mode. They also contain appropriate data variables. A C-header file called ssound.h was also developed to control the OPL chip. This made it possible to easily generate many sonification examples using mathematical functions, probability distributions, and multivariate high-order Markov chains.

In FY97 the OPL chip software was applied to MULTIVAR, making it possible for it to use volume and stereo panning as additional dimensions for data display. The polyphonic properties of the OPL chip enabled simultaneous display of several data elements as chords. Auditory illusions including Shepard tones were demonstrated.

Additional programs were written to produce simultaneous moving sources. Linear and Doppler ramps, starting and ending positions, frequencies, volumes, and their rates of change were driven by data tables.

Faster processors and sound-generating hardware have recently become available. This will make it possible to expand the repertoire of near real-time sonification tools far beyond the limits of the OPL chip.

Point of Contact: J. Stevenson
(650) 604-5720
jims@eos.arc.nasa.gov

X-36 Tailless Fighter Agility Research Aircraft

Mark Sumich, Rodney O. Bailey

The X-36 Tailless Fighter Agility Research Aircraft is a remotely piloted aircraft that was developed to demonstrate that a tailless aircraft, whose aerodynamic and systems configurations are driven by low-observables considerations, often referred to as stealth, can achieve the maneuverability and agility of current-class fighters without the directional stabilization and control power provided by vertical tails.

The 28%-scale X-36 is about 18 feet long, 10 feet wide, and 3 feet high. It weighs 1250 pounds fully fueled. The aircraft is powered by a Williams International F-112 turbofan engine which produces about 700 pounds of thrust.

The aircraft was conceived and developed by Ames Research Center in conjunction with the Boeing Phantom Works. The X-36 Project is an example of a better, cheaper, faster development philosophy, called rapid prototyping, that uses computer-aided design and manufacturing methods to create technologically advanced aircraft on a very short schedule and limited budget. A small, highly skilled, dedicated team designed, built, and shipped two identical X-36 aircraft to NASA Dryden Flight Research Center for flight testing in only 28 months. The total program cost was significantly less than it would have been if more traditional aircraft development methods had been used.

Removing the vertical tails eliminates weight and reduces aerodynamic drag, providing improved aircraft performance. The tailless design also reduces radar signature, an important characteristic for stealthy flight. The aircraft is unstable in both the longitudinal, or pitch, axis and in the directional, or yaw, axis. The X-36 uses conventional aerodynamic control surfaces along with split ailerons and a thrust-vectoring nozzle for aircraft control. An advanced digital flight-control system stabilizes the aircraft.

The X-36 flight-test missions are directed from a ground-control station where the Boeing/NASA test team and the aircraft's pilot are located. The aircraft is remotely piloted using a virtual cockpit. A monitor directly in front of the pilot provides out-the-nose video imagery downlinked from the aircraft. A head-up display is overlaid on the video image to provide flight-critical information. The cockpit displays provide the pilot with excellent situational awareness, making maneuvering flight and precision landings routine. The X-36 takes off and lands conventionally from the lake-bed runways or from the main base runway at Edwards Air Force Base.

The first flight of the X-36 was made on May 17, 1997. The flight was preceded by several months of hardware integration testing, structural modes interaction (SMI) testing, hardware in-the-loop simulations, piloted simulations, test team training, and ground taxi tests. By September 30, 1997, the aircraft had completed a total of 22 flights with a total flight time of 10 hours 54 minutes at angles of attack up to 40 degrees. The rate at which these test flights were flown and the rapid expansion of the flight envelope were made possible by using analysis programs during flight that verified the performance of the flight-control system in stabilizing the aircraft. Data on the aerodynamic characteristics of the X-36 were also generated using sophisticated parameter identification techniques. The photograph shows the X-36 in flight above Rogers Dry Lake bed, Edwards Air Force Base, California.

At the test altitude of 17,000 feet, fighter-type maneuvers such as 360-degree rolls and rolling pullouts were performed to demonstrate the agility of the X-36. A rolling pullout is a classic maneuver when dogfighting. The aircraft is banked sharply in one direction, then quickly rolled in the opposite direction while pulling g's. Classified flight-test data

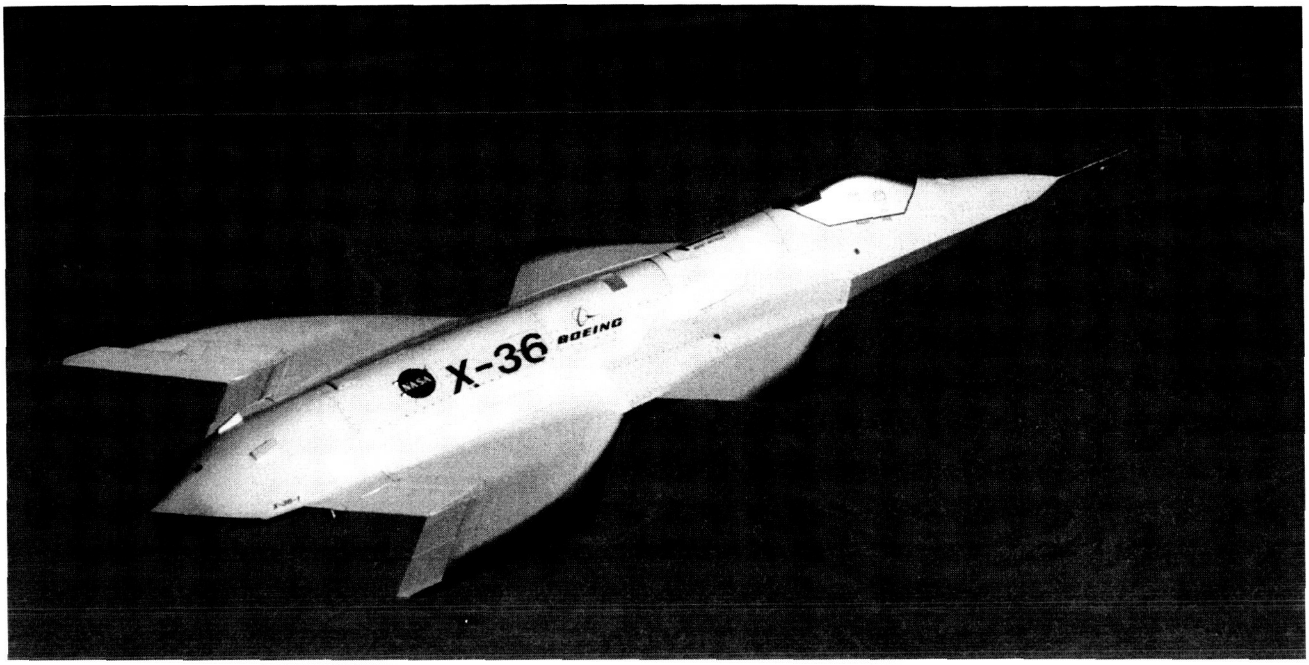

Fig. 1. The X-36 Tailless Fighter Agility Research Aircraft in flight over Rogers Dry Lake bed, Edwards Air Force Base, California.

show that the X-36 aircraft successfully demonstrated that a tailless aircraft can achieve levels of agility and maneuverability exceeding those of present-day fighters.

The X-36 is also an excellent example of how subscale, remotely piloted aircraft can demonstrate advanced technologies at a fraction of the cost and development time required by full-scale aircraft with the pilot aboard. The X-36 Project was a complete success and provides a preview of what fighter aircraft of the future will look like.

Point of Contact: M. Sumich/R. Bailey
(650) 604-6193/6265
msumich@mail.arc.nasa.gov
rbailey@mail.arc.nasa.gov

Aeronautics Design/Test Environment Condition-Based Maintenance for the 12-Foot Pressure Wind Tunnel

Ann Patterson-Hine

In support of the Aeronautics Design/Test Environment effort to enhance operations at wind tunnel facilities, researchers collaborating with wind tunnel experts implemented a software application to monitor system performance and to diagnose anomalous behavior in the make-up air (MUA) compressor subsystem of the 12-Foot Pressure Wind Tunnel at Ames Research Center. This project combined the efforts of the System Health Management team, the Ames Fluid Mechanics Laboratory, and the Applied Research Laboratory at Pennsylvania State University. Condition-based maintenance (CBM) can increase facility efficiency by reducing or eliminating costly repairs required because of unnecessary maintenance and failures. CBM is a systematic approach that focuses on continuous monitoring of equipment combined with model-based reasoning software to indicate the need for maintenance that, if ignored, could lead to failure. Unlike a traditional maintenance program based on manufacturers' time and performance statistics, the condition-based approach determines when maintenance is required based on actual conditions. It can provide advanced warning of possible failures by estimating "remaining useful life" for the component rather than warning only of imminent catastrophic failure. Such advanced warning allows efficient scheduling of downtime.

A Solatron data-acquisition system was installed in the MUA compressor subsystem of the Ames 12-Foot Pressure Wind Tunnel, along with a Rule-Based Expert System (RBES) constructed using RTWorks, an off-the-shelf application that simplifies the process of building complex mission-critical systems. The RBES was encoded with expert knowledge in vibrational analysis and other critical parameters, which then evaluated the monitoring data received and provided wind tunnel operators with alerts of off-nominal behavior. Once the system is tuned properly and the nominal behavior of the compressor is characterized, it will also be used to determine recommendations for system maintenance, including estimates of the remaining useful life of various system components, as shown in the figure. This system was successfully installed in September of 1997 and continues in operation, demonstrating the feasibility of condition monitoring of complex machinery such as that used in wind tunnels. This technology has widespread application not just to all of NASA's tunnels, but to aerospace vehicles at large.

Point of Contact: A. Patterson-Hine
(650) 604-4178
apatterson-hine@mail.arc.nasa.gov

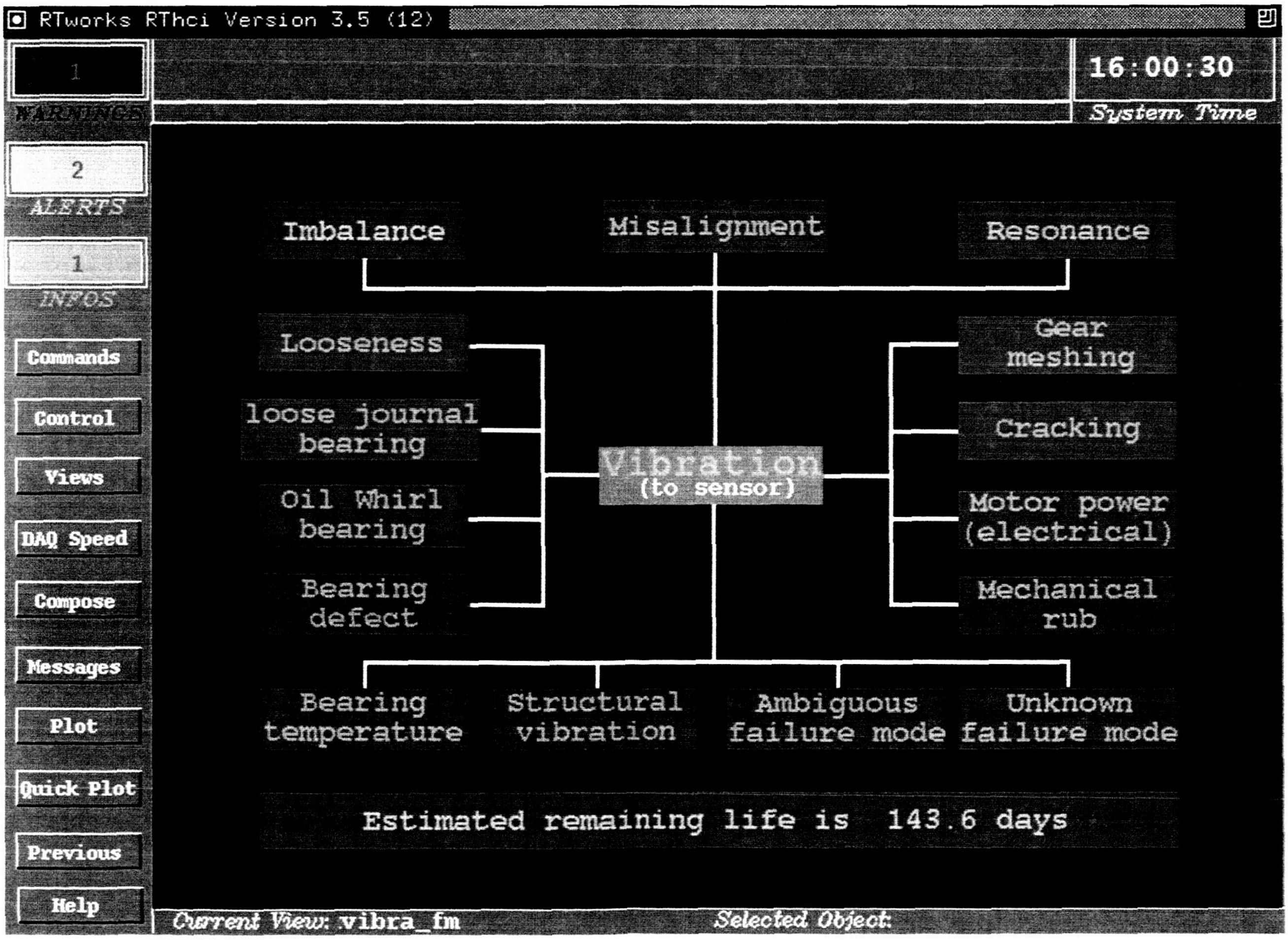
RTworks RThci Version 3.5 (12)
1
WARNINGS
2
ALERTS
1
INFOS
16:00:30
System Time
Commands
Control
Views
DAQ Speed
Compose
Messages
Plot
Quick Plot
Previous
Help
Imbalance
Misalignment
Resonance
Looseness
loose journal bearing
Oil Whirl bearing
Bearing defect
Vibration (to sensor)
Gear meshing
Cracking
Motor power (electrical)
Mechanical rub
Bearing temperature
Structural vibration
Ambiguous failure mode
Unknown failure mode
Selected Object:

Estimated remaining life is 143.6 days

Current View: vibra_fm

Fig. 1. Vibration monitoring system failure mode summary window.

DARWIN

David Korsmeyer

Creating a more dynamic role for wind tunnels in the design process is the goal of a NASA information technology concept for redefining the classic approach to wind tunnel and other aeronautical testing. The project, called DARWIN (Developmental Aeronautics Revolutionizing Wind tunnels with Intelligent systems of NASA), combines custom and commercial software and hardware and advanced experimental instrumentation to create an extended version of the Remote Access Wind Tunnel system. In 1997 the DARWIN Workspace was developed, a user interface that allows secure remote access via the World Wide Web to wind tunnel data. The emphasis of DARWIN is on reducing the cycle time of the wind tunnel process, extracting more pertinent and accurate data from the wind tunnel environment, and changing the role of the wind tunnel from primarily one of a validation process to one of a dynamic and real-time participant in the overall design process.

Traditionally, a wind tunnel test requires bringing a group of technicians and engineers to a single location. In some cases engineers have to wait weeks or months for test data, or if available on-site, data are in the very crude form of streams of numbers which have to be fed into computers, run through custom-written FORTRAN programs, and the results loaded into Excel spreadsheets before the data can be plotted and analyzed. DARWIN makes aeronautics test results available to industry and researchers faster, cheaper, and better. And because it is Web-based, DARWIN can be accessed by multiple users (up to 1000 at a time), and is accessible to any computing platform that supports a Web browser.

Another advantage to being Web-based is that DARWIN uses Java applets to allow remote users to begin their analysis of wind tunnel data as they receive it. Data can be plotted and graphed, and results compared across a series of runs—even multiple runs across multiple tests—because DARWIN maintains a searchable database of test results. Data received from additional instrumentation on the wind tunnel model, such as pressure taps and pressure sensitive paint, can be used to produce visual images of features such as the pressure gradients over the surface of a wing. These can be automatically refined by DARWIN into animated images, allowing engineers to visualize the pressure changes on the model surface as the wing moves.

DARWIN has been operational since April 1997, and currently supports wind tunnels at both Ames and Langley Research Centers. In addition to the completion of the DARWIN Workspace, DARWIN was used in support of the MD-11 Test (High Wing Transport Externally Blown Flap Test) in the Ames 12-Foot Pressure Wind Tunnel and in the implementation of SIMNet support in DARWINnet.

To further enhance remote-user access to wind tunnel data, an application called the Wind Tunnel Sequential Run Predictions was developed, a nonlinear curve-fitting program that takes the points already measured in a run, plus runs from earlier tests, and accurately predicts the remainder of a run. Along with the predictions, the error bars of the predictions are also given. Currently, test engineers rely on experience and intuition to gauge how a test run is progressing. The ability to predict the remainder of a run will give test engineers immediate feedback on whether the run measurements are sensible, on whether fewer points could be sampled within a run (thus saving time), and on how the current run compares to earlier tests.

Point of Contact: D. Korsmeyer
(650) 604-3114
dkorsmeyer@mail.arc.nasa.gov

New Technique for Visualizing Unsteady Flow

David Kao, Han-Wei Shen

A new technique for accurately visualizing time-varying phenomenon in unsteady flow fields has been developed at Ames Research Center. The resulting images captured through the Unsteady Flow Line Integral Convolution (UFLIC) technique reveal complicated flow behavior and help scientists detect important flow features for computational fluid dynamics analysis.

UFLIC employs a new algorithm that takes into consideration the time-variable and flow patterns from previous time steps. In unsteady flows, there are no well-defined flow lines because the flow is dynamic, and particles can advance to new locations easily. The UFLIC algorithm uses a time-dependent particle-tracing scheme to trace flow textures.

This time-dependent algorithm uses the original Line Integral Convolution technique as its underlying form. To model unsteady flow, it uses a successive feed-forward convolution method that maintains coherence between animation frames and a time-accurate value-depositing scheme that models local changes in flow. The feed-forward method does not create each successive frame from the original, but creates it with the previous frame's output to ensure that consecutive frames are highly coherent. Time-accurate value-depositing ensures that as the algorithm repeatedly computes the evolution of pathlines, the pixels involved advance only in a forward pathline direction—thus reflecting physical reality, because particles in flows cannot move backward in time. In addition, by using a high-pass filter, image clarity and texture are improved.

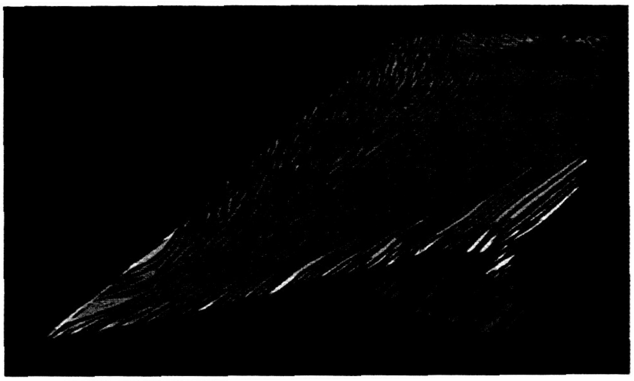

Fig. 1. Surface flow on a tail of a F/A-18 jet.

The figure shown is the surface flow generated by UFLIC using a tail of the twin-tailed F/A-18 jet. At a high angle of attack, the flow is highly unsteady, and vortex bursting is frequent along the leading edge. The velocity magnitude changes rapidly along the leading edge, which indicates cycles of vortex bursting. The results generated clearly show unsteady flow patterns and highlight flow evolution.

Point of Contact: H-W. Shen
(650) 604-4451
hwshen@nas.nasa.gov

New Release of Field Encapsulation Library

Patrick Moran, Chris Henze, Steve Bryson, David Kenwright

The second generation of a software library supporting work related to the design and evaluation of new aircraft has been developed at Ames Research Center. The Field Encapsulation Library (FEL) is designed to support the rapid development of applications involving both computational and experimental fluid dynamics data. The library contains many new features, including a derived-field capability and added support for mesh-independent algorithm development. The new library design also employs a technique known as "lazy evaluation" that makes it easier for the user to write applications that work with large data sets.

The derived-field functionality in the FEL facilitates the creation of new fields in terms of existing ones. For example, many computational fluid dynamics (CFD) solver applications output fundamental solution variables, such as density, momentum, and energy. A typical derived field would be pressure, which can be computed in terms of the fundamental values. There are many derived fields that the user could be interested in viewing. For instance, in the CFD postprocessing application PLOT3D there are over 50 predefined derived fields. The FEL derived-field capability supports all the standard derived fields of PLOT3D; in addition, the library makes it easy for the application programmer to develop custom derived fields.

Another new feature in the FEL is its support for gradient, divergence, and curl differential operators. The built-in support for these commonly used operators makes it easier for users to quickly develop new applications, since more of the necessary field functionality can be used "off the shelf" from the FEL. The library supports computing differential-operator results by either first-order or second-order techniques.

Both the differential-operator fields and derived fields in the FEL employ the lazy evaluation technique. With lazy evaluation, field values are computed when requested, rather than in advance. Lazy evaluation is particularly useful in cases in which an application needs derived values only within small subregions of a field. Many standard visualization techniques, such as streak-line advection or displays on an aircraft surface, fall into this category. The advantages of lazy evaluation are savings in both computation and memory use. Since derived values are only computed on demand, the library never computes values that go unused. Furthermore, no memory is allocated for storing derived values. The benefits of lazy evaluation are especially apparent when working with large time-series data sets, where the drawbacks of precomputing derived values are multiplied by the number of time steps in the data.

Point of Contact: P. Moran
(650) 604-1660
pmoran@nas.nasa.gov

Portable Batch System Expands Its Customer Base

Robert Henderson

The Portable Batch System (PBS) project was started at Ames Research Center to produce a modern resource-management and job-queuing system that was compliant with the formal standards and was flexible and extensible in order to meet the changing needs of computing within the Agency. Although the initial effort concentrated on traditional supercomputers, PBS quickly gained wide acceptance on parallel systems such as the IBM SP series and on clusters of workstations. By providing a common command interface and job-management system across the complete range of modern computers, together with a flexible site and determined scheduling policy, PBS has gained wide acceptance in academie, industry, and the military.

In 1997, the emphasis in the research and development of PBS centered on metacenter computing. Metacenter computing is the management of multiple systems scattered across geographical or administrative domains. Initial work centered on two parallel systems, one at Ames and the other at Langley. This work identified study areas involving peer job scheduling and data movement. The research continued with the creation of a local metacenter consisting of four Cray systems. Current efforts are based on a large number of the Silicon Graphics Inc. Origin systems that are multiple processor systems.

Interest in metacenter computing is also high in other areas. Two of the four Department of Defense Major Shared Resource Centers (MSRC) are exploring ways of sharing computing resources. Both the Aeronautics Research Center at Wright-Patterson Air Force Base in Ohio and the Army Corp of Engineers Waterways Experiment Station in Mississippi have selected PBS as a major component of this research area. With PBS as a common job-scheduling and resource-management tool, the two centers are working to provide resources to each other.

Partly because of the metacenter work, Ames was presented with a NASA Space Act Award. This award was presented for "creative development of a technological contribution, which has been determined to be of significant value in the advancement of the space and aeronautical activities of NASA."

A second developmental effort within PBS during 1997 centered on the area of parallel job task management. When a distributed parallel job runs on multiple computer systems, there are the issues of starting the separate tasks that make up a parallel job, monitoring and controlling the tasks, and accounting for resources used by the tasks. A team of Ames researchers, together with representatives from other national laboratories and several major companies, worked to define a standard for a portable interface implementation that provides the service required to start, control, and monitor tasks.

Point of Contact: B. Henderson
(650) 604-4515
hender@nas.nasa.gov

Adaptive Refinement and Structured Grids for Unsteady Aerodynamics

Robert Meakin

The objective of this research is to develop robust adaptive refinement methods for unsteady geometrically complex (moving-body) applications that exploit the computational advantages inherent in structured data.

The physical domain of complex problems is decomposed into near-body and off-body regions. The near-body domain is discretized with "Chimera" overset grids that need to extend only a short distance into the field. The off-body domain is discretized with overset structured Cartesian grids (uniform) of varying levels of refinement. The near-body grids resolve viscous boundary layers and other flow features expected to develop near body surfaces. Off-body grids automatically adapt to the proximity of near-body components and evolving flow features (first figure).

The adaption scheme automatically maintains solution accuracy at the resolution capacity of the near-body system of grids. The approach is computationally efficient and has high potential for scalability. Grid components are automatically organized into groups of equal size, facilitating parallel scale-up on the number of groups requested. The method has been implemented in the OVERFLOW-D2 code being developed within the Computational Fluid Dynamics–Computational Technology Area of the Common High Performance Computing Software Support Initiative (CHSSI). CHSSI is, in turn, part of the Department of Defense High Performance Computing Modernization Program.

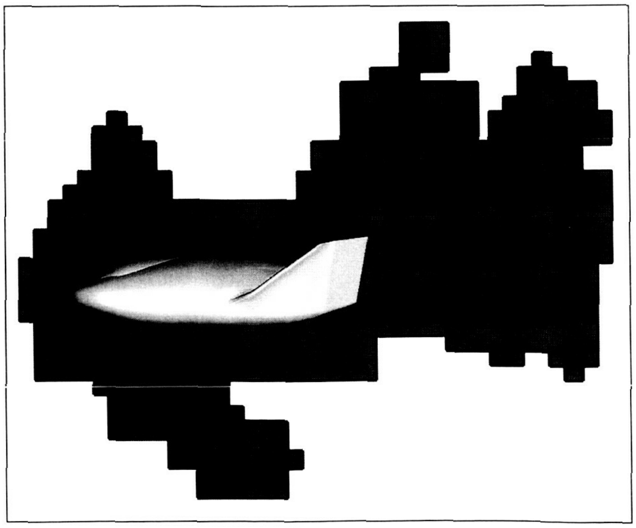

Fig. 1. Boundaries of finest off-body grids.

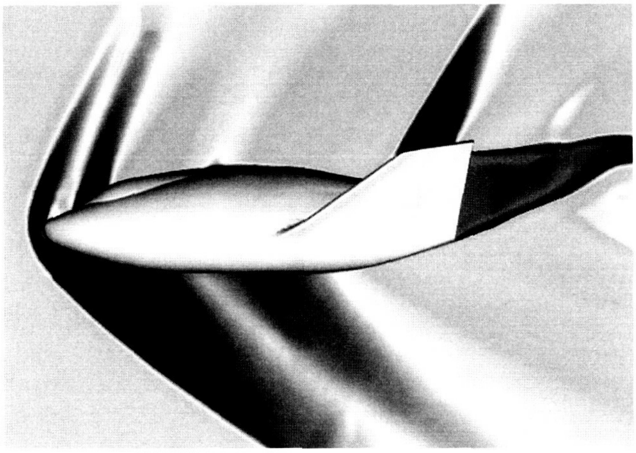

Fig. 2. X-38 Mach field after one adapt cycle.

The adaptive refinement capability within OVERFLOW-D2 has been demonstrated on the X-38 Crew Return Vehicle in a Mach 1.5 free stream (second figure), at an angle of attack of 15 degrees, and at a Reynolds number of 25 million. Test conditions and the near-body grid system were provided to the CHSSI CFD-4 software development team by R. Gomez of Johnson Space Center.

Demonstration of OVERFLOW-D2 on a large-scale application such as the X-38 is significant because of the broad class of problems of interest to the DoD and NASA. These problems require the accuracy available through adaption and the computational efficiency realizable through structured data. Some of the target problems for the method are unsteady moving geometry applications such as aircraft store separation, helicopter rotor-body interaction, crew escape systems, flight maneuvers, and launch vehicle staging.

Point of Contact: R. Meakin
(650) 604-3969
meakin@nas.nasa.gov

Multi-Level Parallelism: A New Computing Technique

James R. Taft

High-performance computing platforms are evolving toward systems with ever larger numbers of processors. These systems utilize standard off-the-shelf microprocessors at the heart of their design. Virtually all hardware vendors have adopted this design approach because it dramatically reduces their costs. Unfortunately, this usually forces researchers to embark on large code-conversion efforts (often consuming work-years) to take advantage of the new parallel systems. Codes used in heavy production environments were often deemed impossible to convert.

Several events have occurred that are changing that attitude. First, the vendors are now building systems that share many of the hardware features of the Cray vector systems. In particular, the new designs are moving toward true shared memory architectures, and instruction sets compatible with vector programming constructs. These new hardware attributes have made it possible to approach parallelism in an entirely new way, a way that is more intuitive and simpler to implement.

Ames Research Center has extensively investigated these new approaches to parallelism using the Silicon Graphics, Inc. Origin 2000 as a test bed. The end result is a new technique for parallel computing: multi-level parallelism (MLP). This project demonstrated that new parallel systems, such as the Origin 2000, could be used in a heavy computational fluid dynamics (CFD) production environment. Furthermore, the CFD codes, running on the Cray C90 systems, could be converted to the parallel systems and still maintain their high-performance levels on the vector machines.

The production CFD code OVERFLOW was chosen as the test bed for the MLP effort. OVERFLOW is composed of approximately 100,000 lines of FORTRAN. It was chosen because it represented one of the toughest tests for the resiliency of the MLP programming approach. To further stress-test the method, it was decided to execute only the largest and most complex problems. To this end a 33-million-point problem was selected. This problem was the largest that had ever been solved at Ames. It requires hundreds of C90 hours to converge.

Doing the zones in parallel is not new; the Message Passing Interface version of OVERFLOW already attempts this process. The unique feature of the MLP approach is that it does so with no message passing and only a few hundred lines of code changes. This results in a code that is simple to maintain, that continues to execute well on C90 systems, and that now executes well on parallel systems at very high sustained levels of performance.

The MLP version of OVERFLOW was completed in about 3 workweeks. The initial performance of the code for the 33-million-point problem was 75 percent that of the performance of the dedicated 16 CPU C90 system when executed on a 64 CPU Origin system. This amounts to 3.7 GFLOPS (10^9 floating point operations per second). This relative performance coupled with the dramatically smaller price for the Origin 2000 resulted in a price/performance advantage of over 13.5. Further tests have demonstrated a sustained performance of over 6.3 GFLOPS for this problem on a 128 CPU Origin, with performance scaling still virtually linear at 128 processors. This performance level is approximately 40% better than that of the dedicated C90.

One of the most important features of the MLP technique is that the user can simply comment-out a few lines of code that call the MLP routines, and the code reverts back to the standard vector-friendly C90 version. This minimal change from the C90 version means that new releases of the OVERFLOW code can be converted rapidly to MLP. This was recently demonstrated with the introduction of OVERFLOW 1.8 which was converted to MLP form in less than 1 day.

The MLP technique has general applicability to many CFD codes. MLP offers researchers the possibility of rapidly converting their Cray vector codes to the new machines, and of insuring high performance on each. Even more importantly, NASA researchers are now able to use the new cost-effective parallel platforms to solve problems, the solutions to which were previously unaffordable.

Point of Contact: J. Taft
(650) 604-0704
jtaft@nas.nasa.gov

Carbon-Nanotube-Based Nanotechnology

Subhash Saini

Carbon nanotubes are large linear fullerenes (close-caged molecules) made of sheets of carbon atoms arranged in six-folded hexagonal patterns. Since their discovery in 1991, nanotubes (rolled up sheets of carbon) have been vigorously investigated both theoretically and experimentally. The single-wall nanotubes are the strongest fibers known, and, depending on how the carbon sheet is rolled, a nanotube possesses unusual electronic properties. NASA's primary interest in nanotubes derives from three technologically interesting properties. First, single-wall nanotubes can be either metallic or semiconducting, thus providing the possibility of nanotube heterojunctions for nanoelectronic components in future ultrafast computers. Second, nanotubes are hollow, tubular, caged molecules that can serve as lightweight containers for packing and carrying hydrocarbon fuels on future space missions. Third, nanotubes have very good elasto-mechanical (strongest, yet highly flexible, tubular fiber known) properties that can be used in a lightweight, highly elastic, and very strong fibrous material for use in fabricating future spacecraft components.

At Ames Research Center, two-, three-, and four-terminal nanotube heterojunctions have been designed as a prototype of carbon-based nanoelectronic devices. Carbon atoms in a single nanotube are arranged in hexagonal arrays. However, by introducing topological defects such as pentagons and heptagons, it is possible to connect metal and semiconducting tubes into prototypes of carbon-based diodes and transistors. At Ames, the two-terminal heterojunctions have been modeled and observed in experiments that are done in collaboration with researchers at Stanford University. The three-terminal heterojunctions, however, will be necessary if any current-driven carbon-based logic device is to be realized in experiments. An example of the Ames carbon nanotube three-terminal "T" heterojunction is shown in the first figure, in which a semiconducting nanotube (red) serving as a gate can modulate the current flowing in a metallic nanotube (green) connecting external source and drain terminals. Three-terminal nanotube heterojunctions are computer-simulated models that are yet to be made in experiments. However, these quasi-two-dimensional (2-D) junctions could be the building blocks of nanoscale tunnel junctions in a 2-D network of nanoelectronic devices. The electronic transport through nanotubes, as interconnects and switching devices, in the form of current versus voltage relationship, is also calculated. These will help in guiding experimentalists toward better characterization of nanotubes and their electronic behavior.

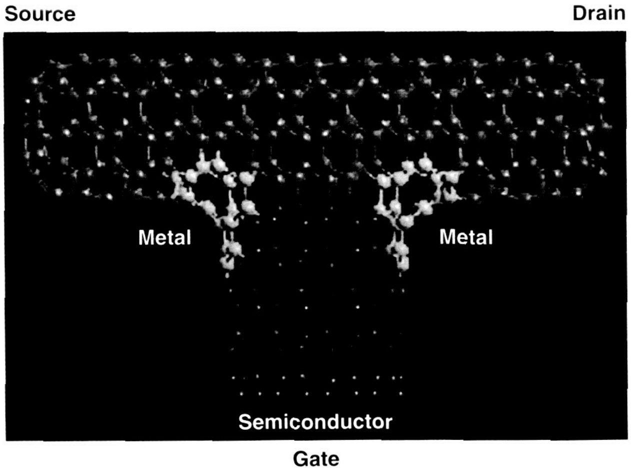

Fig. 1. Carbon-nanotube-based molecular electronics: carbon-nanotube three-terminal "T" heterojunction; red denotes semiconducting nanotube and green denotes metallic nanotube.

To exploit the elasto-mechanical properties of nanotubes, researchers at Ames Research Center and Stanford University have focused on using the nanotube as the tip in scanning-probe microscopes (SPM) to perform nanolithography on semiconductor surfaces. Simulations and experiments have shown that nanotubes are the smallest and strongest nanopencils that can read and write in nanoscale. Nanotube tips have enabled continuous lithography of 10 nanometer features, at a speed of up to 0.5 millimeters per second, over large silicon surface areas while simultaneously minimizing the tip-wear problem in conventional SPM-based nanolithography.

The search for low-cost, lightweight molecular hydrogen fuel storage and carrier material in solid booster rockets is crucial because of the potential it holds for effecting big reductions in overall system weight. Fullerenes, or nanotubes, are excellent candidates for they are lightweight, have large surface-to-volume ratios, and provide good adsorption characteristics for molecular hydrogen. Ames has shown in computer simulations that if nanotubes can be opened or closed in a controlled way, inner cavities of the nanotubes can be accessed for storing molecular hydrogen at higher pressures and densities than possible by any other means. The second figure shows that interstitial spacings in nanotube rope provide less volume to the stored hydrogen than storage within a closed-end nanotube. Computer simulations in conjunction with experimental efforts investigate the possibility of storing molecular hydrogen in nanotubes as nanoscale gas cylinders that can be carried on future space missions.

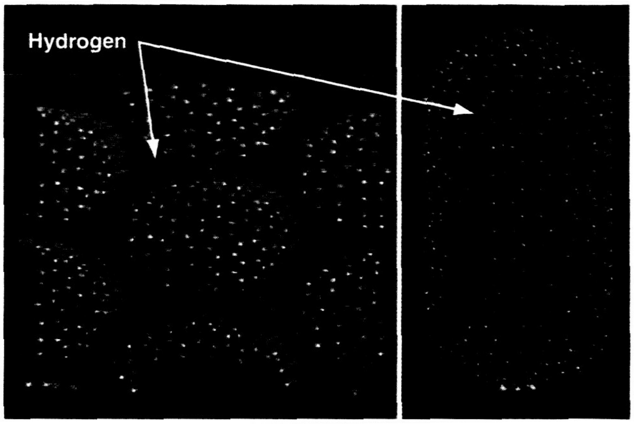

Fig. 2. Hydrogen storage in carbon nanotube: interstitial spacings in a carbon-nanotube rope; red denotes molecular hydrogen.

Point of Contact: S. Saini
(650) 604-4343
ssaini@mail.arc.nasa.gov

Nanoelectronic Devices for the 21st Century

M. P. Anantram, Bryan A. Biegel, T. R. Govindan, Subhash Saini, Toshishige Yamada

Both physical and economic considerations indicate that the scaling era of complementary metal oxide semiconductor will run out of steam around the year 2010. However, physical laws also indicate that it is possible to compute at a rate of a billion times the present speeds with the expenditure of only 1 watt of electrical power. NASA has long-term goals for which ultrasmall semiconductor devices will be needed in critical applications: high-performance, low-power, compact computers for intelligent autonomous vehicles and petaflop (10^{15}) computing technology are two key examples.

Ames Research Center has developed a Green's-function-based code to calculate the transport properties of carbon nanotubes (CNTs). The single most important promise of CNTs with regard to device application is their use as quantum wires. An important question is how disorder affects the conductance of these low-dimensional systems. To obtain an understanding of this, both the low-bias conductance, as a function of the gate voltage (Fermi energy), and the conductance as a function of the applied bias in a CNT for two models of disorders, have been computed. These calculations show that in the presence of weak uniform disorder, the low-bias conductance exhibits a dip as the Fermi energy is swept across the intersection of the first and second sub-bands, as shown in the first figure; otherwise, the CNTs behave as a robust quantum wire. It was also found that in the presence of strong isolated defects, the conductance is significantly affected at the band center, also shown in the first figure.

Silicon-based transistor electronics face daunting technical challenges because of the dramatic miniaturization that is anticipated in the next decade. At that point of miniaturization, identically designed transistors will begin to show different characteristics, a result of uncontrollable deviations in microscopic structure.

A solution to the problem is to greatly simplify the device structure and to build electronics only with atomically precise elements on a regulated surface, as shown in the second figure. This so-called "atomic chain electronics," proposed by Ames as an alternative to silicon-based transistor electronics, will lead to the small and light electronics that will be needed for future NASA space missions. The electronic properties of silicon and magnesium chains have been studied at Ames, with a tight-binding method, and it has been found that silicon chains are always metallic and that magnesium chains are always semiconducting, unlike their three-dimensional counterparts. This indicates that even basic properties have to be reexamined in a microscopic world.

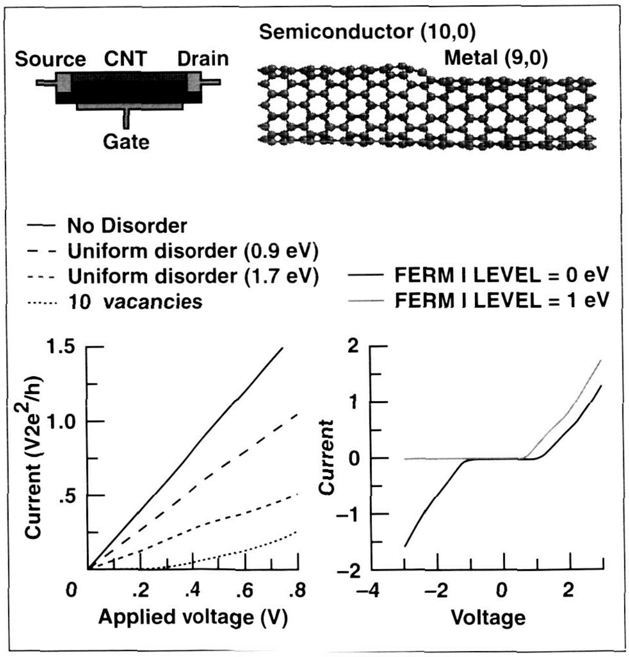

Fig. 1. Comparison of the low-bias conductance versus gate voltage for a defect-free CNT wire and a wire with a weak uniform disorder and strong isolated defects.

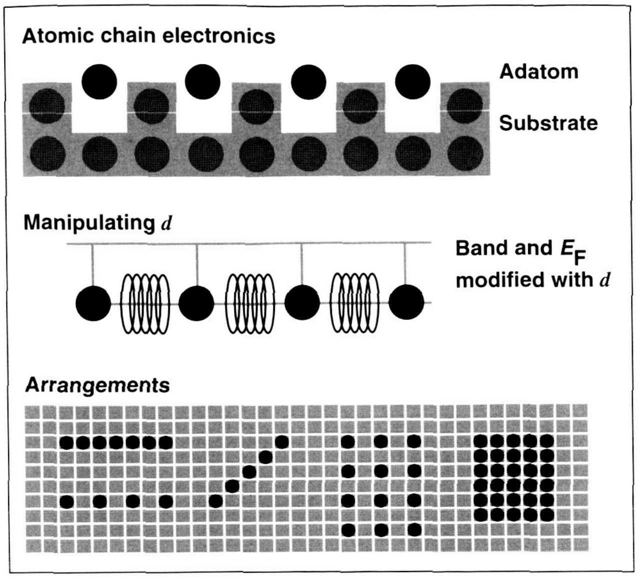

Fig. 2. Device evolution: classic macroscopic (10 years ago), quantum mesoscopic (in next 10 years), and atomic devices (in next 20 years).

Ames is also developing simulation tools that are appropriate for modeling future electronics devices in which both classic and quantum effects are important. The density-gradient model has been incorporated into the partial differential equation solver PROPHET, which was used for quantum-corrected simulations of P-N diodes. A simulation tool called SQUADS, based on the quantum Wigner function and transfer-matrix methods, was used to model devices such as the resonant tunneling diode (RTD), which are quantum-scale in only one dimension. One investigation determined the detailed physics behind strong bistability and 2.5 terahertz oscillations observed in simulations of a particular RTD. These effects were found to be very sensitive to scattering rate and temperature, and it was shown that they could be enhanced with careful modifications of the RTD structure.

Point of Contact: S. Saini
(650) 604-4343
ssaini@mail.arc.nasa.gov

Modeling Carbon Nanotube Electronic Devices

Richard L. Jaffe, Jie Han

Research is ongoing at Ames Research Center to characterize carbon nanotubes in order to exploit their remarkable properties for applications involving strong and lightweight composite materials and nanometer-scale electronic and electromechanical devices and sensors.

Discovered less than 10 years ago, carbon nanotubes are a form of elemental carbon that exhibits interesting electronic and mechanical properties. They can be visualized as resulting from rolling up a single layer of graphite (called a graphene sheet) to make a cylinder. Graphene sheets are hexagonal arrays of carbon atoms. They can be rolled up in a variety of directions (as denoted by two indices, e.g., (10,10), (12,8), and (17,0), which indicate how many steps up and across the array are taken to close the tube). The more interesting variety of nanotubes is *single-walled* (that is, they are a single cylinder), with diameters in the range of 1–3 nanometers and lengths of approximately 1 micron. Other nanotubes consist of concentric cylinders and are called *multi-walled*. Multi-walled nanotubes are observed with diameters up to 100 nanometers. Carbon nanotubes are produced in energetic environments, such as in carbon arcs and by laser ablation of graphite.

Depending on the way in which they are rolled up (called the helicity), carbon nanotubes can have metallic, semiconductor, or insulator properties. Metallic tubes could be used as a kind of molecular wire, and junctions between tubes of different helicity could operate as nano-scale diodes or transistors. Scientists at Ames are using computational chemistry, molecular modeling, and solid state physics techniques to study the electronic properties of hypothetical nanotube junctions. Experiments at Stanford University and elsewhere are under way to verify the results of this modeling study.

One example of this work is presented here. A perfect nanotube consists of only hexagonal rings of carbon atoms. If defects in the form of pentagonal and heptagonal rings are introduced into the hexagonal lattice, the tube will experience a change in helicity and either a change in diameter or a sharp bend. Some examples of bends are shown in the figure along with the indices of the tubes on either side of the junction and the bend angle (the amount of deviation from a straight tube). The pentagonal and heptagonal defects are denoted p and h. Although these junctions are created by modeling, actual tubes with these bend angles have been observed by transmission electron microscopy of nanotube samples.

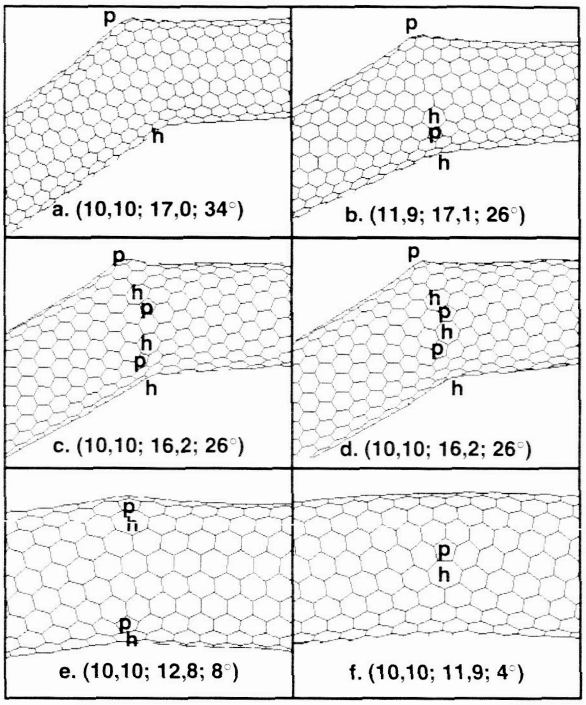

Fig. 1. Representative nanotube junctions.

The (10,10; 17,0) junction shown in part (a) of the figure is of particular interest because it connects a metallic and semiconducting tube. Calculations of the electron density of states at the junction indicate that this junction is electrically conducting and should function as a diode. This tube is nearly 100 times smaller than transistors in the most powerful microprocessor being made today.

Point of Contact: R. Jaffe
(650) 604-6458
jaffe@pegasus.arc.nasa.gov

Interaction Energy of Nitrogen Molecules

Harry Partridge, James R. Stallcop

The interaction energy between two nitrogen molecules is an important basic property needed to determine certain input data required for a real-gas analysis of aerodynamic flows. An accurate representation of the rigid-rotor interaction potential has been constructed by combining the ab initio data and the experimental second virial data to determine the interaction energy in the van der Waals region in a manner consistent with the physics of the interaction. The construction of the potential energy surface is based on the potential function developed by Tang and Toennies for the atom-atom van der Waals interaction.

Extensive electronic structure calculations have been performed to determine the interaction energy of two rigid nitrogen (N_2) molecules, using the coupled-cluster singles and doubles approach, including a perturbational estimate of the triple excitations (denoted CCSD(T)). Full configuration-interaction benchmark studies have shown that the CCSD(T) method accurately determines the electron correlation for systems that are reasonably well described by a single reference. The principal limitation in determining the interaction energy will be basis set incompleteness. The ab initio results define the potential energy surface at small intermolecular separation, as well as the anisotropic behavior of the interaction energy for large intermolecular separations.

Adapting previous work, the strength and slope of the repulsive potential are adjusted in order to increase the well depth to reproduce the measured values of the second virial coefficient B(T). Since the contribution to B(T) from repulsive orientations is small, the virial coefficient is relatively insensitive to errors in the potential energy of these orientations. Hence, the physics of the interaction must be taken into account to obtain a realistic potential energy surface from a fit to measured data for the virial coefficient. The present interaction potential is more anisotropic than the potential of Van der Avoird, Wormer, and Jansen. For example, the angular contribution from the first-order quantum-mechanical correction to B(T) is larger using the present potential, with the difference rising to about 30% at the lowest temperature (75 kelvin) of the virial measurements.

Point of Contact: H. Partridge
(650) 604-5236
partridg@pegasus.arc.nasa.gov

Clutter-Rejection for Obstacle Detection in Radar Data

Yair Barniv

Because of its needle-like nose, shaped for supersonic flight, and the high angle of attack used during takeoff and landing, the High-Speed Civil Transport (HSCT) has no forward window. The HSCT would have to rely on synthetic vision for detecting infringing airborne obstacles, and "seeing" the runway during landing and takeoff. The sensor of choice for all-weather operations is an airborne radar. However, there are two problems inherent in utilizing conventional radars for vision: (1) although they excel in resolving range, their angular resolution is rather poor, and (2) ground clutter may be confused with targets of interest, especially when looking down during landing.

Two complementing approaches were employed to solve these problems: first, differentiating between ground clutter (stationary), and airborne obstacles (having a nonzero ground speed); and second, improving the azimuth resolution so as to decrease the effective ground area that generates clutter (the elevation resolution is of no concern, because, in the down-slanted geometry of landing, it can be improved by utilizing high range resolution).

The first approach is to use an Airborne Moving-Target Indicator (AMTI) to discriminate targets by their motion. A new version of AMTI has been developed, which is based on azimuth or elevation error corrections for the equivalent-clutter direction on a pulse-to-pulse basis. The equivalent-clutter direction has been found to wander erratically from pulse to pulse, even for a pulse repetition frequency (PRF) as high as 10,000 per second. However, for each pulse, the clutter directions are highly correlated for adjacent range bins. Thus, the temporal correlation is low, while the spatial one is high. This observation was used to construct an algorithm that, for each pulse, cancels the clutter inside every range bin by utilizing the equivalent-clutter direction in the adjacent bins.

The first figure shows how the signal-to-clutter ratio (SCR) depends on the obstacle's ground speed and on the interpulse interval (T = 1/PRF). Choosing PRF = 10,000 yields a high SCR with a relatively narrow notch of hard-to-detect target speeds.

The difficulty of detecting low-speed targets with AMTI was addressed by modifying a radar-processing technique, called synthetic aperture radar (SAR), which has been in use for ground mapping. Conventional radars have poor angular resolution because of the size limits on the antenna diameter (larger aperture yields better resolution). An SAR can achieve an equivalent large antenna aperture in azimuth by synthesizing it along its flightpath. It

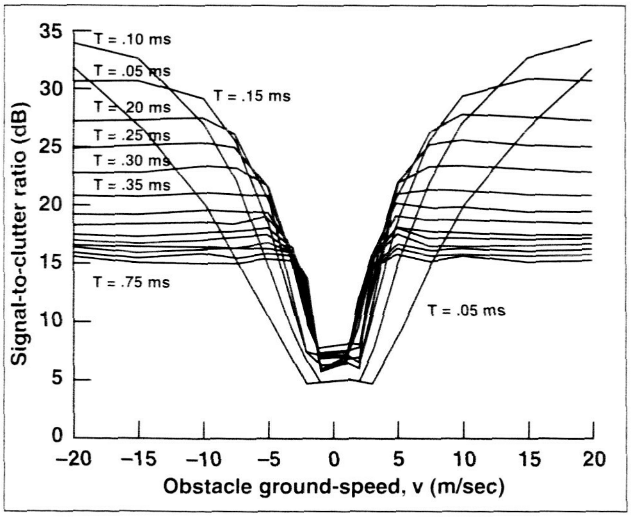

Fig. 1. Obstacle discrimination by ground speed.

illuminates the ground on one side of the aircraft, using a fixed, small, wide-angle antenna. The synthetic aperture equals the distance flown during the observation time of about 0.2 second. Since the aperture is aligned with the flightpath, the conventional SAR is looking sideways at 90 degrees.

The SAR technique has been extended for looking "almost forward"; it now illuminates the angular sectors of 5–45 degrees on both sides of the aircraft flight direction. Thus, the azimuthal resolution becomes a variable that depends on the look direction—it is zero looking straight forward, and improves with the squinting angle.

A conventional SAR, as well as the modified one, images stationary reflectors in their correct azimuthal location (range and elevation are always correct), whereas moving targets appear shifted in azimuth in proportion to their ground speed. This phenomenon is apparent in an SAR image of a moving train, where the train appears to run off the tracks. Incorporating a technique called "monopulse" alleviated this problem for *detecting* low-speed targets—although not for their accurate azimuthal *mapping*. The second figure shows the image of a two-dimensional uniform array of point-size reflectors on the ground on the right side of the flightpath (flying left to right). The smearing shows how the resolution degrades as the look angle approaches the flight direction.

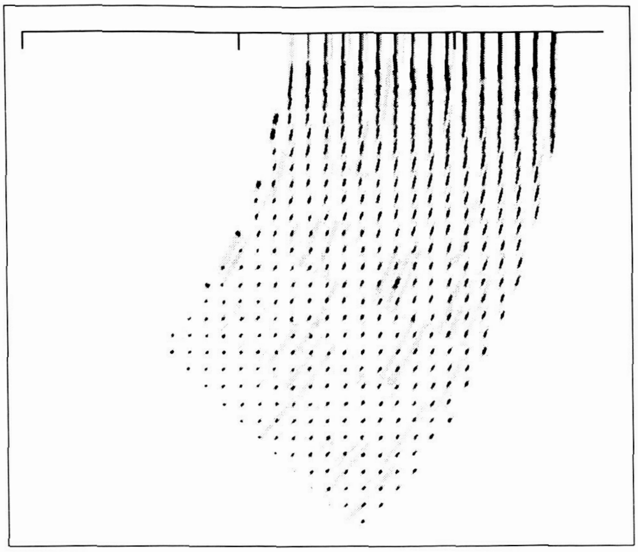

Fig. 2. Azimuthal resolution depends on squint angle.

Contact: Yair Barniv
(650) 604-5451
ybarniv@mail.arc.nasa.gov

Detection of Aircraft in Video Images

Jeffrey W. McCandless, Albert J. Ahumada, Mary K. Kaiser

NASA is collaborating with the aircraft industry to develop technology for a supersonic passenger airplane called the High-Speed Civil Transport (HSCT). One issue that is being examined is the replacement of the conventional forward cockpit windows with synthetic displays. The imagery in these displays would be obtained from video cameras mounted outside the aircraft. A benefit of this configuration is that the video imagery can be examined with computers to determine if another aircraft is in the scene. The goal of this HSCT subproject is to develop computer vision programs to detect aircraft that are moving in the video images.

During FY97, a series of computer programs were written to process video images and to search for moving objects (e.g., other aircraft). Flight tests were conducted in April and May to obtain the video imagery to test the computer programs. Each flight test was conducted with two aircraft. One aircraft was a Boeing 737 with a camera mounted below the nose. With a field-of-view of 13 degrees, this camera recorded the images of a second aircraft (the target plane) flying in various trajectories. For example, one trajectory consisted of the target plane flying from

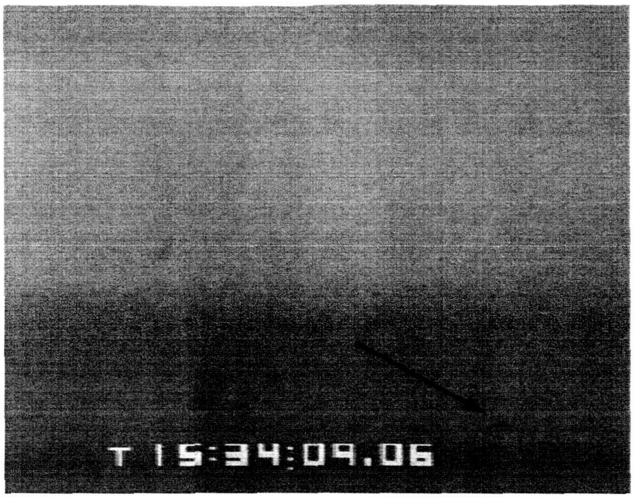

Fig. 1. Video image showing another aircraft flying in the field of view of the camera mounted on the Boeing 737.

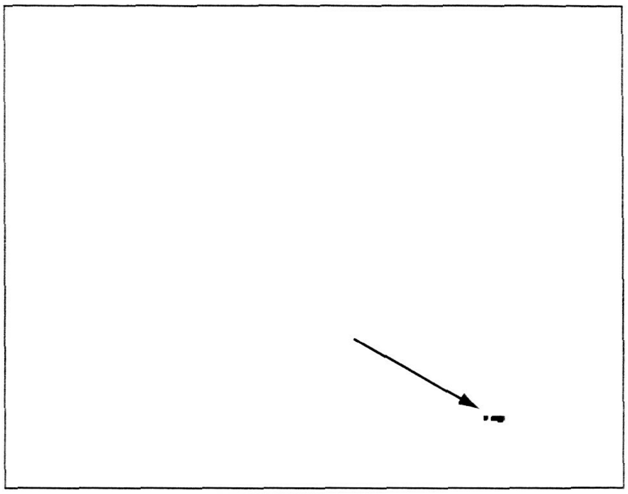

Fig. 2. Results of the computer program. The black region indicates the position of the aircraft in figure 1.

right to left across the path of the Boeing 737, producing the image in the first figure. The position of the target plane is indicated by the arrow in the figure. In this instance, the target plane was a Beech King Air 200 flying at a distance of 1 nautical mile from the Boeing 737. At this distance, it appears relatively small in the image. A computer program based on an optical flow algorithm located the aircraft, as shown in the second figure. In this latter figure, the area corresponding to the aircraft is shown in black.

Point of Contact: J. McCandless
(650) 604-1162
jmccandless@mail.arc.nasa.gov

Surface Operations Research and Evaluation Vehicle

Mary K. Kaiser

The new research vehicle sited at Moses Lake Airport in central Washington doesn't look like it has much in common with the conceptual drawings for the next-generation supersonic airliner, the High-Speed Civil Transport (HSCT). In fact, the Surface Operations Research and Evaluation Vehicle (SOREV) bears more passing resemblance to the large, wheeled irrigators used in the wheat fields surrounding the airport than it does to the sleek, delta-winged HSCT that will one day fly the Pacific Rim at over twice the speed of sound. Yet to researchers addressing issues associated with HSCT taxi operations, the SOREV is a thing of beauty.

The SOREV (shown in the figure) accurately captures the gear and flight-deck geometry of the full-scale HSCT. On the HSCT, there will be an unusually large distance between the flight deck and the nose gear (the pilot sits over 50 feet in front of the gear), and the SOREV provides test capabilities not available in existing test vehicles. Further, the SOREV permits researchers to investigate a number of issues and options associated with the development of an eXternal Visibility System (XVS), which replaces conventional forward-facing windows with synthetic displays. Like the HSCT, the SOREV is equipped with side windows, and the structure supports the mounting of cameras and other sensors.

The SOREV is fully equipped as an experimental vehicle, with extensive onboard position tracking and data collection facilities. Onboard monitoring systems also provide for vehicle safety; both they and the safety driver (who has a bubble-top view of the test arena) can perform safety shutdowns if performance envelopes are pushed too far.

The SOREV will play a significant role in ensuring that the HSCT can perform safely and that it will integrate seamlessly into the airport operations of the 21st century. The test vehicle was built by Martinez & Turek of Rialto, California, under a contract with Boeing, one of the industry partners of the NASA High-Speed Research Program. The other SOREV team partners are Honeywell and the NASA Ames and Langley Research Centers.

Point of Contact: M. Kaiser
(650) 604-4448
mkaiser@mail.arc.nasa.gov

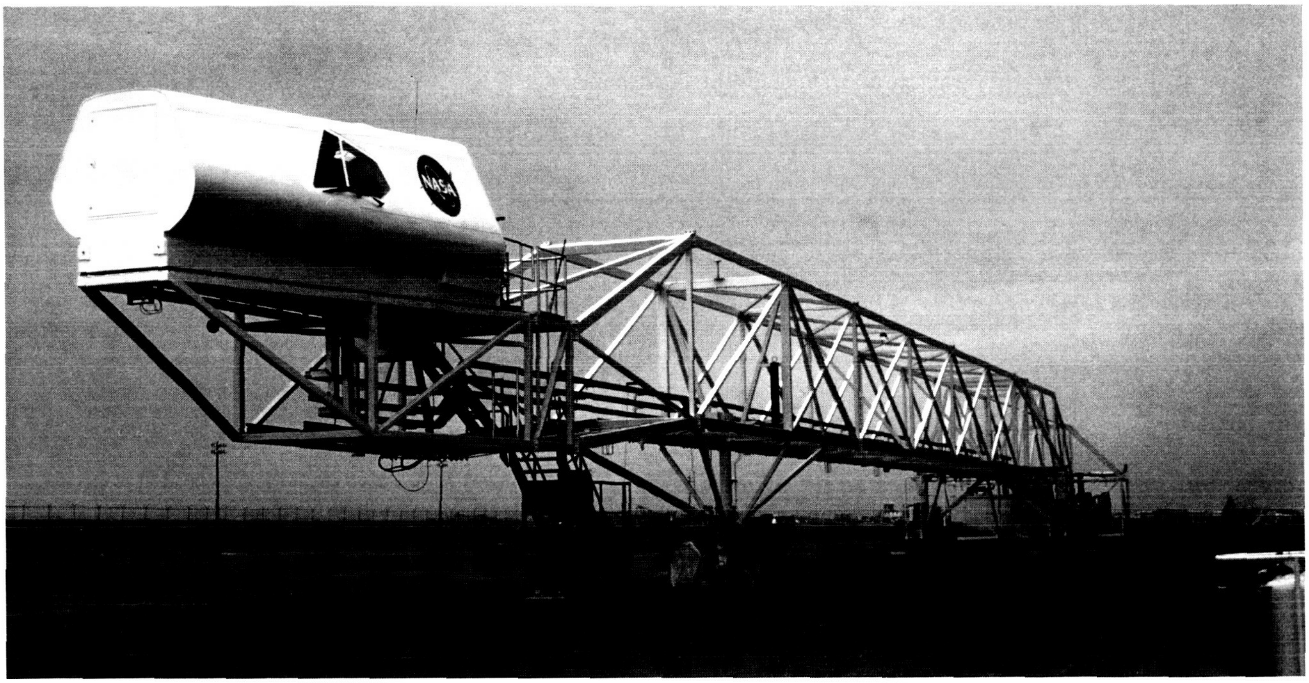

Fig. 1. The Surface Operations Research and Evaluation Vehicle (SOREV). This experimental vehicle accurately models critical aspects of the high-speed civil transport's geometry (e.g., gear and flight-deck placement) and ground maneuvering dynamics (acceleration, braking, turn capabilities).

Direct Simulation of a Supersonic Turbulent Boundary Layer

S. Guarini, R. D. Moser, K. Shariff

Turbulence modeling introduces one of the major sources of uncertainty in the prediction of aeronautical flows. This statement is even truer for supersonic flows for which physical insight is lacking and for which any modeling ideas that do exist remain unvalidated because of lack of data.

Physical understanding and proper modeling of turbulent supersonic flow have seen a new beginning, however, thanks to a number of direct simulations by several groups in the last decade. For instance, an important effect which has recently come to light in free shear flows is a significant reduction with Mach number in the ability of the flow to produce turbulent shear stress from turbulent energy.

A direct simulation of a supersonic boundary layer at Mach 2.5 has just been completed. The turbulence is treated as being homogeneous (times a slow variation) along a transformed streamwise coordinate. The slow variation produces extra terms in the resulting equations. This technique not only obviates the need for an extended length in order for the turbulence to develop, but also allows the use of highly accurate Fourier expansions in the streamwise direction. A highly accurate B-spline representation is used in the wall-normal direction.

The supersonic boundary layer has been traditionally regarded, on the basis of experiment and analysis, as having weak compressibility effects, which can be accounted for by variations in mean fluid properties across the layer. One such analysis is due to Morkovin (1962); it proposes relationships between temperature and velocity fluctuation. The relationships are based on the hypothesis that fluctuations of stagnation temperature are much smaller than those of static temperature. However, the hypothesis itself is found to be invalid, a fact noted by Morkovin himself. Yet, a relationship for root-mean-square intensities which derives from the hypothesis was found to be valid. Its true basis remains to be uncovered.

Another relationship that follows from the hypothesis is that velocity and temperature fluctuation should be anti-correlated. The first part of the figure compares the correlation coefficient $R_{u'T'}$ of these two quantities in the simulation (solid line) with three experiments (symbols) at a similar Mach number. The disagreement is obvious: the experiments indicate a much better agreement with Morkovin's hypothesis than do the simulations. However, the second part of the figure shows that the simulation result (solid line) falls in the middle of several incompressible experiments. The reason for the discrepancy with compressible experiments remains to be explored. For example, is it the result of the low Reynolds number of the simulation compared with that of the experiment?

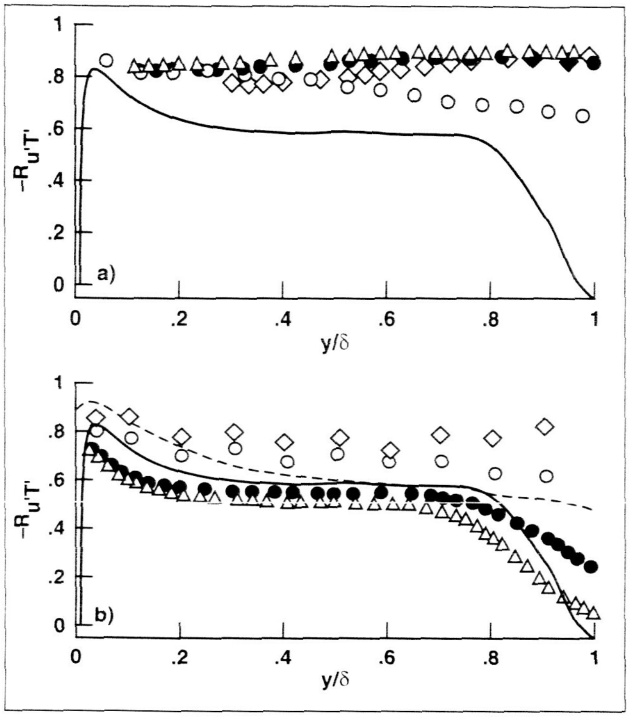

Fig. 1. Correlation coefficient $R_{u'T'}$ of velocity and temperature fluctuations: (a) comparison of simulation (solid) with various compressible experiments (symbols); (b) comparison with incompressible simulation (dashed) and incompressible experiments (symbols).

Point of Contact: K. Shariff
(650) 604-4729
shariff@nas.nasa.gov

Aerothermal Analysis of the X-33 Vehicle

Mike Green, Dinesh Prabhu, Grant Palmer, Mark P. Loomis, Ethiraj Venkatapathy, Dean Kontinos, William Henline, Susan Polsky, Periklis Papadopoulos, Carol B. Davies

High-fidelity hypersonic acreage aerothermal environments have been computed using state-of-the-art numerical methods for three configurations of the Lockheed-Martin Skunkworks X-33 Phase II vehicle. The aerothermal environments, which include the surface pressures, radiative equilibrium surface temperatures, surface streamlines, and loads, have been computed in two paradigms: (1) a trajectory paradigm in which solutions are computed at several points along design trajectories, and (2) a design space paradigm in which solutions have been computed at several points in a space, parameterized by the free-stream Mach number, angle of attack, and Reynolds number, independent of flight trajectories. These computed aerothermal environments have been used in conjunction with an engineering method to define and design the thermal protection system of the X-33 vehicle. Further, the aerothermal environments for deflected control surfaces (on both the canted and vertical fins of the vehicle) and the effect of yaw have been computed. The effect of configuration changes, an evolutionary process unavoidable in design, has also been studied.

The primary objectives of the work were to integrate high-fidelity numerical methods into the design cycle of the X-33 and to put into place the necessary tools and methods for designing the next generation of reusable launch vehicles (RLVs). During the course of acreage computations of the X-33 aerothermal environments, an attempt was also made to define the aerothermal environment of a 2x-scale X-33 (representative of the RLV) at Mach 25, and to address, in a limited sense, the traceability of the X-33 environment to that of the RLV. The first figure shows, in four views, the comparison of the computed surface isotherms of the X-33 and the RLV at peak heating points on their respective trajectories. The surface is assumed to be fully catalytic with emissivities that are typical of the candidate materials for the thermal protection system. The figure shows that at the peak of the heat pulse during the descent phase, both vehicles experience nearly the same thermal environment, even though the X-33 is at a lower altitude.

The present work clearly establishes the feasibility of integrating high-fidelity numerical methods into the design cycle of hypersonic vehicles, either directly or indirectly, as anchor points for engineering methods. The work also establishes the usefulness of the design space paradigm wherein the aerothermal environment definition is effectively decoupled from the trajectory. Although this approach requires more numerical solutions than the traditional trajectory-based approaches, it speeds up the process of trajectory evaluation and is very useful in studying trajectory dispersions and their influence on the design of the thermal protection system.

The thermal protection system on the windward side of the Lockheed-Martin X-33 technology demonstrator vehicle consists largely of metallic panels. As the vehicle travels through Earth's atmosphere at hypersonic speeds, thermal gradients between the top and bottom face sheets cause the metallic panels to bow. Steps and gaps will exist at the panel/panel and panel/nosecap interfaces. This study used Navier–Stokes flow analysis to assess the effects of the bowing, steps, and gaps on the surface heating of the vehicle. A parametric study was performed at the peak heating: peak Mach, Mach 10 turbulent, and peak negative bowing locations of the Mach 15 trajectory. A series of surface-heating augmentation factors was generated that provides the increase or decrease in heating rate as a function of bow height, step height, and gap width. The existence of reverse flow at the panel interfaces, because of panel bowing, was demonstrated.

The phenomenon of thermal-protection-system panel bowing was also studied in a more rigorous manner. Three numerical models, one for the flow

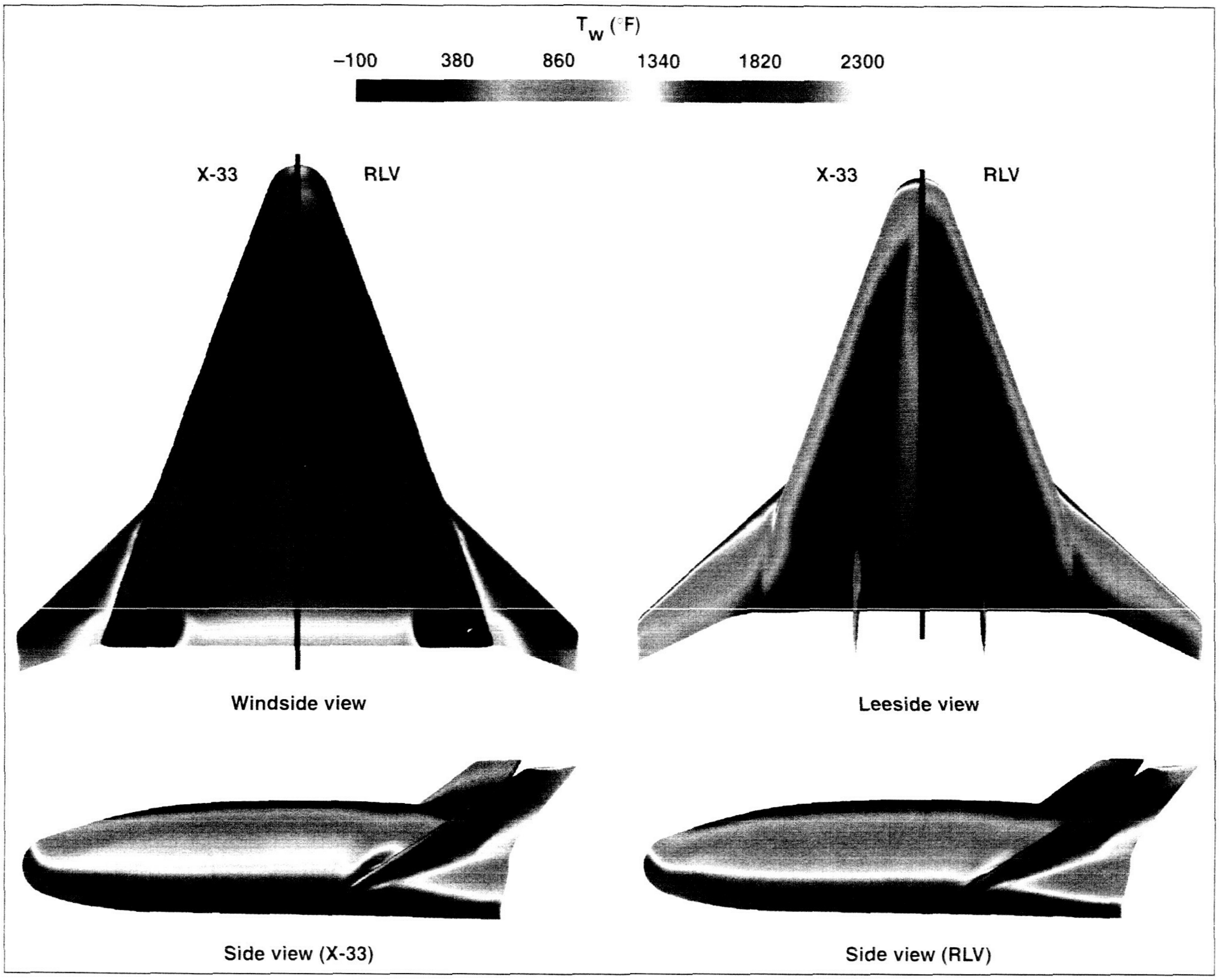
T_w (°F)
–100
380
860
1340
1820
2300
X-33
RLV
X-33
RLV
Windside view
Leeside view
Side view (X-33)
Side view (RLV)

Fig. 1. Comparison of the computed radiative equilibrium surface temperatures.

field, one for the in-depth heat transfer, and one for the thermoelastic deformation, were coupled in sequence to yield the transient response of the metallic panel. The aerothermal loads were derived from computational fluid dynamic solutions and were prescribed as a distribution function with maximum bow height as the governing parameter. Finite-element models were used to simulate the thermal and structural response. The coupled simulation was compared to a single-pass uncoupled solution. Results showed negligible feedback between the structural deformation and the deformation-induced perturbation of the aerothermal heat load. Yet, significant temperature variations were produced on

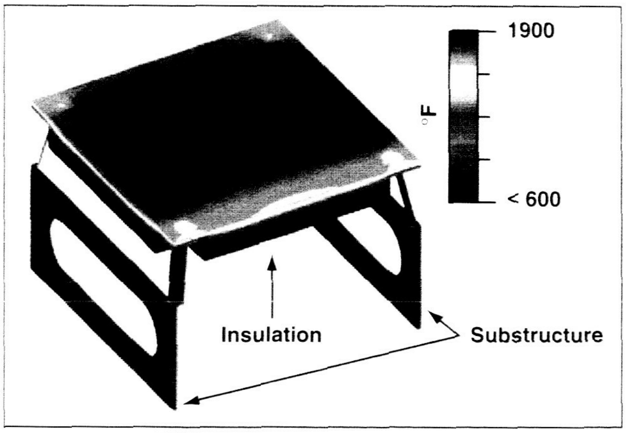
1900
°F
< 600
Insulation
Substructure

Fig. 2. Surface and in-depth temperatures, peak heating point.

the surface of the panel. The deformations induced lateral temperature gradients that increased the thermal stress within the panel. Finally, it was shown that panel bowing does not appreciably alter the trajectory-integrated heat load. The second figure shows computed surface and in-depth temperatures on a panel/support structure stack-up at the peak heating trajectory point.

Point of Contact: M. Green
(650) 604-5595
mgreen@mail.arc.nasa.gov

Aerothermal Analysis of the X-34 Vehicle

Grant Palmer, Susan Polsky

The X-34 vehicle will provide the first flight demonstration under NASA's Reusable Launch Vehicle (RLV) program of a fully reusable launch vehicle. Under a fixed-price contract with NASA, Orbital Sciences Corporation (OSC) is to provide a Mach 8 suborbital RLV technology demonstrator. The vehicle is 18.3 meters in length, has a wingspan of 8.4 meters, and is powered by a single LOX-kerosene engine. The X-34 is carried below an L-1011 aircraft to an altitude in excess of 9 kilometers, where the vehicles separate, the X-34 engine starts, and the X-34 vehicle continues along its flight trajectory. The first flight is scheduled for 1999.

Under a cooperative agreement with OSC, Ames Research Center was given the responsibility for designing, analyzing, and fabricating the thermal protection system (TPS) of the X-34 nosecap, wing leading edges, and rudder leading edge. Temperature, pressure, and heating rates on the surface of the X-34 were computed at six points along the X1004701 Mach 8.5 no-bounce trajectory. The work focused on the nosecap, wing/strake leading edges, and the rudder leading edge. These areas are protected from the thermal environments experienced during flight by silicone-impregnated reusable ceramic ablator tiles.

The computational data provided anchor points from which a time history of surface heating and pressure could be generated. This time history will be used to analyze and design the tiles. The figure shows computed surface-temperature contours at the peak heating point on the descent portion of the trajectory. The Navier–Stokes solutions were, when possible, compared with data from engineering correlations.

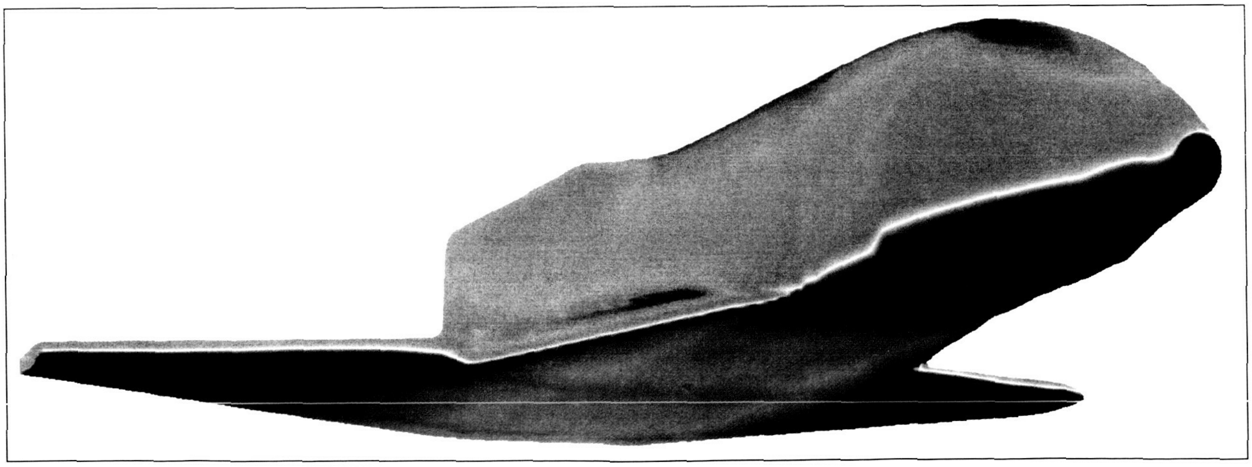

Fig. 1. Surface temperature contours.

The bow shock-wave impingement on the wing leading edge was also investigated. The location of impingement was a function of free-stream Mach number and vehicle angle of attack; no bow shock-wave impingement was seen on the rudder leading edge. A detailed grid sensitivity study was undertaken to establish an acceptable level of grid independence of the computed solutions.

Point of Contact: G. Palmer
(650) 604-4226
gpalmer@mail.arc.nasa.gov

Sharp Leading Edges for Hypervelocity Vehicles

Joan S. Salute, Paul Kolodziej, Jeffrey D. Bull

Recent research shows that ultra-high temperature ceramics (UHTCs) may enable sharp leading edges to be used on space vehicles. Sharp leading edges (≤1 centimeter) could enable an entire new design space for hypervelocity vehicles with decreased drag, increased cross-range capability, and reduced cost-to-orbit. These factors, combined with results from ground-based testing and analysis, led to the implementation of the first UHTC flight demonstration. The objective of this flight was to validate the nonablating performance of a UHTC "sharp" leading edge by comparing flight data with theorized material performance data.

Implementation of the UHTC flight demonstration was a joint effort by Ames Research Center, Sandia National Laboratories, and the U.S. Air Force. A Minuteman III (MM III) launch/reentry opportunity was secured.

Ames designed a UHTC nosetip that sharpened the conventional Mk12A nose from a radius of 0.861 inch to 0.141 inch, as shown on the SHARP reentry vehicle, at the left in the figure. A microminiature thermocouple sensor was designed to measure the temperature within the nosetip. These articles were successfully fabricated, tested in the Ames arc-jet facility, and taken to Sandia National Laboratories for environmental testing. The reentry vehicle (RV) was flown to Vandenberg Air Force Base (VAFB) for further testing and integration with the MM III.

SHARP-B01 was launched from VAFB at 1:27 A.M., May 21, 1997. Once exoatmospheric, SHARP-B01 was deployed and entered Earth's

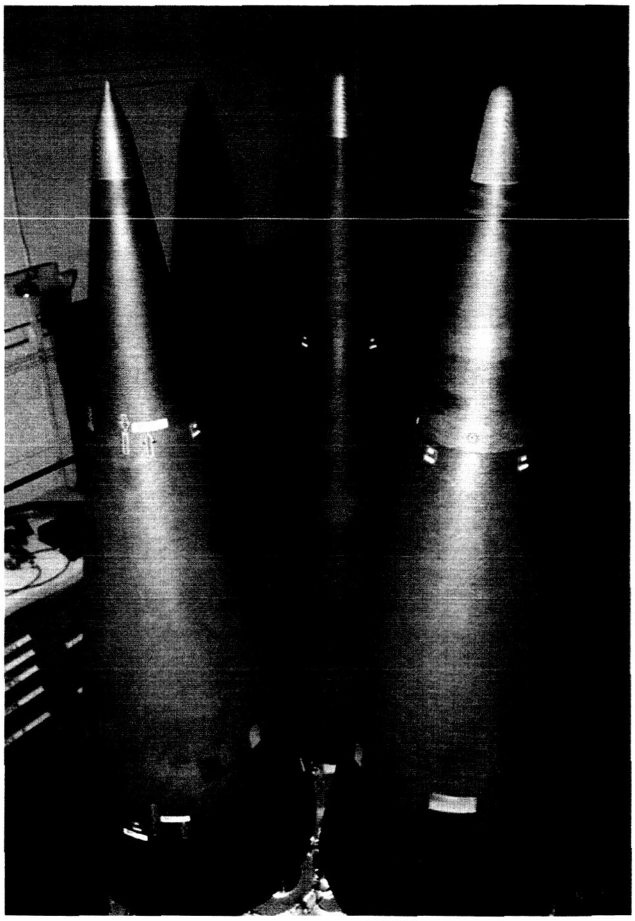

Fig. 1. The 0.141-inch radius nosetip SHARP-B01 reentry vehicle shown with standard Mk12A reentry vehicles.

atmosphere at velocities up to 22,700 feet per second. The nosetip sensor indicated that initial ablation occurred near an altitude of 191,000 feet at a velocity of 22,700 feet per second. Before and during nosetip ablation, SHARP-B01 dynamics were nominal.

These flight results validate the preflight expectations of the UHTC nosetip performance. Arc-jet tests, integrated design tools, and now flight data all demonstrate the material's ability to operate at a temperature of 5100°F before it degrades.

The results of this flight demonstration of sharp leading edges have generated great interest in the aerospace industry.

Point of Contact: D. Rasky
(650) 604-1098
drasky@mail.arc.nasa.gov

Arc-Jet Flow Characterization

Douglas G. Fletcher

Arc-jet facilities have been used extensively to evaluate materials for use in the thermal protection of aerospace vehicles, from Apollo spacecraft and the shuttle to the X-33 and the X-34. Although arc-jet tests are indicative of how well a material will perform in extreme aerothermal heating environments, it has not been possible to directly relate arc-jet test results to flight applications. The main obstacle has been an inability to determine the total enthalpy of the nonequilibrium arc-jet flow, and its distribution among kinetic, thermal, and chemical modes. The objective of this work is to develop diagnostic techniques to determine these quantities, thereby improving our understanding of the relationship between arc-jet test and flight environments.

As part of this effort, a laser-spectroscopic instrument has been developed to characterize the flow environment by measuring the free-stream enthalpy in large-scale arc-jet facilities. This approach involves making flow-property measurements using two-photon laser-induced fluorescence (LIF) of atomic nitrogen; it was recently demonstrated in a series of tests conducted in the Aerodynamic Heating Facility (AHF). The flow properties, which include velocity, translational temperature, and species concentration, were measured simultaneously over a range of facility operating conditions. When combined with facility measurements of mass flux and pitot pressure, an analysis of the flow properties obtained using the two-photon LIF technique yields the kinetic, thermal, and chemical enthalpy components of the free-stream flow directly; the total flow enthalpy is calculated from the sum.

Example two-photon LIF excitation spectra from atomic nitrogen obtained from the arc-jet flow and from a flow reactor, which is used to calibrate the arc-jet measurements, are presented in the first figure as a function of the dye fundamental wavelength.

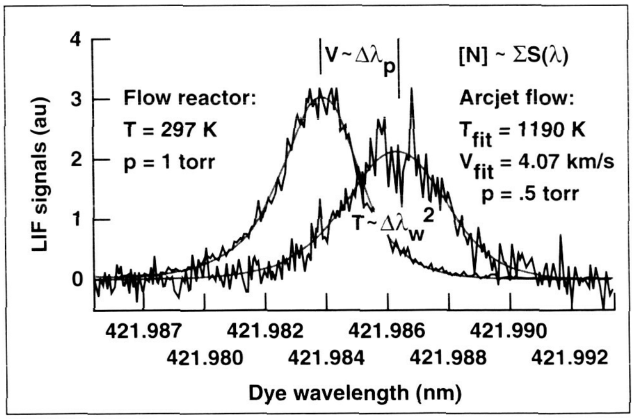

Fig. 1. Excitation spectra from two-photon LIF of atomic nitrogen from the arc-jet flow and from the flow reactor. The narrower spectrum is from the room-temperature, low-pressure flow reactor; the broader spectrum is from the higher-temperature, lower-pressure, nitrogen/argon arc-jet flow.

Nonlinear, least-squares fits to the spectra using a numerical model of the two-photon absorption line shape are also shown for both the reactor and flow data. The thermodynamic conditions of the flow reactor are given in the figure. The arc-jet flow conditions were deduced from the spectra by using the analytical methods that are summarized in the figure: velocity is determined from the Doppler shift of the absorption line center; translational temperature is derived from the absorption line width; and atomic nitrogen number density is proportional to the spectrally integrated LIF signal.

Measurements in the AHF, which was configured with a 30-centimeter-diameter nozzle, were obtained during experiments in which the arc current was varied at constant pressure for two different pressures in a nitrogen/argon mixture. Experimentally determined free-stream total enthalpies for these tests are shown in the second figure; the values range from 16 megajoules per kilogram at the lowest current of the low pressure test case to 28 megajoules per kilogram at the highest current of the high-pressure test. For both chamber pressures, a trend of increasing total enthalpy with increasing arc current is indicated within the uncertainty of the measurements. Trends in enthalpy distribution among the three modes, as current and pressure vary, also provide useful insight into the kinetic processes that govern the nonequilibrium expanding nozzle flow.

Total stream enthalpy and its apportionment into kinetic, thermal, and chemical contributions in the nonequilibrium arc-jet free-stream flow have been sought for over 30 years. The two-photon LIF technique that has provided these measurements represents a unique instrumental capability, and its use in further characterization of the arc-jet facilities at Ames Research Center will establish the relationship between the arc-jet test and flight environments.

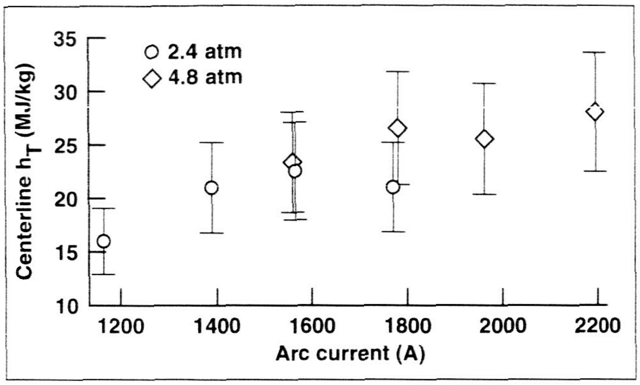

Fig. 2. Centerline enthalpy values that were measured during constant pressure, variable current nitrogen/argon flow tests conducted in the AHF. Uncertainties are indicated by the vertical bars.

Point of Contact: D. Fletcher
(650) 604-1647
dfletcher@mail.arc.nasa.gov

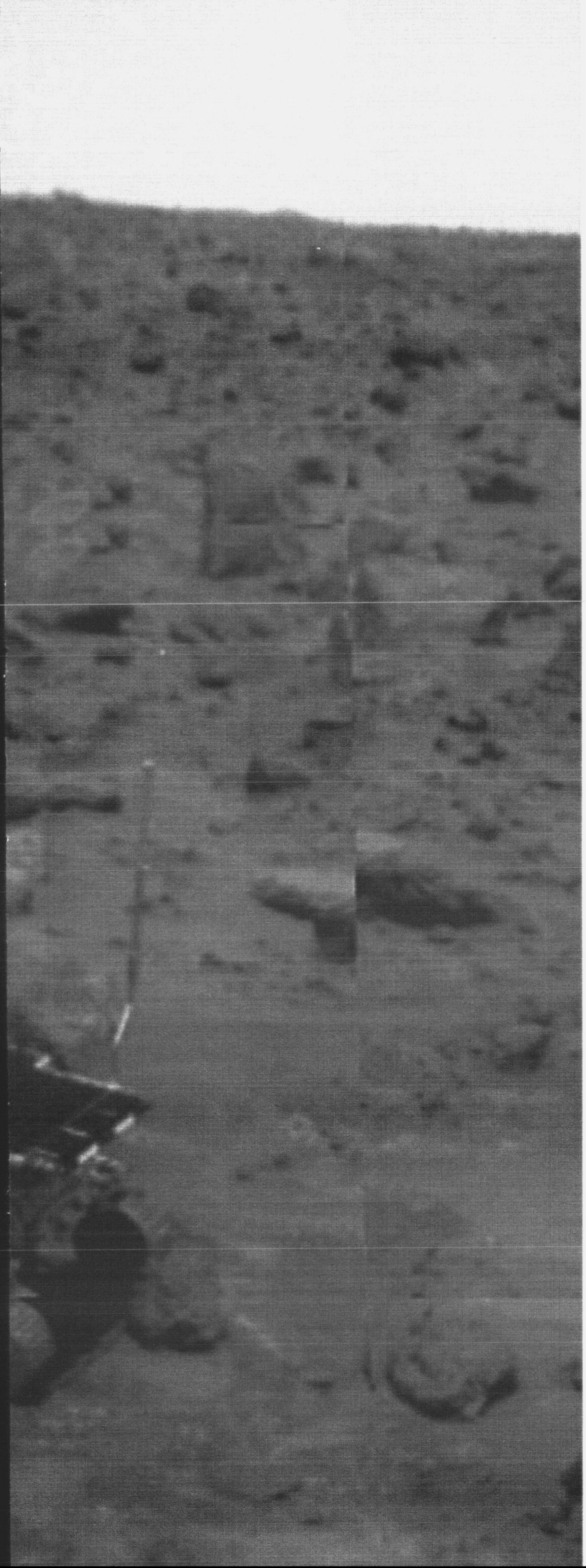

Overview

Scientists in NASA's Space Science Enterprise seek to answer fundamental questions about the origin and evolution of life and celestial objects (planets, planetary systems, stars, galaxies, etc.) in the Universe. Ames Research Center is recognized as a world leader in astrobiology, the study of life in the Universe and of the chemical and physical forces and adaptations that influence life's origin, evolution, and destiny. In pursuing its primary mission in astrobiology, Ames performs pioneering basic research and technology development to further fundamental knowledge about the origin, evolution, and distribution of life within the context of cosmic processes.

Research and technology development are conducted to:

- Study extrasolar matter such as cosmic rays and interstellar gases
- Explore the characteristics of the heliosphere
- Explore the other planets of the solar system
- Identify locations on other planets within the solar system where conditions conducive to life exist or have existed
- Locate planets and planet-forming regions around other stars
- Determine the abundance and distribution of the biogenic compounds that are conducive to the origin of life
- Study the mechanisms of the origin, evolution, and distribution of life in the Universe

Exobiology

Ames' Exobiology Program is a key element of NASA's Astrobiology Initiative, and Ames serves as NASA's lead Center in exobiology. Research in exobiology at Ames ranges from studies of the mechanisms of the origin of living systems, to the processes governing the evolution of life, to the distribution of life on other planets. When coupled with Ames' pioneering research on the dynamics of galaxies, molecular gases and clouds, planetary systems, and the solar system, the study of life is facilitated by the enhanced understanding of the cosmic environment within which life originates and evolves.

Molecules of exobiological significance are ubiquitous in the Universe. It is important to understand the sources and interactions of these building blocks and how living systems emerge from prebiotic molecular chaos.

This report highlights studies in the following areas:

- The synthetic pathways that produce the amino acids found on meteorites
- The energetics of intermolecular interactions
- Chemical biomarkers that represent ancient terrestrial life in the fossil record
- Sites on Mars where chemical biomarkers would most likely have been deposited by ancient Martian life
- Prebiotic synthesis of activated amino acids
- The thermodynamic constraints that govern carbon chemistry related to the identification of good candidates for the first replicating molecules
- Modeling of the dynamics of biological systems with networked interactions

Planetary Systems

Scientists in the Space Science Enterprise are interested in how and where in the Universe planets form, and the geophysical, geochemical, and atmospheric processes that occur over the lifetime of a planet. Further, understanding the dynamics between planetary processes and the origin and evolution of life will help in understanding the distribution of life in the Universe.

Scientists at Ames conceived of and initiated 7 of NASA's 11 planetary missions that have flown since 1972. Of all the planets in the solar system, Mars is most like Earth, especially in that its weather and climate are dynamically similar to Earth's and in that its history may have included life. On July 4, 1997, Mars Pathfinder made history when it bounced to a safe landing on Mars and deployed the small, but capable Sojourner rover. The world watched daily as Sojourner sent back so many detailed images of the Martian landscape that even individual rocks became recognizable.

Planetary Systems research highlighted in this report include the following:

- Numerical simulations of the process of accretion, by which comets and asteroids are formed from micron-sized dust grains in protoplanetary nebulae
- Modeling of meteoritic impacts which provides new insights into geophysical phenomenon such as the magnetic signatures of rocks
- Studies of the reactions of nitrogen and oxygen to better understand the distribution of nitrogen and nitrous oxides in Earth's thermosphere
- Twenty-four-hour monitoring of meteor activity across the entire Northern Hemisphere in order to improve predictions of the returns of long-period comets
- Modeling of the early phases of the growth of planets, including calculations of accretion rates and simulations of the evolution of planetary orbits
- Production and use of a three-dimensional photo-realistic virtual reality model of the Martian surface to enhance the remote data collection performed by Mars Pathfinder
- Estimating the ages of the geologic surfaces of the Galilean satellites, Io, Europa, Ganymede, and Callisto, from the absolute cratering rates resulting from cometary impacts

Astrophysics

As NASA's lead center in airborne astronomy, scientists at Ames pioneered the field of astrophysics. Study topics range from star-forming regions and processes to interstellar photochemistry to protoplanetary disks. Understanding cosmic processes—the evolution of the universe itself—is a vital part of the Origins Initiative.

Ames' astronomers and astrophysicists utilize a wide variety of methods. Ground-based telescopes, such as the Keck and Mount Lemon Observatories, are regularly used to make observations of celestial objects and processes. Development continues on the Stratospheric Observatory for Infrared Astronomy, an infrared telescope to be carried aboard a Boeing 747 aircraft that was specially modified for the task. Space-based observations are also made through instruments such as the Hubble Space Telescope, the European Infrared Space Observatory, and the Japanese Mid-Infrared Spectrometer mission. Computer modeling and laboratory analogs of chemical processes complement the observational astronomy performed.

Astrophysics research highlighted in this report include the following:

- Numerical modeling of the structure of solar nebulae and its relation to planet formation
- Modeling of stellar photospheres and emergent spectra and its application to studies of the infrared spectra of sunspots
- Observations of at least one dense protoplanetary disk (proplyd) and several pairs of binary stars in the belt of the constellation Orion, the nearest region to the Earth where massive stars are being formed
- Studies of the effects of nearby stars on protoplanetary disks and planet-formation processes
- Studies of the photochemistry resulting from ultraviolet irradiation of laboratory analogs of interstellar and cometary ices
- Observation of polycyclic aromatic hydrocarbons in the nebula NGC 1333

Space Technology

To support the Space Science Enterprise in conducting future space science and exploration missions, Ames scientists and engineers develop and validate technologies and instruments, develop calculational and modeling algorithms, and refine analytical methods. The following developments are described in this report:

- A submicron optical aerosol spectrometer to study the particulate components of planetary atmospheres
- A guide-star telescope detector for use on the Gravity Probe B Project
- A significantly improved algorithm for calculating the opacity of water, which enables detailed analysis of the experimental spectrum of water, particularly at high temperatures
- An improved method for preparing analytical microcolumns for miniaturized instruments for future planetary spacecraft missions focusing on in situ or returned samples analysis

Implementing a Strategy for Mars Exopaleontology

Jack D. Farmer, David J. Des Marais

In exploring for a record of ancient Martian life, the goals, methods, and assumptions differ substantially from those required in exploring for extant life. To differentiate this activity from the conventional discipline of exobiology, the exploration of ancient extraterrestrial life is referred to as exopaleontology. The practical task facing exopaleontology is to define a strategy for exploring Mars' fossil record during the decade-long exploration program that lies ahead. Consideration of the quality of paleontological information preserved under different geological conditions is important in order to develop a strategy with broad applicability. To help guide site selection during the Mars Global Surveyor (MGS) Program, a site-selection strategy for exopaleontology—based on microbial fossilization processes in a variety of extreme environments regarded to be good analogs for early Earth and Mars—was developed.

The microbial fossil record encompasses a wide range of information, including cellular remains (organic-walled, permineralized replacements, and external molds of cells), trace fossils (microborings in rocks), biofabrics (micro-textural features of sediments attributed to the behavior of microorganisms), stromatolites (finely laminated biosedimentary structures), biominerals (biomediated mineral precipitates), and chemofossils (biomarker organic compounds, isotopic and trace-element signatures). The preservation of fossils is strongly influenced by the physical, chemical, and biological factors of the environment, which together ultimately determine the kinds of information that will be captured and retained in the rock record. In detrital sedimentary systems, preservation is favored by rapid burial in fine-grained, clay-rich sediments. In chemical sedimentary systems, preservation is enhanced by rapid entombment in fine-grained chemical precipitates. For long-term preservation, host rocks must be composed of stable minerals that resist chemical weathering and that form an impermeable matrix and closed chemical system capable of protecting biosignatures from extensive alteration during subsequent diagenetic changes or metamorphism. In this context, host rocks composed of highly ordered, chemically stable mineral phases, like silica or phosphate, are especially favored. Such lithologies tend to have very long crustal residence times and (along with carbonates and shales) are the most common host rocks for the Precambrian microfossil record on Earth. An important goal in implementing the strategy for Mars exopaleontology is the discovery of surface exposures of these and related minerals during upcoming Mars missions. Efforts continue to define high-priority sites for exopaleontology using Viking data, but site priorities will be refined in the future as new data are incorporated from the Mars '96 Global Surveyor orbiter (beginning in March 1999). Present emphasis is on locating sites that are likely to have sustained long-lived aqueous sedimentation. This approach has identified a large number of potential sites for exopaleontology.

A critical step in implementing a strategy for exploring for evidence of past or present Martian life and prebiotic chemistry is to locate accessible surface outcrops of aqueously formed mineral deposits of the type known to be good long-term repositories for microbial fossil information in the Precambrian rock record on Earth. One limitation is a lack of high spatial resolution remote-sensing data at wavelengths that can provide information about surface mineralogy. The thermal emission spectrometer, which is presently in orbit at Mars, will obtain a global map of surface mineralogy at a spatial resolution of ~3 kilometers per pixel during its nominal mission. But to optimize the selection of sites for a sample return in 2005 and beyond will require infrared mapping at a spatial resolution capable of resolving individual outcrops. Results from ongoing analog remote-sensing studies in the Great Basin of western North America indicate that a resolution capability of about 100 to 300 meters per pixel will likely be needed to precisely locate sedimentary deposits of the right mineralogy (i.e., rock types most favorable for preserving a fossil record of past life) in order to effectively plan rover operations. The 2001 MGS orbiter is presently slated to carry a high-resolution, mid-infrared mapping spectrometer called THEMIS which will be capable of attaining this resolution at selected high priority sites.

Point of Contact: D. Des Marais
(650) 604-3221
ddesmarais@mail.arc.nasa.gov

Molecular Biomarkers in Living Stromatolites

Linda L. Jahnke, Jack D. Farmer, Harold P. Klein

Stromatolites, among the most common fossils in the geologic record, are defined as organosedimentary structures formed by sediment trapping and binding or by mineral precipitation (or both) of microbial communities living in shallow water environments. The microfossil record in stromatolites traces Earth's history since the oldest life, over 3.5 billion years ago. During most of this time, microbial life has dominated Earth, and has been responsible for transforming the primitive anaerobic environments of early Earth, devoid of free molecular oxygen, to the modern aerobic world that supports contemporary biology. Microbial mats are "living" stromatolites, modern day analogs that provide an opportunity (a window to the past) to study the way ancient microbial communities lived and evolved. Today, a variety of these "living" analogs, representing a range of environmental and organismal parameters, are available for study throughout the world. For the most part, the dominate members of recent mats are oxygenic photosynthetic bacteria, the cyanobacteria. The evolution of oxygen-producing photosynthesis within the cyanobacteria heralded the beginnings of our modern aerobic world, and the timing of this event is of particular interest in attempts to understand the process of Earth's evolution.

A variety of stable organic compounds, generally referred to as chemical fossils or biomarkers, have been extracted from stromatolites. Indigenous fossil biomarkers can provide clues to the identity of the original mat-building community and provide insights into the paleoenvironment in which this community existed. The challenge is to understand the link between such molecular fossils and their "living" counterparts, the biomarker molecules synthesized by contemporary mat-building bacteria, and then to apply this information to the study of contemporary microbial mats. Efforts at Ames Research Center are focused on a type of columnar (or conical) stromatolite, the Conophyton, which is one of the most distinctive groups of Precambrian stromatolites. A "living" Conophyton analog is currently forming as the result of silicification of a mat constructed by a fine filamentous cyanobacterium called *Phormidium* in hot springs located in Yellowstone National Park.

The study began by isolating a variety of *Phormidium* cyanobacteria from columnar, microbial mats found in Yellowstone. Two important types of organic molecules have been identified in these cyanobacteria: a group of branched alkanes having 17 to 20 carbons (C_{17}–C_{20}), and hopanoids, a highly cyclized C_{30} molecule (see figure). Both methylalkanes and hopanes are excellent biomarkers for cyanobacteria, are resistant to biodegradation, and are presently known to be the oldest biomarkers dating to Proterozoic rocks 1.7 billion years old. Interest at Ames is in the processes involved in the deposition or degradation of organic material during early mineralization of microbial mats, particularly as this relates to the potential for preserving biomarkers such as branched alkanes and hopanes, which are thought to be more highly resistant to microbial degradation.

In order to relate biomarker analysis of *Phormidium* cultures to their natural environment, the study at Ames is concerned with a type of submerged, columnar *Phormidium* mat widely prevalent in the terraced pools found in the Midway Geyser Basin in Yellowstone. As the pools dry up, the mat surface is gradually covered with a silica layer.

Organic analysis of the distribution of branched alkanes and hopanoids in the submerged and silicifying *Phormidium* mats shows that these cyanobacterial biomarkers dominate the surface photic zones, and that the relative amount of branched alkanes increases in the silicified mat surface. Surprisingly, another cyanobacterial biomarker, esterified polyunsaturated fatty acid (PFA), which is considered a measure of the number of viable cyanobacteria present, was at comparable levels in the surface zones of both the submerged and exposed mats. The cyanobacteria in the top layer of this silicifying, heavily encrusted mat were still very much alive, although an increase in the amount of PFA in the exposed mat does suggest an adaptive response.

There are, however, clear differences in biomarker preservation in the layers below the top photic zone. The relative compositions of the branched alkanes and hopanoids in the submerged mat are actually higher in the lower layers than in the top layer; in the exposed mat, these compounds are greatly reduced in the lower layer relative to the top photic zones of either submerged or silicified types. These changes in lipid biomarker composition suggest an adapting cellular response during the early diagenesis of this mat. It will be important to understand how such adaptation relates to further preservation of these biomarker fossils as mineralization and diagenesis continue toward the rock record.

Point of Contact: L. Jahnke
(650) 604-3221
ljahnke@mail.arc.nasa.gov

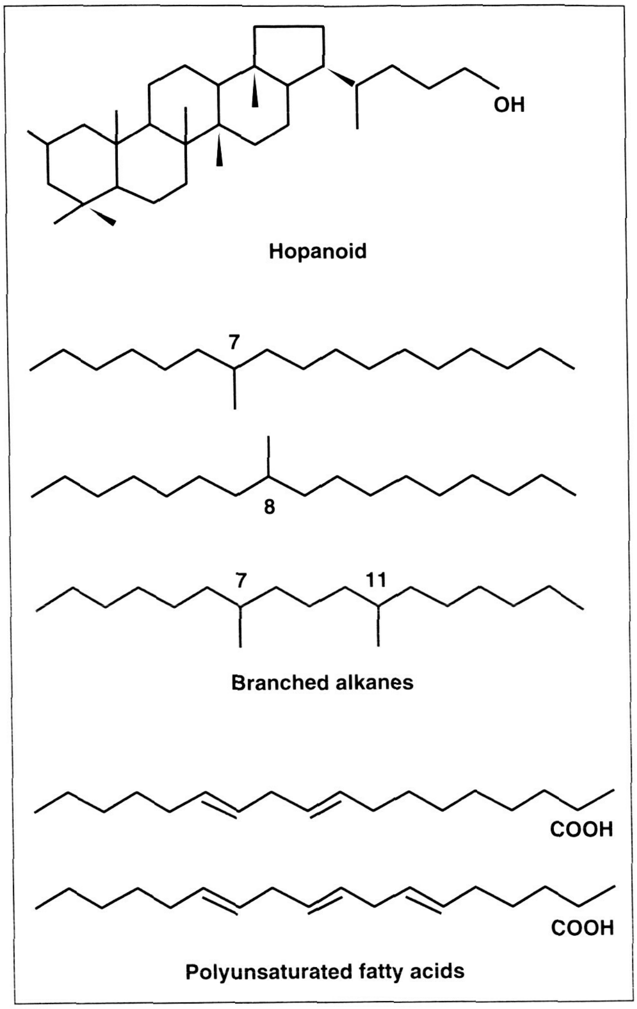

Fig. 1. Molecular biomarkers from Phormidium *cyanobacteria isolated from microbial mats in Yellowstone National Park.*

Amino Acids in Meteorites

Narcinda R. Lerner

The Strecker synthesis,

$$R_2C = O + HCN + NH_3 \leftrightarrow R_2C(NH_2)CN + H_2O \rightarrow R_2C(NH_2)CO_2H$$

has been proposed as a source of amino acids in meteorites. Detection in the Murchison meteorite of carbonyl compounds, the precursors of the amino acids in the Strecker synthesis, and of α-hydroxy acids, important by-products of the Strecker synthesis, supports this conjecture.

The amino acids and hydroxy acids found on Murchison are deuterium enriched, with $\delta D = +1751$ per mil for the unseparated amino acids, and $\delta D = +573$ per mil for the hydroxy acids. Several explanations consistent with a Strecker synthesis could account for this discrepancy, including the following: (1) It is generally accepted that the water responsible for the aqueous alteration that occurred on the Murchison parent body was deuterium-depleted with δD of the order of -100 per mil. If during synthesis, hydroxy acids retain less of the isotopic signature of their carbonyl precursors than their amino acid counterparts, or if the hydroxy acids exchange carbon-bonded hydrons more rapidly with water than the corresponding amino acids, a lower δD for the hydroxy acids is to be expected, even if they and the amino acids arose from common precursors. (2) Individual pairs of α-amino acids and α-hydroxy acids arising from common precursors retain the isotopic signature of their precursors equally well, but the abundance of the amino acid in a particular amino acid-hydroxy acid pair relative to the total amino acids is different from the abundance of the corresponding hydroxy acid relative to that of the total hydroxy acids, resulting in quite different collective isotopic signatures for total amino acids and total hydroxy acids.

With the objective of determining if the discrepancy in deuterium enrichment between the amino acids and the hydroxy acids found on Murchison is consistent with their formation in a Strecker synthesis, measurements have been made of the deuterium content of α-amino and α-hydroxy acids produced in solutions of deuterated carbonyl compounds, potassium cyanide (KCN) and ammonium chloride (NH_4Cl), and also in mixtures of such solutions and Allende dust at temperatures of 263 kelvin and 295 kelvin. Retention of the isotopic signature of the starting carbonyl by both α-amino acids and α-hydroxy acids is more dependent on temperature, concentration, and pH (a measure of acidity and alkalinity) than on the presence of meteorite dust in the solution. For acids with carbonyl precursors that have β-hydrons, the retention of the isotopic signature of their carbonyl precursors is favored by high concentration, low pH, and low temperature. For such acids, loss of the isotopic signature of the carbonyl precursor is frequently greater for the amino acids than for the corresponding hydroxy acids. In order to determine if hydroxy acids retain their carbon-bonded hydrons better than amino acids, deuterium exchange of α-hydroxy acids in deuterium oxide (D_2O) was investigated at temperatures in excess of 393 kelvin. No measurable loss of hydrogen was observed. Considerable deuterium exchange is observed for α-amino acids under such conditions. These results suggest that the Strecker synthesis is not responsible for the amino acids and hydroxy acids in the Murchison meteorite. In order to completely rule out the Strecker synthesis, the deuterium content of amino acid-hydroxy acid pairs such as glycine-glycolic acid or alanine-lactic acid need to be measured.

Point of Contact: N. Lerner
(650) 604-6941
nlerner@mail.arc.nasa.gov

Genetic Network Modeling

Shoudan Liang, Zoltan Szallasi, Stefanie Fuhrman, Roland Somogyi

A cell processes genetic information through transcription and translation of its genes. Understanding the organization of the genetic network and its minimum complexity requirement is among the important theoretical questions about the origins and evolution of life. With the advent of large-scale gene recognition techniques such as GeneChip and MicroArray, theoretical modeling of the genetic networks will also have applications in the biotechnology industry.

In the first project, Boolean networks are used to address complex problems in the cell cycle. First, a general strategy is formulated to generate Boolean genetic networks that incorporate all relevant biochemical and physiological parameters and cover all of their regulatory interactions in a deterministic manner. Second, "realistic Boolean genetic networks" are introduced that produce time-series measurements very similar to those detected in actual biological systems. This project will lead to a better understanding of constraints required for modeling a realistic gene network.

A related project addresses the question of whether it is possible, in principle, to completely infer a complex regulatory network architecture from input-output patterns of its variables. This possibility is investigated again using the Boolean networks. Trajectories, or state transition tables of Boolean nets resemble time-series of gene expression. By systematically analyzing the mutual information between input states and output states, the sets of input elements controlling each element or gene in the network are inferred. This process is unequivocal and exact for complete state transition tables.

The Reverse Engineering Algorithm based on information theory is implemented in a C program for a 50-element network with three inputs per element. The simulations show that a network can be completely reconstructed using only a surprisingly small amount of expression data. The method developed in this work will lead to a practical way of constructing computer models of gene networks. Although this study is limited to synchronous Boolean networks, the algorithm is generalizable to include multistate models, essentially allowing direct application to realistic biological data sets. The ability to adequately solve the inverse problem may enable in-depth analysis of complex dynamic systems in biology and other fields.

Point of Contact: S. Liang
(650) 604-6631
sliang@mail.arc.nasa.gov

Dynamical Behavior of Networks and Cellular Automata

Jeffrey Scargle, Silvano Colombano, Shoudan Liang

Successful initial steps toward improved understanding of the dynamics of biological systems with network-style communications have been achieved. They will lead toward the ultimate objective of elucidation of some elements of the origin of life on Earth and perhaps elsewhere.

A novel data processing algorithm, which addresses the inverse problem of deducing internal network structure from behavior, as represented by time-series data on signals at one or more output nodes, has been developed. Data analysis techniques, based on information theory and Bayesian change-point determination methods (originally developed for astrophysical systems) are being applied to this reverse engineering of biological systems, as well as to automatic genetic sequence decoding.

Models of normal and neoplastic cell dynamics incorporate all relevant biochemical and physiological parameters and describe regulatory interactions in a deterministic manner. Because these realistic Boolean networks behave very much like actual biological systems, they aid in addressing a series of essential questions in cancer biology and therapy. With some extensions, the same models describe the origin and development of primitive cellular life.

A program to study continuous-time networks, with time-delay factors, starts from known exact solutions to such systems when the interactions are linear. The nonlinear interactions, which characterize biological organisms, are being addressed with novel computational techniques developed especially for such networks.

All of this work is carried out in a context of modern information technology, including the use in the models of neural networks, genetic algorithms, and their combinations and extensions, and with the goal of incorporating new large-scale data acquisition efforts in the biotechnology industry and elsewhere.

Point of Contact: J. Scargle
(650) 604-6330
jeffrey@sunshine.arc.nasa.gov

Prebiotic Synthesis of Activated Amino Acids

Arthur L. Weber

About four billion years ago chemical processes occurring on the primitive Earth yielded molecules that had the ability to make copies of themselves (i.e., replicate). These rudimentary replicating molecules eventually developed into today's life that uses both protein and DNA molecules for replication. Since the DNA of today's life is too complex to have been chemically made on the primitive Earth, the first replicating systems may have been composed solely of small proteins, called peptides. Peptides are good candidates for the first replicating molecules because they are constructed from very simple building blocks—activated amino acid molecules that could have been made by chemical processes on the primitive Earth.

In order to understand how activated amino acid and peptide molecules could have been generated 4 billion years ago on the primitive Earth, work centered on three principal study areas: (1) The synthesis of activated amino acids was investigated in the laboratory under simulated primitive Earth conditions. (2) The thermodynamics of carbon chemistry was systematically explored to establish the chemical constraints that govern the synthesis of molecules (amino acids, etc.) needed for the operation and origin of life. (3) Techniques were developed to analyze amino acids from extraterrestrial sources, such as Martian meteorites.

In the past year, significant progress has been made in each of the three research areas listed above. A new prebiotic pathway has been discovered that generates activated amino acid thioesters which are capable of forming peptides. This synthetic pathway functions by converting formaldehyde and glycolaldehyde (one- and two-carbon aldehydes) into sugars that subsequently react with ammonia in the presence of thiol catalysts to give alanine and homoserine thioesters. This "one-pot" synthesis of amino acids operates under mild aqueous conditions, and like modern amino acid biosynthesis, uses sugar intermediates which are converted to amino acids by energy-yielding redox (reduction and oxidation) reactions. Additionally, in order to identify the thermodynamic constraints that govern carbon chemistry related to the origin of life, the free energy was calculated for making and breaking all the possible aliphatic carbon-carbon bonds. This thermodynamic analysis of carbon chemistry revealed that the biosynthetic processes of life are driven by chemical energy made available by redox disproportionation of carbon groups of sugars. It was established that the favorable energy of redox disproportionation was based on the universal reduction potentials of carbon groups. This thermodynamic perspective reveals that the high energy content of sugars makes them the optimal substrate for the synthesis of the molecules needed for life and its origin.

Finally, in preparation for the analysis of Martian meteorite samples, an improved analytical method of detecting amino acids was developed. Together with upgrades in high-performance liquid chromatography (HPLC) instrumentation, the improved method is capable of detecting 1 femtomole (a femtomole is 10^{-15} mole) of amino acid enantiomer. By combining this improved HPLC analytical system with a new electrophoretic method of sample preparation, 26 femtomoles of the meteoritic amino acid, α-aminoisobutyric acid, was detected in 1 gram of Cretaceous-Tertiary boundary sediment. Knowledge of the amino acids in extraterrestrial materials (like Martian meteorites) contributes to understanding the chemistry of amino acid synthesis on the primitive Earth during the origin of life.

Point of Contact: A. Weber
(650) 604-3226
aweber@mail.arc.nasa.gov

Mars Pathfinder Virtual Reality Model (MarsMap)

Ted Blackmon

Researchers at Ames Research Center (ARC) provided Pathfinder Mission scientists at the Jet Propulsion Laboratory (JPL) with three-dimensional (3-D) digital topographic models and an advanced interface for interaction with the virtual environment of the Martian surface. Because of the photographic realism of the 3-D models, scientists were able to learn more quickly about the Pathfinder landing site than they could have from a static view of the rock field that surrounded the lander. The virtual reality aspect of the display allowed them to move around the field, even to project a bird's eye view from above it. Moreover, 3-D measurements of positions, distances, and angles could be easily extracted from the topographic models, providing valuable tools for science analysis and mission planning.

Images of Mars captured by the Imager for Mars Pathfinder (IMP) stereo camera aboard the Pathfinder spacecraft were relayed to JPL through the Deep Space Network. After initial downlink of the images, an automated file-transfer protocol system sent the digital information through the Internet to Ames Research Center, where the 3-D models were rapidly processed by the stereo pipeline. A computer algorithm automatically matched features in a left-eye camera image with the identical features in a right-eye camera image, thus providing the necessary correspondence to compute a 3-D location for that image pixel.

Immediately following processing, the 3-D models were transmitted from ARC through the Internet back to computers at JPL for display in the Science Operations Center, using "MarsMap," a 3-D virtual reality interface for the scientific exploration of Mars. A significant achievement of the stereo pipeline was the total turnaround time of model production and display for the Mars Pathfinder Mission. For the first set of IMP stereo images returned from the surface of Mars, scientists at JPL were able to virtually fly through the 3-D Martian landscape within 15 minutes of receipt of the downlink data at JPL.

Beyond its spectacular visualization capabilities for navigating Mars in 3-D by using stereo eyewear and virtual reality goggles, MarsMap provided the Pathfinder Operations Team with a valuable tool for performing science analysis and mission planning. After the arrival of Pathfinder on Mars, MarsMap was used to verify the angle of the rover ramps for safe deployment, to generate 3-D pointing coordinates for IMP imaging sequences, to determine positions and sizes of rocks at the landing site, to measure the direction of wind tails behind the rocks, and to locate and display other science data markers on the topographic map of Mars.

Another important use of MarsMap was in assisting with past archiving and future planning of Sojourner traverses through the Martian landscape. A virtual model of the Sojourner rover was placed in the 3-D topographic map to show the history of the rover journey on the surface of Mars. Images captured by Sojourner were also integrated into the 3-D model as 2-D "billboards" projected from a virtual camera in the model. When faced with a potentially tight fit between rocks, an operator could use the same virtual model of the rover to determine if the real rover had suitable clearance for the maneuver. The accompanying image shows Sojourner looking at the side of the rock named "Yogi."

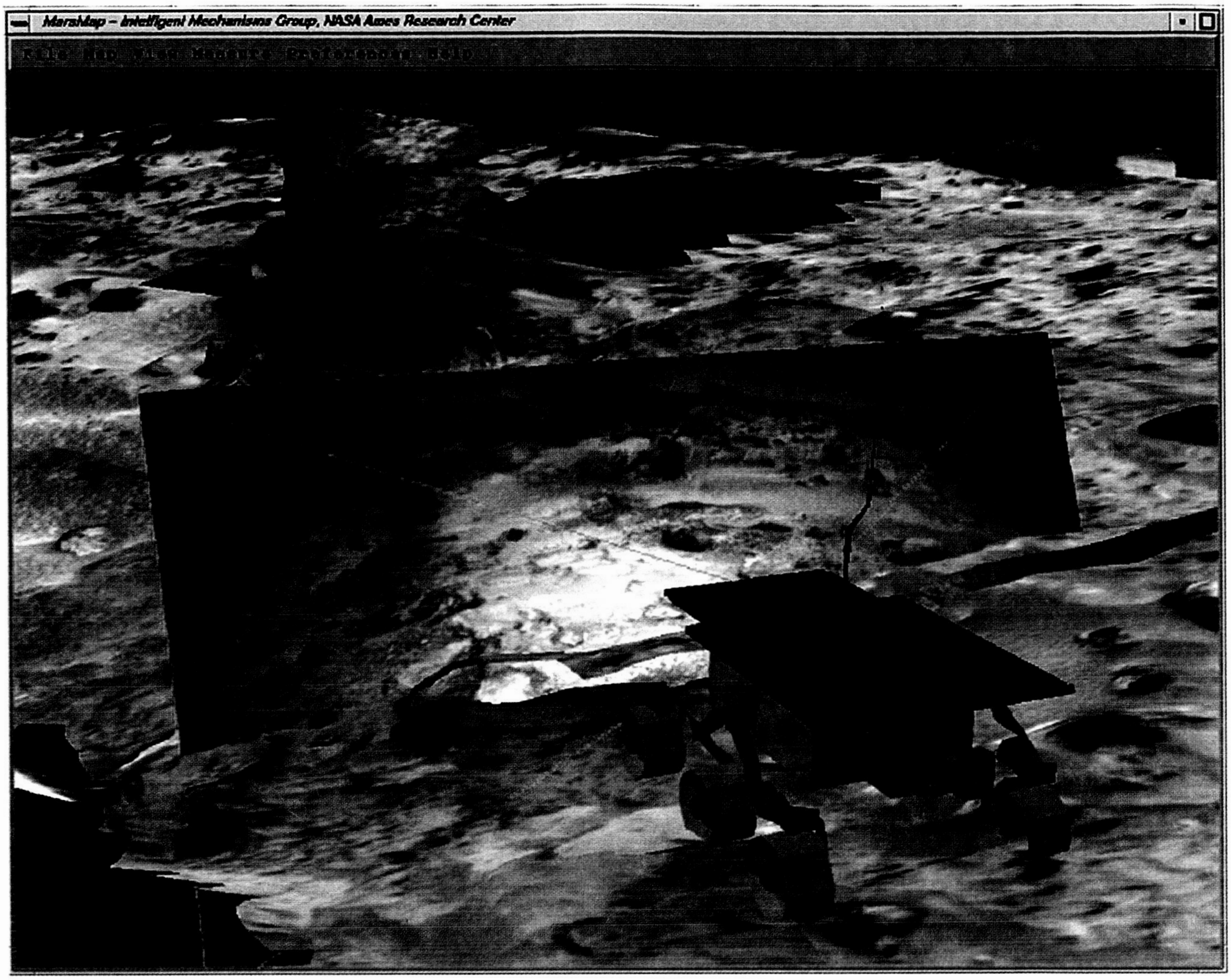
MarsMap – Intelligent Mechanisms Group, NASA Ames Research Center

Fig. 1. A computer-generated image from the virtual reality software MarsMap shows a perspective view of the large rock "Yogi" in the background. Analysis of the steep overhang of this rock using MarsMap was instrumental to the successful navigation of Sojourner during the Pathfinder mission. A rover image and CAD model are also projected into the 3-D scene and substantiate the steep overhang predicted by the virtual reality model.

MarsMap was also used quite extensively for the Pathfinder Mission as a visual cataloging tool. Data markers such as 3-D text symbols were superimposed on the terrain model to indicate the sequence of Alpha Proton X-Ray Spectrometer measurements taken by the Sojourner rover, soil mechanics experiments, and other science-related events. These data markers assisted mission scientists in keeping track of the past activities of Sojourner, as well as planning for future events.

Point of Contact: T. Blackmon
(650) 604-4710
blackmon@artemis.arc.nasa.gov

Primary Accretion in the Protoplanetary Nebula

J. N. Cuzzi, R. C. Hogan, J. M. Paque, A. R. Dobrovolskis

One of the major unsolved problems regarding the origin of planetary systems is the process by which the first sizeable objects (comets, asteroids, etc.) formed from solids that entered the protoplanetary nebula as micron-sized dust grains. Until recently there was little or no theoretical understanding of the key processes that characterize this epoch. The focus at Ames Research Center has recently been on three-dimensional (3-D) direct numerical simulations of particles in turbulence. Previously, it has been shown that the size of particles most strongly concentrated (by orders of magnitude) is in good agreement with the millimeter-size, molten "chondrules" which dominate primitive meteorites—and which show evidence for aerodynamic sorting which has never been explained before.

In FY97, numerical predictions were obtained of the size distribution of particles residing within densely concentrated zones in 3-D turbulence—zones thought to possibly represent the first stage of planetesimal accretion. The code can handle Taylor microscale Reynolds numbers as high as 140 (Reynolds number as high as 1300), and it can handle a million particles at each of 16 Stokes numbers simultaneously (the Stokes number is the ratio of particle stopping time to the Kolmogorov eddy turnover time, and is proportional to the particle radius and density). To test the models, a study was completed in which primitive meteorites were disaggregated and the size distribution of their chondrules was measured directly. The data so obtained are far superior to similar data obtained by examining slices of rock in a microscope, because the slicing process can bias size estimates. These new results also provide direct determination of the chondrule density, which is unattainable in any other way. Finally, these results provide the best measurements yet of the volume of fine-grained dust rims that surround many chondrules—generally believed to have been acquired by sweep-up of fine dust from the nebula gas.

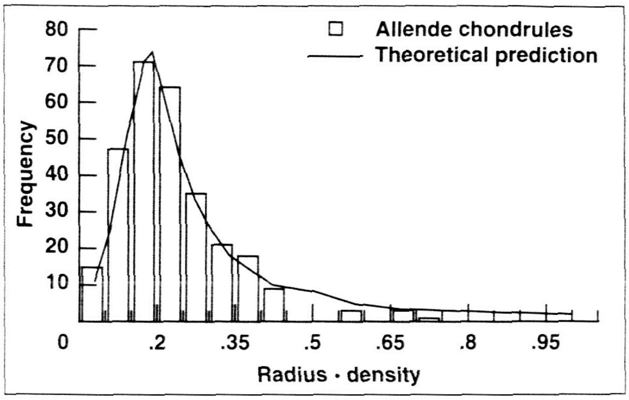

Fig. 1. Comparison of theoretical predictions for the size distribution of particles within a dense clump (smooth curve), proposed as the precursor of primitive meteorite parent bodies, with the observed size distribution of disaggregated chondrules (histogram). Similarly good agreement is found with data obtained by another group for a different kind of meteorite.

Comparison of measurements and theoretical predictions has been very encouraging. The first figure shows a comparison of model predictions with the actual relative abundance of chondrules, as a function of the product of their radius and density (the primary determinants of the Stokes number). The data and the predictions are normalized together at their peaks, and the shapes agree very well. The asymmetry of the theoretical prediction is a natural outgrowth of the model, if a binning volume of one Kolmogorov eddy scale on a side is adopted as proposed. Comparably good fits are found with data from a different team on a different meteorite.

The discovery at Ames (FY96) of the multifractal nature of the particle density field connects the particle concentration process with the same cascade process that partitions the dissipation of turbulent kinetic energy. The scaling properties of cascade processes can then be used to make reliable predictions of various particle-density-related quantities under nebula conditions. The second figure shows the volume having concentration factor C (C is the ratio of local particle density to the mean). The "data" are binned from simulations at three Taylor microscale Reynolds numbers, and the "models" are parameterized only by Reynolds number (once the Reynolds-number-independent

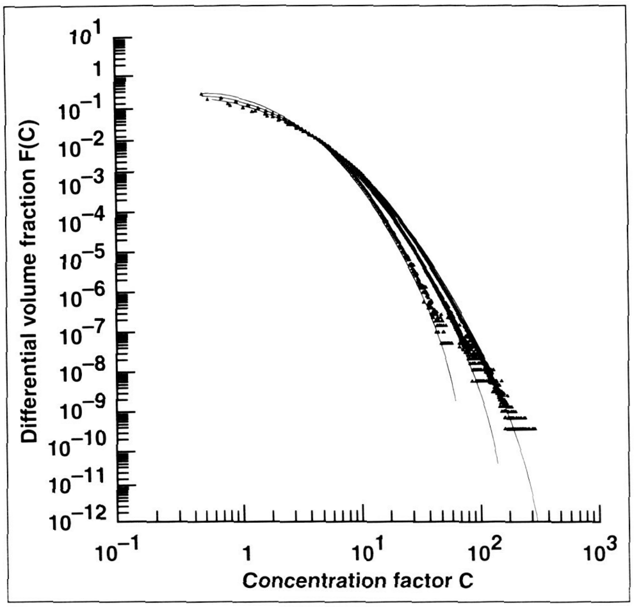

Fig. 2. Comparison of theoretical predictions of volume per unit volume occupied by particles with concentration factor C (lines) with actual binned probability distribution functions. The predictions used only the single fractal descriptor known as the singularity spectrum, which was defined by averaging over data at all three Reynolds numbers. The multifractal approach makes very good predictions of this and other quantities related to the particle-density field.

"singularity spectrum" is determined from the fractal properties of the data). The agreement is very good.

Using this formulation for the nebula, it is predicted that there will be about one clump with a typical dimension of a few kilometers on a side, with a concentration factor of 10^5 to 10^6, for every volume that is 10^4 (1 followed by 4 zeros) kilometers on a side. There will be numerous such clumps in the nebula region of interest, 10^7 kilometers thick and 10^8–10^9 kilometers wide (and even more common concentrations of lower degree). The multifractal formalism is thought to be a fundamental advance in two-phase fluid dynamics; it will be extremely useful in quantitatively describing the properties of selectively concentrated particles in turbulence. For instance, the expected encounter times for chondrules with clumps sufficiently dense to remove the chondrule from circulation, and collision rates within such clumps which augment sticking and accumulation of particles, can also be calculated.

Point of Contact: R. Hogan
(650) 604-0780
hogan@cosmic.arc.nasa.gov

Telltale Electric Currents During Impacts on Rocks

Friedemann Freund, Jerome G. Borucki, Marshall Lisé

Impact studies lead to new insights into geophysical phenomena ranging from electric signals accompanying earthquakes to magnetic signatures of past meteorite impacts on Earth, the Moon, and Mars.

Dry rocks, in particular dry igneous rocks, are known to be good insulators, meaning that they are unable to generate and to transport sizable electric currents. However, evidence has accumulated over the past few years that there is something special about the traces of "water" (H_2O) which nominally anhydrous minerals, the main constituents of igneous rocks, incorporate into their crystal structures when solidifying from water-laden magmas. When water molecules enter a mineral structure, they usually turn into hydroxyls, $\mathrm{H_2O + Si/^{O}\backslash Si = Si/^{OH}\ {}_{HO/}Si}$, but the hydroxyls reshuffle their electrons in such a way that a hydrogen molecule and a peroxy link, $\mathrm{Si/^{OO}\backslash Si}$, are formed for each hydroxyl pair.

Since all igneous rocks on Earth and presumably on Mars solidified from water-laden magmas, the presence of peroxy links deserves attention because, when peroxy links can break apart, they generate electric charges. These charges are defect electrons, also known as "positive holes," similar to the holes in semiconductors which are necessary, together with electrons, to build a transistor. Peroxy links dissociate upon heating, but it has now been recognized that they also break apart when subjected to a sudden mechanical shock. A relatively weak shock suffices; for example, the shock supplied by a steel ball impacting a piece of rock at 100 meters per second. The shock causes the peroxy links to momentarily release positive holes. These act as highly mobile charge carriers and propagate through the mineral structure, jumping from mineral to mineral grain and thus flowing through a rock that would otherwise be considered a good insulator.

To demonstrate the effect, a series of shock-impact experiments was conducted, using for lower velocities a crossbow that can accelerate steel balls up to 100 meters per second, and for higher velocities, 1–6 kilometers per second, the Ames Vertical Gun Range. This paper focuses on the low-velocity impact experiments.

Cylindrical rock cores were fitted with a photodiode for light detection, two capacitive sensors, one at the front near the impact point and one at the far end, and an electrical ground, as shown in the inset in the first part of the figure. When a small steel ball was fired at a velocity of 90 meters per second, the moment of impact manifested itself by a weak, short light pulse, marked by the vertical arrow. Less than 100 microseconds after impact, the front end ring capacitor, about 20 millimeters from the impact point, began to record a positive voltage which eventually rose to +0.5 volt. Another 150 microseconds later, the far-end capacitor (7.5 centimeters downrange) began to record a similar voltage, rising to +50 millivolts, indicating the propagation of a cloud of positive charges at about 300 meters per second. As the front-end capacitor reached +0.5 volt, a second light pulse, much stronger and longer lasting than the first, was emitted from the front end.

In another configuration, depicted in the inset in the second part of the figure, two electrodes were applied to a rectangular piece of the same gabbro (an igneous rock). A photodiode was aimed at the impact point and a pickup coil was installed (not shown) for registering the magnetic field. The electrodes were connected to a 25-volt power supply via a 1-megawatt resistor; the current flowing through this resistor was measured by measuring the voltage

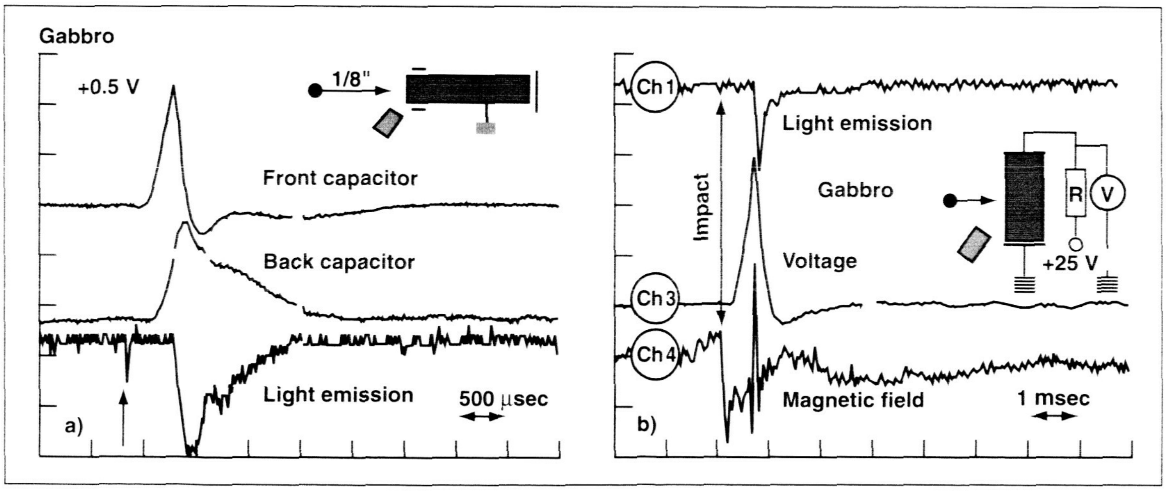

Fig. 1. Example of two low-velocity impacts on gabbro, an igneous rock without piezoelectric quartz. (a) Impact on a cylindrical core resulting in a small light pulse (lower trace, arrow), the appearance of a positive charge, 0.5 volt, at the front-end ring capacitor (upper trace) about 150 microseconds after impact, and after another 150 microseconds of a positive charge at the far-end capacitor (middle trace). Then a strong light pulse occurs from the front end of the rock. (b) Sidewise impact on a rectangular piece of rock with 25 volts applied between two electrodes. The magnetic field pulse (Channel 4) marking the impact is followed by a current of 25 microamperes flowing through the rock (Channel 3) and a strong light pulse (Channel 1) when the current reaches its maximum.

across it. The instant-light emission upon impact was too weak to detect, but the pickup coil registered a magnetic field (Channel 4). After about 125 microseconds the voltage measured across the resistor began to rise (Channel 3), indicating a current of about 25 microamperes. Then the photodiode recorded a sudden light pulse (Channel 1), and the magnetic pickup coil (Channel 4) recorded a brief, but strong magnetic field oscillation.

Point of Contact: F. Freund
(650) 604-5183
ffreund@mail.arc.nasa.gov

Nitrogen Dissociation in Earth's Lower Thermosphere

Winifred M. Huo, Christopher E. Dateo

The reaction of nitrogen atoms (N) with oxygen (O_2) is important in the formation of nitric oxide (NO) in Earth's lower thermosphere. This reaction is particularly sensitive to the internal state of the N atom. The reaction proceeds very slowly if the N atoms are in their ground electronic state (^4S), but becomes much faster for electronically excited N atoms (^2D or ^2P). Thus the amount of NO in the lower thermosphere is dependent on the population of excited-state N atoms. Employing current models of the lower thermosphere, a change in the population of N ^2D from 60% of the total N atom population to 50% results in an 80% decrease in the NO density. Given this uncertainty in the current models, a better understanding of the N atom population distributions is necessary.

Nitrogen atoms in the lower thermosphere are produced by electron impact dissociation of N_2 and the dissociative recombination of N_2^+. Laboratory measurement of electron-impact dissociation of the ground state N_2 ($X^1\Sigma_g^+$) molecule found that equal amounts of ^2D and ^4S nitrogen atoms were produced. This distribution of N atoms gives less ^2D than is used in the model, resulting in an even larger discrepancy between the measured and modeled NO density. To help resolve this discrepancy, large-scale quantum chemical calculations on the dissociation pathways of N_2 have been carried out. The first figure shows

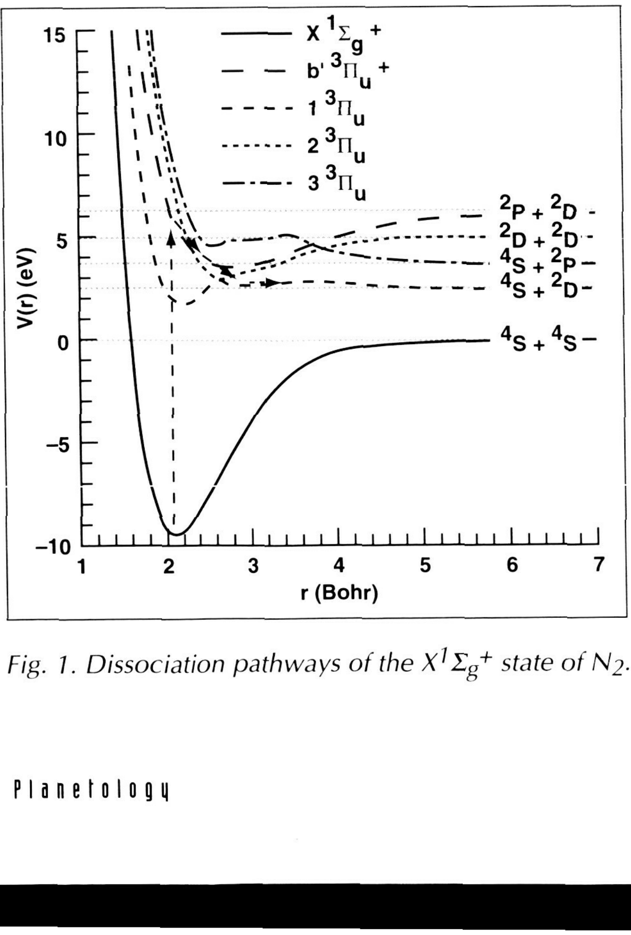

Fig. 1. Dissociation pathways of the $X^1\Sigma_g^+$ state of N_2.

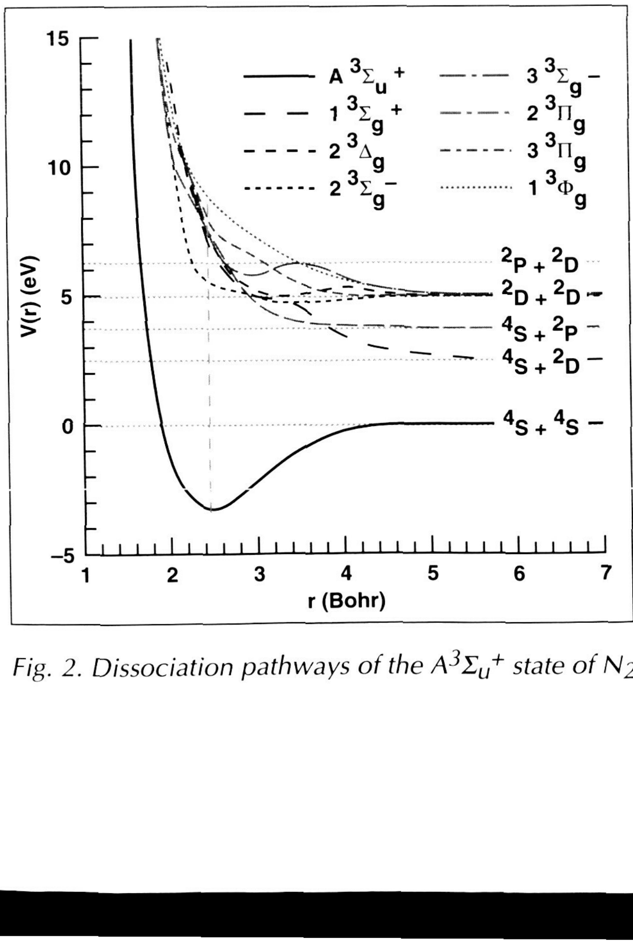

Fig. 2. Dissociation pathways of the $A^3\Sigma_u^+$ state of N_2.

the dominant dissociation pathway of the N_2 ground state. This is a predissociative process in which the dissociation products are $^4S + {}^2D$, in agreement with laboratory measurements.

Electron collisions with the X state of N_2 also produces the metastable $A^3\Sigma_u^+$ state. The A state has been observed in dayglow and in the aurora. The second figure presents a number of dissociation pathways of the A state. Unlike the X state, the dissociation of the A state favors a direct process in which the lower state is directly excited to a repulsive state. The dissociation products distribute among the ^4S, ^2D, and ^2P states.

Calculations of the electron-impact excitation cross sections of the X and A states to the predissociative or dissociative states show that the A state excitation cross sections are of the same magnitude or larger than the X state. Based on these results, the distribution of N atoms with 60% in the ^2D state is favored.

A factor that has not been considered so far in the modeling is the interaction of the A state of N_2 with the O atom to form NO. Since the A state is expected to be more reactive than the ground state, this will provide another source of NO and further lessens the discrepancy between modeling and measurement.

Point of Contact: W. Huo
(650) 604-6161
huo@pegasus.arc.nasa.gov

Transient Meteor Activity

Peter Jenniskens

In 1997, Ames Research Center proved to be uppermost in studies of transient meteor activity. Meteor storms and lesser outbursts are spectacular natural phenomena that have eluded systematic study with modern techniques. During an outburst, meteor rates increase above the normal annual activity for a period that typically ranges from 1 to 24 hours. Little is known about why it sometimes "rains stars" at night. An answer to this question is key to the information that is particular to these events. For example, outbursts provide a unique window on how comets shed the large millimeter-to-centimeter-size dust grains that contain most of the mass lost by comets in the form of dust.

With the archiving center at Ames, a Global Meteor Scatter Network (Global-MS-Net) was made operational this year; it has stations in Finland, Hawaii, Austria, and Belgium, and two stations in Japan, operated by amateur astronomers. For the first time, meteor activity was monitored on a 24-hour and global basis (see the figure), but not yet in the Southern Hemisphere. Three outbursts were detected, all of known meteor streams: the Perseids, Leonids, and Ursids. On four occasions, the network provided upper limits to possible outburst activity reported by meteor observers and amateur astronomers.

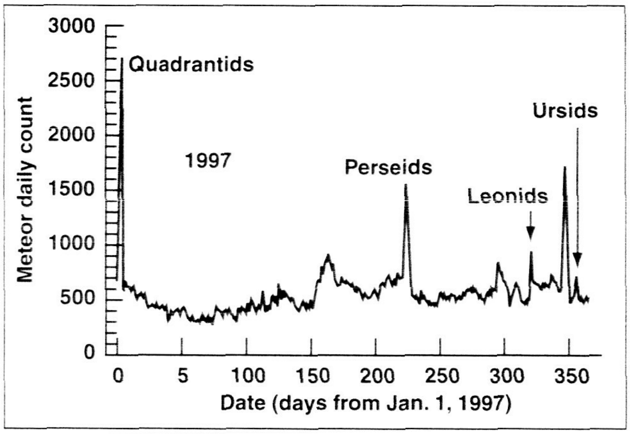

Fig. 1. Graph of the daily meteor count during the year of 1997 as measured by the Finnish Global-MS-Net station of Ilkka Yrjölä in Kuusankoski. The meteor streams discussed in the text are indicated.

Important progress was made toward determining how the Global-MS-Net detection of an outburst from the dust of a long-period comet can help predict its return in future years. The key is in the position of the major planets, because their gravitational perturbations affect the motion of the cometary dust trail that is responsible for the outbursts. Once it has been determined which planetary configurations direct that trail into Earth's path, it is possible to forecast a meteor outburst of the type caused by the dust trail of long-period comets. Typically, that happens only once or twice every 60 years. No new outburst associated with long-period comets was detected with certainty this year.

Work also progressed on studies of the outbursts caused by Jupiter- and Halley-type comets; all three outbursts this year were of those types. They were observed with a mobile photographic and video camera system, tracking the orbits of individual meteoroids, determining their grain morphologies, and measuring the particle-size distribution. Those results revealed that planetary perturbations play a role in the dispersion of cometary ejecta at a very early stage.

A surprising discovery came from similar observations of a well known annual stream, the Quadrantids. The results revealed structure in the distribution of orbits, implying ejecta less than 500 years ago. This stream turned out to have more in common with meteor outbursts than with annual shower activity. The stream does not originate from comet 96P/ Machholz 1, as was thought before. Rather, the source may be hiding as an asteroid-like object in a high-inclination orbit.

Point of Contact: P. Jenniskens
(650) 604-3086
peter@max.arc.nasa.gov

Solar System Dynamics

Jack J. Lissauer

Progress has been made on several theoretical problems related to the dynamical structure of the solar system. Models of the early phases of the growth of solid planetary embryos on eccentric orbits were developed and used to calculate accretion rates and the accumulation of rotational angular momentum. It was found that eccentricities of the magnitude believed to be present during this period modify planetary growth rates and angular momentum accumulation only slightly, relative to the case of planets on circular orbits.

The torque exerted by a satellite on a particulate annulus centered at a mean-motion resonance was studied by using both analytic and numerical techniques. In the linear approximation, the net torque on the disk is the same as that exerted on fluid disks (which were studied previously by P. Goldreich, California Institute of Technology, Pasadena, California, and S. Tremaine, Princeton University, Princeton, New Jersey). The width of the annulus over which the bulk of the torque is exerted shrinks as time increases. The torque in a nondissipative disk is limited in time by nonlinear effects of the interaction close to resonance, which require a few thousand orbits to develop for typical solar system parameters. The same torque is obtained for disks of particles initially on circular orbits as for disks of particles on moderately eccentric orbits with periapses uniformly distributed in longitude. Results of these simulations are applicable to low-optical-depth planetary rings, such as Neptune's Adams Ring, and to planetesimals within the protoplanetary disks.

Systems of planets with orbits initially identical to subsets of the planets within our solar system were integrated for very long periods of time (billions to tens of billions of years) with the Sun's mass decreased relative to the masses of the planets. Systems based on the giant planets show an approximate power-law correlation between the time elapsed until a pair of planetary orbits cross and the solar-to-planetary mass ratio, provided that this ratio is less than 0.4 times its current value. However, deviations from this relationship at larger ratios suggest that this correlation cannot be extrapolated to accurately predict the lifetime of the current system. Detailed simulations of the evolution of planetary orbits through the Sun's postmain-sequence mass-loss epoch suggest that the orbits of those terrestrial planets that survive the Sun's red giant phase are likely to remain stable for longer than a billion years (possibly much longer), and those of the Jovian planets are likely to remain stable for more than 10 billion years (possibly much longer). Pluto is likely to escape from its current 2:3 mean-motion resonance with Neptune within a few billion years beyond the Sun's main-sequence lifetime if subject only to gravitational forces; its prognosis is even poorer when nongravitational forces are included. Higher mass stars, which lose a larger fraction of their mass during their red giant phase, may lose their planetary systems as a consequence of their mass loss.

Point of Contact: J. Lissauer
(650) 604-2293
lissauer@ringside.arc.nasa.gov

Virtual Reality on Mars Pathfinder

C. Stoker, T. Blackmon, M. Sims, E. Zbinden

The objective of this project was to produce a three-dimensional (3-D) photo-realistic virtual reality (VR) model of the Martian surface for use in the Mars Pathfinder mission. Marsmap, the interactive terrain visualization system, creates and renders digital terrain models produced from stereo images of Mars' surface taken by the lander's images for Mars Pathfinder (IMP) camera. A primary benefit of using VR to display geologic information is that it provides an improved perception of depth and spatial layout of the remote site. The VR aspect of the display allows an operator to move freely in the environment, unconstrained by the physical limitations of the perspective from which the data were acquired. Virtual reality also offers a way to archive and retrieve information in a way that is easily understood. Combining the VR models with stereo display systems can enable a feeling of presence at the remote location. The capability, implemented in Marsmap, to interactively perform measurements from within the VR model, offered unprecedented ease in performing operations that are normally time consuming and difficult using standard photogrammetric techniques. This ground-breaking project demonstrated the power of using VR as a cartographic tool.

In the rapid production of digital terrain models (DTMs), a computational algorithm called the "stereo pipeline" was used. The core component of the stereo pipeline is the automatic matching of features in the left-eye camera image with the same features in the right-eye camera image, thus providing the necessary correspondence to compute a 3-D location for the feature. A significant aspect of the project was the rapid production and display of models by using a distributed production team and fast data transfer. The first complete stereo panorama sequence taken after deployment of the IMP, known as the "Monster Pan," was composed of 98 stereo pairs. These data were displayed in VR at mission control at the Jet Propulsion Laboratory within 1 hour of downlink.

The Pathfinder DTMs were displayed with an interactive user interface called MarsMap which includes the following key features: (1) real-time, interactive navigation of the virtual viewpoint through the 3-D model of the landing site; (2) measurement of topographical features, including 3-D positions, distances, and angles; (3) display of daily traverses of Sojourner; (4) display of rover images within the VR model projected from the viewpoint of the rover; and (5) catalog and display of the sequence and location of science experiments conducted by the rover.

MarsMap was designed to be accessed with a standard 2-D mouse and used pull-down menus to call features. Models could be viewed in stereo using Stereographics Crystal Eyes liquid crystal display shutter glasses or with a set of head-tracked "Virtual Binoculars." The two figures show example views of the Martian surface generated using MarsMap.

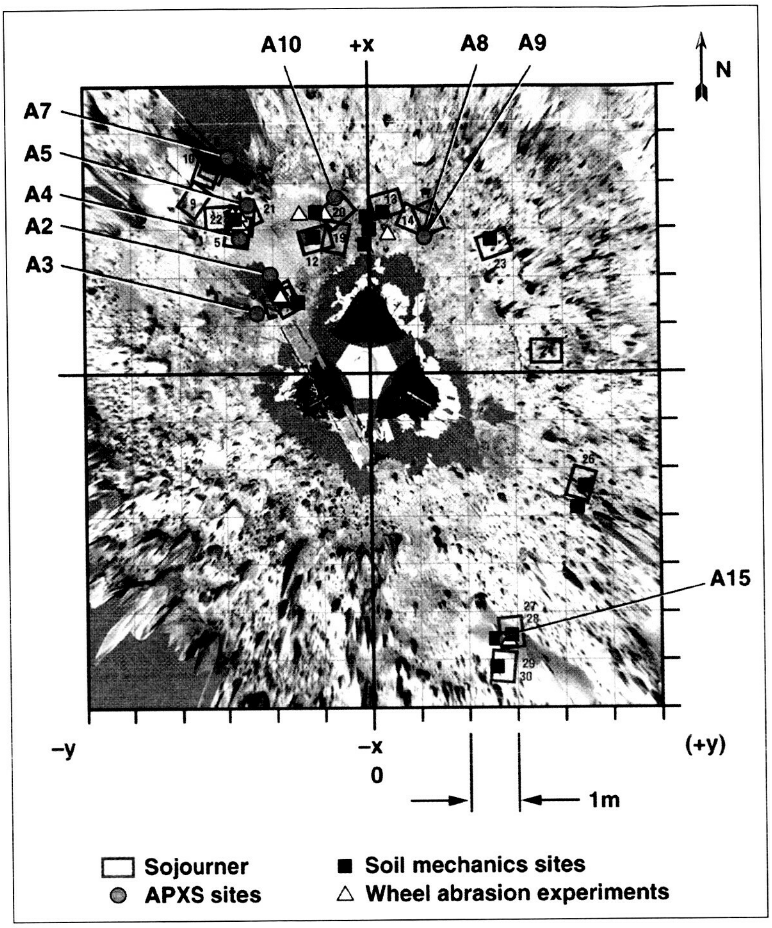
A10
+x
A8
A9
N
A7
A5
A4
A2
A3
A15
–y
–x
0
(+y)
1m
Sojourner
APXS sites
Soil mechanics sites
Wheel abrasion experiments

Fig. 1. Overhead view of the Pathfinder landing site. Data markers indicate the positions of rover activities through the first 30 sols of the mission including rover end-of-day positions (red rectangles), APX measurements (blue dots), soil mechanics experiments (black squares), and wheel-abrasion experiments (yellow triangles). (1 sol on Mars is the equivalent of 1 Earth day or represents one complete rotation of the planet.)

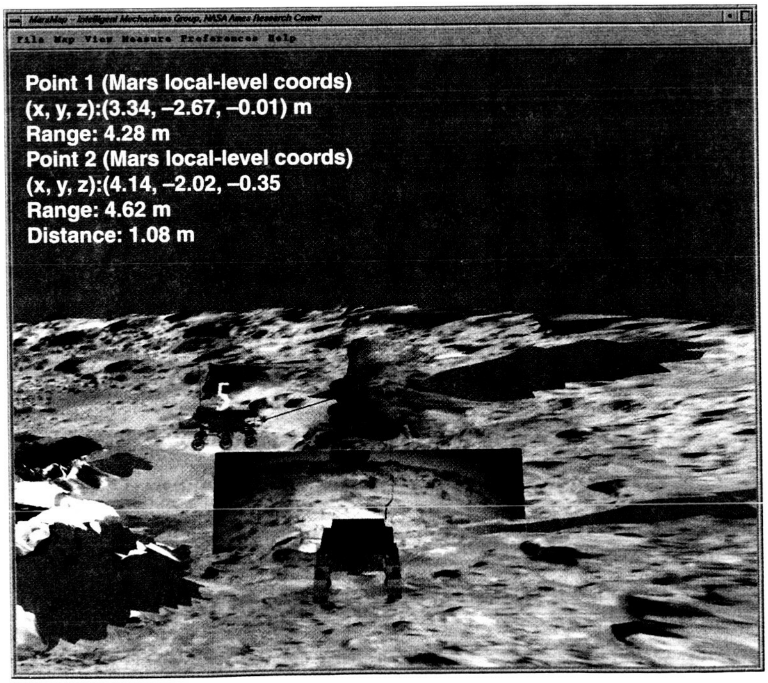
MarsMap - Intelligent Mechanisms Group, NASA Ames Research Center
File Map View Measure Preferences Help

Point 1 (Mars local-level coords)
(x, y, z):(3.34, –2.67, –0.01) m
Range: 4.28 m
Point 2 (Mars local-level coords)
(x, y, z):(4.14, –2.02, –0.35
Range: 4.62 m
Distance: 1.08 m

Fig. 2. Two views of MarsMap showing (a) a measurement of a rock, and (b) a rover image projected into the 3-D model.

Beyond the spectacular visualization capabilities for navigating Mars in 3-D, MarsMap provided the Pathfinder team with a valuable tool for performing mission planning and operations, science analysis, and public outreach. The Marsmap project has shown that VR can be used as a powerful method for analyzing the geology of a remote environment. Virtual reality models can be created and displayed, and analysis and measurements can be performed with unprecedented speed and accuracy. Virtual reality may represent a giant leap forward for scientific analysis.

Point of Contact: C. Stoker
(650) 604-6490
cstoker@mail.arc.nasa.gov

Cratering Rates on the Galilean Satellites

Kevin Zahnle, Luke Dones

In the inner solar system, impact craters are made mostly by asteroids and long-period comets. The Jupiter family of comets, whose comets are in relatively short-period, low-inclination orbits dominated dynamically by gravitational interactions with Jupiter, is relatively unimportant. These roles are reversed in the outer solar system. Asteroids rarely reach as far as Jupiter, and long-period comets are more or less uniformly distributed. The Jupiter-family comets, which swarm about Jupiter, are relatively the most important source of cratering in the vicinity of Jupiter. The purpose of this project was to determine the absolute cratering rates on the Galilean satellites, and to use those rates to estimate surface ages on Io, Europa, Ganymede, and Callisto.

Cratering rates are determined by the numbers and sizes of the comets, by their distribution in space, by their impact probabilities with the various objects, and by their impact velocities. The most important uncertainty is in the size-number distribution of the comets. This must be determined from the properties of observable comets, which are mostly comets that pass near Earth. It has recently become possible to perform extensive numerical simulations of statistically significant numbers of comet orbits as they evolve from their source region in the Kuiper belt to their many fates. These models fill in the orbital distribution of the comets, such that one can calibrate the distribution as a whole to the relatively few comets that are large enough or come near enough Earth to observe.

A single sentence summary of this work is that 20-kilometer-diameter craters, which are made by kilometer-size comets, occur on a Galilean satellite about once in a million years. The uncertainty in this rate is a factor of 5. More than 90% of the craters on the Galilean satellites are caused by the impact of Jupiter-family comets. Long-period comets contribute at the 1%–10% level, as do the Trojan asteroids (asteroids that are coorbital with Jupiter, trailing or leading Jupiter by ±60 degrees). Main belt asteroids are currently unimportant, for each 20-kilometer crater made on Ganymede implies the disruption of a 200-kilometer-diameter parental asteroid, a destruction rate far beyond the resources of today's asteroid belt.

Study results are presented in the figure. All data are expressed in terms of the equivalent number of 10-kilometer craters. The curves are the surface ages that correspond to these crater densities at these apex angles—solid curves are ages relevant to Ganymede, the dotted curves are ages relevant to the higher cratering rate at Europa—calculated according to the assumption that the satellites have been in synchronous rotation throughout. The surface ages are those predicted using a nominal cratering rate, with the additional assumption that the Kuiper belt decays inversely with time. Ages for Callisto are not shown, but are consistent with the age of the solar system.

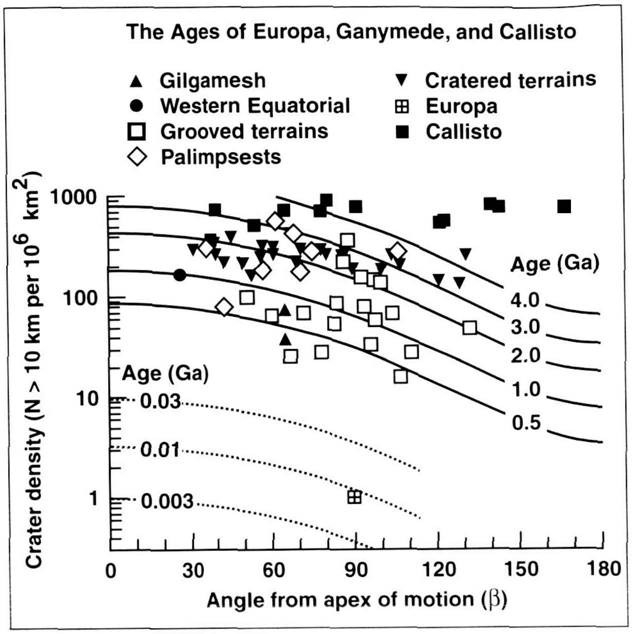

Fig. 1. Crater densities on and nominal ages of various types of surfaces on Europa, Ganymede, and Callisto as a function of the angle β from the apex of the motion.

The paucity of 20-kilometer craters on Europa indicates that its surface is of order 10 million years (in the figure, the datum for Europa is the nominal equivalent of five 20-kilometer craters scattered over the Moon's surface). The figure emphasizes the many ages of Ganymede. Lightly cratered surfaces (including many of the grooved terrains) are nominally 0.5–1.0 billion years old, and the cratered terrains and palimpsests (ghostly imprints of lost impact basins) are comparable to the age of the solar system. The Gilgamesh ejecta blanket in particular is assigned a nominal age of 0.7 billion years (Gilgamesh and Western Equatorial are large young-impact basins). These ages are considerably younger than the 4.56-billion-year age of the solar system and the 3.82-billion-year age of the great Imbriam impact basin on the Moon. Such relative youth is consistent with Ganymede still being alive, in a geological sense, and is more consistent with Ganymede's currently strong magnetic field than a more conventionally ancient age would be.

On a human timescale, the Galilean satellites all rotate synchronously with their orbit; that is, they each are tidally locked to Jupiter, with the same hemisphere always facing Jupiter. They are in this sense like Earth's own Moon. A peculiarity of synchronous rotation is that there are well-defined leading and trailing hemispheres. The leading hemisphere should be more quickly cratering. The technical term for a faster cratering rate on the leading hemisphere is the apex-antapex asymmetry. It is not expected to be a subtle effect: cratering rates at the apex are more than 10 times higher than cratering rates at the antapex. The effect is illustrated by the labeled curves in the figure. But the effect is not obvious in the available data. A lack of apex-antapex asymmetry on Europa could be explained as small-number statistics, but it is not altogether unlikely that the Europan surface moves, either slowly on some glacial timescale, or in response to tidal heating, or catastrophically in the manner of true polar wander. Such phenomena have been predicted. Nonsynchronous rotation seems most likely if the ice is really a shell floating on a liquid ocean. It is harder to envision if the water layer is solid ice everywhere. Ganymede too shows no clear evidence of apex-antapex asymmetry. How, other than by rotation, is Ganymede to avoid a pronounced apex-antapex cratering asymmetry? And if there is no other choice, does this not suggest that Ganymede too was once, and perhaps not so long ago, home to a liquid ocean?

Point of Contact: K. Zahnle
(650) 604-0840
kzahnle@mail.arc.nasa.gov

The Structure of the Solar Nebula

K. Robbins Bell, P. Cassen

The coplanarity of the planets in our solar system suggests that they all formed from a flattened gaseous nebula which has since dispersed (the "solar nebula"). The existence of similar protoplanetary disks in other systems has recently been confirmed by Hubble Space Telescope observations which show flattened nebulae in silhouette against the hot background of the Great Nebula in Orion. Many of the disks observed there are probably being eroded away by radiation from the massive, bright stars that illuminate the nebula and so will never form planetary systems (see also in this report the paper by Hollenbach et al.). Nevertheless, their direct observation confirms that solar nebula analogs and thus planetary systems may be common. This report describes recent research into the structure of the solar nebula which suggests that planets may have formed in darker, colder environments than generally believed.

Even with direct observations of solar nebula analogs, numerical and analytic models must be used to determine conditions deep inside at the planet-forming midplane. Work has been continued in this field by deriving temperature and density profiles for a variety of possible protoplanetary disk phases. The models encompass early solar nebula analogs appropriate for times when material spiraled rapidly in through the disk to land on the young Sun and the disk was thick and dominated the radiation emitted from the systems, to later analogs in which the flow of material was small and the disk was thin and energetically less important. The models also consider systems in which the stellar mass is larger or smaller than the mass of the Sun so that it will be clear which differences are a result of real variation in mechanism and which are merely a result of the differences in the stellar mass of the central star. One of the key conclusions made (along with collaborators T. Henning and H. Klahr of the University of Jena, Germany) was that throughout most of the lifetime of the disk and throughout much of its radial extent, the disk surface is shielded from radiation by the central star.

Because of a lack of detailed models, it has often been assumed that disks are either essentially flat or curve continuously upward so that their surfaces are illuminated everywhere by light from the central star. Detailed studies, however, show that the shape of the disk's surface is controlled by the local temperature-dependence of the opacity. Because the opacity diminishes at lower temperatures, the disk becomes more optically thin as one moves radially outward, and the thickness of the disk decreases. Inner annuli thus shield outer annuli from stellar radiation. At early times, when mass flow through the disk was large and local energy generation strong, this was probably not a large effect. At later times, however, when planet formation is thought to have been most important, a cooler environment may have shortened the timescales of planet formation by enhancing the effect of self-gravitation in the coagulation of micron-size dust particles into macroscopic bodies or by decreasing the relative velocities between planetesimals themselves, thus allowing for speedier assembly into protoplanets.

Point of Contact: R. Bell
(650) 604-0788
bell@cosmic.arc.nasa.gov

Molecules in Stellar Photospheres

Duane Carbon, David Goorvitch, Martin Cohen

Absorption lines from molecular species dominate the spectra of all cool stars, whether they are high luminosity giants and supergiants or faint dwarfs of the lower main sequence. The density and strength of the molecular transitions are so great that their presence profoundly affects the structure of the outermost stellar layers, the stellar photospheres. Because the cool stars are so important in a variety of astrophysical contexts, a program aimed at accurately modeling their photospheres and emergent spectra is being conducted.

A key component of this effort is the development and maintenance of complete molecular line tabulations. These tabulations contain all the line parameters required for computing the strength and broadening of each individual molecular line. In the past year the database has been expanded to include the isotopic line lists developed by Uffe Jorgensen of the Niels Bohr Institute for the CN A-X system, the TiO α, β, γ, γ', ε, δ, and ϕ systems, and the CH vibration-rotation, A-X, B-X, and C-X systems. The tabulations for OH and SiO vibrational-rotational lines based on newly available information have also been upgraded. This molecular line database now contains all the important isotopic lines for the following transitions:

Molecule	Transition	Number of lines
OH	Vibration-rotation	58,000
C_2	b-a	79,000
SiO	Vibration-rotation	93,000
CO	Vibration-rotation	135,000
CH	Vibration-rotation, A-X, B-X, C-X	115,000
CN	A-X	2,200,000
TiO	Vibration-rotation, A-X, B-X, C-X, E-X, b-a, c-a, b-d	12,000,000
H_2O	Vibration-rotation	308,000,000

In FY97, the database has been used in the study of the infrared spectrum of sunspots. This investigation has provided a valuable check on the accuracy of the molecular line parameters in the database. The spectra of cool stars provide relatively poor tests of molecular parameters simply because their temperatures, gravities, and, particularly, compositions are not known with much accuracy. Since accurate sunspot models are available and the solar abundances are well studied, high-resolution sunspot spectra are an excellent standard for comparison. Observed sunspot spectra have been systematically compared with theoretical spectra computed using the molecular line database. In addition to evaluating the accuracy of the massive H_2O line list developed at Ames Research Center, the line parameters for CO, SiO, and OH have been checked. Comparison of theoretical and observed sunspot spectra reveals significant discrepancies in the strengths and positions of many OH transitions. This result strongly suggests the need for additional laboratory and theoretical work on the energy-level structure and dipole-moment function of this important molecular species.

The molecular database has also been used to generate spectra for several cool stars: Alpha Boo, Alpha Tau, and RX Boo. In the case of the red giant Alpha Tau, an important infrared flux standard, observed and theoretical fluxes are being compared over more than three decades of wavelength, from 1 micron to beyond 1 millimeter. Although still in its early stages, the comparison of millimeter fluxes suggests significant modifications to accepted models of Alpha Tau.

**Point of Contact: D. Carbon/D. Goorvitch
(650) 604-4413/5502
dcarbon@nas.nasa.gov
dgoorvitch@mail.arc.nasa.gov**

NICMOS Images of Orion

Edwin F. Erickson, Michael Kaufman, Sean Colgan

The Near Infrared Camera and Multi-Object Spectrometer (NICMOS) was installed on the Hubble Space Telescope during a space shuttle servicing mission in February 1997. Using NICMOS, early release observations of the nearest region to Earth where massive stars are being formed—the belt of the constellation Orion—were obtained. These images (shown in the figure) reveal intricate structures in both the near-infrared continuum and in emissions from molecular hydrogen (H_2).

Numerous H_2-emitting knots have been resolved for the first time. Many of these features exhibit prototypical bow-shock morphologies, elongated structures with roughly V-shaped tips. These are interpreted to be lower-excitation analogs of similar structures observed with ground-based telescopes northwest of the core. Many of the elongated H_2 structures and bow-shock features appear to radiate outward from a region very near a radio continuum source, suggesting that the H_2 energetics are dominated by one or more outflow sources in this region. However, the orientations of some features are unrelated to this apparent outflow pattern. Faint continuum features have been detected near the origin; however, no 2-micron emission coincides with this suspected outflow source. The newly resolved H_2 features with bow-shock morphologies are located in regions previously identified as bow-shocks by highly blueshifted components in their line profiles. In contrast, regions of H_2 emission that are diffuse in the NICMOS image have broad, smooth line profiles. Several continuum features have an arc-like appearance, suggesting interactions of winds with the ambient medium. At least 40 stellar or protostellar continuum sources have been detected, including at least one protoplanetary disk and four pairs of binary stars.

Point of Contact: S. Colgan
(650) 604-0420
colgan@cygnus.arc.nasa.gov

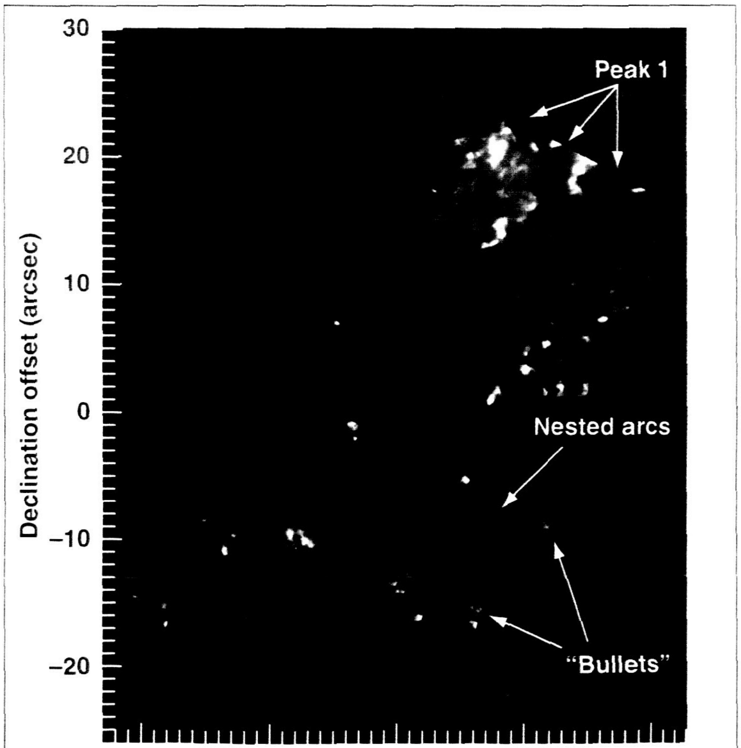

Fig. 1. Molecular hydrogen mosaic of the Orion star-forming region.

Star Formation Studies

D. Hollenbach, K. R. Bell, P. Cassen

The Center for Star Formation Studies, a consortium of scientists from the Space Science Division at Ames Research Center (ARC) and the Astronomy Departments of the University of California at Berkeley and Santa Cruz, conducts a coordinated program of theoretical research on star and planet formation. The Center supports postdoctoral fellows, senior visitors, and students; meets regularly at Ames to exchange ideas and to present informal seminars on current research; hosts visits of outside scientists; and conducts a summer week-long workshop on selected aspects of star and planet formation.

The main focus of the ARC portion of the research work conducted by the Center during 1997 was on the evolution of the protoplanetary disks which ultimately form planets. In particular, considerable effort was devoted to understanding the effect that nearby massive stars would have on the planet-forming disks around low-mass stars like the Sun, and to the interaction of the young low-mass star with its protoplanetary disk. Many low-mass stars like the Sun form in clusters. When stars form in large clusters, the bulk of the stars are low-mass stars, but a few high-mass stars, 5–100 times as massive as the Sun, also form. These stars are 1000 to 1 million times as luminous as the Sun, and radiate mainly ultraviolet photons.

In collaboration with D. Johnstone (University of Toronto) and J. Bally (University of Colorado), the effect of the ultraviolet radiation of a nearby massive star on young stars with protoplanetary disks was studied. It was found that for young star/disks less than about 1 light year from the massive star, a distance typical of cluster size, the effect of the ultraviolet radiation is quite devastating to planet formation. The irradiated surfaces of the gas and dust disks orbiting the stars are heated to thousands of degrees, and the disks evaporate in timescales of less than a million years, which is shorter than the timescale thought to be required to accumulate planets. Comparing their models to Hubble Space Telescope observations of 41 such photoevaporating disks in the Orion Nebula, the study group derived disk masses, sizes, lifetimes, and surface-density distributions and explained the optical and infrared spectra seen from these objects.

Disks observed around low-mass young stars which are not disrupted by nearby bright stars are expected to give rise to planetary systems like our own. Together with T. Henning and H. Klahr of the University of Jena (Germany), the midplane conditions in these solar nebula analogs, where solid material from dust to rocks to planetesimals and planets are formed, were studied. That research (which is described more fully in a separate paper in this volume) indicated that because the disk thickness is controlled by the distribution of dust grains, much of the disk may be shadowed from illumination by the central star. Therefore, planet formation occurs in an environment colder than expected by previous estimates.

The theoretical models of ARC have been used to interpret observational data from such NASA facilities as the Infrared Telescope Facility, the Infrared Astronomical Observatory, the Hubble Space Telescope, and the Infrared Space Observatory, a European space telescope with NASA collaboration, as well as data from numerous ground-based radio and optical telescopes. In addition, the models have been used to determine the requirements of future missions such as that of the Stratospheric Observatory for Infrared Astronomy and the proposed Space Infrared Telescope Facility.

Point of Contact: D. Hollenbach
(650) 604-4164
hollenbach@warped.arc.nasa.gov

Galactic Bulge Observations

Thomas L. Roellig, Kin-Wing Chan

The mid-infrared spectrometer (MIRS) that flew on the joint NASA/Japanese Space Agency Infrared Telescope in Space (IRTS) mission in 1995 yielded a wealth of data that are presently being analyzed and reported on. Here we present the results of MIRS studies of the Galactic Bulge region.

The MIRS operated over wavelengths ranging from 4.6 to 11.7 microns with a spectral resolution of about 0.23 to 0.36 microns. This is an ideal spectral region and resolution for investigations of infrared emissions from solid material, since it covers many of the diagnostic stretching and bending modes of candidate interstellar material. The IRTS/MIRS telescope/instrument combination achieved sensitivities that were orders of magnitude better than those of any other instrumentation previously used for diffuse mid-infrared emission studies.

Analysis of the MIRS results was performed for four locations in the Galactic Bulge region with galactic longitude and latitude coordinates of 8.7°, 2.9°; 8.7°, 4.0°; 8.7°, 4.7°; and 8.7°, 5.7°. The MIRS data were averaged over effective beam sizes of 8 × 20 arcminutes and corrected for interstellar extinction based on results from the Cosmic Background Explorer mission. Analysis of the data from the Infrared Astronomical Satellite (IRAS) mission indicates that the MIRS diffuse emission measurements had at most a 10% contribution from IRAS 12-micron point-sources.

Below galactic latitudes of 4.0° in the Galactic Bulge, the MIRS spectra are very similar to those from M and K giant stars. The unidentified infrared bands at 6.2, 7.7, 8.6, and 11.3 microns were also detected; it is likely they originate from emission from the diffuse interstellar medium in the bulge. Above galactic latitudes of 4.0°, the MIRS spectra are similar to the spectra of evolved stars with the high mass-loss rates seen by IRAS. One likely interpretation is that this emission arises predominantly from a large number of low-luminosity stars that were not detected by IRAS. The age of such low-luminosity stars would have to be at least 12 billion years, and the existence of such a large number of evolved stars with high mass-loss rates in the bulge would have a significant effect on our understanding of the stellar content and evolution of the Galactic Bulge. Furthermore, since the characteristics of the Galactic Bulge region are similar in many ways to those of elliptical galaxies, these results may shed light on the origin of the excess mid-infrared emission that has been observed on some elliptical galaxies.

Point of Contact: T. Roellig/K-W Chan
(650) 604-6426/3118
troellig@mail.arc.nasa.gov
kwc@ssa1.arc.nasa.gov

Photochemistry of Interstellar and Cometary Ice Analogs

Scott Sandford, Max Bernstein, Louis Allamandola, Robert Walker

Ames Research Center has made major contributions to the understanding of the composition and properties of interstellar and cometary ices. This is done, in part, by studying how laboratory ice analogs are modified by various kinds of chemical processing, for example, by ultraviolet (UV) irradiation. These laboratory studies, coupled with telescopic observations, show that the main components of cosmic ices are simple molecules like water (H_2O), methanol (CH_3OH), carbon monoxide (CO), carbon dioxide (CO_2), and ammonia (NH_3). Ultraviolet irradiation of such ices produces "hot" hydrogen (H), carbon (C), oxygen (O), and nitrogen (N) atoms and radicals like formyl radical (HCO) which ultimately combine with other species in the ice to make new, often more complex, organic molecules. Interstellar materials made in this manner may ultimately seed planetary systems that form within dense clouds with molecules crucial to the origin of life.

This paper reports on the chemical processes that occur when polycyclic aromatic hydrocarbons (PAHs) are frozen in H_2O-rich ices and then UV-irradiated. PAHs, large aromatic molecules that consist of fused hexagonal rings of carbon surrounded by peripheral hydrogen atoms (an example is shown in the figure), are known to be abundant and ubiquitous in the gas phase in space where their aromatic structure makes them highly resistant to photodestruction. However, in dense clouds, PAHs are efficiently frozen onto dust grains where they will be exposed to UV radiation. Under these conditions, PAHs will not just be exposed to direct interactions with high-energy photons, but will also experience chemical attack by "hot" atoms and reactive molecular fragments produced when photons strike other molecular components in the interstellar ice.

A large number of experiments were carried out in which various PAHs were frozen in H_2O ices at 12 kelvin and then exposed to varying amounts of UV radiation. After photolysis, the ices were warmed and the remaining room-temperature residues collected. The samples were examined using infrared spectral techniques before, during, and after deposition, irradiation, and warm-up. The room-temperature residues were also examined by the chemistry group of Richard Zare at Stanford University using the technique of laser desorption-mass spectrometry.

The results of the infrared and mass spectrometric studies demonstrate that PAHs frozen in ices are indeed more susceptible to modification by UV irradiation than are PAHs in the gas phase. The alteration of the PAHs appears to occur along several different pathways, represented graphically in the figure, that involve the addition of hydroxyl radicals (OH) groups, O atoms, or H atoms to the peripheral carbon atoms on the PAHs. The result is the production of PAHs containing alcohols, ketones, ethers, and aliphatic hydrocarbons as peripheral functional groups.

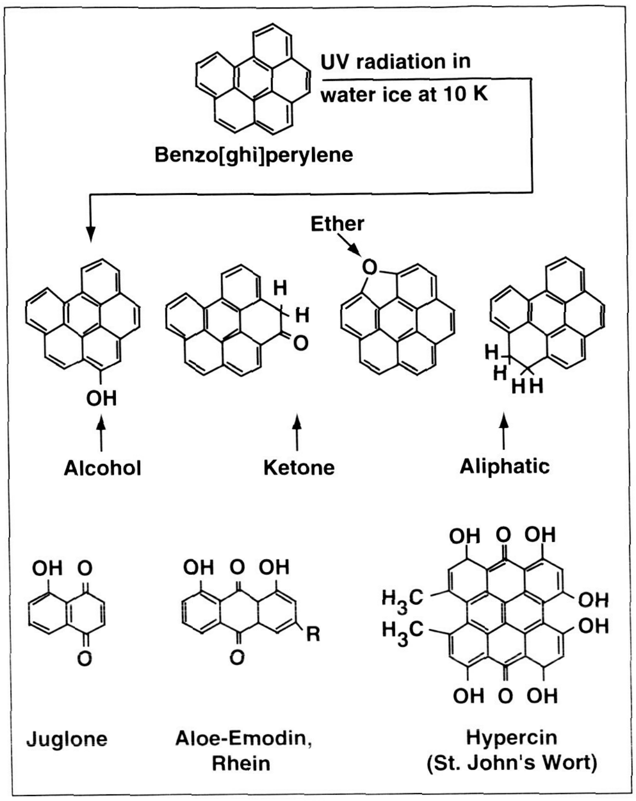

Fig. 1. The molecular structures (top) that are formed when a polycyclic aromatic hydrocarbon (in this case, benzo[ghi]perylene) is UV-irradiated in an H_2O ice at 12 kelvin. The new functional groups produced on the periphery of the molecule include those of alcohols, ketones, ethers, and aliphatics. The structures (bottom) of juglone, aloe extracts, and hypercin, are examples of aromatic molecules that are important in living systems. The peripheral structures of these molecules are very similar to those seen in the upper portion of the figure.

These processes add significantly to the molecular complexity of the material and have several important implications. First, oxidized forms of PAHs are thought to represent important cancer risks, and the photolysis of PAHs in ice grains in the upper atmosphere may represent a significant pollution risk. Conversely, PAHs having these kinds of structures are common in primitive meteorites and, as the figure shows, are very similar to compounds critical to the chemistry of living systems. Thus, the photolysis of PAHs in interstellar and cometary ices may have had a part in the production of compounds that played key roles in the origin of life.

Point of Contact: S. Sandford
(650) 604-6849
ssandford@mail.arc.nasa.gov

Hot Water Decoded

David W. Schwenke

A detailed knowledge of the rotation-vibration spectrum of water vapor is required in a wide variety of disciplines, from atmospheric chemistry, observations through Earth's atmosphere, and the search for water-based life, to the modeling of cool oxygen-rich stars. This is because spectroscopy, the analysis of light intensity as a function of frequency, is the only means available for the study of distant objects, and water has ubiquitous presence in the Universe. Every molecule has a unique set of frequencies at which it absorbs light, and the pattern of line positions and line strengths allows precise identification and concentration analyses from afar.

In order to deduce the temperature variation of the line strengths for widely diverse conditions, it is necessary to know the line positions, the intrinsic line strengths, and the initial-state internal energy. The line positions can be determined very accurately from experiment. However, even under optimum conditions, it is only possible to obtain line strengths of moderate accuracy at fixed temperature. Thus theoretical calculations are required in order to decompose the line strength into its temperature-dependent Boltzman factor, which depends on the internal energy and the intrinsic line strength. Previous theoretical work has not been accurate enough to assign the initial states for regions of the spectrum that are congested or that involve highly excited rotation-vibration levels; however, recent work at Ames Research Center (ARC) has resulted in a significantly improved calculation of the opacity of water. These calculations achieved a level of accuracy that far exceeded that of previous work and now enables detailed analysis of the experimental spectrum of water.

A widely used low-temperature database of water lines is the HITRAN database, the 1996 release of which contains 30,117 lines for the most prevalent isotope of water; of these, 1,725 were unassigned. It is possible to associate 30,092 of the lines with the ARC theoretical database, and in the process, 133 lines were reassigned and 831 of the unassigned lines were assigned with a very high degree of confidence.

The ARC theoretical water database has also been used in the simulation of the spectrum of a sunspot. The line positions predicted were sufficiently accurate to assign the dominant water peaks, which is a significant accomplishment given the very high density of lines at these elevated temperatures. Because this requires both accurate line positions and accurate line strengths, the simulation demonstrated the reliability of the ARC theoretical water database for high temperatures.

Point of Contact: D. Schwenke
(650) 604-6634
schwenke@pegasus.arc.nasa.gov

Discovery of Polycyclic Aromatic Hydrocarbon Ions in NGC 1333

Gregory Sloan, Lou Allamandola, Jesse Bregman, Doug Hudgins, Tom Hayward, Becky Devito

Since the discovery of unidentified infrared emission bands in 1973, their origin has been assigned to several different carriers. Although the first suggestion that these bands were due to polycyclic aromatic hydrocarbons (PAHs) occurred in 1984, the lack of a good match between laboratory spectra of PAHs and the interstellar features prevented a conclusive identification. The large discrepancy between the relative band intensities observed in the laboratory and those observed in astronomical sources has recently been resolved by laboratory spectra of ionized PAHs. Specifically, the relative strengths of the emission features due to C-H bending modes (8.6 and 11.3 microns) are too strong relative to the C-C modes (6.2 and 7.7 microns) in laboratory spectra of neutral PAHs, but ionized PAHs provide a good match with astronomical spectra. The laboratory spectra of ionized PAHs show an additional weak band near 10 microns; they also show that the 11.3-micron band is shifted to shorter wavelengths by 3%–5%.

The reflection nebula in NGC 1333 around the young star SVS 3 has proven to be a fertile region in which to investigate the possible ionization of PAHs. SVS 3 is an early B star, so its ultraviolet output is weaker and cooler than it is in most other PAH sources (e.g., the Orion Bar, NGC 7027), where the PAHs may be completely ionized. Previous observations at coarse spatial resolution had shown that the mid-infrared spectrum changed with position in NGC 1333 in a way consistent with there being a larger fraction of ionized PAHs close to the central star rather than farther away. In order to investigate the spectral variations in the PAH emission at higher spatial resolution, a long-slit spectra of NGC 1333 SVS 3 was obtained at the 5-meter Hale Telescope at Palomar using SpectroCam-10. The slit was oriented N/S and covered a 2- by 16-arcsecond region of the sky covering SVS 3 and the nebulosity to the south.

The combination of high spatial and spectral resolution in the present data set reveals several variations in the shape of the emission features in the 10–13-micron region. The 11.2-micron PAH feature develops a wing on the short-wavelength side close to SVS 3 accompanied by an emission feature at 10 microns. The wavelength of the wing is shifted from the center of the 11.2-micron band by about 4%, just the shift expected for the 11.2-micron feature between neutral and ionized PAHs. As the distance from SVS 3 increases, and as the intensity of the ionizing radiation decreases, both the 10-micron component and the 11.0-micron wing first decrease in strength and then vanish within a few arcseconds. Combining this spatial behavior with the match to features in laboratory spectra of ionized PAHs, it is concluded that both the 10-micron feature and the blue wing of the 11.2-micron feature arise from PAH cations in the nebulosity close to the central star. Specific emission features from ionized PAHs have not been identified before, even though previous spectra of PAH sources show the 10-micron feature.

Point of Contact: J. Bregman
(650) 604-6136
jbregman@mail.arc.nasa.gov

Submicron Optical Aerosol Spectrometer

Mark L. Fonda, David M. Stratton

A light-scattering instrument capable of measuring in situ aerosol particle sizes from 0.02 to 100 microns in concentrations as low as 1 part per billion, under low-pressure conditions (as low as ~0.05 Torr) has been developed. The instrument illustrated in the first figure can provide continuous data monitoring and data collection to encompass the wide dynamic size range and concentration conditions needed in studies of planetary atmosphere models, as well as field experiments addressing Earth air-quality pollution standards. A fiber-coupled argon-ion laser system, which incorporates polarization ratio scattering measurements was used to determine the size distribution at particle sizes smaller than 0.1 micron. As particle concentration and size increases, data collection shifts to angular (diffraction-based) scattering for larger particle measurements (up to 100 microns). A customized software and electronics package automatically shifts from polarization to diffraction-based measurements as the angular scattering detector attains an acceptable signal-to-noise ratio. Results from static experiments utilizing Freon, flow-through experiments utilizing sodium chloride (NaCl) and carbon particles, and dynamic acetylene photolysis experiments were performed that provided comparative particle-size data with data obtained with a scanning electron microscope. The second figure illustrates particle growth in acetylene that was photolyzed with 1800-angstrom ultraviolet radiation. In this set of measurements, the particle diameter ranges from about 0.03 micron to 0.33 micron, and the concentration increases from 0.06 to 0.27 parts per billion.

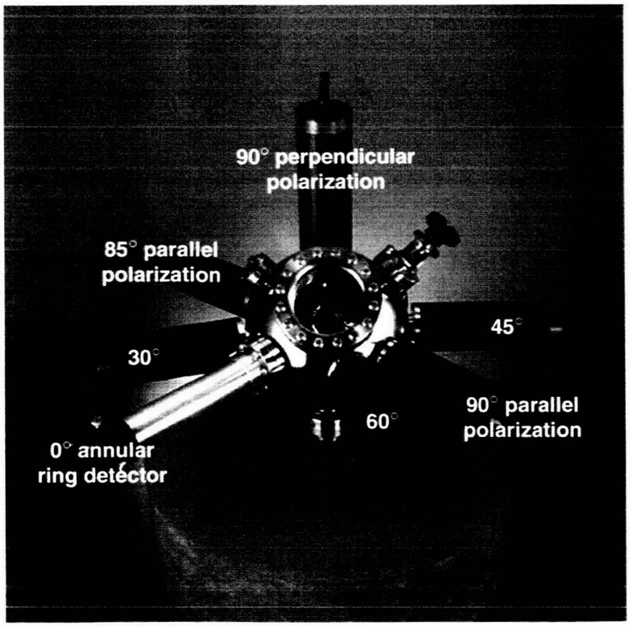
90° perpendicular polarization
85° parallel polarization
45°
30°
90° parallel polarization
60°
0° annular ring detector

Fig. 1. Atmospheric aerosol growth vessel.

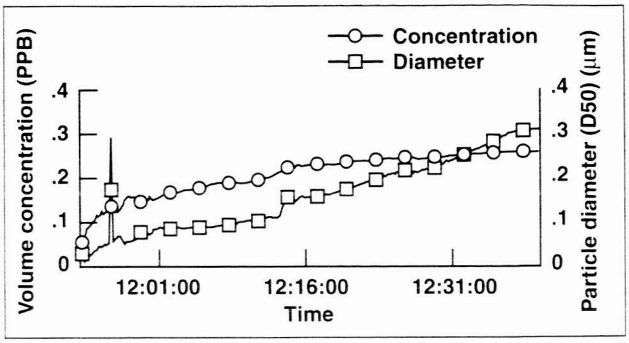

Fig. 2. Dynamic acetylene photolysis test data.

Point of Contact: M. Fonda
(650) 604-5744
mfonda@mail.arc.nasa.gov

Gravity Probe B Project

J. Goebel

Ames Research Center is supporting the development and manufacture of the guide-star telescope detectors of the Gravity Probe B (GPB) Project. GPB is a Stanford University/Lockheed-Martin/Marshall Space Flight Center Physical Science Mission that has called upon Ames Research Center's expertise in cryogenic electronics to help meet the program's launch schedule. The Ames technical contribution has been made over a period of 2 years and is expected to conclude shortly after launch, currently scheduled for March 2000 from Vandenberg Air Force Base.

The GPB fine-motion guide-star tracking system uses a 5.6-inch aperture, all fused-quartz telescope which is attached to a quartz block assembly containing the relativistic-effect sensing gyroscopes. The guide-star telescope rotates about a central axis, thereby providing a constant pointed reference direction to a star fixed on the celestial sphere; this is the distant inertial reference frame. The satellite that contains this assembly will be in a polar orbit about Earth. The precession rate of the sensed gyroscope directional output from the distant inertial reference frame is a possible indication of a general relativistic deviation from that expected by Newtonian gravitational theory. A precession rate is expected to occur at an angular scale of a few arcseconds per year, and it is expected to be measured with an accuracy of about 0.2 milliarcsecond per year. For comparison, the apparent angular diameters of the few nearest stars, visible to all but the largest telescopes as points of light, are less than 10 milliarcseconds.

The first figure is a picture of the quartz telescope with the attached light detectors. The telescope is standing on its base plate. Light enters from above and is reflected into the upper structure, the Knife Edge Divider Assembly, where the beam is divided equally between eight photodiodes. The equality of this division determines the error signal that is sent back to the control circuits which then adjust the spacecraft orientation. Four detectors are needed for complete control; the other four are identical, but redundant. The detectors are at the very top of the figure.

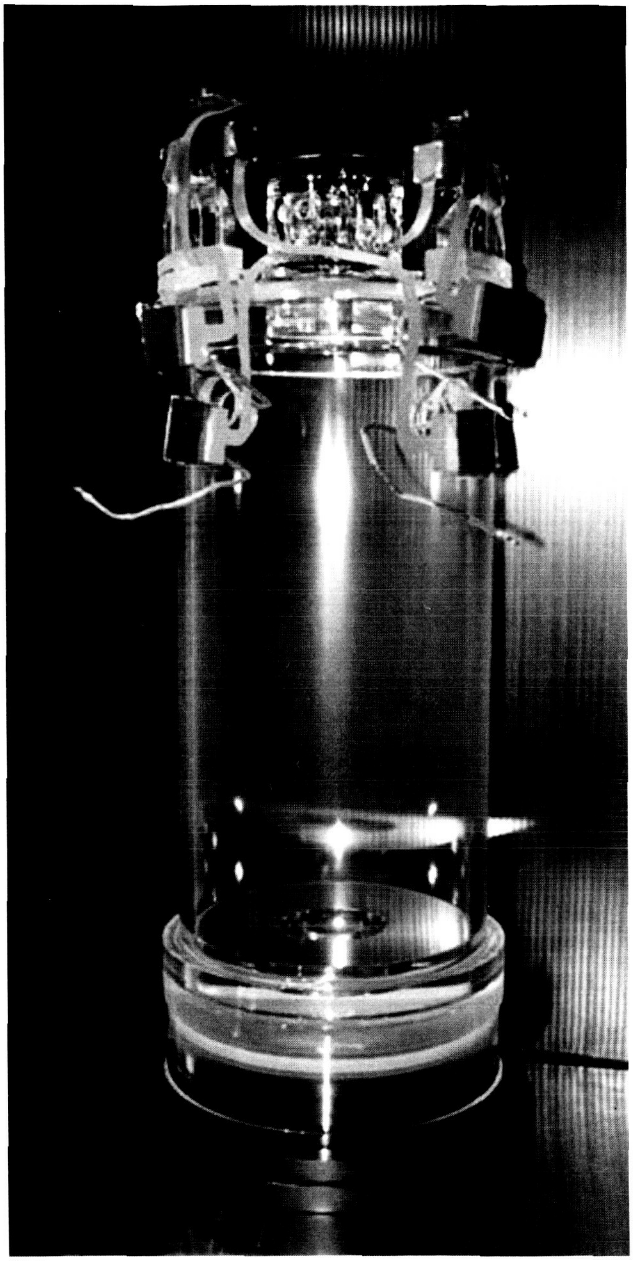

Fig. 1. Gravity Probe B (GPB) 5.6-inch-aperture quartz telescope.

The second figure shows the detector circuit and thermal isolator mounted to its titanium base and flexible cable assembly. Signals are conveyed via flexible printed circuits to connectors that interface the detectors thermally and electrically to a low-thermal-conductivity cable bundle (not shown) which is part of the science instrument assembly.

Ames personnel have been fully matricized into the Telescope Readout Electronics Group of the GPB Project. Significant technical contributions have been made in the areas of cryogenic characterization of electronic components, circuit design, standardization, manufacture, detector circuit acceptance testing, flexible cable design and manufacturing, thermal isolator design and testing, optical calibration, quality assurance, detector package assembly, and acceptance testing.

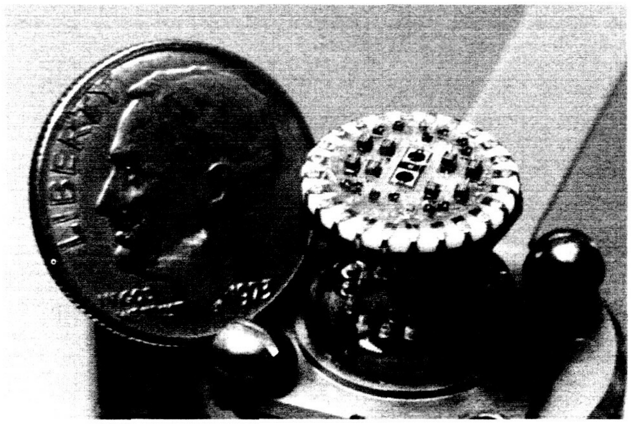

Fig. 2. Guide-star detector circuit and thermal isolator.

Point of Contact: J. Goebel
(650) 604-3188
jgoebel@mail.arc.nasa.gov

Modeling of Steady Secondary Flows in Pulse Tube Cryocoolers

Jeffrey M. Lee, Peter Kittel

A linearized solution for describing steady secondary flows generated by periodic compression and expansion of a gas in a tube has been developed and verified. The small-amplitude series expansion in the inverse Strouhal number at the anelastic limit is applied to the two-dimensional axisymmetric equations for mass, momentum, and energy conservation for an ideal gas. The solution is calculated to higher-order for understanding mass and enthalpy streaming. This work is useful for predicting the streaming losses that are present in pulse tube cryocoolers.

The ordered equations show that the zeroth-, first-, and second-order equations are coupled through the zeroth-order temperature. An analytic solution is obtained in the strong temperature limit where the zeroth-order temperature is constant. The solution shows that periodic heat transfer between the gas and tube, characterized by the complex Nusselt number, is independent of the axial-velocity boundary conditions and the Fourier number. Steady velocities increase linearly for small Valensi numbers and can be of order 1 for a large Valensi number. Decreasing heat transfer between the gas and the tube decreases steady velocities for systems in which nonzero velocity boundary conditions exist at each end of the tube, such as for orifice pulse tubes. For systems in which one end of the tube is closed, such as for basic pulse tubes, increasing heat transfer between the gas and tube decreases steady velocities. The model predicts that a conversion of steady work flow to heat flow occurs whenever temperature, velocity, or phase-angle gradients are present. Additionally, steady enthalpy flows are reduced by heat transfer and are scaled by the Prandtl number times the Valensi number.

Particle velocities from a smoke-wire experiment were compared to model predictions for an orifice pulse-tube configured system (see figure). Mass-streaming and flow reversal between the centerline and diffusion layers of the gas were observed, and velocities were measured. The theory predicted the

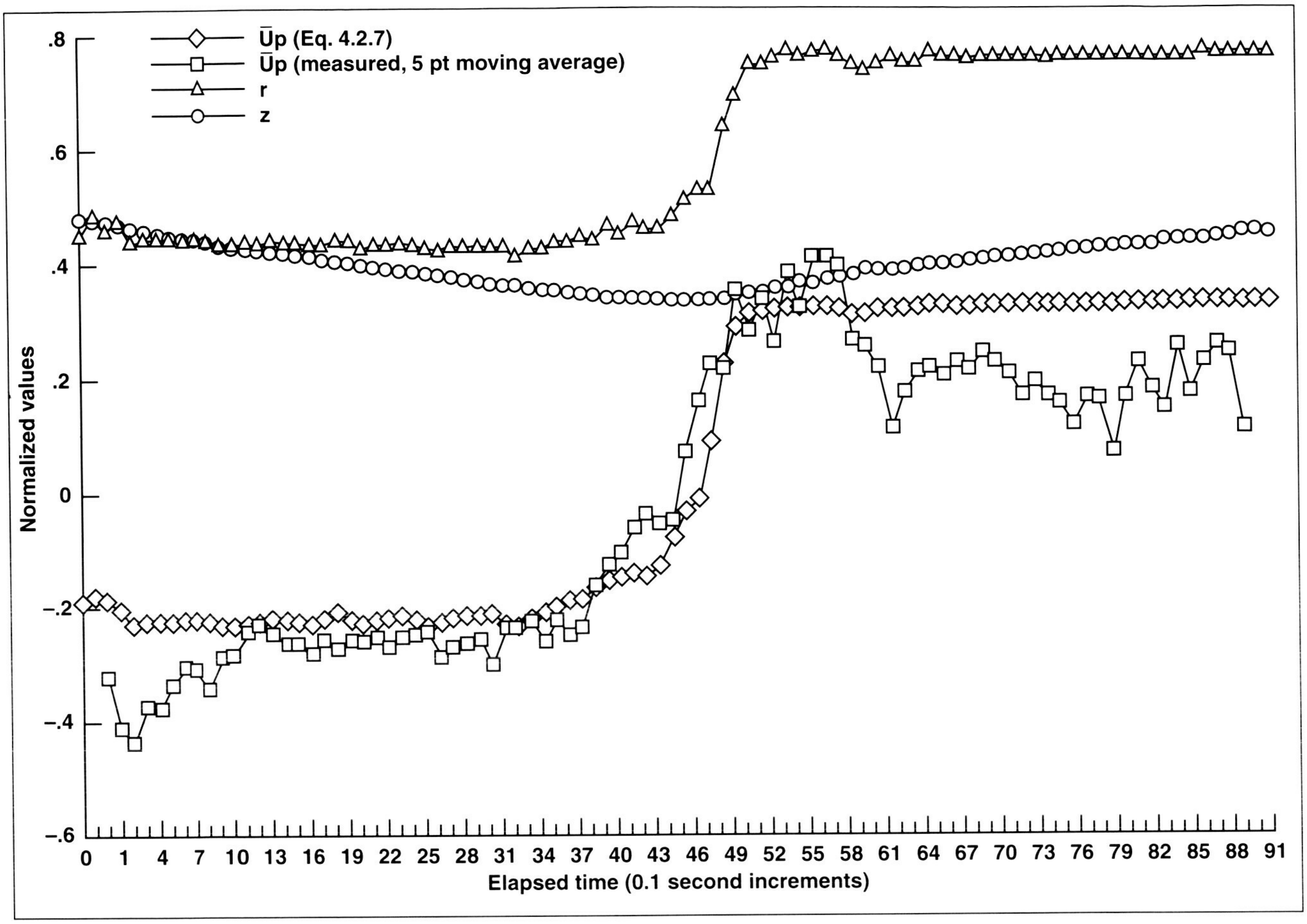

Fig. 1. A comparison of measured and predicted higher-order steady secondary streaming particle velocities in oscillating compressible flow. Data were obtained for a Valensi number of 68 and a velocity phase angle of 90 degrees. The measured velocities were obtained from smoke-visualization experiments.

speed and direction of the mass-streaming, and the locations where the flow reversed. The results indicate that the theory is valid for pulse tubes and that it can be used to solve for the zeroth-order temperature, to compute enthalpy flows, and to determine losses associated with steady secondary streaming. The theory can be used to minimize secondary flow losses when designing pulse tube coolers.

Point of Contact: J. Lee
(650) 604-5693
jmlee@mail.arc.nasa.gov

Validating Requirements for Fault-Tolerant Systems Using Model Checking

Francis Schneider, Jack Callahan, Steve Easterbrook

The objectives of this work were to develop new techniques for validating fault-tolerance requirements in the early stages of software development, and then determining whether the requirements and high-level designs for fault-tolerant systems provide the required reliability before they are implemented. Another purpose was to explore the integrated application of model-checking technology as a verification and validation technique for software requirements.

A case study of a dually redundant spacecraft controller, in which a checkpoint and rollback scheme is used to provide fault tolerance during the execution of critical control sequences, was conducted. The software-requirements specification for the spacecraft established the required behavior for the checkpoint and rollback scheme. Their validity could not be determined through inspection. In other words, it was not possible to determine whether the behavior described in these requirements would provide the desired level of fault tolerance. Testing of the eventual implementation would not necessarily provide this validation either, a result of the difficulty of ensuring test-case coverage for all possible fault-occurrence scenarios. The approach taken was to derive a formal automata-based model from the specification, and to use a model-checker to explore its behavior. Various high-level safety properties were used to validate the generalized system model. Key system functional requirements were validated by using linear temporal logic to define the corresponding liveness properties, which are required to be satisfied when the system responds to faults. The model checker, Spin, identified traces in the model for which these properties were violated, using nondeterministic fault injection.

Validation of fault-tolerant architectures is a difficult problem, and exhaustive testing of the implemented systems is an unsatisfactory approach to its solution. Errors found after implementation are expensive to fix. If the fault-tolerant architecture is found to be deficient during system testing, then much of the development effort may have been wasted. Testing cannot guarantee coverage of all possible fault conditions, for the precise timing of fault occurrences can determine how they are handled. For these reasons, techniques that can be applied earlier in the life cycle are needed.

Model checking can be applied to abstract models of the proposed architecture early in the life cycle, and can explore model behavior in the presence of a wide variety of fault conditions. A model was abstracted from design notes for the dual-redundant system. The model was pruned to remove states that did not affect the properties to be tested, thereby reducing the size of the state space to one that is manageable by current model-checking tools. Five different fault categories were identified, and six separate requirements on the rollback scheme were validated. Each of the requirements involved the exhaustive examination of approximately 100,000 states in the model, and took about 30 seconds. The response and recovery in each case was to the injection of a fault of the appropriate category in all possible ways, based on the model.

Three of the six runs for the six requirements failed in the verification. Three anomalies were identified: two were errors in the requirements that might not occur in the implementation, and the third was a discrepancy in the detailed requirements that could allow for erroneous behavior of the implemented system. This analysis demonstrated that the approach is feasible, and that it is capable of detecting subtle errors that had escaped detection through other means.

Point of Contact: S. Easterbrook
(304) 367-8352
steve@research.ivv.nasa.gov

Bonded Capillary Columns

Thomas Shen, Jr-Lung Chen

The sol gel process has been widely used in a variety of areas including high-performance chromatography, materials science, and nanotechnology applications.

The sol gel technology has been applied for the in situ formation of stationary phases on fused-silica capillary columns. Experience suggests that the sol gel method will provide a better avenue for preparing analytical microcolumns for miniaturized instruments. These microcolumns have the potential to be used for fast and highly efficient separation and analysis of polar as well as nonpolar compounds in future planetary spacecraft missions that will focus on in situ or returned samples analysis. The sol gel process is not a well-defined preparation procedure. Usually, it has to be modified according to the components involved. Therefore, studies of the effects of solvents were conducted, and some particular formulations were found to be excellent for the preparation of columns.

In order to further advance the sol gel process for column preparation in a more definitive and effective way, a more systematic study will be carried out to further resolve this problem. Accordingly, several short (about 10-feet-long) gas chromatography (GC) columns have been prepared. Some of these displayed desirable properties for analytical gas chromatography of small polar and nonpolar molecules (see figure).

Point of Contact: J-L Chen
(650) 604-1156
jlchen@mail.arc.nasa.gov

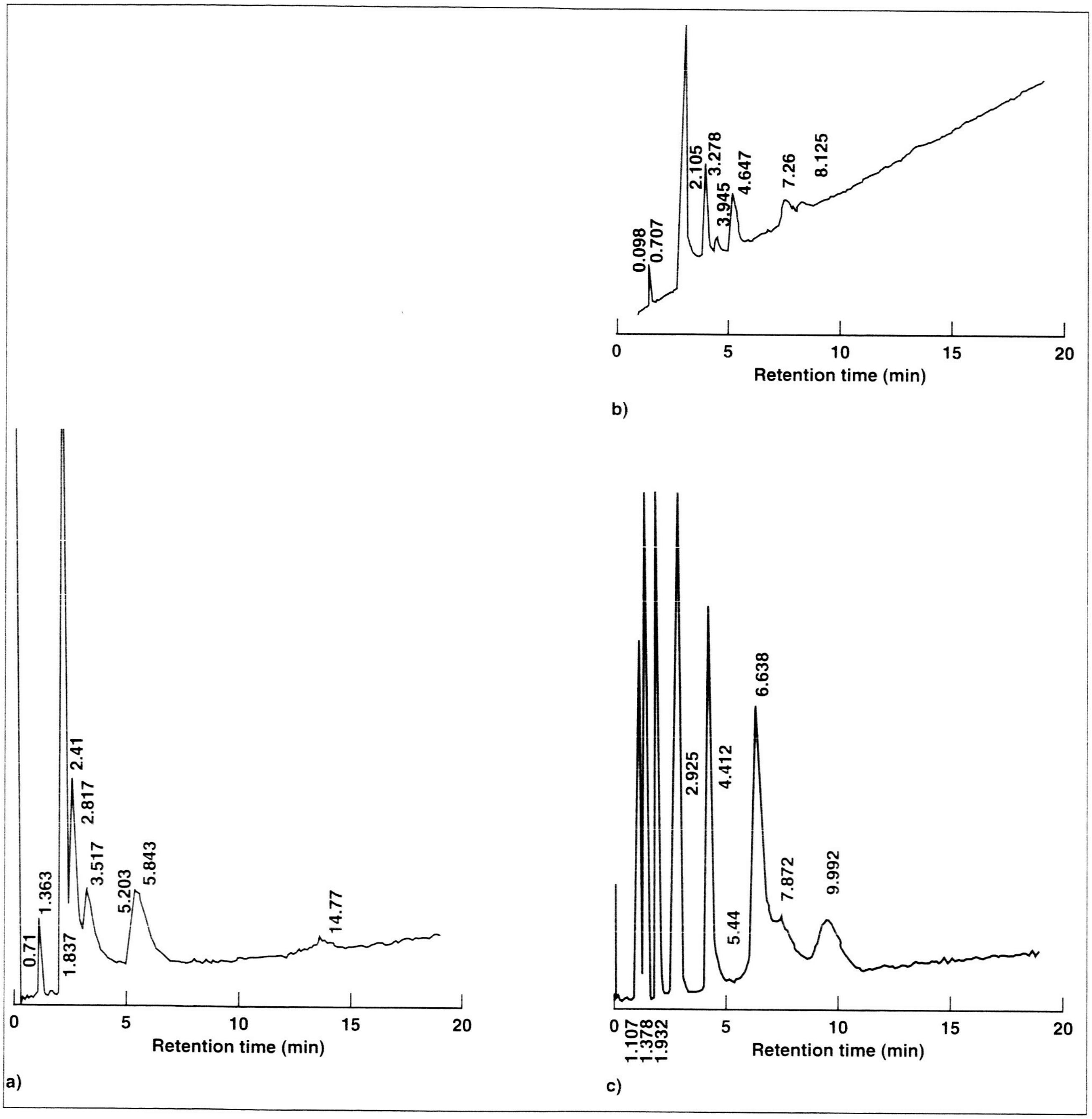

Fig. 1. Chromatographic data based on a 10-foot-long cyanoethyl-containing fused-silica capillary column with inner diameter of 0.530 millimeter. (a) The GC analysis of a mixture of seven amines was run at a flow rate of 1 milliliter per minute of helium at 129° C. (b) The GC analysis of a mixture of six alcohols was run at 3 milliliters per minute of helium at 100° C. (c) The GC analysis of a mixture of 10 hydrocarbons was run at 1 milliliter per minute of helium at 20° C.

2-D Super Resolution Used on Mars Pathfinder

Bob Kanefsky, Peter Cheeseman, C. Stoker

The Data Understanding Group at Ames Research Center is developing the theory and practice of combining information from multiple images. The group has already produced a technique called Two-Dimensional (2-D) Super-Resolution; this technique uses multiple images of the same scene, taken by the same instrument under nearly identical lighting conditions and from nearly identical instrument orientations, and produces a single output image of higher resolution than the input images. The inescapable slight differences in instrument orientation, and in the registration of scene features on the pixel grid of the instrument, ensure that any point in the scene is pixelized differently in each input image. The 2-D Super-Resolution technique exploits these registration differences to create a mathematical model of the original scene—using the information from all the low-resolution input images—which has much higher resolution than those images. The resolution can typically be improved by a factor equal to the square root of the number of input images. This model can then be used to generate a high-resolution output image.

Until 1997, the 2-D Super-Resolution technique had been used only for "data mining." Dramatic improvements had been demonstrated by chance on some identical Viking Orbiter images, and some modest but scientifically used results had been obtained on potential landing sites.

During the Mars Pathfinder mission (July through October 1997), the technique was used by Ames personnel working on the Pathfinder science team. The Imaging for Mars Pathfinder (IMP) camera on the lander was commanded to take image sequences especially designed to be processed by the super-resolution algorithm.

The science team was pleased with the results, and made super-resolution sequences one of the routinely commanded sequences for the rest of the primary mission and into the extended mission. It was to be run at low priority until the final multispectral panorama was complete, and then at high priority. This would have resulted in a flood of data if the spacecraft had survived a few weeks longer and completed the panorama, and automatic processing was put in place to prepare for this. As it is, over a dozen rocks and horizon features were still super-resolved, including both Twin Peaks, Big Crater, Wedge, Half Dome, Stack, and the Flotilla of Flat Tops.

Some early near-field targets were selected, in part, to validate the super-resolution algorithm and

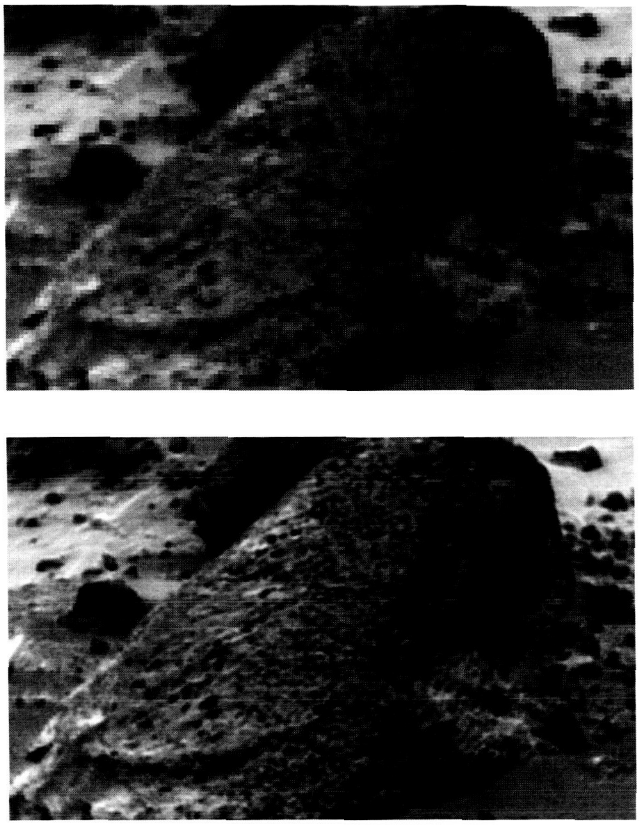

Fig. 1. The top image of Wedge, a rock a few meters to the south of Pathfinder, is one of the 25 images taken on Sol 20 (July 23). The super-resolved image (bottom) was created from the 25 images to demonstrate the 2-D super-resolution technique. It shows the pitted texture for the first time. This was later confirmed when Sojourner rover took closeups of Wedge on Sol 35.

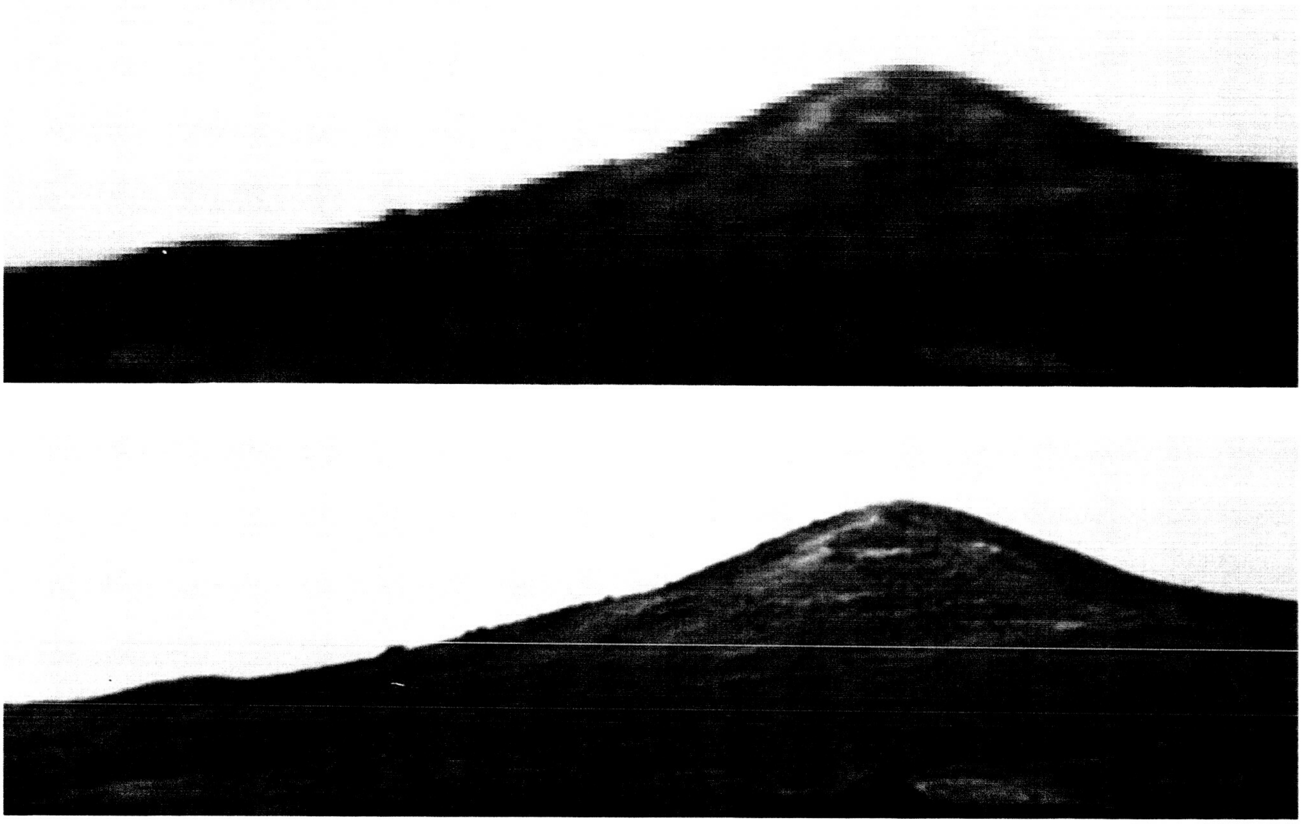

Fig. 2. One (top) of the forty-two images of South Peak—one of the famous Twin Peaks to the west of the Pathfinder landing site—that were processed to create a super-resolved image. The result (bottom) is about five or six times sharper than the input images. This is the sharpest picture of South Peak available anywhere. Note possible outcropping in the foreground.

show that its results could be trusted. The super-resolution algorithm was able to show the pits in the rock named Wedge (see first figure), which no human had ever seen up until that point. In all the raw IMP images, the texture of Wedge was too fuzzy to discern; the science team could not agree whether the rock was bumpy, like granite, or pitted, as a volcanic rock with vesicles might be. This observation was confirmed two weeks later when Sojourner approached Wedge for the first time and took closeups. (This took place just before the rover's entirely too-close encounter, when it was wedged on top of Wedge for more than two days!)

The super-resolved images of the Twin Peaks indicate that the horizontal features, just barely visible in the raw images, probably consist of lines of boulders, rather than layered deposits, and that South Peak is not so different from its twin as it first appeared (second figure). The South Peak image also happens to capture a rock in the foreground, which shows evidence of layering in the super-resolved image. This could be an outcropping, a tempting target for a rover, although it was far beyond Sojourner's range.

Point of Contact: P. Cheeseman
(650) 604-4946
cheesem@ptolemy.arc.nasa.gov

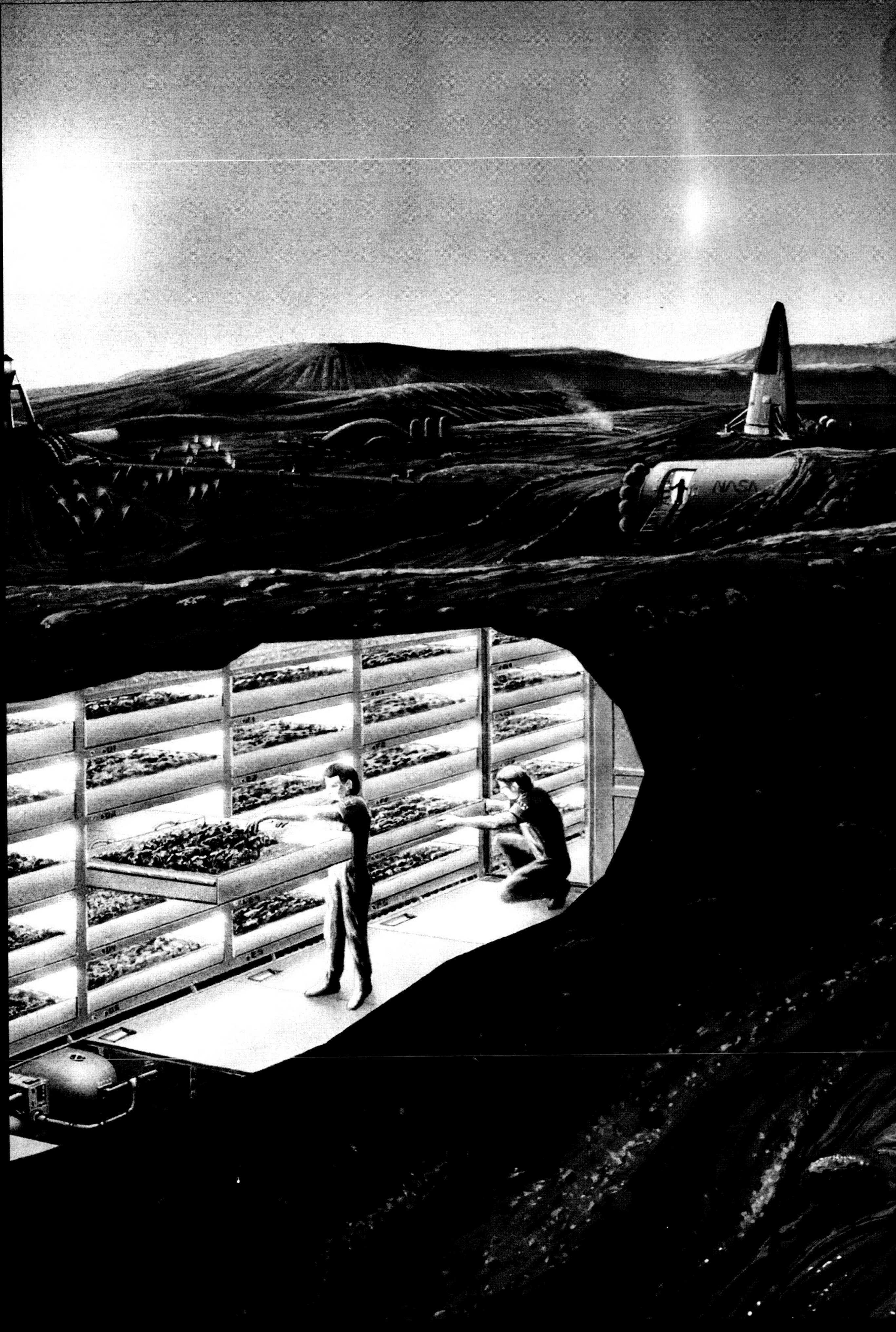
NASA

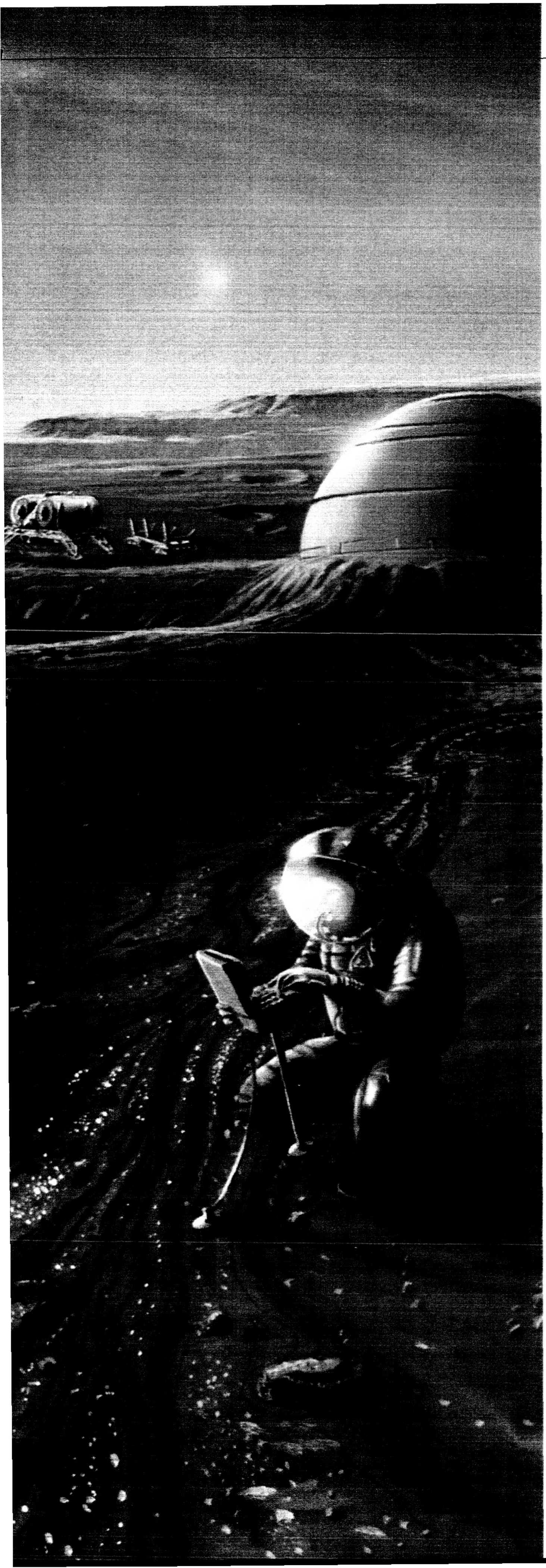

Overview

NASA's Human Exploration and Development of Space (HEDS) Enterprise brings the frontier of space fully within the sphere of human activity. Ames Research Center supports the HEDS Enterprise by conducting research, managing spaceflight projects, and developing advanced technologies. An objective of these efforts is to seek knowledge of physicochemical and biological phenomena that can be fully explored only at very low gravity levels. This objective embraces the quest for knowledge of the role and influence of gravity in living systems—one of the elements of NASA's astrobiology activities. A second objective is to develop technologies for advancing human exploration of space and achieving routine space travel. A complementary objective is to apply knowledge generated in pursuit of these objectives, whenever possible, to enrich life on Earth. In FY97 important research and technology efforts pursuant to the following goals of the HEDS Enterprise were accomplished:

- Increased knowledge of nature's processes using the space environment
- Advanced human exploration of the solar system
- Achieved routine space travel
- Enriched life on Earth through educational, commercial, and technological opportunities in space

New knowledge and an increase in the understanding of nature's processes related to the influence of gravity on living systems are acquired by a two-pronged approach: (1) Research is conducted on the ground and in space over a range of gravitational levels and with a variety of biological specimens; and (2) specialized equipment and advanced technologies are developed to support life-sciences research on the ground and in space. The knowledge acquired is then integrated and disseminated via information technology. Armed with this knowledge, scientists can help to ensure the safe travel of humans in space for extended durations and contribute to the understanding of life on this planet.

In this report, new life-sciences research findings that expand our understanding of the phenomena surrounding the effects of gravity on living things are presented. Research to help secure the health and safety of humans ultimately living and working in space continues to unravel mysteries that surround aspects of our own evolution.

Space scientists have worked for many years to understand the source or sources of two of the most commonly experienced, pervasive effects of weightlessness: space motion sickness and postflight orthostatic intolerance. Previous research has indicated that the headache, nausea, and vomiting experienced by most astronauts during the first days of weightlessness, and the subsequent inability to stand (orthostatic intolerance) upon returning to Earth, are the results of a shift in body fluids toward the head. Two recent studies have focused on this area of concern, furthering both the understanding of the consequences of this fluid shift and the appropriate direction for mitigating its effects with countermeasures.

Recent work suggests that the fluid shift that results from cardiovascular deconditioning increases intracranial pressure (ICP). The increased ICP contributes to the motion sickness that directly impacts crew performance at critical times in space, and may contribute to the readaptation effects as well. Ongoing comparisons of existing invasive methods for measuring ICP with an Ames-developed, noninvasive, ultrasonic measurement device are proving the device to be sensitive and accurate. This method will enable scientists to investigate the association between ICP and physiological symptoms experienced in space. With this knowledge, scientists can refine the countermeasures employed by the astronauts to relieve their discomfort. This device has a strong dual-use potential in the medical community for diagnosing the extent of damage in head-trauma patients.

Additional research toward identifying the most effective countermeasure for cardiovascular deconditioning examined various ground-based models to simulate the effects of this biomedical condition. Researchers found that the most promising ground approaches for inducing a similar physiological response to postflight fainting, head-up tilt, and lower body negative pressure were more effective when combined, providing additional insight into the mechanisms that cause the disorder.

Because changes in ICP can have consequential health impacts on Earth as well as in space, understanding the mechanisms underlying cardiovascular adaptation is vital. Life scientists at Ames have conducted comparative studies of gravity tolerance using two species of snakes with evolutionary divergent backgrounds. Their long body form and widely different behavioral ecologies make arboreal (tolerant against gravitational stress) and aquatic (less able to resist gravitational stress) snakes sensitive models for studying ICP regulation in altered postural configurations. Thus, the arboreal species may be an appropriate model for studying chronic effects of adaptation to gravity, while the aquatic species provides a contrasting example of adaptation to weightlessness in terms of the cardiovascular system and ICP changes.

Other important research in FY97 contributing to the long-term health of humans in space focused on the calcium endocrine system and its role in regulating bone formation in space. The source of exercise-induced immune system depression was examined to improve exercise countermeasure protocols for efficient immune function during extended space travel.

To say that research in the unique environment of space presents engineering challenges is an understatement. Developing a piece of equipment that operates within the bizarre, confined, yet unconstrained environment of spacecraft microgravity is quite a task. For that same piece of equipment to completely satisfy research objectives while posing no health or safety risk on the crew requires technological wizardry. It is largely this challenge that dictates the substantial lead time to develop and assemble a payload, particularly for a spacelab mission in which crew interaction with living subjects is paramount to the success of the investigation.

In spite of this formidable task, Ames has recently developed its most complex spacelab mission in the shortest amount of time. FY97 has seen the culmination of an intense effort to complete substantial modifications to existing facilities, as well as to finish development of unique hardware to meet the requirements of the Neurolab mission. This suite of facilities, combined with novel investigations into numerous neurological phenomena (the study of learned versus adaptive behavior in newborn rats, and the mechanisms associated with memory retention and its role in human aging), will enable this international mission to consummate the 1990–2000 research era designated the "Decade of the Brain."

As part of the HEDS goals to achieve routine space travel and to explore the solar system, Ames continued its pursuit of life-support methodologies. New materials and techniques were examined that hold significant promise in reducing the potential hazards associated with re-release of contaminants during atmosphere regeneration due to on-orbit humidity swings. Investigating a solution to this problem has led to a new method for sampling atmospheric gases that should enable greater data collection from planetary probes.

Toward the vital goal of enriching life on Earth, technologies and procedures developed for space exploration found new applications in both the public and private sectors. The Autogenic-Feedback Training Exercise system and methodology were used by the U.S. Army to evaluate crew performance in a physiologically stressful environment. And, from the singular application to breast cancer imaging to the collaborative linking of clinics to form a virtual hospital, the state-of-the-art virtual environment technologies for three-dimensional interaction continued to expand their strong beneficiary base.

Each of these contributions is key to ensuring a successful space station era that will hopefully lead to one of planetary outposts, then on to permanent planetary inhabitation beyond the confines of our Earth. These individual, unique contributions build on previous findings, eventually leading to giant leaps in understanding. Such are the tools of exploration.

Inducing Presyncope in Men: A Comparison of Two Stimuli

Patricia S. Cowings, William B. Toscano, Bruce Taylor

NASA has identified cardiovascular deconditioning as a serious biomedical problem associated with long-duration exposure to microgravity in space. High priority has been given to the development of countermeasures for this disorder and the resulting orthostatic intolerance experienced by crewmembers upon their return to the unit gravity norm of Earth. Microgravity leads to cardiovascular deconditioning in humans, which is manifested by postflight reduction of orthostatic tolerance and upright exercise capacity. Recent studies tested the effects on orthostasis produced by combining 60 degree head-up tilt (HUT) with lower body negative pressure (LBNP) (see first figure). The procedure for this test consisted of HUT for 20 minutes, then added −20 millimeters mercury (mmHg) negative pressure for 10 minutes, and progressed to −40 mmHg for 10 minutes. The results showed that this combined stimulus test produced presyncope symptoms in 84% of the test subjects (N = 40).

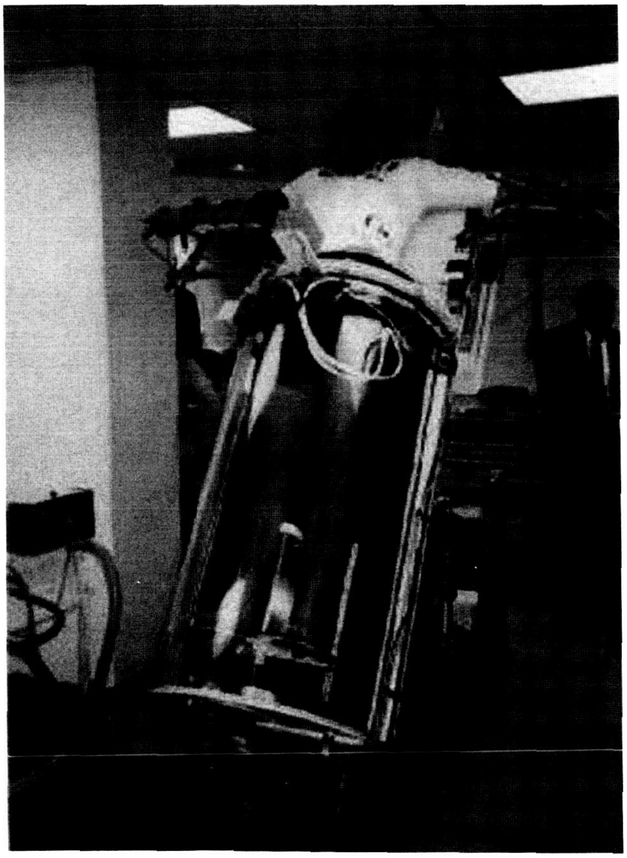

Fig. 1. Subject during 60° HUT and LBNP.

The primary purpose of the present study was to directly compare two tests of orthostatic tolerance in normal adult men. The first was a LBNP test, and the second was a combined test of HUT and LBNP. In order to test countermeasures for postflight orthostatic intolerance, the investigators must understand the nature of physiological responses to a gravitational stress. They believe that each individual will produce a unique physiological response pattern that will reliably describe his/her own symptom levels. The investigators wanted to determine which of these types of tolerance test were best suited for subsequently evaluating treatments or countermeasures that will be used to help future astronauts adapt more readily to microgravity, as well as to facilitate readaptation to Earth.

The specific hypotheses were: (1) The HUT + LBNP will induce presyncopal symptoms at lower levels of negative pressure than the supine LBNP test will, and (2) physiological measures will show distinct changes when test conditions change—that is, at the initiation of each step in the LBNP, at the initiation of HUT + LBNP, and at the point when presyncopal symptoms occurred (termination of the test). These data could be used to objectively characterize symptom levels experienced by individuals and individual differences in tolerance to these tests.

Results on a one-tailed t-test showed that subjects could tolerate the supine LBNP significantly longer than the combined HUT + LBNP ($p < 0.0004$). All physiological data indicated that the combined HUT + LBNP stimulus produced higher stress levels throughout the test than were observed for the supine LBNP. The second figure shows the heart rate data of subjects during both tests under conditions of supine

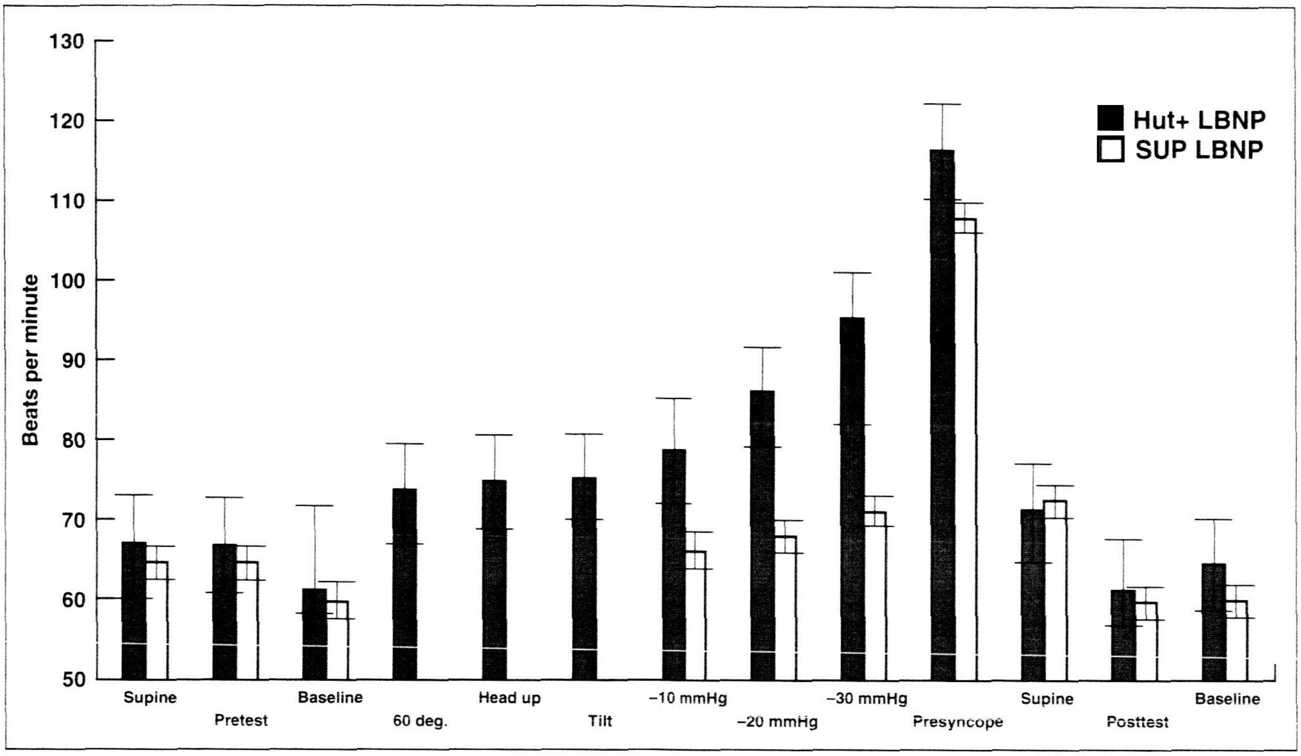

Fig. 2. Heart during supine LBNP and 60° HUT (N = 8).

baseline, minute 10 through –30 mmHg, presyncope, and during supine posttest baseline. Each bar represents a 3-minute mean.

Both hypotheses were successfully met. The HUT + LBNP can be used to reliably induce presyncope in men. However, the physiological data suggest that this device provides too strong a stimulus for testing countermeasures when used with normotensive subjects.

Point of Contact: P. Cowings
(650) 604-5724
pcowings@mail.arc.nasa.gov

Ultrasonic Measurement of Intracranial Pressure Waveforms

Toshiaki Ueno, Richard E. Ballard, Lawrence M. Shuer, William T. Yost,
John H. Cantrell, Alan R. Hargens

Intracranial pressure (ICP) dynamics are important for understanding adjustments to altered gravity. ICP may increase during microgravity due to a fluid shift to the head. As widely observed in clinical settings, elevated ICP causes headache, nausea, and projectile vomiting, which are similar to symptoms of the space adaptation syndrome. At levels over 20 millimeters mercury, ICP may compromise cerebral circulation. However, there are no experimental results to support the hypothesis that ICP is actually altered during microgravity exposure, primarily because of the invasiveness of currently available techniques.

Ames has developed and refined an ultrasonic device that measures changes in intracranial distance noninvasively using a patented pulse phase locked loop (PPLL) technique. Although the skull is assumed to be rigid, many investigators report that the skull moves on the order of micrometers in association with ICP pulsation resulting from variations in arterial pressure. The new ultrasonic device records ICP waveforms noninvasively from skull movements, enabling an evaluation of ICP dynamics by analyses of pulsatile components of ICP waveforms. Amplitudes of pulsatile components of ICP yield information on intracranial compliance, representing the magnitude of ICP change with a change in volume of any intracranial component (brain, blood, or cerebrospinal fluid). Clinically, it is important to monitor intracranial compliance because it represents the volume-buffering capacity of the intracranial tissues and fluid. In addition, because the intracranial volume-pressure curve is generally exponential, an inverse relationship exists between intracranial compliance and pressure. Thus, changes in mean ICP level can also be estimated from pulsatile components of ICP waveforms.

As previously reported, measurements by this ultrasonic device correlate well ($R^2 = 0.80$) with invasively measured ICP in cadavera. In this report, new data are obtained from patients under two different conditions. In the first measurement, waveforms of intracranial distance were collected in a patient who was undergoing a craniotomy. An ultrasonic transducer was placed directly on the surface of the patient's skull after a skin incision was made (the skull was intact at the time of measurement). The first figure shows that pulsatile changes in cranial distance were associated with a cardiac cycle. In the other measurement, changes were compared in cranial distance with invasively measured ICP in a head trauma patient. There was good correlation between the two measurements as shown in the second figure. Although there is still a possibility that cutaneous pulsation affects the measurement when a transducer is placed onto the skin, these results indicate that the technique is sensitive enough to measure pulsatile components of ICP waveforms noninvasively from skull movements in humans.

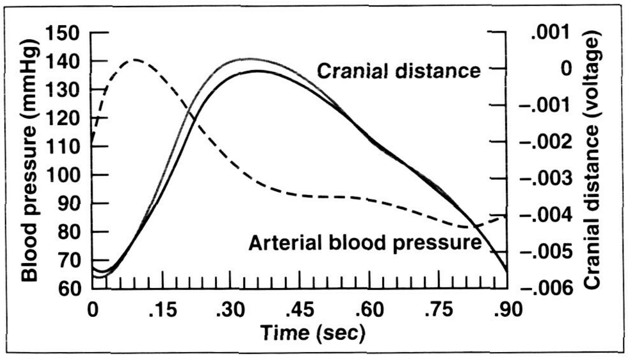

Fig. 1. Waveforms of the cranial distance and arterial blood pressure measured at the brachial artery are shown as solid lines and a dashed line, respectively. Waveforms of the intracranial distance were collected during two separate periods to demonstrate measurement reproducibility. Cranial distance is expressed as output voltages from the PPLL circuit.

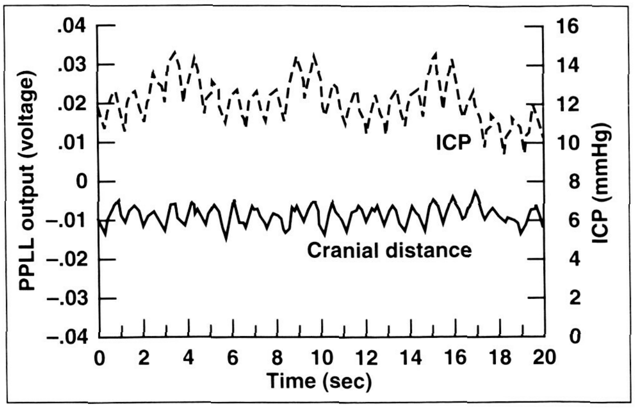

Fig. 2. Waveforms of the cranial distance and invasively measured ICP are shown as a solid line and a dashed line, respectively. Due to a low-frequency cut filter in the PPLL circuit, pulsatile components of respiratory origin are not detected in the cranial distance data.

Point of Contact: T. Ueno/A. Hargens
(650) 604-5747/5746
tueno@mail.arc.nasa.gov
ahargens@mail.arc.nasa.gov

Evolutionary Adaptations of Intracranial Pressure to Gravity

Masayuki Matsuyama, Toshiaki Ueno, Christopher Yang, Shi-Tong T. Hsieh, Harvey B. Lillywhite, Alan R. Hargens

The microgravity environment of spaceflight removes hydrostatic pressure gradients within the human body that are associated with upright posture on Earth. Exposure to microgravity causes a blood shift from legs toward the head, which probably elevates carotid arterial pressure and jugular venous pressure. These factors may elevate intracranial pressure (ICP), cause headache, nausea, and vomiting, and reduce crew performance in orbit. When astronauts return to Earth, about half are unable to stand upright, which may be caused by a combination of blood volume loss, leg muscle loss, and altered baroreflex control of blood pressure and flow to the head. It is important to investigate gravitational effects on ICP from a fundamental biological standpoint.

Snakes provide sensitive animal models for studying cardiovascular adaptation because of their long body form and diversification of behavioral ecology. They also provide sensitive models for investigating ICP regulation with altered posture. In general, arboreal snakes are tolerant against gravitational stress, whereas aquatic snakes have less ability to resist gravitational stress. Presently there is no knowledge of how species from differing gravitational habitats deal with postural effects in terms of their ICP. Therefore, the purpose of this study was to evaluate the gravitational adaptation of ICP in snakes.

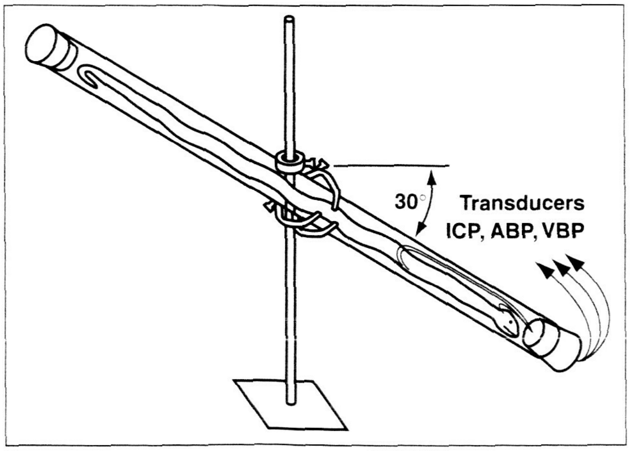

Fig. 1. Drawing of a head-down tilted snake inside the tube. ICP = intracranial pressure, ABP = arterial blood pressure, VBP = venous blood pressure.

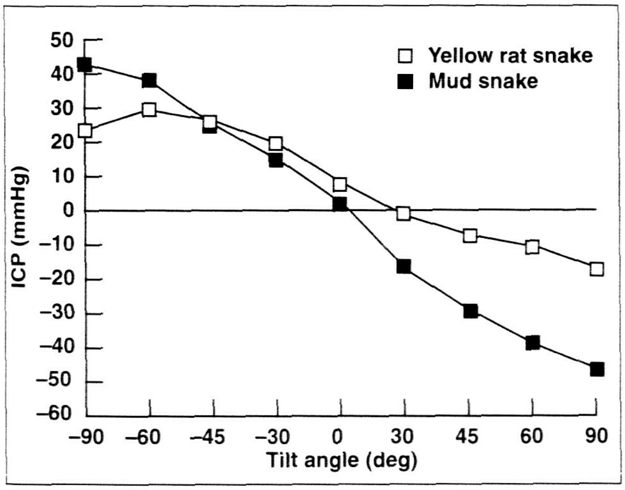

Fig. 2. In the mud snake (aquatic species), ICP increased to 42 millimeters mercury (mmHg) during head-down tilt, whereas in the yellow rat snake (semi-arboreal species), ICP rose to 23 mmHg.

In these studies yellow rat snakes (*Elaphe obsoleta*) represented a semi-arboreal species, and mud snakes (*Farameia abacura*), an aquatic species. Catheters were placed in their right aortic arch, inferior vena cava, and intracranial space in order to measure aortic blood pressure, venous blood pressure, and ICP simultaneously. After surgery, the snakes were confined within an individually-fitted clear acrylic tube and were tilted from 0 degrees (horizontal) to the following angles: 30, 45, 60, and 90 degrees as shown in the first figure. Each angle was held for two minutes. Comparisons of the investigated parameters were made between these two species with contrasting gravity exposure during their respective evolutionary histories.

During head-down tilt in aquatic snakes, ICP increased more rapidly and to higher levels than that in arboreal snakes as shown in the second figure. Compared to arboreal snakes, aquatic snakes have limited ability to counteract gravitational stress by preventing rapid elevations and high levels of ICP in head-down tilt postures. These results help the investigators understand how microgravity affects cerebral circulation and fluid balance in an evolutionary context. Furthermore, snakes may provide an excellent model for contrasting the long-term effects of gravity adaptation (arboreal snakes) versus microgravity adaptation (aquatic snakes) on the cardiovascular system.

Point of Contact: M. Matsuyama/A. Hargens
(650) 604-5747/5746
mmatsuyama@mail.arc.nasa.gov
ahargens@mail.arc.nasa.gov

Calcium Metabolism in Bion 11 Monkeys

Sara B. Arnaud, Richard E. Grindeland, Meena Navidi

The calcium endocrine system regulates the supply of calcium and phosphorus for the mineralization of bone, a process that is known to be depressed during spaceflight. The role of circulating hormones in the localized decrease in bone formation in the weight-bearing skeleton is unresolved and difficult to study in the human because of the effects of exercise itself on calcium metabolism. Additional knowledge would not only improve understanding of the mechanism of adaptation to a weightless environment, but also provide a rationale for the use of the hormones of the calcium endocrine system—parathyroid hormone, calcitonin, and the vitamin D hormone (1,25-D)—in the prevention or restoration of bone loss during spaceflight. Currently, therapeutic trials that include these hormones are under way for the human osteoporoses that can result from systemic factors such as estrogen deficiency.

The Bion mission provided the opportunity to examine the effects of spaceflight on the circulating levels of calcium regulating hormones in rhesus monkeys. Bone tissue obtained by iliac-crest biopsy showed clear effects of weightlessness in flight animals, but not in chair-restrained ground controls.

The calcium endocrine study required validation of the human assays used to measure the peptide hormones, parathyroid hormone, and calcitonin because of structural differences in monkey and human hormones. Validation involved the assay of blood samples obtained before and after a 10-minute calcium infusion, and confirmation of the physiologic response. Assays in the laboratory of Dr. Leonard Deftos from the University of California, San Diego, were successful in showing increases in calcitonin, and decreases in parathyroid hormone after calcium infusion, as illustrated in panels A and B of the first figure.

The third hormone of the calcium endocrine system is a sterol that circulates in the rhesus monkey in concentrations seven to ten times higher than in man. To evaluate changes in the levels during spaceflight, serum 1,25-D was monitored during the development of vitamin D deficiency, induced by removing diet sources of vitamin D and exposure to sunlight for four months. The hormone decreased 30, 48, and 83% from basal levels after 1, 2, and 4 months, respectively.

The most striking changes during the 17-day spaceflight were observed in the concentration of vitamin D hormone, which decreased from 75% to 68% in the serum of flight monkeys, and from 27% to 73% (average 54%) in five ground controls, as illustrated in the second figure. At the whole body level, this hormone functions to facilitate calcium transport in the intestine, kidney, and bone, and to differentiate bone cells. Theoretically, a decrease in the level of circulating hormone would not only reduce intestinal calcium and phosphorus absorption, but also indirectly reduce bone resorption. This might be considered an appropriate physiologic response for an unloaded, inactive skeleton, a view that is supported by results from a human bed-rest study in which isokinetic exercise which loaded bone prevented both a decrease in serum 1,25-D, and an increase in urinary calcium excretion. The spaceflight response was not greater than the response on Earth, an indication that the endocrine regulation of

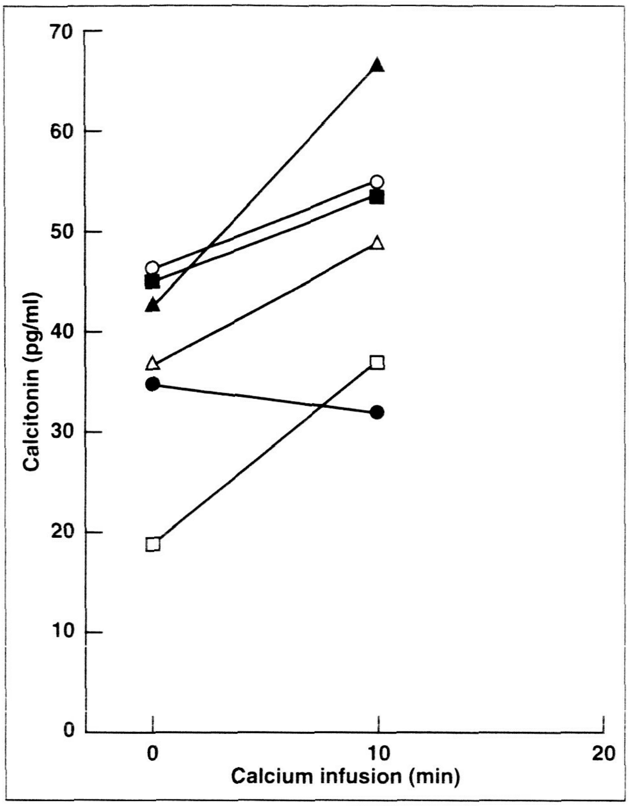

Fig. 1. Panel A: The effect of a 10-minute infusion of calcium on the concentration of serum calcitonin in six monkeys. The infusion increased serum ionized calcium from 1.25 millimoles per liter to 1.44 millimoles per liter.

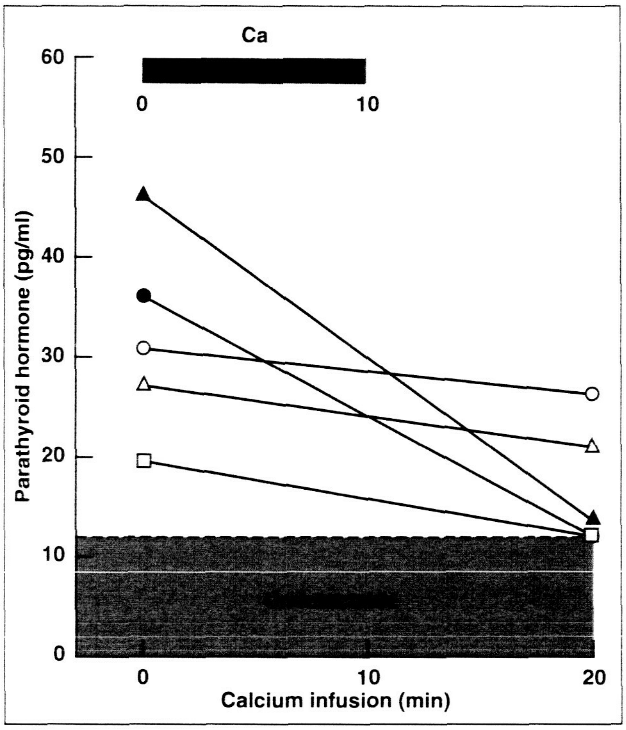

Fig. 1. Panel B: The response in serum parathyroid hormone 10 minutes after the end of the same infusion of calcium in five monkeys as in panel A. In three, circulating levels were depressed to values of 12.1 picograms per milliliter, or the limit of detection of the assay.

calcium metabolism at the whole body level in these spaceflight animals was not impaired. The components of the calcium endocrine system associated with the localized findings in bone tissue were not identified.

Point of Contact: S. Arnaud
(650) 604-6561
sarnaud@mail.arc.nasa.gov

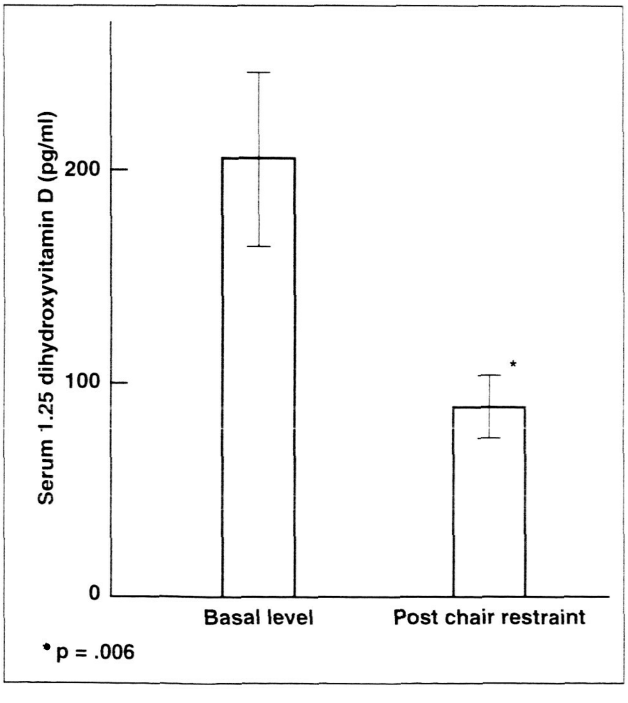

Fig. 2. The effect of chair restraint on the circulating concentration of the vitamin D hormone (1,25-dihydroxyvitamin D).

Human Immunology and Osmolality: An Hypothesis

John E. Greenleaf, Meghan A. McKenzie, Robin Looft-Wilson, Paul R. Barnes

Maintenance of efficient body immune function is essential for successful long-duration spaceflight. Physical exercise training is employed on extended flights to counteract some aspects of weightlessness deconditioning. Exercise also influences the immune system: performance of moderate exercise increases many immune parameters in the blood, while heavy exercise depresses immune function.

However, the mechanism of these exercise-induced immune responses, particularly those involving the white blood cells (WBC, leucocytes) and platelets (Plat, thrombocytes), is not clear. Prior hypotheses have implicated plasma catecholamines (epinephrine, norepinephrine), cardiac output (blood flow), increased rectal temperature (Tre), and changes in plasma volume (PV), with no agreement on the major factors or their possible integrative effect on immune function.

Experimental data from Ames Research Center have indicated that plasma osmotic concentration [Osm] is highly correlated with responses of the WBC and Plat during exercise, but not at rest, as shown in part (a) of the figure. During exercise, the high, significant correlation coefficients (r) between [Osm]

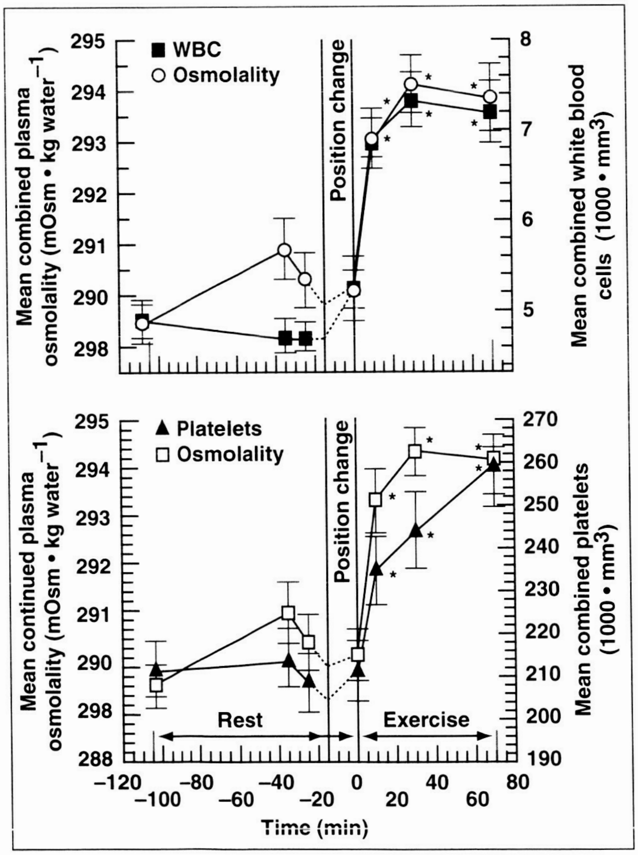

Fig. 1(a). Upper panel: Mean (standard error) plasma osmolality and white blood cells at rest and during exercise in six untrained men (22–39 years). Lower panel: Mean (standard error) plasma osmolality and platelets at rest and during exercise.

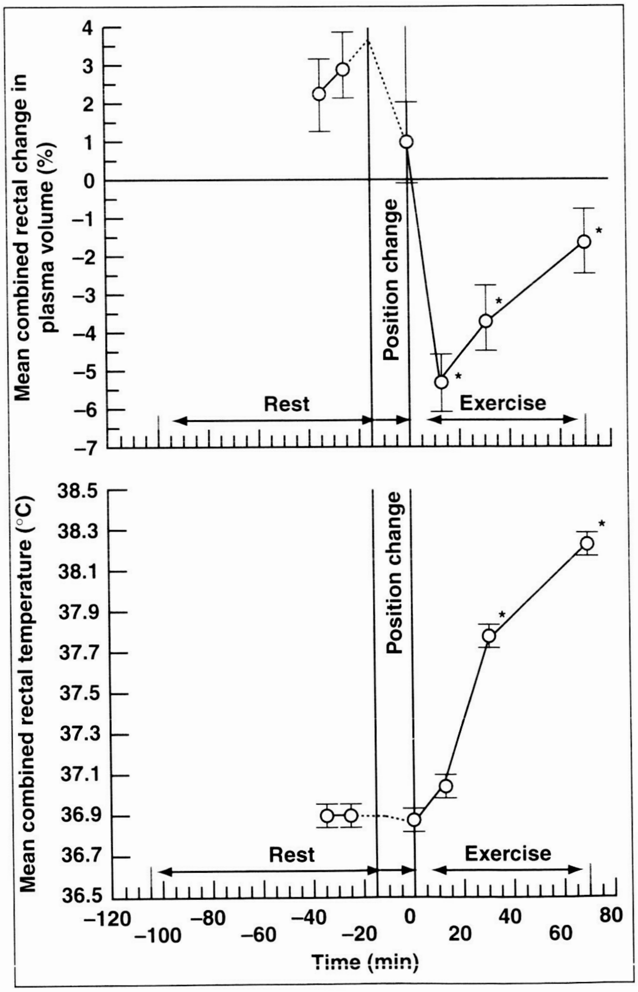

Fig. 1(b). Mean (standard error) percent change in plasma volume (upper panel), and rectal temperature (lower panel), at rest and during exercise in six men.

and WBC ($r = 0.95$, $p < 0.001$), and [Osm] and Plat ($r = 0.94$, $p < 0.01$), indicate that the leucocytes, thrombocytes, and hyperosmolality occur primarily within the first 10 minutes of moderate (71% of the maximal intensity) exercise. Neither the decrease in PV nor the increase in Tre during exercise, as shown in part (b) of the figure, were involved because all respective correlation coefficients between percent change in PV and Tre and WBC, Plat, and [Osm] were less than 0.2 (nonsignificant).

Thus, these high correlations, between [Osm] and WBC or Plat, suggest the hypothesis that changes in plasma osmolality may contribute to the mechanism of leucocytosis and thrombocytosis induced by exercise.

Point of Contact: J. Greenleaf
(650) 604-6604
jgreenleaf@mail.arc.nasa.gov

Neurolab Technologies Enable Space Life Sciences Neuroscience Research

James P. Connolly, Paul D. Savage

The Shuttle Spacelab mission, Neurolab, was the primary focus for the flight support elements of the Life Sciences Division, the Payload and Facilities Engineering Branch, and the Science Payloads Operations Branch. First conceived in 1993, and launched just five years later, Neurolab evolved into the most complex Spacelab mission ever developed by Ames Research Center (ARC). Though the major hardware units had flown previously (for example, the general purpose work station (GPWS), the research animal holding facilities (RAHFs), and the animal enclosure modules (AEMs)), critical modifications were carried out to ensure that the hardware would meet the Neurolab science objectives and improve overall technical capabilities.

The monitoring and process control subsystem (MPCS) was a new element incorporated into the RAHFs. The MPCS is a microprocessor-based process and control system housed in a standard interface rack (SIR) drawer. It replaces both the RAHF upper and lower electronic boxes used on previous flights for environmental system control, RAHF system monitoring, and data retrieval. Consolidation of these functions into a single unit was intended to improve maintainability, increase thermal and power efficiency, add system diagnostic capabilities, improve remote ground monitoring and control, and reduce the overall required rack space. Additionally, incorporation of the MPCS in the SIR drawer ensured its compatibility with future International Space Station experimental systems. Because the Neurolab science objectives required the housing of neonate rats, some RAHF cages were modified to accommodate nursing dams and neonates. A middeck flight with rat neonates on STS-72 in January 1996 was a research "first" by the Ames Life Sciences Division that helped prepare for the sophisticated experiments on Neurolab.

The AEMs, which were previously flown on 20 Shuttle missions and designed for hands-off protocols, were modified for in-flight access to animals. Access and transfer schemes proposed for use on Neurolab were first tested in the parabolic arc environment aboard a KC-135. The AEM lid and transfer unit modifications greatly expanded the science that is possible using this middeck rodent facility (see the first figure). The improved AEM may

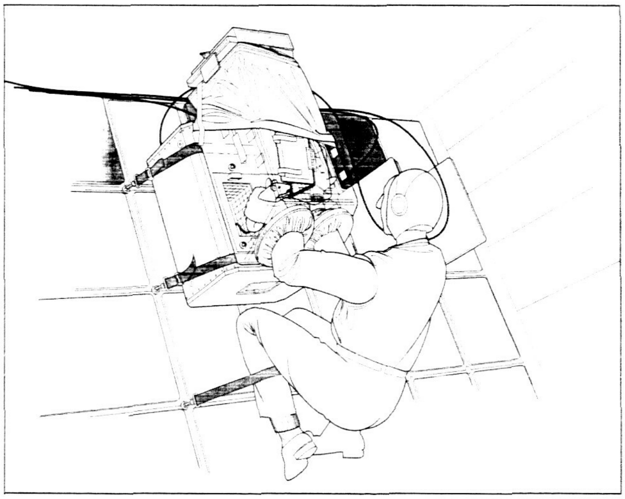

Fig. 1. Crew person at animal enclosure module with modified lid and transfer unit allowing middeck animal access.

well be the mainstay of the life sciences microgravity experiments in the shuttle middeck while the Space Station is being assembled.

Unique flight hardware, designed to support specific experiments on the Neurolab Mission, includes the Neurolab biotelemetry system (NBS) and a sophisticated system to measure and record neural coding signals of place and direction in the microgravity environment. The NBS, based on commercially available hardware, was developed to monitor heart rate, deep body temperature, and activity for 12 rats housed in one of the payload's two RAHF systems (see second figure). The hardware that measures and records neural codings monitored the performance of freely behaving rats on specialized experiment apparatuses during testing sessions inside the GPWS.

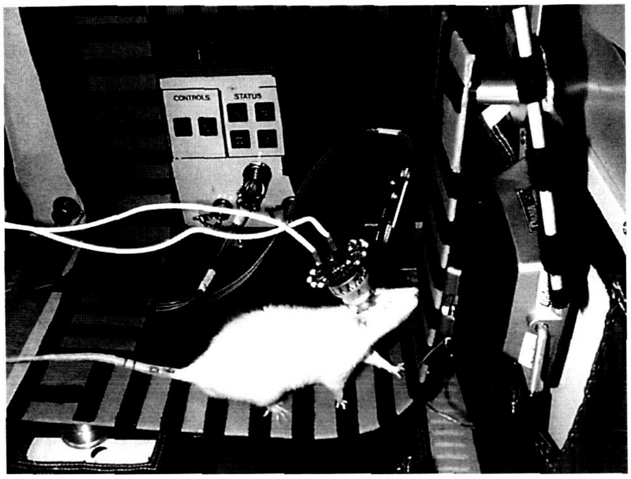

Fig. 2. Ensemble neural coding of place and direction in Zero-G experimental animal, with associated test hardware.

ARC's engineering, science, and operations personnel have successfully managed hardware development, functional testing, biocompatibility testing, and delivery of a highly complex array of flight hardware to support this last Spacelab Mission in commemoration of the "Decade of the Brain."

Point of Contact: J. Connolly/P. Savage
(650) 604-6483/5940
jpconnolly@mail.arc.nasa.gov
psavage@mail.arc.nasa.gov

Advanced Life Support Research and Technology Development Activities

Mark Kliss

Ames Research Center carries out research and development of new technologies that will enable the human exploration and development of space. These activities will reduce life-cycle costs, improve operational performance, promote self-sufficiency, and minimize the expenditure of resources in future space exploration, such as a human mission to Mars. Advanced Life Support technologies for a human Mars mission are depicted in the figure. There are also significant opportunities for Earth application of the developed technologies. The following are some of the key examples of these activities.

Power consumption is a key problem facing carbon dioxide (CO_2) removal technologies for long-duration spaceflight. There are problems with efficiency in using the current sorbent-based techniques to perform the carbon dioxide/water (CO_2/H_2O) split. This research seeks to develop high-efficiency CO_2 removal technologies for closed-loop regenerative systems by improving the CO_2/H_2O separation. Data on the influence of water on the adsorption of CO_2 and trace contaminants show significant reduction in the capacity of sorbents and the possibility of elution back into the cabin environment. In FY97, research on new materials and operating procedures has made significant contributions toward mitigating this safety problem. New knowledge on adsorption processes has also led to a novel passive/low-power method of extracting and pressurizing a nitrogen-argon mixture from the Martian atmosphere. This mixture would be suitable as a carrier/sweep gas for instruments used on planetary probes.

In situ resource utilization (ISRU) is an enabling technology for both robotic and human missions. In robotic missions, the in situ production of consumables from local resources (carrier gas,

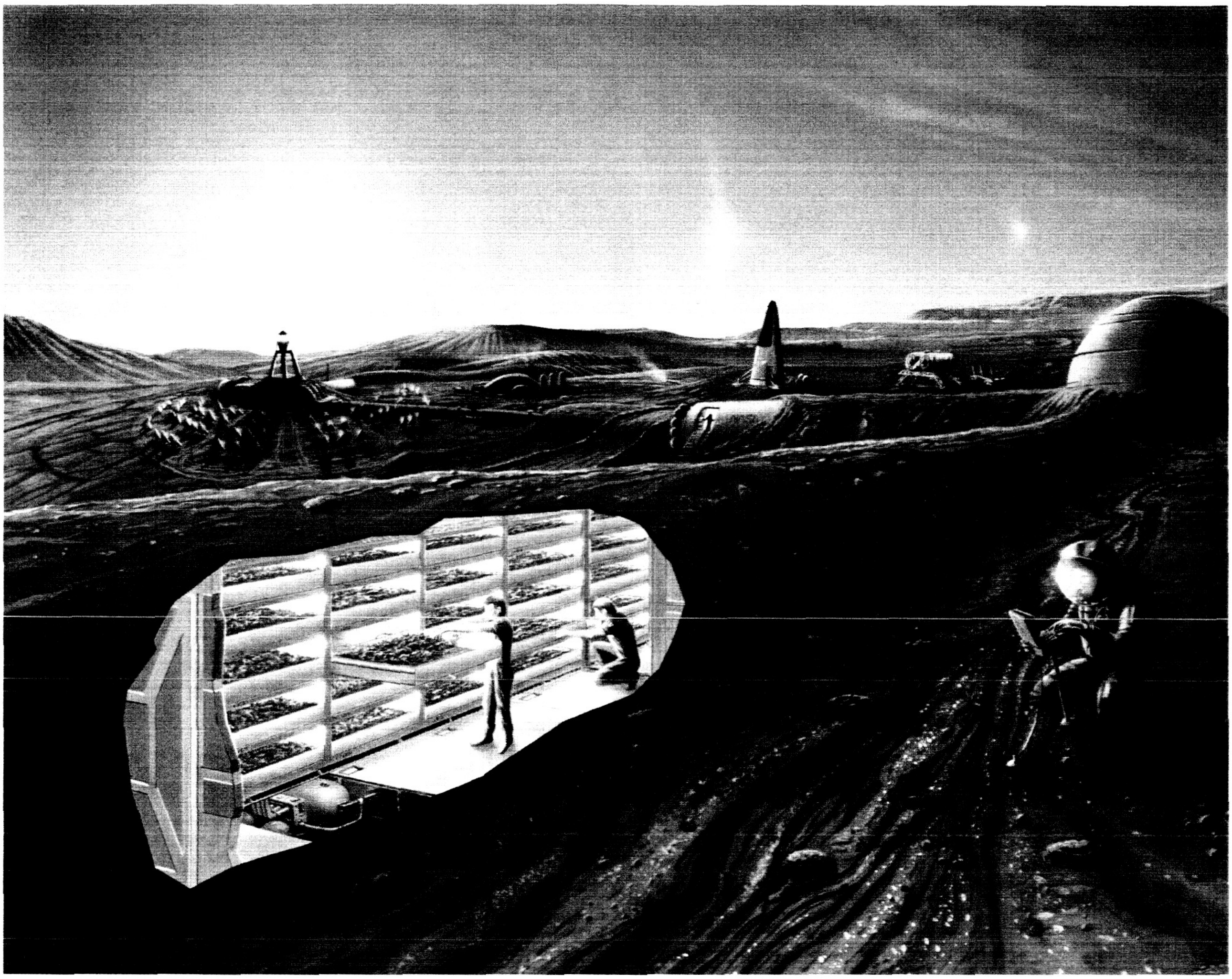

Fig. 1. Artist's rendition of Advanced Life Support technologies for a human Mars mission.

calibration gas, propellants) can extend the range and duration of science payloads. In robotic sample-return missions, fuel and oxygen for the return voyage can be produced locally; such an approach is being considered for the Mars sample-return mission. For human missions, the production of consumables for life support and propulsion from planetary resources significantly reduces cost and risks.

At Ames the core processes related to "mining the atmosphere of Mars" are being researched. Efforts include (1) energy-efficient ways of compressing the predominantly CO_2 atmosphere of Mars for chemical processing needs and utility gas, (2) separation of nitrogen/argon buffer gas for instruments and life support, (3) production of oxygen from CO_2 electrolysis, (4) evaluation of water collection methods, and (5) development of microsensors for ISRU applications. FY97 research has led to the development of a test-bed which has successfully demonstrated Mars atmospheric compression, oxygen generation, and microsensing of oxygen (O_2) and CO_2.

Human and food wastes are not currently recycled, and are key elements in the design of advanced life-support systems that approach self-sufficiency. Both supercritical water oxidation (SCWO) and incineration processors have been developed and are currently under evaluation. Key issues that are being addressed include waste preparation and process feed and product stream clean-up, with a special focus on the acid gases and other trace contaminants produced. A prototype incinerator was delivered to Johnson Space Center as part of an extended closed 90-day manned chamber test. All product gases met Spacecraft Maximum Allowable Contaminant standards, and the CO_2 product gas was used to supply CO_2 to a wheat crop included in the 90-day closed test. The U.S. Navy has expressed interest in SCWO technology because of its potential for reducing hazardous liquids to CO_2 and H_2O while ships are at sea.

Point of Contact: M. Kliss
(650) 604-6246
mkliss@mail.arc.nasa.gov

U.S. Army Application for NASA Technology

Patricia S. Cowings, William B. Toscano, Charles DeRoshia

The purpose of this project was to use NASA technology to assist the U.S. Army in the assessment of motion sickness incidences in the command and control vehicle (C2V). The NASA technology utilized is U.S. Patent No. 5,639,436, Autogenic-Feedback Training Exercise system and method. During this study we determined the frequency and severity of motion sickness in personnel during a field exercise in the C2V. This vehicle contains four workstations where military personnel are expected to perform command decisions in the field during combat conditions. Eight active duty military men (U.S. Army) at the Yuma Proving Grounds in Arizona participated in this study. On the first day, all subjects were given baseline performance tests while their physiological responses were monitored. On the second day of their participation, subjects rode in the C2V while their physiological responses and performance measures were recorded. Self-reports of motion sickness were also recorded, with only one subject experiencing two incidences of emesis. Seven out of the eight subjects reported other motion sickness symptoms; most predominant was the report of drowsiness, which occurred a total of 19 times. The table summarizes symptom reports, hours of sleep obtained on the previous night, seat position in the C2V, and previous experience in this or other tracked vehicles.

Changes in physiological responses were observed relative to motion sickness symptoms reported and the different environmental conditions (i.e., level, hills, and gravel) during the field exercise. The subject who reported the most symptoms (subject 3), and the one who reported no symptoms at all (subject 6), both rode in the C2V on the same day. The first figure shows the physiological data of both individuals which are plotted as 1-minute averages across time. C2V courses are represented as

Table 1. Motion sickness symptoms during the command and control vehicle (C2V) field exercise

I.D.	VMT	TMP	DIZ	HAC	DRZ	SWT	PAL	SAL	NSA	ED	EA	Previous experience	Seat position	Hours sleep
# 1					3							Yes	4	6.5
# 2					2							No	1	4.5
# 3	2	4	3		4	3	1	1	3			No	1	4.0
# 4					1							Yes	4	6.5
# 5			3	1	1				1			No	1	5.0
# 6												Yes	4	4.5
# 7		1		1	4	1		1	1	2	2	No	1	7.0
# 8		2	2		4	1						Yes	4	6.0
Total	2	7	8	2	19	5	1	2	5	2	2			

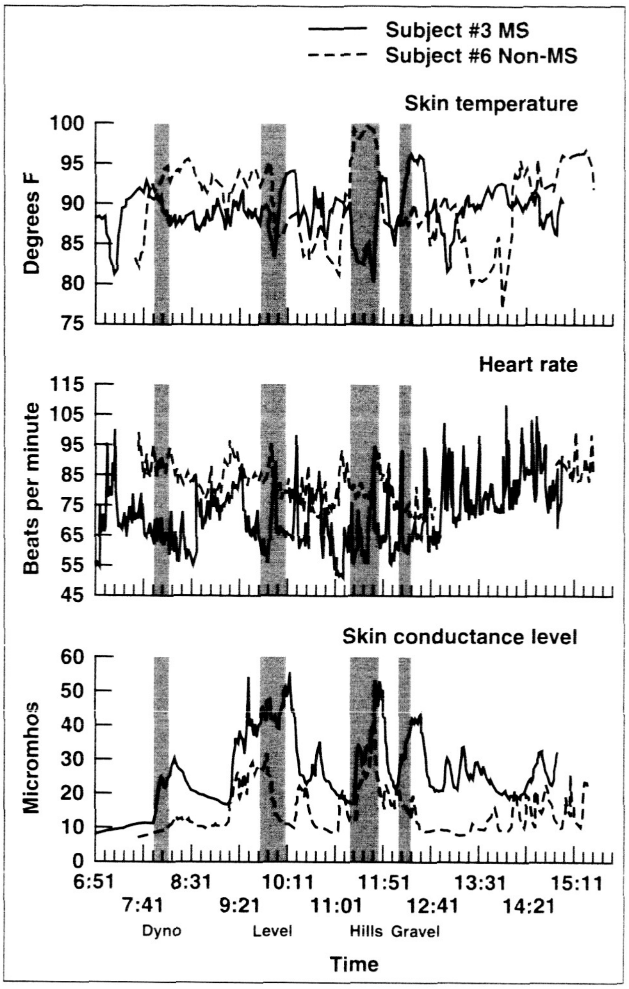

Fig. 1. Comparison of motion sickness and non–motion sickness subjects during the C2V exercise.

bars. The bottom graph shows the skin conductance level of both subjects. This response reflects minute changes in the electrolytic properties of the skin (i.e., sweat), which are generally too small to be perceived as changes in "wetness," and is a very sensitive index of physiological and emotional arousal. Note that both subjects began the day with relatively low levels in skin conductance, and both responded to changes in terrain. The response increases (i.e., arousal) that began several minutes before actually reaching the level course probably reflect the point where they began operating video game terminals and/or the response to movement of the vehicle as they drove to the next course. Subject 3, however, made much larger increases in this response, which were of longer duration than those of subject 6, and which never returned to the prestimulus levels recorded at the start of the day (i.e., less than 10 micromhos).

Performance data show an overall decrement during the C2V exercise. These preliminary results suggest that malaise and severe drowsiness can potentially impact the operational efficiency of the C2V crew. However, a number of variables (e.g., individual's sleep quantity prior to the mission, prior experience in the C2V, etc.) were not controlled for in this study and may have influenced the results. Most notably was the fact that subjects with previous experience in the C2V all occupied seat 4, which was anecdotally reported to be the least provocative position. Subjects were assigned on an "as available" basis, and the investigators had no prior knowledge of the subjects' experience in tracked vehicles. Composite performance latency shows the expected exponential learning pattern over training trials 1 through 8 (see second figure). On the C2V day, task batteries were administered only when the vehicle was not moving. The vehicle doors were opened and Yuma Proving Ground personnel provided lap-top computers for the subjects' use.

It was concluded that a second study is required to further evaluate the impact of seat position, orientation, and C2V experience on motion sickness susceptibility. Further, it was concluded that it is unlikely that pharmacological intervention or crew preselection/screening will mitigate the problem.

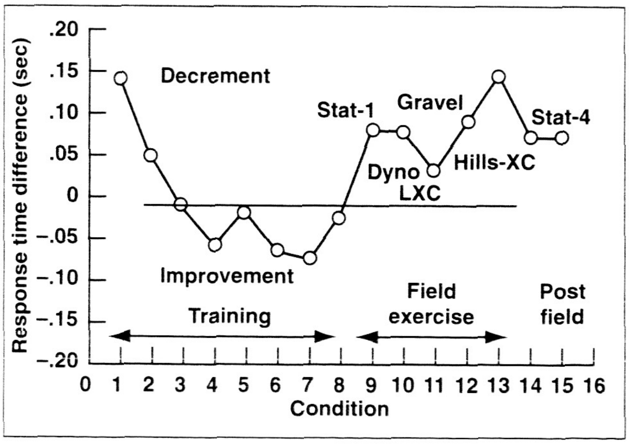

Fig. 2. Mean response latency (5 tests): residuals after subtraction of learning curve.

Investigation of behavioral methods for improving crew alertness, motivation, and performance and reducing malaise is recommended. The value of utilizing three separate converging indicators—physiological measures, performance measures, and standardized symptom reports—has been demonstrated as an effective means of assessing environmental impacts on the safety and well-being of human passengers or crew on land, sea, air, and space vehicles.

Point of Contact: P. Cowings
(650) 604-5724
pcowings@mail.arc.nasa.gov

Virtual Environment Surgery and the Virtual Hospital

Muriel D. Ross, Jeffrey D. Smith

The Biocomputation Center is dedicated to computer-based three-dimensional (3-D) visualization, mathematically based modeling, and 3-D simulation. The emphasis is on teams of broadly based, interdisciplinary investigators, and on a union between computational, theoretical, and experimental research. Virtual environment surgery (VES) technologies of the Biocomputation Center have found several new applications in FY97, including breast cancer imaging research and 3-D ultrasound and computed tomography (CT) visualization tools. In addition, the first steps have been taken toward creating a virtual hospital, linking several clinical institutions using the VES technology and the Next Generation Internet/NASA Research and Education Network (NGI/NREN).

The Biocomputation Center maintains state-of-the-art virtual environment technologies for 3-D viewing and interaction. The Fakespace Immersive Workbench (Fakespace, Mountain View, California) acts as a viewing interface into a virtual environment. The workbench is large and permits several individuals to see the visualization projected above the tabletop in 3-D. Special Crystal Eyes glasses (Stereographics, San Ramon, California) are required for 3-D viewing. Users have full control of viewing angle, position, and perspective. The Fakespace Pinch Glove, in conjunction with a Polhemus radio-tracking device (Framingham, Massachusetts), allows the user to interact with the virtual environment by grabbing and moving objects. The Immersive Workbench, associated hardware, and the VES software are driven by a Silicon Graphics Onyx RE2 workstation.

The Ames Biocomputation Center has a long history of success in processing, manipulation, and visualization of large 3-D biological datasets. In FY97, with the permission of the Stanford Radiology Group, the VES technologies were applied to magnetic resonance imagery (MRI) of breast cancer for visualization, modeling, and virtual environment surgery applications as shown in part (a) of the first figure. Women's health issues are of increasing importance to NASA now that one half of future astronauts will be women. This new research effort improves upon previous methods for breast cancer visualization, and will help to model the motion of the tumor within the breast as a woman's body shifts during diagnosis and surgery. In addition, emerging methodologies resulting from this breast cancer imaging application will apply directly to NASA's interests in other MRI, Ultrasound, and Space applications.

The Biocomputation Center has used its specialized VES software and computing facilities to process 3-D datasets of the heart. A post-operational CT scan of the heart showing a graft was visualized using the same software as shown in part (b) of the figure. In the future, this segmentation and visualization technology will be applied to 3-D ultrasound datasets from the Cleveland Clinic Foundation, Department of Cardiovascular Imaging.

Today, there is a need for a collaborative virtual environment to perform interactive surgical planning, practice, and education activities. The Biocomputation Center has begun the process of creating a virtual hospital to connect Stanford University

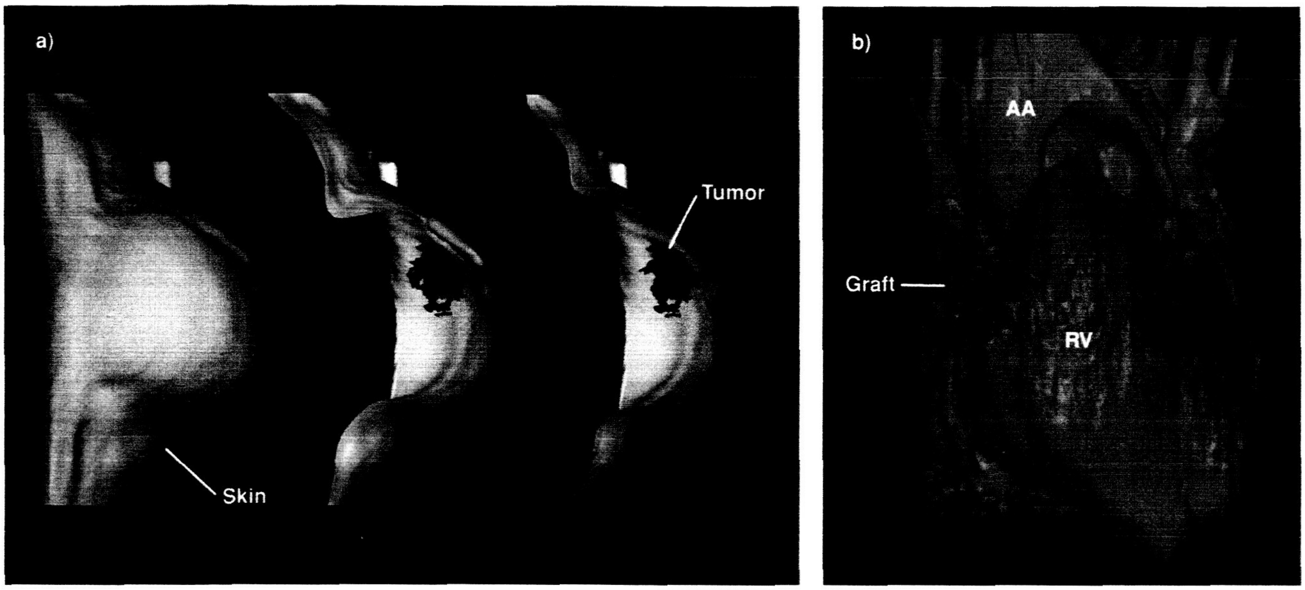

Fig. 1. Research and technology development at the Biocomputation Center in FY97 have found new imaging applications in breast cancer research and cardiology. A three-dimensional cut-away image of the breast (a) made from magnetic resonance imaging data shows a large tumor under the surface of the skin. A three-dimensional heart image (b) made from computed tomography data displays a graft from the aorta (AA) to the muscle of the right ventricle (RV).

Medical School, The Cleveland Clinic Foundation, and the Salinas Valley Memorial Hospital. The VES technologies will be used to process raw data, and to provide an interactive work environment between institutions. Through these interactive sessions, doctors will be able to discuss diagnoses, share preoperative planning strategies and techniques, or even perform "virtual surgeries" as a group, thus linking experts across the globe in an unprecedented way.

The virtual environment technology will be useful to the Human Exploration and Development of Space (HEDS) Enterprise for training astronauts for long-term missions in space. It will provide simulation capability during spaceflight to help astronauts respond appropriately to unanticipated emergencies. Advances in telemedicine and collaborative virtual environment tools developed for the Virtual Hospital will lay the groundwork for interaction between people on Earth and in Space. Today, Ames Research Center and the Biocomputation Center are poised to take a leading role in 3-D imaging technologies for both Earth-bound and space-based applications.

Point of Contact: M. Ross
(650) 604-4804
ross@biocomp.arc.nasa.gov

AeroVironmen
Pathfind
AeroVironmen
Pathfin

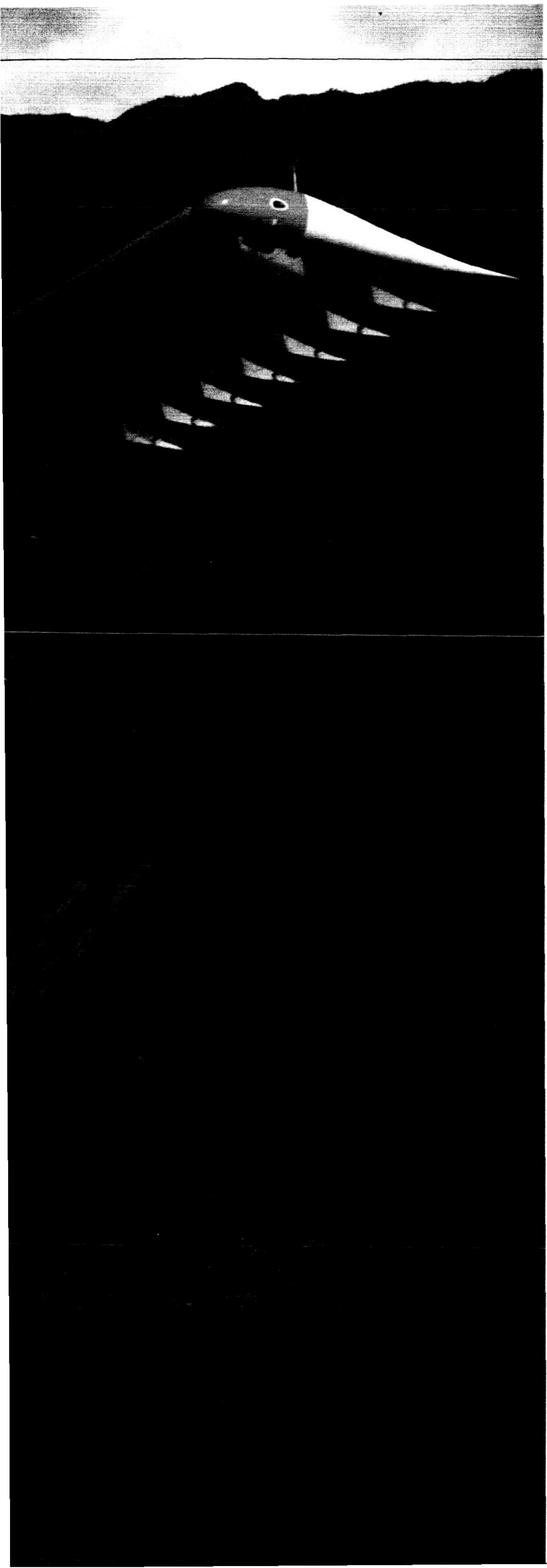

Overview

NASA's Earth Science Enterprise (formerly Mission to Planet Earth) studies the total Earth environment—atmosphere, ice, oceans, land, biota, and their interactions—to understand the effects of natural and human-induced, near-term changes on the global environment and to lay the foundation for long-term environment and climate monitoring and prediction. Ames Research Center supports the Earth Science Enterprise by conducting research and by developing technology with the objective of expanding the knowledge of Earth's atmosphere and ecosystems. This is also one of the goals of the Agency's Astrobiology research and technology efforts, which are led by Ames. A complementary objective is to apply the knowledge thus gained to practical, everyday problems and to transfer the technology and knowledge to users outside NASA. During FY97, numerous research and technology efforts were undertaken, the results of which address the following goals of the Earth Science Enterprise:

- Expand scientific knowledge of Earth's environmental system
- Enable the productive use of Earth Science Enterprise science and technology
- Disseminate information about Earth's systems

Earth Science research is particularly concerned with atmospheric and ecosystem science and with biosphere/atmosphere interactions. Key components of the research include the study of physical and chemical processes of biogeochemical cycling; the dynamics of terrestrial and aquatic ecosystems; the chemical and transport processes that determine atmospheric composition, dynamics, and climate; and the physical processes that determine the behavior of the atmosphere on Earth and on other solar system bodies. Of special interest are the development and application of the new technologies that are required to develop insight into these science topics. Significant contributions were made in three areas: in the analysis of critical gaseous emissions, in the development of models and instruments, and in radiation research.

Research highlights include a focus on important environmental concerns related to stratospheric ozone depletion, to perturbations in the chemical composition of the atmosphere, and to climatic changes resulting from clouds, aerosols, and greenhouse gases. Numerous state-of-the-art instruments were flown successfully, and significant data were collected for stratospheric and tropospheric research. For stratospheric experiments, the following are included: the Meteorological Measurement System (MMS), which measures pressure, temperature, and the wind vector, and a dual-channel tracer instrument for stratospheric dynamics studies (ARGUS). These instruments were flown on the ER-2 aircraft for the Airborne Southern Hemisphere Ozone Experiment and for the Stratospheric Tracers Atmospheric Transport study.

For tropospheric experiments, instruments were flown on several aircraft to measure carbon monoxide, nonmethane hydrocarbons, carbonyls, and reactive nitrogen species. Specifically, fluxes of important biogenic gases from terrestrial ecosystems were quantified, as were the Subsonic Aircraft: Contrail and Cloud Effects Special Study and Tropospheric Aerosol Radiative Forcing.

The enormous growth in aviation has given rise to concerns that emissions from aircraft may be modifying the atmosphere in important ways. Ames led the planning and development of the DC-8 SONEX (Subsonic Assessment Ozone Nitrogen Oxide Experiment) mission, which was conducted during the period September–November 1997 in the vicinity of the North Atlantic flight corridor to study the effect of aircraft emissions on the nitrogen oxide families (NO_x) and ozone.

Technology developments were realized on two fronts: modeling and instruments. Model developmental efforts or simulations based on developed models are presented for the following phenomena: the effect of gravity waves generated by convection or stratospheric circulation; the effects of climate and land-cover interactions in the Amazon rain forest; the solar radiation regime of vegetation canopies; and paleoenvironment studies using pollen data and leaf-area development. Newly developed instruments include a miniaturized, lightweight, tunable, diode-laser spectrometer; an MMS on the NASA DC-8 aircraft to provide science-quality state variables and wind data; an airborne disaster assessment sensor; a digital array scanning interferometer; and a fully automated, 14-channel sunphotometer to fly on remotely piloted aircraft and other platforms. Also, a new program was created (Environmental Research Aircraft and Sensor Technology) to focus critical technology development and flight demonstration for remotely piloted vehicles.

Radiation research focuses on phenomena associated with the interaction of solar radiation with the atmosphere and with solar system bodies. The high-resolution infrared spectroscopy is devoted to basic experimental and theoretical research into the absorption of radiation by gases. The purpose is to determine the molecular spectroscopic parameters needed for the design and interpretation of field measurement programs related to the atmospheric environments of Earth and other planetary and stellar bodies.

Using Earth Science Enterprise data and technology, commercial firms can expect to expand their businesses, and public-sector managers can exercise stewardship of the nation's natural resources. The enabling, productive use of Earth science and technology is exemplified by a number of accomplishments, including the effects of land-use change on the methods and assumptions currently in use to estimate the influence of land cover in Earth's carbon budgets in the boreal forest and in Oregon. Other reported data, analyses, and technologies can be used by researchers seeking answers to key Earth science questions and by educators teaching Earth Sciences.

Remote-Sensing Data in Estimating Inputs to Ecosystem Models

Joseph Coughlan, Jennifer Dungan

To better understand carbon cycling in forest ecosystems, several process-based ecosystem models have been developed. The forest leaf-area index (LAI) and other variables describing plant biomass are necessary to run these models. The only feasible means of estimating these forest variables for spatial extents of tens of meters and larger depend on remote-sensing instruments. In the past, reflectance index measurements based on optical remote-sensing data have been used to estimate LAI. This work involves developing algorithms for combining remote-sensing data in the microwave and optical regions of the electromagnetic spectrum (1) to increase the accuracy of LAI estimates, as well as the estimates of other variables; and (2) to extend the range of validity of LAI estimates beyond that achieved from optical data alone.

The first step was to assemble data from the Boreal Ecosystem-Atmosphere Study campaigns. Airborne synthetic aperture radar and Landsat Thematic Mapper images obtained for the Southern Study Area (SSA) were calibrated to physical units and georectified. Statistical relationships between the image and ground measurements were examined for 15 plots within the SSA along with the general covariance between the optical and radar data. The second step was to determine if the radar data detect and provide additional information or augment the optical measurements. This work is one of the few efforts to combine the diverse technologies of passive and active remote sensing for the purpose of answering ecological questions. Mahta Moghaddam of the Jet Propulsion Laboratory in Pasadena was a co-investigator on this project.

Point of Contact: J. Dungan
(650) 604-3618
jdungan@gaia.arc.nasa.gov

Paleoenvironmental Studies

Hector L. D'Antoni

A revision of a pollen profile was undertaken in order to start astrobiological research in South America. Gruta del Indio del Rincón del Atuel (GIRA) is a rock shelter located at lat. 34° 45′ S and long. 68° 22′ W, east of the Andes. The stratigraphy of GIRA includes fossil traces of archeological, paleontological, and paleoecological events. Previous research in this important site showed three groups of ecological indicators: (1) plants of the Monte ecosystem that depend on the groundwater table (phreatophytes), (2) Monte ecosystem plants that are independent of the groundwater (nonphreatophytes), and (3) plants of the Patagonia ecosystem. These groups of indicators were used to piece together plant succession in this area in a time frame of more than 32,000 years before present (BP). Such history includes a first occupation by the Patagonia ecosystem during the last 20,000 years, corresponding to the last Ice Age, then a Monte occupation from 10,000 years to the present. The latter is subdivided into a phase of phreatophytic dominance that ends about 2500 years BP and a nonphreatophytic dominance that persists through the present. This time, a thorough analysis of its paleoenvironmental content was performed in looking for indicators of declining ecosystems. The first figure shows the results of such analysis.

The paleoenvironmental record was divided into three major zones. Zone I (from 32,000 years to about 10,000 years ago) is characterized by indicators of the Patagonian ecosystem, suggesting climate controlled by the Pacific high pressure cell, with 200 millimeters of annual precipitation (mostly in winter), and a mean annual temperature of 8°C. Zone II (from 10,000 to about 3000 years ago) is characterized by indicators of riparian environments

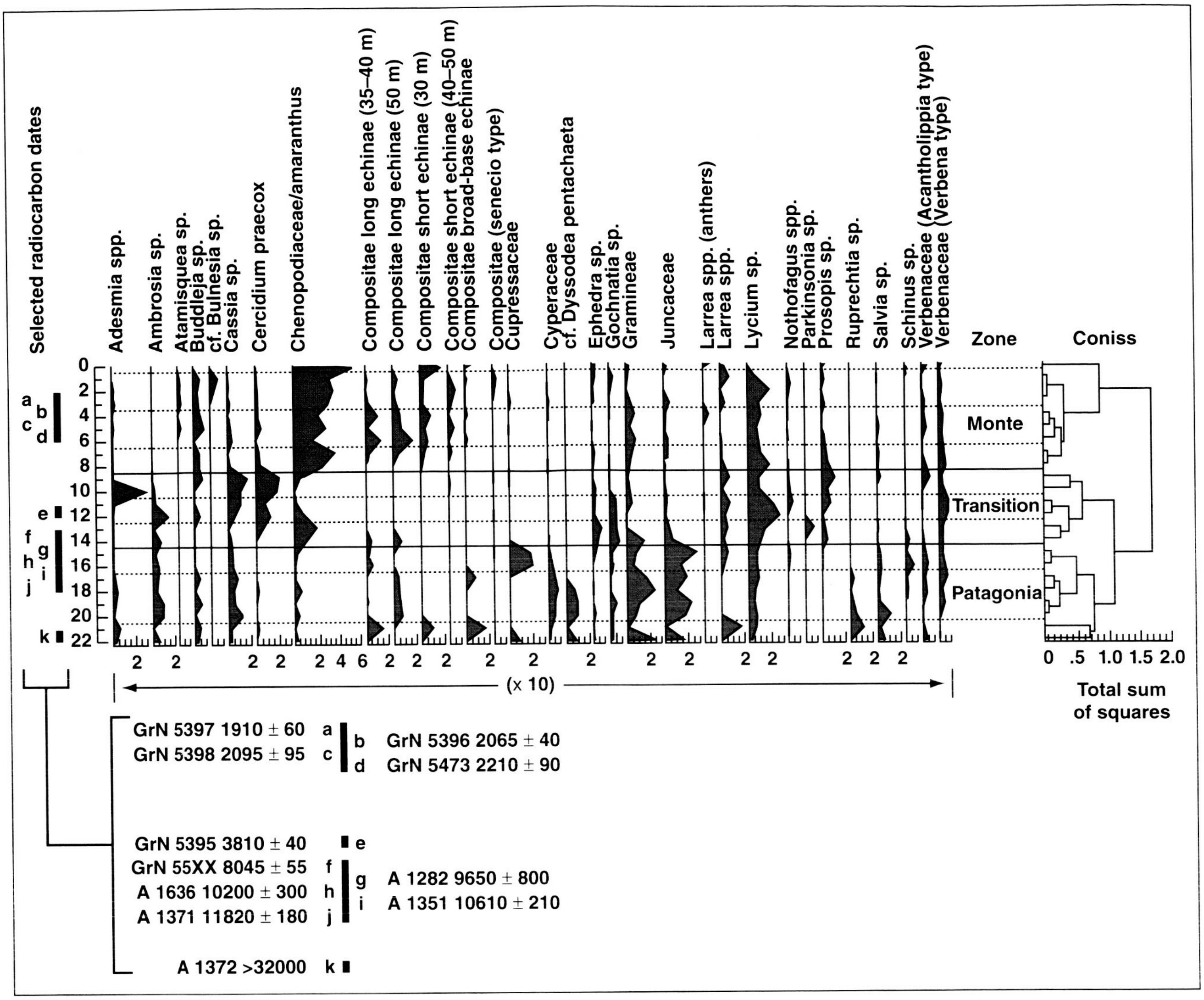

Fig. 1. The Gruta del Indio Profile pollen profile. Depth corresponding to age before present is shown on the y-axis.

in the desert such as *Prosopis julliflora* (algarrobo, mezquite), small trees like *Cercidium praecox* (brea, palo verde), and a high frequency of *Lycium* sp., a woody Solanaceae, and *Cassia* sp., a bush of the Leguminosae. These indicators suggest more precipitation and higher temperature. GIRA is not far from the Atuel River, which originates in the Andes and, at the time of transition from glacial to postglacial time, may have had a much larger flow volume than at the present, thus enlarging the area of riparian environments. Increased precipitation and higher temperatures may be linked to a stronger influence of the Atlantic high pressure cell in this region. Zone III (from 3000 years ago to the present) is characterized by dominance of annuals (Chenopodiaceae plus *Amaranthus* sp. and several types of Compositae). *Lycium* sp. is an important indicator. This zone reflects Monte plant geographic province conditions (similar to those of the Sonoran Desert in the Northern Hemisphere), with 300 millimeters of annual precipitation, most of which occurs in summer, and a mean annual temperature of 14°C. This profile shows that climate change between Pleistocene and Holocene times triggered changes in ecosystems such that, by about 10,000 years ago, the Patagonian ecosystem declined locally, giving place to a relatively fast succession of dominant taxa in Zone II (Transition) leading to Zone III (Monte) with a deep reorganization that preserved some indicators of the previous ecosystem (i.e., *Lycium* sp.), and passed dominance to annual herbs (Chenopodiaceae + *Amaranus*) and several types of Compositae. Some indicator genera are absent in the new ecosystem: *Adesmia, Ambrosia,* Cupressacea, *Cyperaceae, Dyssodea, Parkinsonia, Ruprechtia,* and *Salvia.*

Indicators replaced in the past from one ecosystem to the next may be provisionally assigned to either competition or genetic limitations. When environmental conditions change, several plant groups are pushed to local extinction because their minimum environmental needs are no longer met. GIRA's record makes a good case for local extinction of *Ruprechtia, Schinus,* some Juncaceae, Cupressaceae, Cyperaceae, some Compositae, and *Adesmia* sp. at the onset or at the end of the Transition zone. At the same time, other indicators are established during the Transition time, *Cercidium, Prosopis, Parkinsonia, Ephedra ochreata,* some Compositae, and others. In order to identify indicators of a process of ecosystem decline, more research is needed in ecosystems as well as in population ecology in order to obtain mechanistic explanations for displacement or extinction. An additional, very valuable indicator in GIRA's record is *Mylodon listai,* the giant sloth that left this latitude at the end of Pleistocene, migrated south, and became extinct at mid-Holocene time.

The process described above shows that the boundary between Patagonia and Monte ecosystems moved northward during the Ice Age and toward the south in the postglacial time. Locally, about 9000 years ago such displacement resulted in the extinction of most of the Patagonia ecosystem and the giant sloth. Intensive research of both local disappearance and extinction of ecosystem components will provide further insight into the astrobiology question of rapid environmental changes and their consequences on ecosystem properties.

Data analysis of the Oregon Pollen Transect is finished and the results are shown in the second figure. Cluster analysis of samples ordered along the Dayville-Newport + Cascade Head transect resolved

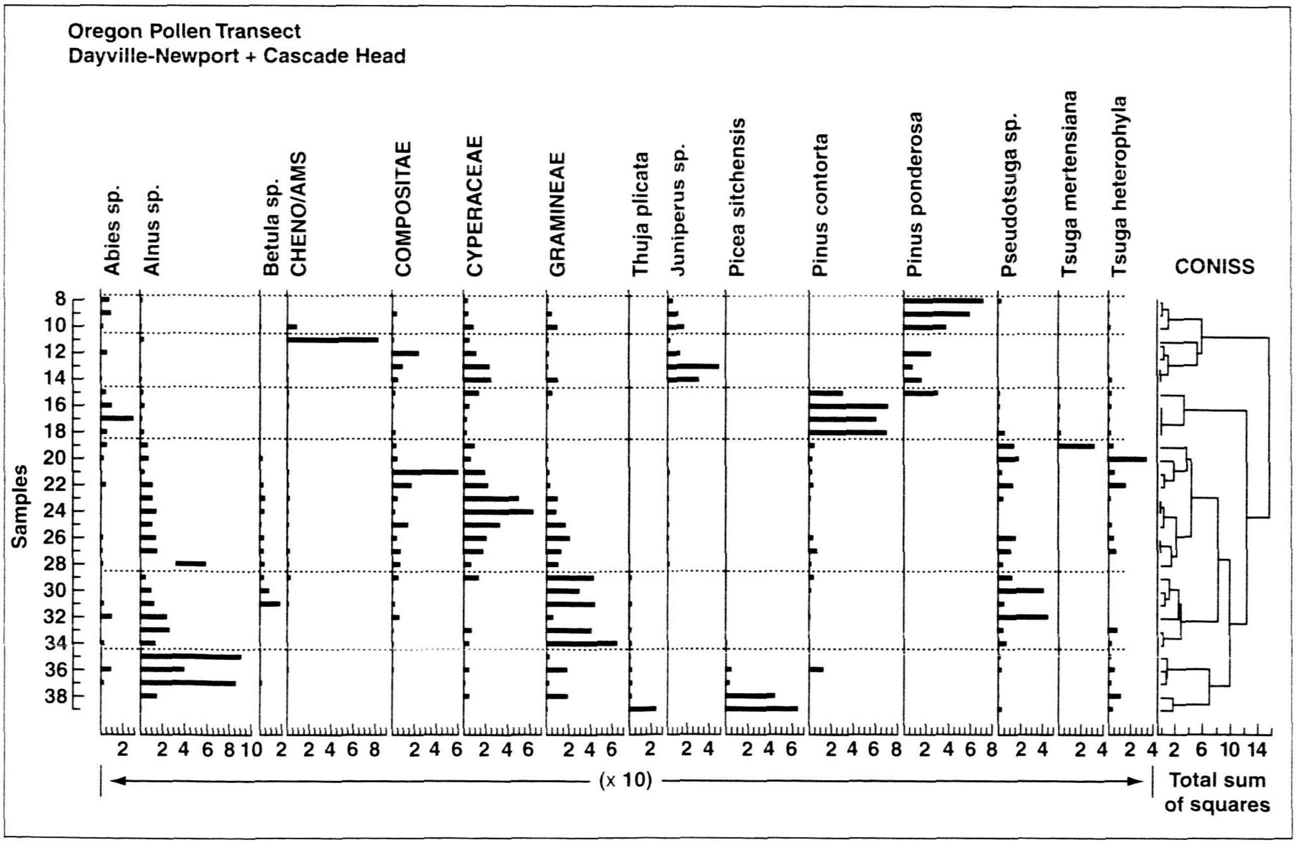

Fig. 2. Oregon Pollen Transect pollen profile.

vegetation zones quite clearly. Thus, samples 8–10 correspond to the Ponderosa pine (*Pinus ponderosa*) zone; samples 11–14 correspond to the Western juniper (*Juniperus occidentalis*) zone; samples 15–18 correspond to the Grand fir (*Abies grandis*) zone east of the Cascades; samples 19–28 correspond to the Pacific silver fir (*Abies amabilis*) zone above an elevation of 1000 meters and the Western Hemlock (*Tsuga heterophylla*) zone west of the Cascades; samples 29–34 correspond to the Willamette Forest and Prairie zones; and samples 35–39 correspond to the Sitka spruce (*Picea sitchensis*) zone. This high correspondence of pollen and vegetation illustrates that pollen is a strong predictor of vegetation. Using results from the OTTER Project (Oregon Transect Ecosystem Research Project), and assuming a linear relation between pollen variables and vegetation indices, a model was produced; the improved model can be used to reconstruct past environments in order to create vegetation indices from fossil pollen data (i.e., "hindcasting").

Point of Contact: H. D'Antoni
(650) 604-5149
hdantoni@mail.arc.nasa.gov

Global Land Surface Monitoring with Low-Resolution Satellite Imagery

Christine A. Hlavka, Jennifer Dungan

The only practical way to produce maps of large regions of the globe is to use remotely sensed data that have coarse spatial resolution, such as data from the advanced very-high-resolution radiometer (AVHRR) at 1.1-kilometer resolution, or the soon-to-be launched moderate-resolution imaging spectroradiometer (MODIS) instrument at resolutions of 250 meters to 1 kilometer (MODIS is a "moderate-resolution" instrument by today's standards). However, the accuracy of the resultant maps is in doubt, especially for mapping highly fragmented land-cover types such as burn scars in forests and grasslands and ponds in Arctic tundra. These land-cover types are important in climatology, hydrology, and other Earth sciences. The objective of this project is to develop an approach for improving area estimates by modeling the distribution of patch sizes of homogeneous land cover, such as open water or the ash layer left by fire.

Digital maps of fire scars in Brazil from both the Landsat multispectral scanner imagery (56-meter resolution) and AVHRR imagery and of water bodies in Alaskan tundra from the Earth Resources Satellite ERS-1 synthetic aperture radar imagery (at resolutions of 12.5 and 100 meters) have been developed. Statistical analysis has confirmed the important contribution of small patches to the overall extent of these land-cover types and has identified candidate models, exponential or power curves, for the fine-scale distributions. Comparison of Landsat and AVHRR maps revealed the types of pixelation effects, caused by low spatial resolution, that can cause errors in area measurements. Software to simulate patch-size distributions at various resolutions has been created and will be used to investigate the relationships between size distributions observed at different resolutions and to develop a new procedure for improving area estimates. Gerry Livingston, School of Natural Resources, University of Vermont, was a co-investigator on this project.

Point of Contact: C. Hlavka
(650) 604-3328
chlavka@mail.arc.nasa.gov

CRUSH Project

Lee F. Johnson, Brad Lobitz

Ames Research Center, together with the Robert Mondavi Winery (Oakville, California) and Terra Spase Vineyard Consulting (Napa, California), is evaluating the use of geospatial technology (remote-sensing, geographic information systems) in a "precision agriculture" context. In the Canopy Remote-Sensing for Uniformly Segmented Harvest (CRUSH) project, high-spatial resolution multispectral images were collected at midseason 1997 with an airborne ADAR-5500 digital camera system.

In a technology demonstration, an image of a 7.5-acre Mondavi chardonnay study block was processed to a Normalized Difference Vegetation Index to improve sensitivity to grapevine canopy density. The Index values were then stratified and color-coded for visual discrimination. A georegistered output image was delivered to the winery for input to the grower's geographic information system. NASA and winery researchers field-sampled vines within the study block for canopy density (light interception), vine physiology (leaf-water potential, chlorophyll concentration), fruit characteristics (maturity, potential quality), and yield. The grower used a laptop computer with image display and onboard Global Positioning System to physically subdivide (with flagging tape) the study block for harvest based on vine vigor (high, medium, and low). Grapes from each field segment were fermented separately and the resulting wines were formally evaluated by the winery.

Field measurement of canopy density and leaf-water potential agreed well with image patterns of density, which was in turn related to grape maturity and malic acid concentration. Most significantly, the winery realized for the first time "reserve" wine (highest quality and value) from a portion of the study block. In addition to the technology demonstration, Ames staff transferred image processing methods and expertise to Terra Spase, who was then able to add value to the raw imagery and sell the product to some 25 North Coast wine-producing clients. Partially as an outcome of this project, Mondavi Winery has led an effort to establish the Wine Country Geographical Information System, a regional user group dedicated to sharing spatial data and processing techniques.

Point of Contact: L. Johnson
(650) 604-3331
ljohnson@mail.arc.nasa.gov

Modeling Leaf and Canopy Reflectance

Lee F. Johnson, Christine A. Hlavka

The goals of this project are to build a leaf reflectance model (LEAFMOD) that incorporates the absorbance properties of biological chemical components, to test the validity of the model, and to evaluate the sensitivity of canopy reflectance to changes in leaf chemical composition by coupling the leaf model to a canopy model. This research will contribute to a better understanding of the radiative transfer processes of plant canopies and will be useful in interpreting remote-sensing data, that is, images from airborne and satellite platforms, used for ecological and biogeochemical research. The results should be useful in determining the minimum sensing requirements for future high-spectral-resolution instruments.

The LEAFMOD computer simulation program was developed to run in two modes: (1) a forward mode that simulates leaf reflectance and transmittance given the optical properties of the leaf material, and (2) an inverse mode that computes the optical properties given reflectance and transmittance by finding values that reproduce the observed reflectance and transmittance in forward mode. Tests of LEAFMOD confirmed that the model predicts realistic scattering and absorption coefficients for leaf material in the inverse mode and predicts reflectances and transmittances similar to laboratory values in the forward mode.

A canopy model was developed and linked with LEAFMOD, and LEAFMOD was modified so that it would compute leaf absorbance properties given the concentration of the main chemicals in the leaf (water, chlorophyll, protein, cellulose, and lignin). The linked models were used to simulate hypothetical trends in plant canopy reflectances resulting from such factors as leaf dry-out and chlorosis (chlorophyll depletion). Barry D. Ganapol, Department of Aerospace and Mechanical Engineering, University of Arizona, Tucson, collaborated with the Ames investigators on this project.

Point of Contact: C. Hlavka
(650) 604-3328
chlavka@mail.arc.nasa.gov

Amazon Ecology from Space

Christopher Potter

The degree to which primary production, soil carbon, and trace-gas fluxes in tropical forests of the Amazon are limited by moisture availability and other environmental factors has been examined using a new ecosystem modeling application for Brazil. A regional geographic information system serves as the data source of climate drivers, satellite "greenness" images, land cover, and soil properties for input to the NASA-CASA model over an 8-kilometer-grid resolution. This study describes the first published use of satellite remote sensing to simulate regional carbon and nitrogen fluxes and associated "greenhouse" gas emissions in the rain forests and savannas of Brazil.

Major findings of this modeling research include the following. Simulation results imply that net primary production (NPP) is limited by cloud interception of solar radiation over the humid northwestern portion of the region, with peak annual rates for NPP of nearly 1.4 kilograms of carbon per square meter per year localized in the seasonally dry eastern Amazon in areas that we assume are primarily deep-rooted evergreen forest cover. Regional effects of the conversion of Amazon forest to pasture on NPP and soil carbon content are indicated in the model results, especially in seasonally dry areas (see figure). Pasture plants and annual crops planted in areas of cleared Amazon rain forest are less tolerant of drought and less capable of tapping deep soil moisture supplies than the forest tree species that they replace. Comparison of model flux predictions

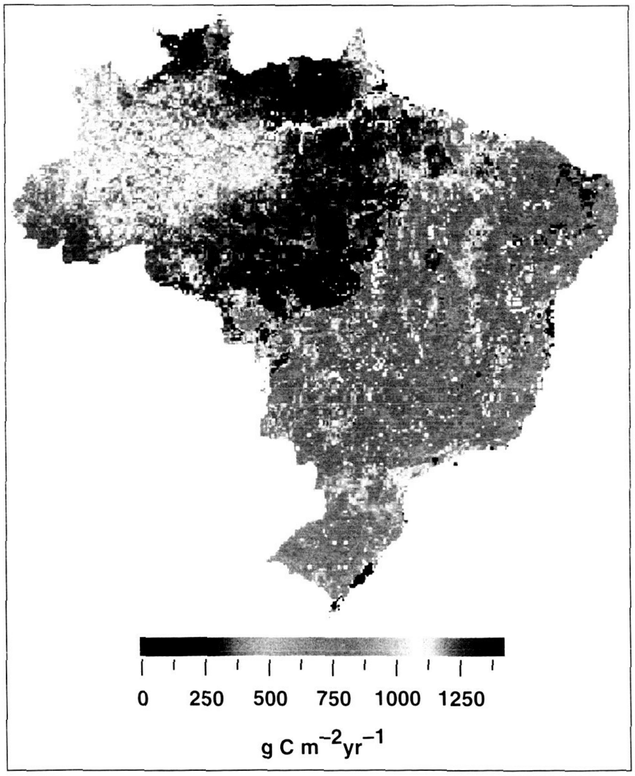

Fig. 1. Net primary production estimated at 8-kilometer cell resolution by the NASA-CASA model for Brazil, ca. 1990.

along selected ecoclimatic transects reveal moisture, soil, and land-use controls on gradients of ecosystem production and soil trace-gas emissions (carbon dioxide (CO_2), nitrogen dioxide (N_2O), and nitric oxide (NO)).

Building upon this research, ecosystem scientists at Ames Research Center have been selected for the NASA Science Team component of the Large-Scale Biosphere-Atmosphere Experiment in Amazonia.

Point of Contact: C. Potter
(650) 604-6164
cpotter@mail.arc.nasa.gov

Ultraviolet Radiation Effects on Carbon Isotope Fractionation

Lynn Rothschild, David DesMarais, Anne Tharpe

The objective of this project is to determine if ultraviolet (UV) radiation affects stable carbon isotope ratios. If so, is there an ecologic (e.g., microbial mat vs. phytoplankton) or taxonomic (e.g., prokaryote vs. eukaryote, alga vs. plant) correlation with the effect? These data will provide the basis for presenting the phenomenon to the scientific community, for estimating how widespread the phenomenon is, and for suggesting ways to begin to elucidate the mechanisms underlying the effect. Ultimately this work could lead to a re-interpretation of isotopic ratio studies, including a re-interpretation of the fossil record.

Isotopic measurements and, more specifically, ratios of ^{13}C to ^{12}C (isotopes of carbon) in organic relative to inorganic matter, play an important role in interpreting biological activity. In the interpretation of the fossil record, stable carbon isotope ratios are one of the most critical sources of data next to morphological fossils. They are a possible approach to searching for life on Mars. Stable carbon isotope ratios are playing an increasingly important role in the analysis of global carbon fluxes, of biogeochemical features of modern ecosystems, and of community structure. They have even been used to determine diet in archeological studies.

The stable carbon isotopic composition (d ^{13}C) of a plant or photosynthetic microorganism growing on carbon dioxide (CO_2) is determined principally by the isotopic composition of the CO_2 as well as by any isotopic discrimination associated with CO_2 uptake. Bulk isotopic composition can be further modified somewhat by enzymatic discrimination during the biosynthesis of amino acids, lipids, and nucleotides, and during respiration. To the extent that UV irradiation alters the patterns of carbon flow in an organism, it can also alter isotopic composition.

An experiment was conducted to determine if UV could affect stable carbon isotope ratios in algal communities. Screens were set up that were UV-transparent or that filtered out UVA or UVA+UVB, over two types of microbial ecosystems in Yellowstone National Park; one dominated by the red alga *Cyanidium* sp., and one dominated by the green alga *Zygogonium* sp. After 90 days of the treatments, the samples were collected, frozen, and turned over to DesMarais' laboratory for analysis. The results (first figure) are clear: In these two mats, UV radiation does affect the carbon isotopic signature.

Experiments were then conducted on radishes to examine UV effects on isotope fractionation. Radish seeds were grown in flats on the roof of the laboratory under different types of UV screening, with approximately 50 plants germinating per treatment. The plants were rotated periodically and were grown

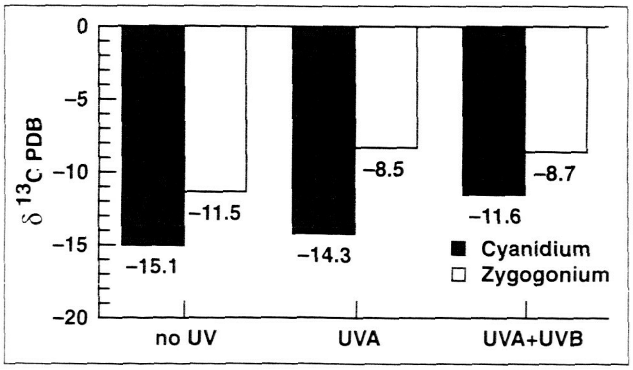

Fig. 1. Carbon isotope values for red and green algae grown under three different UV treatments.

near a blower that controlled temperature. Isotopic analysis of leaf tissue, which at the site of photosynthesis should be the most sensitive to isotopic shifts, showed no difference among the three UV treatments: full solar UV+PAR (photosynthetically active radiation, 400–700 nanometers), –UVB, and –UVA+UVB (second figure). Unlike the microbial mats, in which the absence of UV led to a depletion of ^{13}C relative to ^{12}C of several per mil, there was no detectable difference among plant treatments.

Isotopic discrimination in plant leaves is largest when the rate at which CO_2 is supplied to the enzyme ribulose bisphosphate carboxylase (RubisCO) exceeds the enzymatic uptake rate. Discrimination is suppressed to the extent that CO_2 fixation draws down the CO_2 concentration inside the leaves because of leaf stomatal resistance. The d ^{13}C values of the radish plants were identical under all growth conditions. This indicates that the balance between the rates of CO_2 diffusion through the leaf stomata and CO_2 fixation by RubisCO were unchanged under the three UV irradiation regimes.

In contrast, the d ^{13}C values of the microorganisms did increase with higher levels of UV exposure. This trend cannot be attributed to slower rates of photosynthesis at higher UV exposures, because d ^{13}C values would be expected to decrease with a decrease in the rate of photosynthetic CO_2 assimilation, relative to the rate of CO_2 supply to the microbes. This isotopic trend compels another interpretation that invokes changes in carbon flows elsewhere in metabolism, related perhaps to the synthesis of nucleotides, proteins, or lipids, or to respiration. If the influence of UV on isotopic discrimination in metabolism could be understood, it might allow us to delineate more precisely the metabolic effects of UV irradiation.

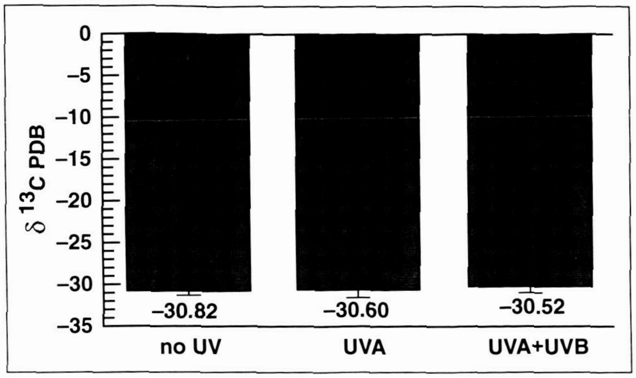

Fig. 2. Isotopic fractionation for radishes.

The conclusion is that UV can effect isotope fractionation in some, but not all photosynthetic organisms. Aruna Balakrishnan, a student, collaborated with the Ames researchers on this project.

Point of Contact: L. Rothschild
(650) 604-6525
lrothschild@mail.arc.nasa.gov

Perceptual Image-Compression Prototype

Andrew B. Watson

NASA missions have generated and will continue to generate immense quantities of image data. For example, the Earth Observing System is expected to generate data in excess of one terabyte per day. NASA confronts a major technical challenge in managing this great flow of imagery: in collection, preprocessing, transmission to Earth, archiving, and distribution to scientists at remote locations. Expected requirements in most of these areas clearly exceed the capabilities of current technology. Part of the solution to this problem lies in efficient image-compression techniques. As part of a larger program of human factors research, Ames has developed a new technology called DCTune to improve image compression.

For much of this imagery, the ultimate consumer is the human eye. In this case, image compression should be designed to match the visual capacities of the human observer. DCTune is based on a model of human vision, and DCTune technology is compatible with JPEG (Joint Photographic Experts Group), the current international standard for still-image compression. Two patents have been awarded for DCTune technology.

DCTune calculates the best JPEG quantization matrices to achieve the maximum possible compression for a specified perceptual error, given a particular image and a particular set of viewing conditions. In DCTune, a target perceptual error of 1.0 means that for the specified viewing conditions the compressed JPEG image is perceptually lossless; that is, it will appear exactly the same as the original uncompressed image.

DCTune offers three key benefits:

1. Accurate specification of visual quality. DCTune incorporates a scale that relates directly to perceptual quality. A value of 1 indicates perceptually lossless quality.

2. Custom quantization matrices optimized for specific applications (printing, internet, web-TV, medical imaging, TV, digital video disks, digital video camcorders, digital TV, high-definition TV, teleconferencing, etc).

3. Reduced file size. For a given level of visual quality, DCTune will produce a smaller file than standard JPEG.

To expedite transfer of this NASA technology to the commercial sector, we have developed a prototype application and made it available to potential developers. DCTune1.1 is a minimal implementation of DCTune technology that is offered free for demonstration purposes only. It takes a color image, computes the optimal quantization matrix, and generates both the matrix and the compressed image.

The figure shows an original image (left) and the same image after compression using the DCTune prototype. The amount of compression was selected so that original and compressed images would be indistinguishable.

Point of Contact: A. Watson
(650) 604-5419
abwatson@mail.arc.nasa.gov

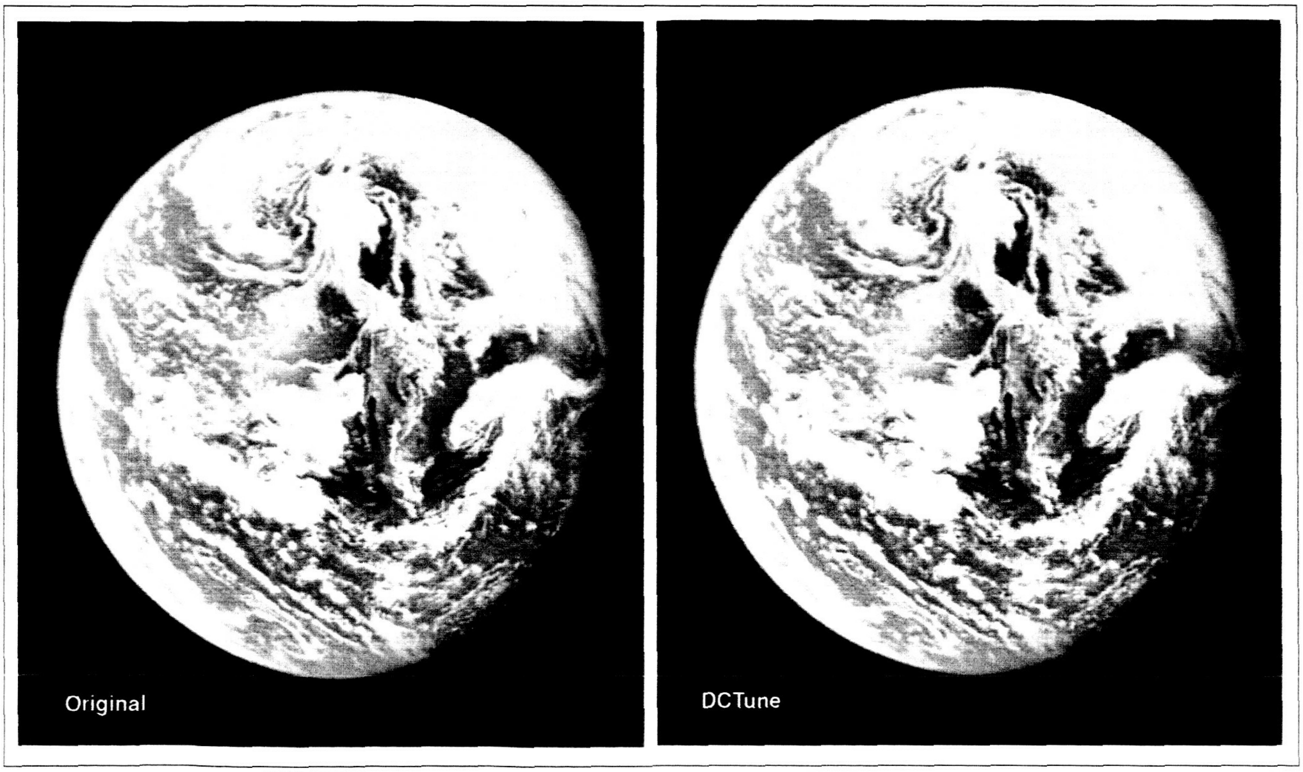

Fig. 1. An original image (on the left) and the image (on the right) resulting from application of DCTune perceptually optimized image compression. The image on the right has been compressed as much as possible while still ensuring that it is visually indistinguishable from the image on the left

Aircraft-Borne Meteorological Measurement Systems

T. Paul Bui, K. Roland Chan, Leonhard Pfister, Antonio A. Trias, Stuart W. Bowen, Jonathan Dean-Day, Cecilia Chang, Elizabeth Moore, David Bui

The aircraft-borne Meteorological Measurement System (MMS) provides high-resolution meteorological parameters (pressure, temperature, and the three-dimensional wind vector). The MMS consists of three major systems: (1) an air-motion sensing system to measure the velocity of the air with respect to the aircraft, (2) an aircraft motion-sensing system to measure the velocity of the aircraft with respect to Earth, and (3) a data-acquisition system to sample, process, and record the measured quantities. Because much of the instrumentation is attached to the aircraft at carefully chosen locations, the MMS is a platform-specific instrument and cannot be moved from one aircraft to another.

The MMS is uniquely qualified for investigation of atmospheric mesoscale (gravity and mountain lee waves) and microscale (turbulence) phenomena. An accurate characterization of the turbulence phenomenon is important for the understanding of dynamic processes in the atmosphere, such as the behavior of buoyant plumes within cirrus clouds, diffusions of chemical species within the wake vortices that are generated by jet aircraft, and microphysical processes in breaking gravity waves. Accurate temperature and pressure data are needed to evaluate chemical reaction rates, as well as to determine accurate mixing ratios. Accurate wind-field data establish a detailed relationship with the various constituents and the measured wind also verifies numerical models used to evaluate air-mass origin. Because the MMS provides quality information on atmospheric state variables, MMS data have been extensively used by many investigators to process and interpret the in situ experiments aboard the same aircraft.

Over the past decade, the MMS on board the ER-2 aircraft has successfully participated in major NASA field missions: STEP in 1987, AAOE in 1987, AASE I in 1989, AASE II in 1991–1992, SPADE in 1992–1993, ASHOE/MAESA in 1994, and STRAT in 1995–1996. In 1997, the ER-2 MMS completed a series of three campaigns of the POLARIS (Photochemistry of Ozone Loss in the Arctic Region in Summer) mission. The campaigns were based in Fairbanks, Alaska, and in Barbers Point, Hawaii.

The MMS on board the DC-8 aircraft has successfully participated in two major field campaigns: the Subsonic Aircraft: Contrail and Cloud Effects Special Study in 1996, and the SONEX (Subsonic Assessment Ozone Nitrogen Oxide Experiment) in 1997. SONEX concentrated in the North Atlantic flight corridor to study the effect of airline traffic on the atmosphere.

New software was developed for both platforms in order to automate the operation of the dedicated laser gyro Embedded GPS Inertial Reference System (GPS is the Global Positioning System). The fundamental pressure measurements were also improved with active thermal controls, thus improving final meteorological data.

Point of Contact: P. Bui
(650) 604-5534
bui@mms.arc.nasa.gov

Studies of Stratospheric Bromine Compounds

Timothy J. Lee, Srinivasan Parthiban

The current understanding of stratospheric ozone depletion chemistry resulting from halogen compounds indicates that in spite of the fact that the concentration of bromine in the stratosphere is much smaller than that of chlorine, bromine accounts for approximately the same degree of ozone depletion as chlorine because of its much greater ozone-depletion potential. The effectiveness of bromine in promoting ozone loss in the lower stratosphere is related to the fact that most of the bromine resides in more labile forms, relative to chlorine, capable of taking part in the ozone-removal cycles. A greater percentage of bromine is in reactive forms, because the conversion of reactive bromine to the reservoir form hydrogen bromide (HBr) from reactions with methane (CH_4) or hydrogen (H_2) is negligible, whereas chlorine atoms can be diverted from the catalytic ozone depletion cycles through the formation of hydrochloric acid (HCl) by reaction with CH_4, H_2, or hydrogen dioxide (HO_2). Further, the destruction rates of HBr and bromine nitrate ($BrONO_2$) are much faster than those of the analogous chlorine reservoir species. In response to these findings, there have been a number of experimental and theoretical studies aimed at the detailed characterization of stratospheric bromine compounds over the last several years. It seems natural that $BrONO_2$ would figure prominently in these studies since the chlorine analog, chlorine nitrate ($ClONO_2$), is an important reservoir species. In the lower stratosphere, the formation of $BrONO_2$ occurs by the termolecular reaction coupling bromine oxide (BrO) and nitrogen dioxide (NO_2):

$$BrO + NO_2 + M \rightarrow BrONO_2 + M \qquad (1)$$

(where M is a third body). The destruction of $BrONO_2$ involves photolysis at ultraviolet wavelengths during the day, leading to a catalytic cycle for ozone destruction. At night, with no photolysis, it has been suggested that $BrONO_2$ can be removed by heterogeneous reactions. Recently a proposal was made that these heterogeneous reactions of $BrONO_2$ may also contribute to catalytic destruction of ozone. However, it is proposed here that a more likely explanation for both the elimination of $BrONO_2$ and the destruction of ozone (O_3) is provided by an observation made by researchers in 1974; that is, it was shown that $BrONO_2$ and O_3 react at 195 kelvin to form a bromide nitrate (O_2BrONO_2) molecule (a structure was never determined):

$$BrONO_2 + 2O_3 \rightarrow O_2BrONO_2 + 2O_2 \qquad (2)$$

Reaction (2) is likely to be more complicated than the single-step termolecular process presented, probably involving two successive bimolecular processes

$$BrONO_2 + O_3 \rightarrow OBrONO_2 + O_2 \qquad (3)$$

$$OBrONO_2 + O_3 \rightarrow O_2BrONO_2 + O_2 \qquad (4)$$

Using the tools of computational quantum chemistry, the equilibrium structures, dipole moments, harmonic vibrational frequencies, and infrared intensities of the reactants and products of reactions (3) and (4) have been determined. In order to assess the reliability of these calculations, results for $BrONO_2$ have been compared with very-high-level singles and doubles coupled cluster theory calculations with a perturbational estimate for triples (denoted as CCSD(T)) and also with experiment where available. Heats of formation of some of these compounds have been evaluated, and the energetics of possible dissociation pathways assessed. We are not aware of any experimental data for the $OBrONO_2$ and O_2BrONO_2 compounds. The transition state for reaction (3) has been examined and the barrier height has been determined.

The implications of this work are significant: if this reaction occurs in the stratosphere, particularly during low Sun conditions, then it may greatly enhance the role of bromine in catalyzing ozone destruction in the stratosphere. Also significant is the very real possibility that $BrONO_2$ may not be a reservoir species for bromine under any stratospheric conditions, a result of its reaction with ozone, contrary to common understanding.

Point of Contact: T. Lee
(650) 604-5208
tlee@pegasus.arc.nasa.gov

Analysis of Stratosphere-Troposphere Exchange

Lenny Pfister

This project has provided meteorological coordination for the ER-2 aircraft POLARIS field mission along with the computer support for project scientists. (The POLARIS acronym stands for Photochemistry of Ozone Loss in the Arctic Region in Summer.) Meteorological satellite products, both imagery and cloud parameters along ER-2 flight tracks, were also provided. The POLARIS mission undertook three major field campaigns in FY97, each with a duration of about 3.5 weeks.

Work has continued on the analysis of lidar data from the Tropical Ozone Transport Experiment. An important result is evidence that subvisible cirrus clouds near the tropical tropopause can be formed by local cooling because of a combination of large-scale uplift and inertia-gravity waves. This is in addition to

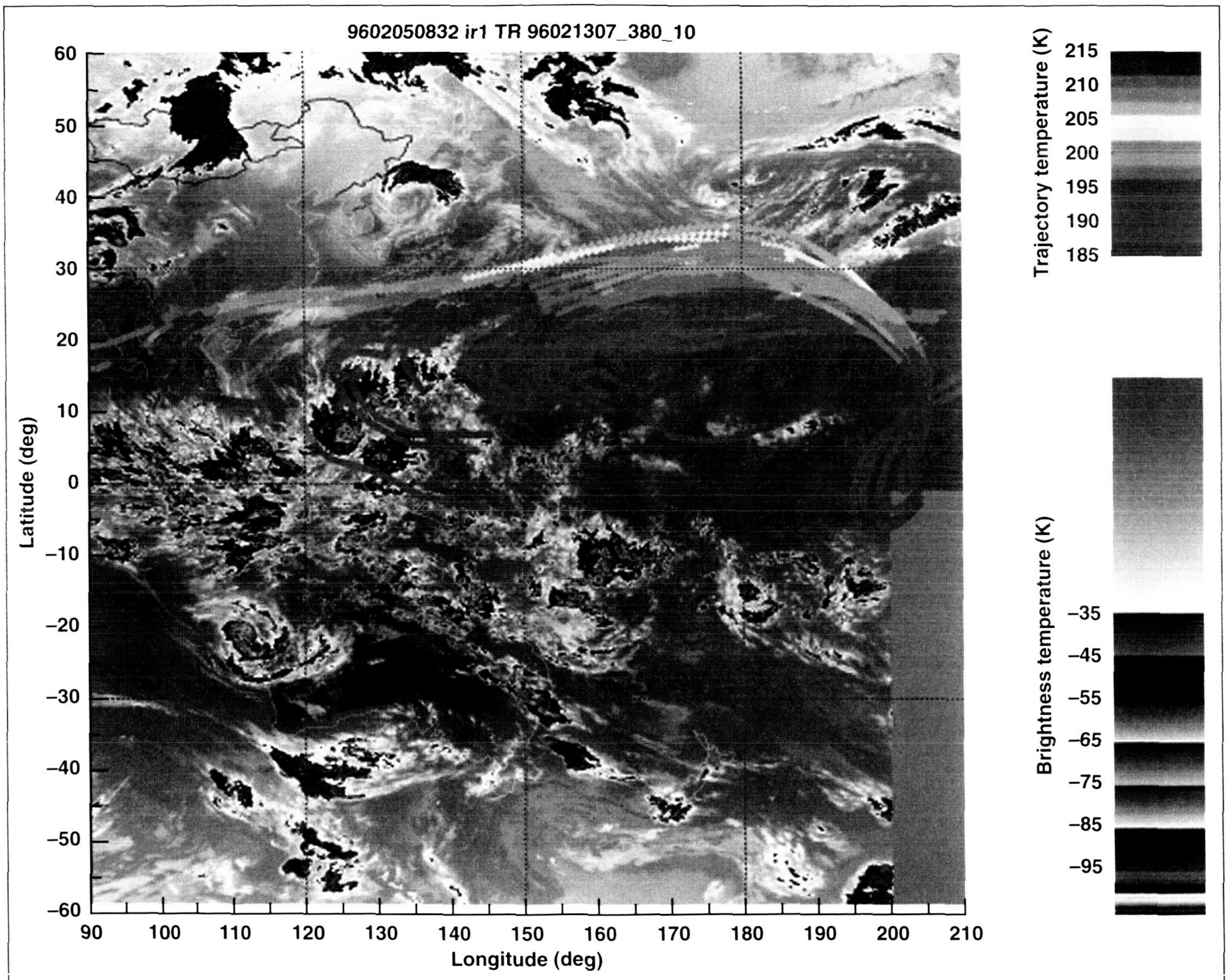
9602050832 ir1 TR 96021307_380_10
Latitude (deg)
60
50
40
30
20
10
0
−10
−20
−30
−40
−50
−60
Longitude (deg)
90
100
110
120
130
140
150
160
170
180
190
200
210
Trajectory temperature (K)
215
210
205
200
195
190
185
Brightness temperature (K)
−35
−45
−55
−65
−75
−85
−95

Fig. 1. Brightness temperatures of 10.5-micron over the western and central Pacific region on February 5, 1996. Superimposed thereon are 10-day back trajectories on the 380-kelvin surface (near the tropical tropopause) from 16 points along the DC-8 flight track from the TOTE/VOTE flight of February 13, 1996. Parcel temperatures along the trajectories are color coded. Back trajectories are calculated using analysis fields from the NASA Goddard Space Flight Center Data Assimilation Office.

the well-established convective outflow mechanism for forming subvisible cirrus clouds. The figure shows the back trajectories on the 380-kelvin isentropic surface from 16 points along the flight track on February 13, 1996. Subvisible cirrus clouds were observed near the tropopause at north latitude 5 and 10 degrees. Most of the parcels have originated in the western Pacific where convection is prevalent, have been transported northward and eastward and warmed as a result of adiabatic descent, and then cooled by adiabatic ascent as they travel southward. The warming is about 5 degrees, implying a doubling of the saturation mixing ratio. This means that any cloud particles left after convective outflow are unlikely to have survived. Thus, the observed thin cirrus clouds are almost certainly a result of recondensation in response to cooling.

A technique for forecasting air masses that have been convectively influenced—which uses trajectory analysis combined with meteorological satellite data—has also been developed. This, along with satellite image display tools that have been developed, will be used in future missions, such as the examination of the North Atlantic flight corridor for evidence of pollution by nitrogen oxides and their effects on upper tropospheric ozone. The back trajectories combined with meteorological satellite data have already been used to evaluate the effect of convection on tropospheric measurements of hydroxyl radical (OH) by the ER-2 during the Stratospheric Tracers Atmospheric Transport Study.

Point of Contact: L. Pfister
(650) 604-3183
pfister@telsci.arc.nasa.gov

Convectively Generated Gravity Waves

Lenny Pfister

Convectively generated gravity waves are one of the major uncertainties in the momentum budget of the stratosphere. Recent momentum budget studies have shown that several phenomena, including the polar night jet in the Antarctic winter stratosphere, the zonal winds in the summer midlatitude stratosphere, and the quasibiennial oscillation, cannot be explained by topography gravity-wave forcing and planetary-wave forcing alone. It is clear that convection generates significant gravity-wave energy; the problem is that convection is a sufficiently complex phenomena, and the data sufficiently sparse, that a clear picture of the amplitudes and phase speeds of convectively generated gravity waves has yet to emerge.

Progress has been made in two areas. First, an analysis was made of a case study of gravity waves generated by convective systems, since recent theoretical and modeling work suggests that the simple "transient-mountain-at-the-tropopause" conceptual model can explain only part of the mesoscale gravity-wave variance. Evidence was found for waves with horizontal wavelengths of about 50 kilometers and vertical wavelengths of about 5–10 kilometers. Also found was evidence of inertia-gravity waves with horizontal wavelengths of 1000 kilometers, which is consistent with studies that inferred horizontal wavelengths using vertical profiles and inertia-gravity wave dispersion relationships.

Second, the study team has participated in an international group that is doing some preliminary planning for an international convective gravity-wave experiment using ER-2 aircraft. One of the products of this group is a white paper describing the motivation, participation, and venue of the experiment.

In addition, the team has arranged for some rapid satellite scans of convective systems being overflown by the ER-2 during the Photochemistry of Ozone Loss in the Arctic Region in Summer campaign. The purpose is to isolate some of the high-frequency forcing of gravity waves in the stratosphere. Joan Alexander, University of Washington, collaborated with the study team on this project.

Point of Contact: L. Pfister
(650) 604-3183
pfister@telsci.arc.nasa.gov

Measuring Tropospheric Nitrogen

James R. Podolske

Assessing the effect of the current fleet of commercial subsonic aircraft on Earth's atmosphere requires detailed knowledge of the nitrogen chemistry of the upper troposphere and lower stratosphere. Understanding of this problem has been hampered by large uncertainties both in the abundances of the odd-nitrogen reservoir species and in the partitioning of reactive nitrogen between nitric oxide (NO) and nitrogen dioxide (NO_2). Among the nitrogen reservoir species, nitric acid (HNO_3) is expected to be one of the predominant compounds. Current instrumentation is inadequate for measuring HNO_3 and NO_2 with the speed and accuracy required to advance understanding in this area.

The open path tunable infrared monitor of the atmosphere (OPTIMA) instrument measures gas phase HNO_3 and NO_2 in the free stream of the NASA DC-8 aircraft. The instrument uses an infrared laser spectrometer coupled to an actively aligned multiple-pass Herriott sampling cavity whose open absorption path between the fuselage and the inner engine pylon achieves a free-stream absorption path length of 384 meters. To further enhance the detection sensitivity of this tunable infrared diode-laser system, high-frequency wavelength modulation spectroscopy is employed. Detection sensitivity for HNO_3 is currently in the range of 25–50 parts per trillion by volume (pptv), and NO_2 at about the 5 pptv range. In 1997, instrument design, construction, and testing were successfully completed. OPTIMA was then used in the NASA Subsonic Assessment Ozone Nitrogen Oxide Experiment mission, sampling air in and around the North Atlantic flight corridor to look for signatures of aircraft emissions that perturb the natural chemistry of the upper troposphere and lower stratosphere. Data analysis is under way.

Point of Contact: J. Podolske
(650) 604-4853
jpodolske@mail.arc.nasa.gov

Atmospheric Effects of Aircraft Emissions: SONEX

Hanwant B. Singh, James Eilers

The enormous growth in aviation has given rise to concerns that emissions from aircraft may be modifying the atmosphere in important ways. SONEX (Subsonic Assessment Ozone Nitrogen Oxide Experiment), a NASA-sponsored DC-8 aircraft mission, was conducted in October–November 1997 in the vicinity of the North Atlantic flight corridor to study the effect of aircraft emissions on the nitrogen oxide families (NO_x) and ozone (O_3). SONEX was managed by Ames Research Center. The major SONEX science objectives were (1) to obtain high-quality measurements of reactive nitrogen species (NO_x family), key ozone precursors (hydrogen oxide families (HO_x)), and tracers from the upper troposphere/lower stratosphere; and (2) to use these observations in conjunction with models to assess the effect of air-traffic emissions on NO_x and O_3. Shannon, Ireland, and Bangor, Maine, were the two primary deployment sites; they allowed access from latitudes 35° N to 70° N over the Atlantic. The Azores provided a secondary deployment site that allowed access to subtropical air masses. Survey flights, as well as maneuvers across fresh aircraft exhaust tracks in the Organized Track System between North America and Europe, were carried out. These DC-8 efforts were closely coordinated with the European DLR/POLINAT (Deutsche Forschungsanstalt für Luft- und Raumfahrt/ Pollution in North Atlantic Tracks) program, which used a higher-flying and smaller Falcon 20 aircraft as the primary research platform. Coordinated missions between the DC-8 and Falcon were performed successfully to accomplish both data-gathering and intercomparison objectives. Results from the SONEX mission are expected to allow an assessment of NO_x and HO_x upper-tropospheric photochemistry that will be greatly improved over any that have been possible to date. Anne M. Thompson of NASA Goddard Space Flight Center collaborated on this project.

Point of Contact: H. Singh
(650) 604-6769
hsingh@mail.arc.nasa.gov

Airborne Tracking Sunphotometry

Philip B. Russell, John M. Livingston, Beat Schmid, Damon Ried

Atmospheric aerosols (suspensions of airborne particles comprising hazes, smokes, and thin clouds in the troposphere and stratosphere) play important roles in determining regional and global climates, the chemical composition of the atmosphere, and atmospheric transport processes. As knowledge has advanced in each of these fields, so has recognition of the importance of aerosols. National and international bodies have called for increased efforts to measure aerosol properties and effects, as a means of improving predictions of future climate, including greenhouse warming, ozone depletion, and radiation exposure of humans and other organisms.

A fundamental measure of any aerosol is how much it attenuates light beams of various colors (i.e., various wavelengths). This attenuation is usually described in terms of the quantity known as *optical depth*. The dependence of optical depth on light wavelength is the optical-depth spectrum.

The Ames airborne sunphotometers determine the optical-depth spectrum of aerosols and thin clouds. They do this by pointing detectors at the Sun (tracking it) and measuring the (relative) intensity of the solar beam in several spectral channels. The tracking head of each instrument mounts external to the aircraft cabin, thereby increasing data-taking opportunities relative to in-cabin sunphotometers and avoiding data contamination by cabin-window effects. Each channel consists of a baffled entrance tube, interference filter, photodiode detector, and integral preamplifier. The filter/detector/preamp sets are temperature-controlled to avoid thermally induced calibration changes. Each instrument includes an entrance-window defogging system to prevent condensation (a problem otherwise common in aircraft descents). Solar tracking is achieved by azimuth and elevation motors driven by differential Sun sensors. In general, Sun tracking is achieved continuously, independent of aircraft pitch, roll, and yaw, provided that change rates in those axes do not exceed about 8 degrees per second and that the Sun is above the aircraft horizon and is unblocked by clouds or aircraft obstructions (e.g., tail, antennas). Data are digitized and recorded by an onboard data-acquisition and control system. Real-time data processing and color display are routinely provided. The science data set includes the detector signals, derived optical depths, detector temperature, Sun tracker azimuth and elevation angles, tracking errors, and time. Each instrument must maintain its radiometric calibration (including window and filter transmittance, as well as detector responsivity and electronic gain) to within 1% in each spectral channel for periods of several months to a year.

The 6-channel Ames Airborne Tracking Sunphotometer made its first flights on the NASA CV-990 aircraft in 1985. Since then, it has flown on a wide range of NASA and other aircraft. Its measurements have been used to validate NASA satellite data bases and to discover new information on urban and marine hazes, desert dust, biomass- and fuel-burning smokes, cirrus clouds, and volcanic aerosols. Most recently, it measured U.S. pollution haze from a C-131 over the Atlantic in the Tropospheric Aerosol Radiative Forcing Observational Experiment (TARFOX, July 1996), and European pollution aerosols, African dusts, and water vapor from a ship in the Second Aerosol Characterization Experiment (ACE-2, June–July 1997).

The 14-channel Ames Airborne Tracking Sunphotometer was developed under the NASA Environmental Research Aircraft and Sensor Technology Program. It made its first science flights on the Pelican (modified Cessna) aircraft of the Center for Interdisciplinary Remotely Piloted Aircraft Studies during TARFOX in July 1996. Mountain calibrations were conducted at the Zugspitze in Germany as part of the Pre-ACE-2 Radiometer Intercalibration in October 1996. Airborne calibrations and further test and science flights were made in California and over coastal waters in conjunction with Navy flights of the Pelican in November 1996. After calibration at Mauna Loa Observatory (Hawaii) in May 1997, it again flew on the Pelican in ACE-2 (June–July 1997), measuring European and African aerosols, water vapor, and ozone. The analysis of measurements will help in understanding the effect of man-made and natural hazes on Earth's climate.

Point of Contact: P. Russell
(650) 604-5404
prussell@mail.arc.nasa.gov

Environmental Research Aircraft and Sensor Technology

Steve Wegener

The Environmental Research Aircraft and Sensor Technology (ERAST) Program provides focus for critical technology development and flight demonstration that reduce the technical and economic risk of using remotely piloted aircraft (RPA) as a means of collecting scientific data in a timely and cost-effective manner. The ERAST Sensor and Science Mission Element provides focus for sensor (science and platform) and mission development and demonstration.

Fiscal Year 1997 saw the completion of a 3-year development program designed to provide the Atmospheric Effects of Aviation Program and the Upper Atmosphere Research Program with a new generation of small, lightweight, low-power RPA-class sensor systems. Although the development of high-altitude RPAs has been beset by many problems, the following ERAST-developed sensors have provided valuable contributions in 1997: STRAT (Stratospheric Tracers of Atmospheric Transport), POLARIS (Photochemistry of Ozone Loss in the Arctic Region in Summer), OMS (Observation from the Middle Stratosphere), ACE 2 (Second Aerosol Characterization Experiment), and Pathfinder science campaigns worldwide. New surface acoustic-wave sensor technologies were explored that have the potential to significantly reduce the size of instruments designed to make in situ measurements of trace gases in the low-pressure atmospheres.

Technologies for over-the-horizon (OTH) communications, which are key to extending the range of RPAs beyond line-of-sight telemetry, were explored and developed in 1997. Preparations for a trans-Pacific flight of the General Atomics Altus RPA were developed to evolve, test, and assess the policies and procedures for operating these unique aircraft in national airspace. Development priorities of Altus shifted focus to demonstrating new payload and satellite-communication technologies on the surrogate RPA testbed platform (Piper Navajo aircraft). The system, built on the Tracking and Data Relay Satellite System Surface Movement Advisor demonstrated in 1996, complemented with a mechanically steered planer-array high-gain antenna, provided continuous cockpit teletype communications, interactive operation on remote-sensing experiments (sea surface temperature measurements), real-time status and command of platform and experiment, and web-based monitoring of experiment location and status. The new antenna allowed higher bandwidth (38.8 kilobytes-per-second data), in a smaller, lower-weight, lower-power OTH communications package.

The Ames-managed ERAST element deployed the first Mission to Planet Earth RPA science mission in 1997. The ERAST-funded, Ames-developed digital array scanned interferometer (DASI) and Airborne Real-Time Imaging System (ARTIS) were integrated on the Solar Electric Pathfinder at the ERAST RPA flight-test facility at the Pacific Missile Range Facility on Kauai, Hawaii. The DASI instrument system, developed to provide an interferogram for each pixel in the pushbroom scanner, operates interactively via the internet. The ARTIS color infrared 6-megapixel digital camera system provides near real-time imagery on the web with interactive control. Integration, testing, and operation of both imagers on this unique platform required extensive collaboration between RPA operators and the science investigators to develop new safe, efficient, and flexible procedures to exploit the advantages of these exciting new systems. Pathfinder set an altitude record of 71,530 feet in July 1997. Integration was accomplished in August and September.

The science and sensor element of ERAST endeavors to reduce obstacles to the emergence of a new aerospace market developed around remotely piloted aircraft by driving new regulatory and operational procedures, developing operational experience, and expanding applications.

Point of Contact: S. Wegener
(650) 604-6278
swegener@mail.arc.nasa.gov

Multidimensional Simulations of Marine Stratocumulus Clouds

Andrew Ackerman

The effects of aerosols on cloud albedos contributes the single greatest uncertainty in estimates of global radiative forcing since preindustrial times. A dramatic example of these effects is provided by ship tracks, which are long, linear regions of enhanced cloud reflectivity that sometimes form downwind of ships. Previously, ship tracks and a number of other topics in the area of aerosol-cloud interactions have been investigated with a one-dimensional numerical model, which is composed of three components: a size-resolved aerosol and cloud microphysics model, a detailed radiative transfer model, and a turbulent kinetic energy closure scheme. An advantage of using a one-dimensional model is that its computational efficiency allows simulations of processes with long time constants; it also permits large numbers of simulations to test model sensitivities. However, there are shortcomings to a one-dimensional approach. For example, peak supersaturations, which determine the fraction of aerosols that nucleate cloud droplets, are underestimated because of horizontal averaging; and the covariation of vertical winds and supersaturations are oversimplified, resulting in droplet activation at cloud top rather than at cloud base. To overcome these shortcomings, a newly rewritten microphysics model and a multidimensional eddy-resolving dynamics model have been merged with the radiative transfer model.

Also, by simply replacing the subroutines specific to warm cloud (liquid water) microphysics with their ice counterparts, a new model was created that is being used to study upper-troposphere ice clouds such as contrails and subvisible cirrus.

The first topic relevant to marine stratocumulus clouds under investigation with the new model is the collapsing boundary layer. With the one-dimensional model, it was found that when aerosol concentrations are depleted to very low values, cloud-top radiative cooling can no longer support the turbulent mixing that provides surface moisture to the cloud layer and maintains the boundary layer against subsidence of dry, warm, upper-troposphere air. In such a case, the cloud-topped boundary layer collapses to a fog layer driven by surface shear. However, there are questions regarding the time scales involved, which determine how frequently such a mechanism can occur when boundary conditions (such as sea-surface temperature) are changing. Preliminary two-dimensional simulations with the new model confirm previous calculations, as seen in the figure.

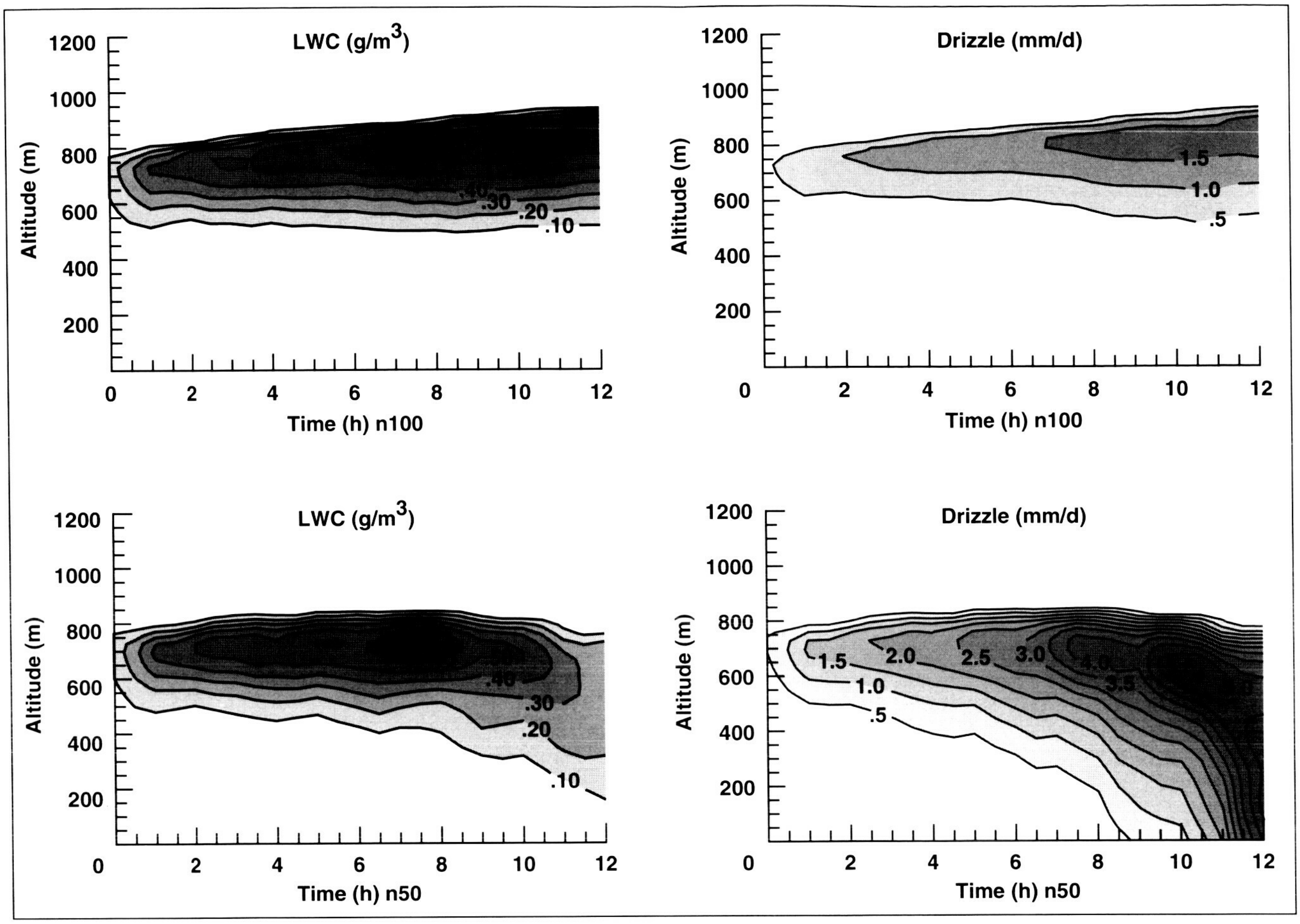

Fig. 1. Time-height contours of horizontally and 2-hour-temporally averaged liquid water mixing ratio (grams per kilogram) and drizzle flux (millimeters per day) in 40 × 40 simulations with initial uniform particle concentrations of 100 (top panels) and 50 (bottom panels) per cubic centimeter.

In the upper (lower) panels the initial particle concentration is 100 (50) per cubic centimeter. In the simulation with lower particle concentrations, the drizzle process develops more rapidly, not only producing a greater sink of cloud water, but also depleting particle concentrations more rapidly. At 18 hours, the maximum droplet concentrations are 52 and 1 per cubic centimeter (a surface source of sea salt particles would likely keep the concentrations from falling much below 5 per cubic centimeter in nature—no consideration of any particle sources was used for these calculations). It is seen that by 18 hours the simulation with a lower initial particle concentration has resulted in a catastrophic collapse of the marine boundary layer.

Point of Contact: A. Ackerman
(650) 604-3522
ack@sky.arc.nasa.gov

Quantitative Infrared Spectroscopy of Minor Constituents of Earth's Atmosphere

Charles Chackerian, Jr., Lawrence P. Giver

Infrared spectroscopic techniques have become extremely powerful tools for use in achieving a number of observational objectives in understanding and monitoring the "health" of Earth's atmosphere. Prerequisite to designing appropriate instruments as well as to interpreting the observations that monitor the important molecular species, quantitative laboratory spectroscopic measurements must be done. The measurements provide (1) line and band intensity values that are needed to establish limits of detectability for as yet unobserved species and to quantify the abundance of those species that are observed; (2) line positions, half-widths, and pressure-induced shifts, all of which are needed for remote and in situ sensing techniques; and (3) data on these basic molecular parameters at temperatures and pressures appropriate to the real atmosphere.

Good progress has been made in calibrating the BOMEM Fourier Transform Spectrometer (FTS) intensity determinations with measurements obtained with the Kitt Peak interferometer on carbon dioxide (CO_2). The analysis for line intensities has begun for nitric acid (HNO_3) using infrared spectra previously obtained.

An experimental study was completed which demonstrates that magnetic rotation spectroscopy can detect free radical molecular species (in situ) in the part-per-trillion mixing ratio range. In connection with this work, measurements were done to establish Zeeman tuning rates in the infrared spectrum of nitrogen dioxide (NO_2).

Preliminary measurements have been made to measure line intensities and shapes of gaseous water in the 1-millimeter spectral region to help in understanding the apparent anomaly associated with absorption of solar radiation by clouds in Earth's atmosphere. The signal-to-noise ratio (S/N) on these spectra, recorded with the high-resolution BOMEM FTS and 25-meter base-path multiple-traversal absorption cell, were greatly enhanced by incorporating an infrared band-limiting filter wheel with S/N ratios greater than 1000 achieved in 30 minutes of integration.

This research was performed in collaboration with Linda Brown, Jet Propulsion Laboratory/ California Institute of Technology; Mike Dulick, National Solar Observatory; Guy Guelachvili, University of Paris XI; Sumner Davis, University of California, Berkeley; Aaron Goldman, University of Denver; Ginette Tarrago, University of Paris XI; Nelly Lacome, University of Paris VI; Tom Blake, Battelle, Pacific Northwest Laboratory; and Chris Mahon, Space Physics Research Institute.

Point of Contact: C. Chackerian
(650) 604-6300
chack@hertz2.arc.nasa.gov

Spreading and Growth of Contrails in a Sheared Environment

Eric Jensen

The evolution of persistent contrails (condensation trails) has been modeled over time scales of 15–180 minutes using a large-body simulation model with detailed microphysics. Model results have been compared to satellite and in situ measurements of persistent contrails from the Subsonic Aircraft: Contrail and Cloud Effects Special Study. In particular, the evolution of the persistent contrail observed on May 12, 1996, was simulated. In simulations with large ambient supersaturations and moderate wind shear, crystals with lengths greater than 200 microns are generated within 35 minutes by depositional growth. In situ measurements in the May 12 contrail case showed that these large crystals did in fact form. The large crystals fall rapidly and the contrail's horizontal extent increases as a result of wind shear (see figure). Strong radiative heating (with

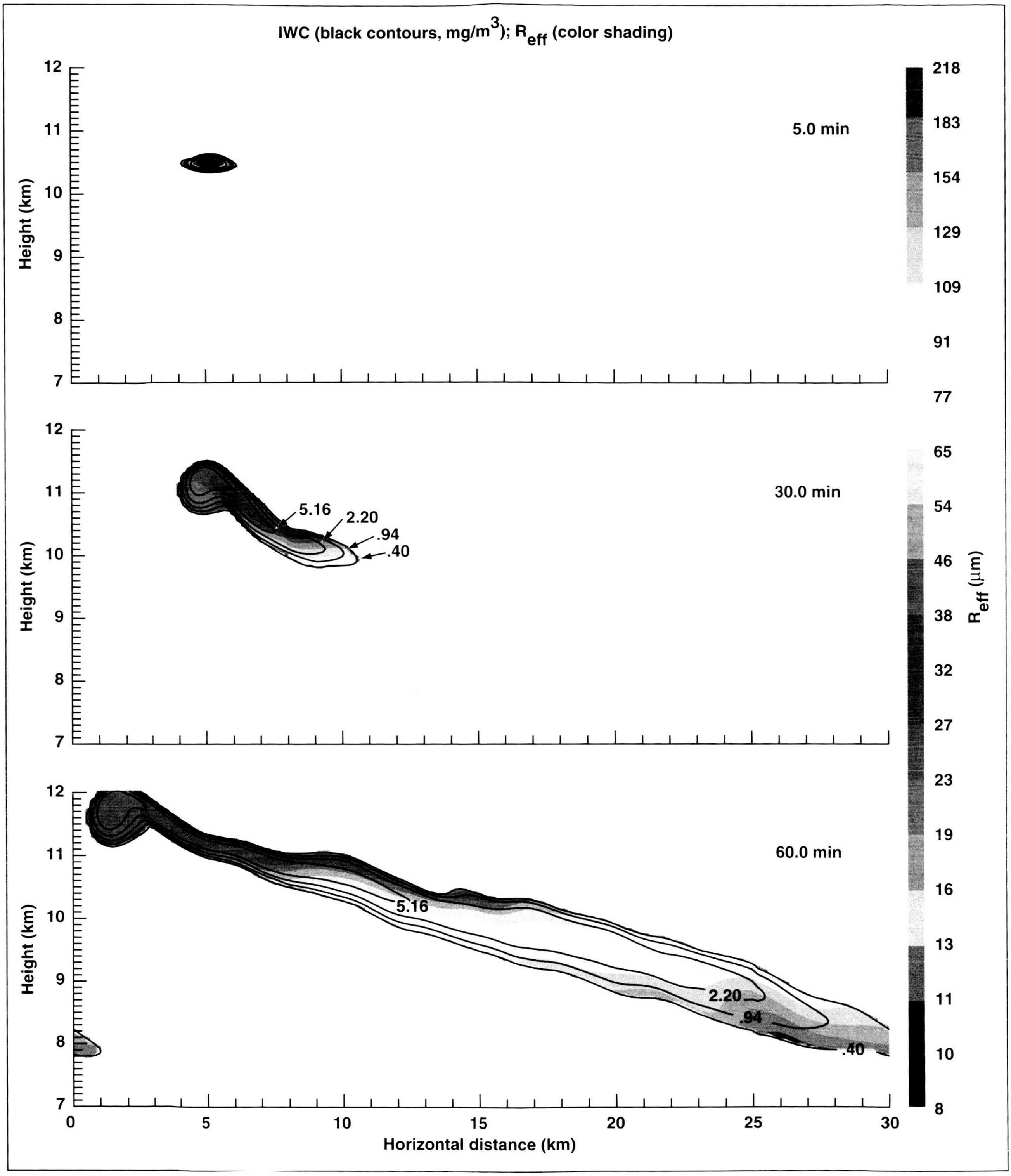

Fig. 1. Contours of ice water content (IWC) are plotted versus cross-track horizontal distance and height at three different times in the baseline simulation. The color shading shows the effective radius (R_{eff}) of the ice crystals. The sorting of crystal size with height as well as the contrail spreading are evident.

rates up to 30 kelvin per day) drives a local updraft and lofts the contrail core several hundred meters. The observed rate of contrail spreading and maintenance of optical depths larger than 0.1 can be explained simply by the growth and precipitation of ice crystals that nucleate during the initial contrail formation if the environmental humidity is high enough (relative humidity with respect to ice greater than 125%). This result is consistent with the high humidities observed in regions where the persistent contrails formed on May 12. Also, the simulations indicate that the humidity must be high throughout a depth of at least several hundred meters below the contrail to allow the crystals to continue growing as they fall.

Point of Contact: E. Jensen
(650) 604-4392
ejensen@sky.arc.nasa.gov

The Roles of Aerosols in Stratospheric Ozone Chemistry

Anthony W. Strawa, Rudolf F. Pueschel, Guy V. Ferry

Stratospheric aerosol can affect the environment in three ways. Sulfuric acid aerosols have been shown to act as sites for the reduction of reactive nitrogen and chlorine and as condensation sites to form (under very cold conditions) polar stratospheric clouds, which facilitate ozone depletion. Recently, modeling studies have suggested a link between black carbon aerosol (BCA) and ozone chemistry. These studies suggest that nitric acid (HNO_3), nitrogen dioxide (NO_2), and ozone (O_3) may be reduced heterogeneously on BCA particles. The ozone reaction converts ozone to oxygen molecules, while HNO_3 and NO_2 react to form nitrogen oxide (NO_x). Finally, a buildup of BCA could reduce the single-scatter albedo of aerosol below a value of 0.98, a critical value that has been postulated to change the effect of stratospheric aerosol from cooling to warming. Correlations between measured BCA amounts and aircraft use have been reported. Attempts to link BCA to ozone chemistry and other stratospheric processes have been hindered by questions concerning the amount of BCA that exists in the stratosphere, the magnitude of reaction probabilities, and the scarcity of BCA measurements.

Recently the Cloud and Microphysics Group participated in the NASA-sponsored Photochemistry of Ozone Loss in the Arctic Region in Summer (POLARIS) mission, which studied ozone depletion mechanisms in the Arctic summer and was completed in Alaska in 1997. The Ames Wire Impactors (AWI) were used in this mission as part of the complement of experiments on the NASA ER-2 aircraft, with the objective of measuring the character of the stratospheric aerosol during POLARIS and providing this information to the scientific community. A main objective of the study was to determine the amount of aerosol surface area, particularly that of BCA, available for reaction with stratospheric constituents and to assess, if possible, the importance of these reactions. The AWI collect aerosol and BCA particles on thin palladium wires that are exposed to the ambient air in a controlled manner. The samples are returned to the laboratory for subsequent analysis. The product of the AWI analysis is the size, surface area, and volume distributions, and the morphology and elemental composition of the aerosols and BCA. Modifications to the AWI data analysis procedures were required in which the collection of BCA is modeled as a fractal aggregate. The new analysis results in an increase in BCA surface area of approximately 24 and an increase in mass of 10 from the previous method. The character of the BCA and its area distributions measured during POLARIS are compared with those made by the AWI on past missions; the comparisons show trends in the spatial and temporal distribution. One trend confirms that the amount of BCA in the Northern Hemisphere is much greater than in the Southern Hemisphere. For the current study, BCA surface area is used in computer models that attempt to predict measured nitrogen oxide/reactive nitrogen (NO_x/NO_y) ratios.

Preliminary analysis attempts to relate BCA surface area to the nitrogen cycle of ozone chemistry. Inclusion of the HNO_3 reaction with BCA in one model improves the agreement of calculated to measured NO_x/NO_y ratios, but more work is yet to be done. The effect of the other reactions on the ratio needs to be explored. An assessment of the accuracy of the reaction probabilities should be made, if possible. Radiative effect must also be evaluated.

Katja Drdla of the National Research Council, Ross J. Salawitch of Jet Propulsion Laboratory, Sunita Verma of Science Systems and Applications Inc., and Steve Howard of Symtech collaborated with the investigators on this project.

Point of Contact A. Strawa
(650) 604-3437
astrawa@mail.arc.nasa.gov

Developing and Validating an Aerosol Model for the Upper Troposphere

Azadeh Tabazadeh

The main purpose of this research was to develop and validate an upper tropospheric aerosol model (UTAM). With this model it is possible to calculate the following quantities: (1) the equilibrium partitioning of various species between the gas and aqueous phases for a wide variety of environmental conditions, (2) the variation in the inorganic aerosol composition as a function of temperature and relative humidity, (3) the solution compositions at which inorganic salt precipitation might occur in upper tropospheric aerosols, and (4) the deliquescence relative humidity (in the atmosphere this is the ambient relative humidity at which a completely dry aerosol becomes thermodynamically unstable and will transform into an aqueous solution droplet) of ammoniated or nitrated aerosols under upper tropospheric conditions. Predicting the equilibrium partitioning has important applications in both gas- and aqueous-phase chemistry modeling calculations, and determining the aerosol composition and salt precipitation can play a significant role in predicting the frequency of cirrus cloud occurrence in the upper troposphere.

Currently, thermodynamic electrolyte models are available for calculating the properties of inorganic aerosols for the conditions found in the lower troposphere and stratosphere. In the lower troposphere, such models are often used in air-quality studies to assess the effects of aerosols on health, gas-phase partitioning, and visibility. In the stratosphere, aerosol models have been used to simulate the formation and growth of polar stratospheric clouds, which are linked to stratospheric ozone depletion. However, these thermodynamic treatments are not suited for calculating the properties of inorganic aerosols under upper tropospheric conditions. Since these aerosols participate in the nucleation and growth of cirrus clouds, understanding their physical properties is crucial for accurately predicting the occurrence of cirrus clouds in the upper troposphere and their subsequent radiative effects.

Simulating the thermodynamic properties of the upper-tropospheric aerosols would require a complex mixed-electrolyte model that accounts for the various ionic interactions in the aqueous solution. This project is developing a mixed-electrolyte model of upper-tropospheric aerosols to address in detail how the current model of cirrus formation from pure sulfuric acid solution droplets can be affected by the presence of ammonium or nitrate ions in solution. Basically, the research shows that ammoniated aerosols are more efficient in nucleating cirrus than are pure sulfuric acid droplets. Further, crude analysis of the recent Subsonic Aircraft: Contrail and Cloud Effects Special Study data indicates that most of the aerosols collected during this campaign were composed of acidic solutions of ammonium sulfate instead of pure sulfuric acid, which is commonly used as the main source of cloud condensation nuclei for microphysical modeling of cirrus clouds in the upper troposphere. In general, it is essential to determine the phase of the background particles that exist in the upper troposphere since the barrier to ice cloud formation by vapor deposition on dry salt surfaces is significantly higher than that of homogeneous freezing from aqueous solution droplets. Also, detailed investigations of the role of aerosol composition and phase transformation in the nucleation and growth of cirrus clouds have been done. In the figure, the three main particle transport pathways to the upper troposphere are depicted and will be used to investigate how these various pathways may alter the nucleation of cirrus clouds in the upper troposphere.

Collaborators on this project were Jin S. Lin, Bay Area Environmental Research Institute and O. B. Toon, LASP Institute, University of Colorado, Boulder, Colorado.

Point of Contact: A. Tabazadeh
(650) 604-1096
taba@sky.arc.nasa.gov

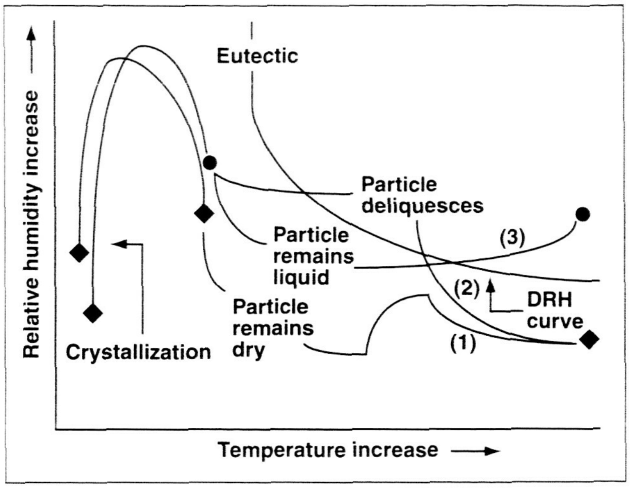

Fig. 1. Particle transport pathways to the upper troposphere. Three general temperature-relative humidity pathways are shown in the plot. Dry and liquid particles are designated as diamonds and circles, respectively. Above the deliquescence relative humidity (DRH) curve the liquid particles are stable, and below this curve liquid particles become supercooled. Solid particles can only exist below the DRH curve for temperatures above the eutectic point.

REPORT DOCUMENTATION PAGE

Form Approved
OMB No. 0704-0188

Public reporting burden for this collection of information is estimated to average 1 hour per response, including the time for reviewing instructions, searching existing data sources, gathering and maintaining the data needed, and completing and reviewing the collection of information. Send comments regarding this burden estimate or any other aspect of this collection of information, including suggestions for reducing this burden, to Washington Headquarters Services, Directorate for information Operations and Reports, 1215 Jefferson Davis Highway, Suite 1204, Arlington, VA 22202-4302, and to the Office of Management and Budget, Paperwork Reduction Project (0704-0188), Washington, DC 20503.

1. AGENCY USE ONLY *(Leave blank)*

2. REPORT DATE
September 1998

3. REPORT TYPE AND DATES COVERED
Technical Memorandum

4. TITLE AND SUBTITLE
Research and Technology 1997

5. FUNDING NUMBERS

6. AUTHOR(S)
Ames Investigators

7. PERFORMING ORGANIZATION NAME(S) AND ADDRESS(ES)

Ames Research Center
Moffett Field, CA 94035-1000

8. PERFORMING ORGANIZATION REPORT NUMBER
A-9810764

9. SPONSORING/MONITORING AGENCY NAME(S) AND ADDRESS(ES)

National Aeronautics and Space Administration
Washington, DC 20546-0001

10. SPONSORING/MONITORING AGENCY REPORT NUMBER
NASA/TM–1998-112240

11. SUPPLEMENTARY NOTES
Point of Contact: Stephanie Langhoff, Chief Scientist, Ames Research Center, MS 230-3,
Moffett Field, CA 94035-1000 (650) 604-6213 or contact the person(s)
designated as the point of contact at the end of each article

12a. DISTRIBUTION/AVAILABILITY STATEMENT

Unclassified — Unlimited
Subject Category 99

12b. DISTRIBUTION CODE

13. ABSTRACT *(Maximum 200 words)*

This report highlights the challenging work accomplished during fiscal year 1997 by Ames research scientists, engineers, and technologists. It discusses research and technologies that enable the Information Age, that expand the frontiers of knowledge for aeronautics and space, and that help to maintain U.S. leadership in aeronautics and space research and technology development. The accomplishments are grouped into four categories based on NASA's four Strategic Enterprises: Aeronautics and Space Transportation Technology, Space Science, Human Exploration and Development of Space, and Earth Science.

The primary purpose of this report is to communicate knowledge—to inform our stakeholders, customers, and partners, and the people of the United States about the scope and diversity of Ames' mission, the nature of Ames' research and technology activities, and the stimulating challenges ahead. The accomplishments cited illustrate the contributions that Ames is making to improve the quality of life for our citizens and the economic position of the United States in the world marketplace.

14. SUBJECT TERMS
Aeronautics, Space transportation, Space sciences, Earth sciences, Life sciences, Information technology, Research and technology

15. NUMBER OF PAGES
191

16. PRICE CODE
A09

17. SECURITY CLASSIFICATION OF REPORT
Unclassified

18. SECURITY CLASSIFICATION OF THIS PAGE
Unclassified

19. SECURITY CLASSIFICATION OF ABSTRACT

20. LIMITATION OF ABSTRACT

NSN 7540-01-280-5500

Standard Form 298 (Rev. 2-89)
Prescribed by ANSI Std. Z39-18
298-102